Microwave Studies of Molecules with Asymmetric Internal Rotors: CH_2DNO, CHD_2NO and ClF_2CCHO

By

David W. Knight

A thesis submitted in fulfilment of the requirements for the Degree of Doctor of Philosophy at the University of Bristol, October, 1985

DECLARATION

This thesis is based on work, carried out under the supervision of Dr. A.P. Cox, at the Physical Chemistry Department of Bristol University, between October 1981 and October 1984. No part of the work presented here has been submitted for any other Degree. The work is believed to be original except where otherwise indicated.

D.W. Knight

October 1985

ACKNOWLEDGEMENTS

I would like to thank my Supervisor, Dr. A. Peter Cox, for his help and encouragement throughout this work. I would also like to thank my friends and colleagues, particularly Stuart Hubbard, Ben Gracey, Rob Barr, Todd Marder and Sue Miller, for making my time at Bristol University enjoyable. I would like to thank Dr. David Field for allowing time away from other duties so that this account could be completed. I would also like to thank Dr. Peter Goggin, for the FTIR spectrum of chlorodifluoro-acetaldehyde, and Jeremy Randell and Dr. A. Peter Cox for the microwave spectrum of $ClF_2CCH^{18}O$. Thanks is also due to Ruth Jenkins, for typing the manuscript. Finally, I would like to thank Jenny Rosenfeld, for good humour and support while this Thesis was being written.

Financial support from the S.E.R.C. is gratefully acknowledged.

ABSTRACT

Microwave spectra of the partially deuterated nitrosomethanes CH_2DNO and CHD_2NO have been re-examined. Analysis of the gauche (C_1) forms using a coupled-level, reduced axis system Hamiltonian gives zero-point torsional splittings of ΔE^{-}_{+} = 922.01 (19) MHz in CH_2DNO and 190.16 (14) MHz in CHD_2NO. Cis-gauche tunnelling perturbations have been interpreted to determine the cis (C_S form) - gauche zero-point separations. The gauche conformer lies above cis by 11.20 cm^{-1} in CH_2DNO. Cis lies above gauche by 10.31 cm^{-1} in CHD_2NO. These results, taken with the CH_3 and CD_3 data, indicate an approximately incremental change in the effective torsional potential with successive deuterium substitution, which can largely be rationalised on the basis of a difference in the in-plane and out-of-plane C-H force constants. Acetaldehyde is found to be closely analogous.

In CH_2DNO, a (+) - (-) near degeneracy at J=1 gives rise to perturbed ^{14}N quadrupole hyperfine structure. This has been analysed by constructing mixed wavefunctions which depend on the tunnelling parameters.

The microwave spectrum of chlorodifluoroacetaldehyde, ClF_2CCHO, has been measured for several isotopic species. The spectrum is dominated by μ_c transitions of a gauche form, which has a chlorine dihedral angle of 109.5°. An accidental planarity relationship has permitted determination of the ^{35}Cl quadrupole coupling tensor, which is cylindrically symmetric, with χ_z = -71.7(4) MHz orientated in the C-Cl bond direction. Vibrational satellite data indicate a high barrier to gauche-gauche inversion of ~820 cm^{-1}, consistent with no observable splitting up to v=3 in the torsion and $\nu(1 \leftarrow 0) \simeq 95$ cm^{-1}. Other satellite spectra suggest the existence of another form, ~200 cm^{-1} above the gauche, displaying non-rigid behaviour.

The published torsional data for trifluoronitrosomethane and trifluoroacetaldehyde (fluoral) have been re-investigated in order to reconcile

discrepancies in the interpretation of microwave and optical results. Vibrational coupling causes the effective internal rotation constant to deviate from the rigid top-rigid frame value. Allowing for this, all of the torsional data up to v=8 for CF_3NO have been fitted to a single degree of freedom model requiring only three constants /cm^{-1}; F_0 = 1.982 (4), V_3 = 238 (2), V_6 = -6 (2). Similar fitting of data for CF_3CHO and CF_3CDO indicatesan incorrect location of the torsional fundamental among hot bands in these cases.

CONTENTS

Cont/d

CHAPTER 1

Introduction

For a system consisting of a single molecule travelling in a field-free region of space, the total energy, referred to the centre-of-mass of the system, is given by the expression;

$$E = E_o + E_{elec} + E_{vib} + E_{rot} + E_Q$$

the term E_o contains all that has been neglected elsewhere, such as nuclear and gravitational energy. The other terms are in order; the electronic, vibrational and rotational energies of the molecule, and the energy due to the orientating effect that electrons have on quadrupolar (non-spherical) nuclei.

The separation of the energy into components is not rigorous. Indeed, it is the breakdown of the vibration-rotation separation which permits the experimental determination of barriers to internal rotation by microwave spectroscopy. Such barriers, hindering rotation about chemical bonds, are of great interest to chemists. It is well known that the orientation of the parts within a molecule affects its physical properties. What is desirable, therefore, is a theory to explain the barrier in terms accessible to the chemist. Such a theory has not been readily forthcoming[1,2,3]. This is not because any hitherto unsuspected basic forces come into play, but because of the mathematical complexity of the problem.

The fundamental approach to the origin of the molecular potential energy surface is the ab-initio calculation. For such a calculation, the molecule may be regarded as an assembly of charged point-masses held together by electrostatic forces. The total energy is then;

$$E = T_n + T_e + V_{nn} + V_{ee} + V_{ne}$$

where the terms are; the kinetic energies of the nuclei and electrons, and

the potential energies of internuclear repulsion, inter-electron repulsion and nucleus-electron attraction.

Ab-initio calculations of barriers to internal rotation[4] give the variation of the total energy with conformation. The barrier is analogous to a vibrational force-constant and as such may be calculated on the basis of the Born-Oppenheimer approximation. In this case, the term T_n is set to zero. The total energy is then regarded as the total electronic energy, which may be calculated using some assumed configuration of nuclei, and using approximate electronic wavefunctions.

Nearly all ab-initio calculations of barrier heights are done using the LCAO-MO-SCF (Linear Combination of Atomic Orbitals - Molecular Orbital - Self-Consistent Field) method[4]. Within this scheme, the molecular wavefunction is constructed using molecular orbitals, which are one-electron functions depending only on the spin and position of the electron. For a system with an even number of spin-paired electrons, orbital wavefunctions which satisfy the Pauli principle are solutions of the Hartree-Fock (Self Consistent Field) equations. These equations can only be solved for atomic systems. The molecular orbitals must therefore be constructed from linear combinations of atomic orbitals. The nominally infinite atomic orbital basis sets must also be truncated in any practical calculation. The procedure for calculating the barrier is then to evaluate the total energy at two conformations and to subtract the results.

The stringent requirements placed on any ab-initio calculation of barrier height are apparent when it is realised that the barrier constitutes only a minute fraction ($\sim 10^{-3}$%) of the total energy[5]. This is in contrast to its importance in determining the gross molecular shape. Errors incurred in the calculation can therefore not only affect the accuracy of the calculated barrier, but can also, at worst, cause the model to give the wrong preferred conformation.

Possible sources of error, within the Hartree-Fock approximation, lie in the neglect of electron correlation and relativistic effects. Electron correlation energy arises because the probability of finding two electrons at the same point simultaneously is zero. It amounts to $\sim 0.5\%$ of the total energy[4]. For molecules containing light elements, errors due to the neglect of relativistic effects amount to $\sim 0.1\%$ of the total energy[4]. Both of these quantities are greater than the barrier height, successful calculation therefore depends upon them remaining unchanged on moving from ground-state to transition-state geometry.

Outside of the Hartree-Fock approximation, errors may arise due to truncation of the atomic-orbital basis set, uncertainty of the molecular geometry and neglect of zero-point vibrational effects. Truncation of the basis set may seriously affect the computed total energy, but its effect on the calculated barrier height is, in some measure, under the control of the investigator. This is because the computed barrier values can be seen to converge as the basis set is expanded. The other effects, however, although usually smaller than the barrier height, are more difficult to eliminate completely.

The molecular geometry is an important assumption which is injected into the ab-initio calculation. There is a difficulty here because, although an experimental probe (e.g. microwave spectroscopy) exists for the structure of the molecule in its ground state, there is no such probe for the transition state. The only approach to the transition state structure is therefore through geometry optimisation. This entails adjustment of the atomic co-ordinates (whilst maintaining a fixed internal-rotation angle) in order to minimise the total energy. Unfortunately, to do so effectively requires some knowledge of the complete molecular potential energy surface. On the other hand, an accurately known ground-state structure can be regarded, to some extent, as a naturally optimised geometry. It is therefore to be

expected, and usually found[4], that rotation of a molecule into its transition-state conformation, without allowing for relaxation of bond lengths and angles, results in a calculated barrier height which is greater than the experimental value.

As mentioned earlier, for the purpose of the ab-initio calculation, the kinetic energy of the nuclei, T_n, is neglected. This will introduce errors because the molecular force-constants, and hence the zero-point energy, will change with configuration. This point is illustrated by the study of nitrosomethane in Chapter 2, which is an example of an experiment to determine the change in the internal rotation potential as a result of isotopic substitution. (Ab-initio calculations, which regard the nuclei in a molecule as immobile point-charges, are unaffected by isotopic substitution). It must therefore be recognised that there is a contribution to the barrier from zero-point energies (a few tens of wavenumbers)[6] which, again, cannot be evaluated without some knowledge of the potential energy surface.

Despite the difficulties, ab-initio (SCF) calculations are generally successful in predicting the preferred conformations and approximate barrier heights in small molecules. Nitrosomethane, which is an example of interest here, has been the subject of calculations, using truncated basis sets, and without geometry optimisation, which calculate the barrier quite accurately in agreement with experiment[7,8]. A theory of the origin of barriers to internal rotation is therefore embedded within the framework of the Hartree-Fock approximation. A problem with this theory, however, is that it entails consideration of the molecule as a whole, and cannot be generalised to very large molecules without the development of electronic computers of ever-increasing sophistication.

What is needed is a theory to describe the barrier in terms of local phenomena, such as might be discussed under the following headings;

(i) Resonance and Hybridisation

(ii) Electrostatic forces

(iii) Steric Hindrance

(iv) Hydrogen bonding

(v) Valence co-ordinate zero-point energies

(vi) Dispersion (Van der Waals) attraction.

all of which are concepts familiar to the chemist and which are associated with the idea of transferability from one molecule to another. Some progress has, of course, been made in this direction[2,3,9]. To begin with, it is obvious that (v) and (vi) are of less importance than the others because they are neglected in the Hartree-Fock approximation (dispersion forces arise as a consequence of electron correlation). It is also quite sensible to make predictions on the basis of observed trends within homologous series of molecules. However, no general theory is yet available, and theories which attempt to account for particular groups of molecules are frequently upset by troublesome exceptions. This point will be discussed further, using collected data, at the end of Chapter 3.

Apart from the theoretical difficulties in predicting barriers to internal rotation, there are also experimental difficulties in measuring such barriers accurately. These come about because it is often necessary to interpret internal rotation data using a simplified model. The model adopted, unless there are very large amounts of data, is usually the one-dimentional Schroedinger equation;

$$H = -\frac{d}{d\alpha} F(\alpha) \frac{d}{d\alpha} + V(\alpha)$$

where $F(\alpha)$ is related to the effective moment of inertia for the internal rotation process, $V(\alpha)$ is the potential energy, and α is the internal rotation co-ordinate. Both $F(\alpha)$ and $V(\alpha)$ are normally expressed as series expansions. It is then found that there are linear relationships between the terms in the expansions[10] of V and F. As a consequence, the simultaneous determination

of the coefficients of V and F, by least-squares fitting to the torsional energy spacings, is an ill-conditioned problem. Determination of $V(\alpha)$ therefore requires that $F(\alpha)$ be obtained from a precise knowledge of the molecular structure. This takes us back to the difficulty mentioned earlier, that there is no experimental probe for the transition-state configuration. In addition, as will be illustrated in Chapter 4, there is a difficulty with the definition of the internal-rotation coordinate α when using a model with a single degree of freedom. Nonetheless, with due attention to possible model errors, barrier heights can be reliably obtained from spectroscopic data, especially if the results of far-infrared (FIR) and microwave experiments are combined[11,12].

Microwave spectroscopy is, of course, a principal source of structural data in the form of molecular moments of inertia. It is therefore interesting to note that, since powerful electronic computers have become available, there has been considerable progress in the field of ab-initio structure prediction. The calculations involved need to go beyond the SCF approach, if they are to agree with the accurate results of microwave experiments, and do so by including the so-called 'configuration-interaction' (CI) terms to take account of electron correlation. The results are impressive, and it is now fair to say that the ground-state equilibrium structures of small molecules ($\lesssim$ 30 electrons) can usually be predicted accurately[13]. Such methods may not be applicable to very large molecules, such as those of biological importance, but they do underline the basic validity of the electrostatic model.

One phenomenon that cannot be accounted for, in a theory that describes molecules as collections of point-charges, is nuclear quadrupole coupling. This arises because certain nuclei have a non-spherical charge distribution. Nuclear spin angular momentum then becomes coupled to the overall angular momentum of the molecule as the quadrupolar nucleus orientates with the

electric field gradient in its vicinity. This causes the lines in the molecular rotation spectrum to be split into hyperfine components representative of the nuclear spin states. Interpretation of this nuclear-quadrupole hyperfine-structure (NQHFS) then, in favourable circumstances, permits a tensor-analysis of the electrostatic field gradient in the region of the coupling nucleus. Quadrupole coupling is therefore an important source of information about chemical bonding, and microwave spectroscopy, again, is an important source of such data.

If this section appears to over-emphasize electronic theory, then it does so because such issues will be largely neglected elsewhere. The work, as a whole, is more concerned with the pragmatic business of collection and interpretation of experimental data. Specifically, it is a study of internal-rotation in small molecules, where an sp^3 hybridised atom is connected to an sp^2 hybridised atom. The molecules for which new data are reported are the partially deuterated nitrosomethanes, CH_2DNO and CHD_2NO, and chlorodifluoro-acetaldehyde ClF_2CCHO.

Chapter 2 describes the assignment of the microwave spectra of gauche-CH_2DNO and gauche-CHD_2NO, both of which are complicated by quantum-mechanical tunnelling between left and right handed versions of the gauche conformer. Also given is an analysis of the ^{14}N quadrupole coupling, again complicated by quantum-mechanical tunnelling, and a precise determination of the cis-gauche zero-point energy difference by identifying perturbations in the rotational energy manifolds of these otherwise-localised conformers.

Chapter 3 describes the microwave spectrum of ClF_2CCHO, studied as the starting point for a microwave analysis of chlorodifluoronitrosomethane, ClF_2CNO, which is iso-electronic to it. Four isotopic modifications of the aldehyde; $^{35}ClF_2CCHO$, $^{37}ClF_2CCHO$, $^{35}ClF_2CCDO$ and $^{35}ClF_2CCH^{18}O$ are used to determine the molecular structure of the gauche-form. The isotopic data are also used to determine the complete ^{35}Cl quadrupole coupling tensor.

Excited state studies of the C-C torsion indicate a high barrier ($\sim$820cm^{-1}) for gauche-gauche interconversion. There is also evidence of a higher-energy form, which is probably a cis-form. This form however gives rise to an unusual microwave spectrum, which seems to indicate that it is involved in some facile tunnelling process.

Work in Chapter 4 tackles a long-standing problem; the apparent discrepancy between optical and microwave torsional data for two molecules having heavy symmetric internal rotors. These molecules are trifluoro-nitrosomethane, CF_3NO, and trifluoroacetaldehyde (Fluoral), CF_3CHO. It turns out that the discrepancies arise for different reasons. For CF_3NO, a reliable data adjustment is given using the torsional-potential least-squares fitting program of appendix six. The result gives the barrier height (238.4(1.6) cm^{-1}) without recourse to structural data, and the problem of determining the internal rotation constant, $F(\alpha)$, from structure is discussed. For CF_3CHO and CF_3CDO, on the other hand, it appears that the frequency positions of the torsional fundamentals, in the FIR spectra, have been mis-assigned due to superposition of several torsional hot-bands.

CHAPTER 2

NITROSOMETHANE

Introduction

The microwave spectrum, barrier to internal rotation and preferred conformation of nitrosomethane (CH_3NO) were first reported by Coffey, Britt and Boggs[14]. The molecule has a bent C-N-O group, due to the presence of a lone electron-pair on the nitrogen atom, and undergoes hindered rotation about the C-N bond. Isotopic species with a symmetric methyl group (CH_3NO and CD_3NO) therefore give A-E type spectra[15], which were analysed for the barrier height. Identification of the preferred conformation by microwave spectroscopy, however, required study of the partially deuterated species (CH_2DNO and CHD_2NO). A molecule with a greater than two-fold symmetric internal rotor has the same moments of inertia regardless of conformation. The partially deuterated species (CH_2DNO and CHD_2NO) however have measurably different moments of inertia for different orientations of the methyl group. It was thus established that nitrosomethane, in the electronic ground state, adopts the conformation with hydrogen atom eclipsing the oxygen atom, and that the partially deuterated species exist in *cis* (planar-symmetric) and *gauche* (asymmetric) forms (see Figure 1).

The microwave study of nitrosomethane was continued at the Bristol Laboratory by Paul Turner and Dr. A. Peter Cox[16,17]. These authors reported an accurate structure for the molecule, based on ten isotopic species, and confirmed the methyl barrier determination on the basis of additions to the CH_3NO and CD_3NO data sets. They also undertook a centrifugal distortion study for comparison with the harmonic force-field derived from the vibrational fundamentals reported by Lüttke[18] and Barnes et al[19]. It was found that reliable distortion constants could not be obtained by studying species with

Nitrosomethane Rotamer Definitions.

CH_2DNO

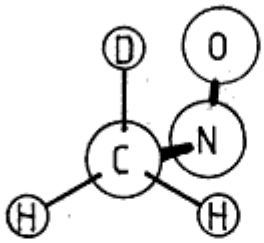

Cis.

$\alpha = 0°$

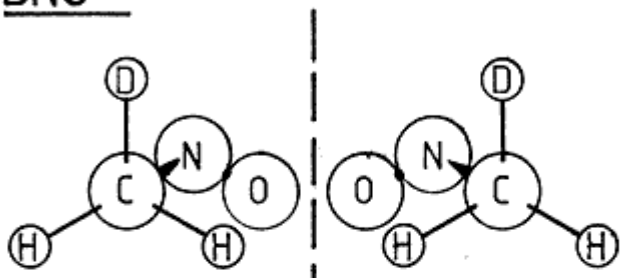

Gauche.

Spectroscopically Indistinguishable Forms.

$\alpha = \pm 120°$ (nominally).

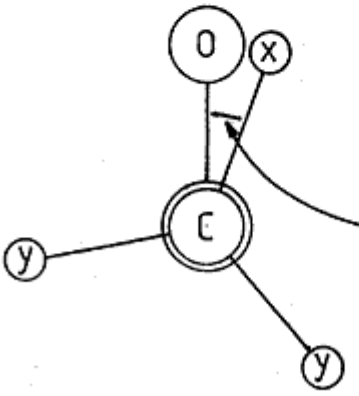

α

Dihedral Angle here defined in terms of the hetero atom 'X'. α is the angle between the projections of the N–O and C—X bonds on to a plane perpendicular to the internal rotation axis.

Figure 1

a symmetric internal rotor because of approximations necessarily introduced into the torsion-rotation Hamiltonian. This difficulty was effectively overcome by studying the partially deuterated species.

On partial deuteration of nitrosomethane, the A-E type spectrum disappears to be replaced by a spectrum due to three non-degenerate torsional substates (see Figure 2). These substates, using the notation of Quade and Lin[20], are denoted by the subscripts 0, + and - attached to the limiting high-barrier torsional quantum number. The O_0 state is localised in the region of the cis potential minimum and, therefore, at infinite barrier, corresponds to the cis form. The O_+ and O_- states are symmetric and anti-symmetric combinations of wavefunctions localised in the gauche potential minima.

Prior to the nitrosomethane work, it had been noted by Kilb, Lin and Wilson[21], that the microwave spectra of the cis (O_0 state) partially deuterated acetaldehydes, CH_2DCHO and CHD_2CHO, followed the ordinary asymmetric rotor pattern. Turner and Cox[22], in adopting acetaldehyde as a model for nitroso-methane (the two molecules being inertially alike), went on to show that these spectra could be fitted to a Watson centrifugal-distortion Hamiltonian. Spectra of cis-CH_2DNO and cis-CHD_2NO were then subsequently fitted in the same way[17]. These species therefore proved to be a source of structural, centrifugal distortion and dipole moment information relatively free from the complicating effects of internal rotation; this extremely useful phenomenon being due to an unexpectedly large separation of the O_0 and $O_\pm$ zero-point energies.

The difference in the cis and gauche zero-point energies, in the partially deuterated species, must arise out of the effect of isotopic substitution on the kinetic and the potential energies. However, the kinetic energy effect, which depends on the internal rotation constant, F (α), can be calculated from structure and shown to be too small to produce the

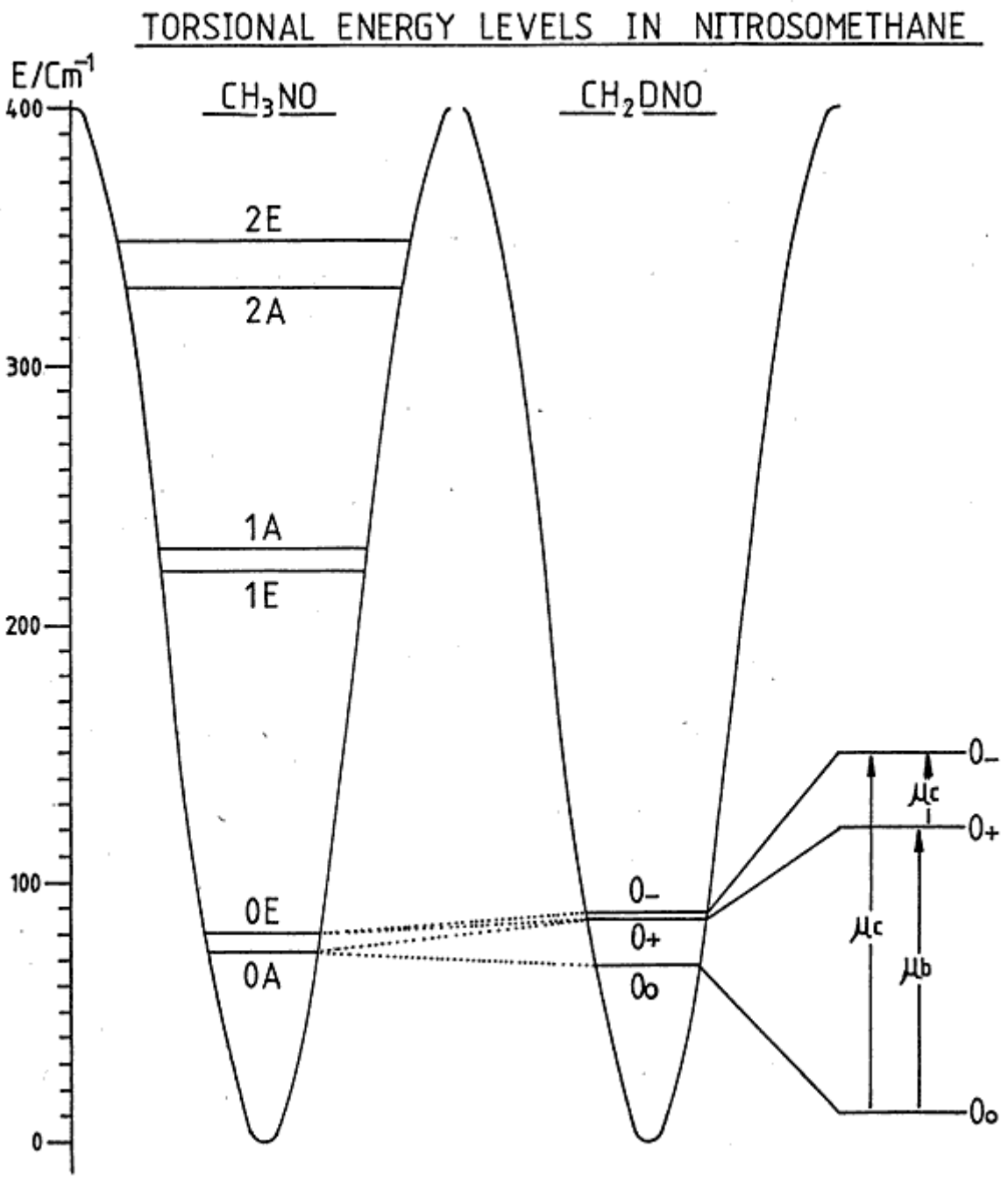
TORSIONAL ENERGY LEVELS IN NITROSOMETHANE
E/Cm⁻¹
400
300
200
100
0
CH3NO
CH2DNO
2E
2A
1A
1E
0E
0A
0-
0+
0o
μc
μb

Figure 2

observed shift. The zero-point separation therefore arises principally out of the change in the potential, $V(\alpha)$, with substitution. This change must originate in a contribution to the effective potential from other vibrations in the molecule, and is therefore due to an α dependence of the zero-point energy of the other vibrations. Such a dependence is to be expected since it is well established from infrared studies[23], and supported by ab-initio calculations[24], that C-H bond lengths and force constants show a strong α dependence. The consequence, in nitrosomethane and acetaldehyde, is that the 0_0 and $0_\pm$ states become energetically isolated to an extent which largely supresses cis $\leftrightarrow$ gauche tunnelling. The cis form therefore behaves like an ordinary asymmetric rotor to a high degree of approximation. This approximation does however break down for certain states of rotational energy.

During the course of centrifugal distortion work on cis part-deuterated acetaldehyde[22] and nitrosomethane[16,17], Turner and Cox noted that, although the overall fit to the Watson Hamiltonian was good, there were occasional perturbations. These were attributed to cis-gauche interactions, which occur when 0_0 state rotational sublevels lie close to 0_+ or 0_- sublevels of appropriate symmetry and the same J (neglecting quadrupole coupling). It was then apparent that, if the mutually perturbing energy levels could be identified, and if the gauche energy levels could be calculated, it would be possible to determine accurately the cis-gauche zero-point energy difference. This would, of course, require detailed assignment of the $0_\pm$ state rotational spectra which, because of facile gauche $\leftrightarrow$ gauche tunnelling, do not obey the asymmetric rotor pattern.

Detailed assignments for acetaldehyde of gauche-CH_2DCHO and gauche-CHD_2CHO were subsequently carried out by Turner, Cox and Hardy[25,26]. These authors were successful in fitting their observations to a Pickett Hamiltonian[27] (see later) which included centrifugal distortion terms. It was thus found that some of the gauche energy levels were also perturbed by interaction

with energy levels from the cis form. It was then established that the cis form of CH_2DCHO lies 15.55 cm^{-1} lower in energy than the gauche form. This result, and the opportunity to study a more complicated case in which quadrupole coupling occurs, provided the motivation for the present study of gauche-CH_2DNO and gauche-CHD_2NO.

PREPARATIVE CHEMISTRY OF NITROSOMETHANE

Nitrosomethane was first discovered in 1947 by Coe and Doumani[28]. It exists in equilbrium with its dimer such that, except at high temperatures, the dimer is the predominant species. Both the dimer and the monomer also have a tendency to isomerise irreversibly to formaldoxime. The chemistry of this system, identified by Gowenlock and Trotman[29] and later clarified by Frost, Lau, McDowell and Westwood[30] is summarised in Figure 3.

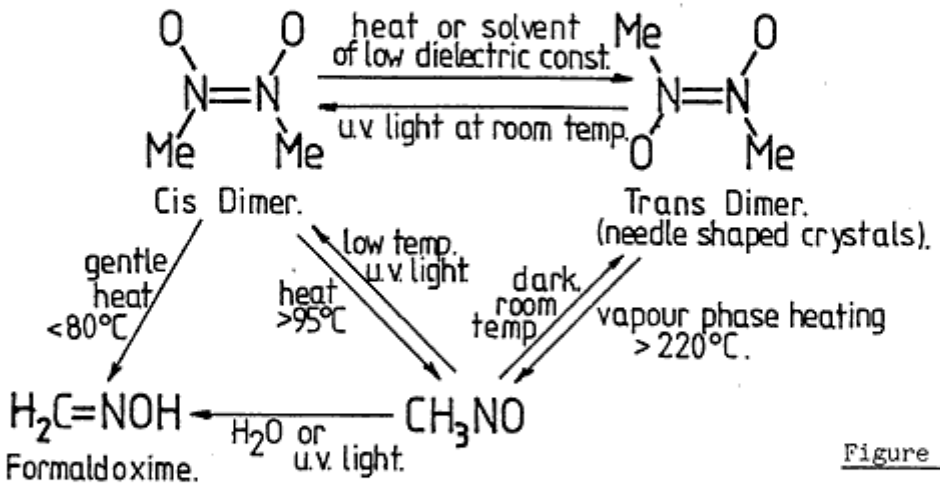

Figure 3

Chemistry of Nitrosomethane.

Nitrosomethane was originally prepared by photolysis of tertiary butyl nitrite, but a variety of starting materials are suitable for the photo-synthetic route[31]. The mechanism in these cases has been shown to involve the re-combination of nitric oxide and methyl radicals[32,33]. For the purposes of this work, iso-propyl nitrite was chosen as the starting material[34] because it can be readily prepared from acetone. The methyl hydrogen atoms in acetone are labile as a consequence of the enolisation process, which

makes the preparation of deuterated acetone[35] very straightforward. After acetone deuteration, the reaction scheme used was as follows:

$$Me_2CO \xrightarrow{NaBH_4} Me_2CHOH \xrightarrow{HONO} Me_2CHONO$$

$$Me_2CHONO \xrightarrow{h\nu} [Me^{\cdot}, NO^{\cdot}, \text{etc}] \rightarrow MeNO \rightarrow (MeNO)_2$$

Experimental

Two samples of nitrosomethane were required for the present work, one 33% deuterated and the other 67% deuterated. Deuteration was accomplished by mixing the starting material (Acetone B.D.H. Aristar) with D_2O (Aldrich 98 atom % D) in the presence of a catalytic quantity of K_2CO_3. 5ml of acetone and about 25mg of K_2CO_3 was used in each case. The amount of D_2O used was calculated on the basis of complete hydrogen scrambling. Reactants were left in contact, in air-tight evacuated tubes, for several weeks at room temperature (~20°C) and then checked for the presence of a C-D stretching band in the gas phase I.R. spectrum. In the case of the lightly deuterated acetone sample, this band was very weak.

In order to remove water and D_2O, acetone samples were distilled onto anhydrous $MgSO_4$ and then onto calcium oxide (distilling directly onto CaO is not recommended because the reaction between CaO and water is strongly exothermic). After drying, samples were then distilled onto 10g quantities of $NaBH_4$. Drying was sufficiently thorough to eliminate the troublesome evolution of hydrogen during the borohydride reduction, enabling the reactants to be sealed in a confined space. Reactions were allowed to proceed overnight and the resulting isopropyl alcohol, apparently adsorbed on the remaining solid material, was liberated by gentle flaming.

Two different methods were tried for the nitrosylation of iso-propyl alcohol. The first, a traditional bench method, involved treating the alcohol with a mixture of sodium nitrite and dilute sulphuric acid ('nitrous acid') at 0°C, decanting the resulting isopropyl nitrite with a syringe.

This method was wasteful on account of the high volatility of the product. A far better method, compatible with vacuum-frame technique, involved the use of N_2O_3 gas. Air-free water (3ml) was distilled onto isopropyl alcohol (3ml); the apparatus was then repeatedly filled, up to one atmosphere pressure, with N_2O_3. The gas was absorbed into the liquid phase by periodically freezing the reactants with liquid nitrogen. The mixture separated into two layers, an upper straw coloured layer being the crude product. N_2O_3 treatment was discontinued when the lower aqueous layer began to show a persistent blue colour. Residual N_2O_3 was removed from the product by distilling it onto 2ml of strong aqueous NaOH, the product was then dried by distilling it out of a methylated-spirit/dry-ice bath ($\sim$ -60°C) onto anhydrous $MgSO_4$.

Isopropyl nitrite was photolysed in small portions (0.2 $\sim$ 0.5ml) in a 500ml silica bulb with a borosilicate finger. The light source was a 400W input Hanovia mercury vapour lamp surrounded by a water filled silica jacket. Brief sessions of photolysis (5 ÷ 15 min), with the bulb as close as possible to the lamp, resulted in a blue colour in the gaseous phase and the appearance of fine needle shaped crystals of trans-$(MeNO)_2$ at the surface of the glass. The borosilicate finger was used for periodic collection of the product to protect it from U.V. light. Freezing the finger in liquid nitrogen and flaming the bulb caused the crystals to evaporate and a bright blue ring of nitrosomethane monomer to appear at the glass-nitrogen interface. On warming, the monomer changed into the colourless dimer. Completion of photolysis was judged on failure to produce a significant crop of crystals. The bulb was then pumped briefly to remove unchanged isopropyl nitrite and gaseous byproducts before flaming to transfer the product into a sample tube for spectroscopy.

Sample Handling

Coffey, Britt and Boggs[14] obtained the microwave spectrum of nitrosomethane by dosing from a sample of the trans dimer. For this work, however, the dosing method used was that devised by Turner and Cox[16,17] (see Figure 4). Samples were stored at room temperature in evacuated borosilicate 'U' tubes. Dimer in one arm of the tube was dissociated by flaming and collected as blue monomer in a liquid nitrogen Dewar on the other arm. On warming, the monomer either dimerised or evaporated into the spectrometer cell.

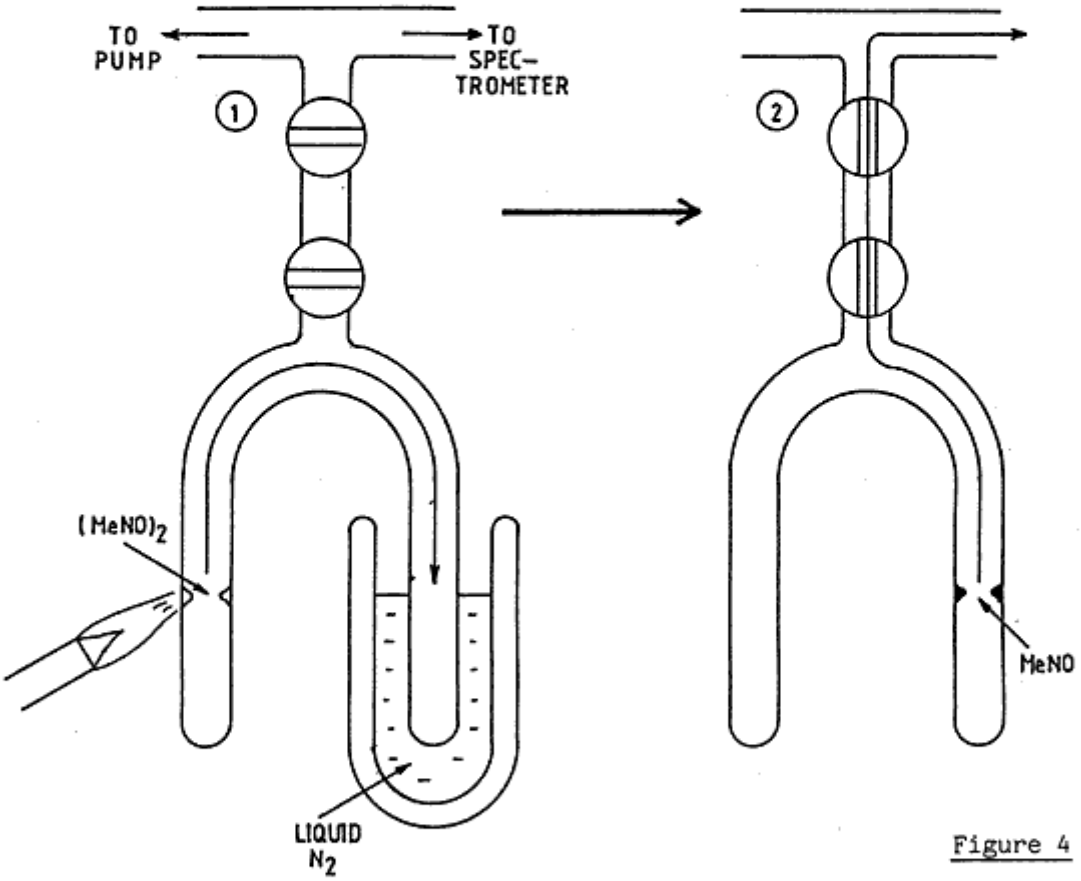

Figure 4

Spectra were recorded at dry-ice temperature with pressures in the region 0.01 ~ 0.05 torr. Throughout a spectroscopic run, the pressure in the cell dropped continuously with a half life of about half an hour. This effect, due to dimerisation or isomerisation of the sample, was not always a disadvantage because it caused the resolution of quadrupole hyperfine structure to improve with time.

The samples, being inhomogeneous mixtures, were hard to assess for purity. Formaldoxime gives a microwave spectrum at room temperature but not at dry-ice temperature[36] and so was not a source of interference. CH_2DNO was the most abundant component of the 33% deuterated sample as expected. Moreover, since most of the species present had already been assigned in detail, ambiguities as to the origin of a line of interest could often be resolved by comparing the relative intensity with that of a known line and seeing if the relationship held on changing to a sample with different deuteration content.

PRELIMINARY THEORETICAL CONSIDERATIONS

For an extremely non-rigid species such as gauche-CH_2DNO it is not possible to make a detailed assignment of the microwave spectrum on the basis of an ordinary asymmetric rotor model. Some theory descriptive of the internal rotation process is required from the outset. It also becomes necessary to include centrifugal distortion corrections at an early stage in the analysis. Nevertheless, it has been possible to account for the observed spectra on the basis of a model having only one large amplitude internal degree of freedom, and it has been possible to predict transition frequencies on the assumption that rotation-vibration coupling occurs entirely along the 'a' principal axis.

The initial approach, restricted to low J or particularly well behaved lines, was to treat the 0_+ and 0_- states separately wherever possible and to introduce the internal rotation perturbation by diagonalising 2x2 matrices containing the most heavily interacting energy levels. This treatment is similar to that used by Hirota Hirooka and Morino[37] in their analysis of $CH_2D\text{-}CH{=}CH_2$ and, since only a-axis coupling is considered, is equivalent to applying the Hamiltonian

$$H = \left[\begin{array}{c|c} A_+P_a^2 + B_+P_b^2 + C_+P_c^2 & Q_aP_a + N_a(P_bP_c + P_cP_b) \\ \hline & A_-P_a^2 + B_-P_b^2 + C_-P_c^2 + \Delta E_{\pm} \end{array}\right]$$

In practice, only the off diagonal term in Pa is retained, so that the perturbation calculation becomes simply;

$$T^{-1}\begin{bmatrix} E_{+\,J\tau}^{(0)} & K_aQ_a \\ K_aQ_a & E_{-\,J\tau'}^{(0)} \end{bmatrix} T = \begin{bmatrix} E_{+\,J\tau}^{(1)} & 0 \\ 0 & E_{-\,J\tau'}^{(1)} \end{bmatrix}$$

with the assumption that Qa is the same for all pairs of levels considered.

Obviously, this approach cannot be carried too far but the formulation has the major advantage of being constructed in terms of the gauche principal axis system. The expectation values $\langle Pg^2 \rangle$ (g = a,b,c) are therefore appropriate to the calculation of first-order quadrupole energies, and have been sufficient to account for most of the observed hyperfine splittings. It will be shown in a later section that, where the usual quadrupole theory has been inadequate, discrepancies arise as a consequence of torsional (+ ↔ -) rather than rotational near degeneracy.

Accurate fitting and prediction of hypothetical line centres has been accomplished using a computer program written by L. Halonen and P.H. Turner (see Appendix 7). This program sets up a Hamiltonian in Pickett's Reduced Axis System[27] (RAS) and includes centrifugal distortion in Watson's A-reduction[38]. The Hamiltonian, including quadratic and quartic angular momentum terms, is as follows;

$$H = \begin{bmatrix} H_0 & H_{10} \\ H_{10} & H_1 \end{bmatrix}$$

where 0 refers to the (+) and 1 to the (-) substate and, with V = 0 or 1;

$$H_v = X_v P_x^2 + Y_v P_y^2 + Z_v P_z^2 - \Delta J_v P^4 - \Delta JK_v P^2 P_z^2 - \Delta K_v P_z^4 - \delta J_v [P^2, (P_x^2 - P_y^2)]_+ - \delta K_v [P_z^2, (P_x^2 - P_y^2)]_+ + E_v$$

$$H_{10} = (T_{xz} + T_j P^2)[P_x, P_z]_+ + T_{k1}[P_z^2, [P_x, P_z]_+]_+ + T_{k2}[(P_x^2 - P_y^2), [P_x, P_z]_+]_+$$

where $[A,B]_+ = AB + BA$

Only y axis coupling is included so that representation II^r (X = C, Y = A, Z = B) is fixed for this application. In practice, E_0 is set to zero so that $E_1 = \Delta E_{\mp}$, the zero-point energy difference between the 0_+ and 0_- torsional substates.

The philosophy underlying the derivation of this Hamiltonian is that, for a molecule with a single aperiodic tunnelling co-ordinate, there is a choice of inertial axis system which will eliminate the vibration-rotation (Coriolis) interaction[27]. Assuming that the chosen axes pass through the centre of mass of the molecule and that electronic angular momentum can be neglected, the classical Hamiltonian for such a molecule becomes;

$$H = \underbrace{\frac{1}{2}\tilde{\omega}I\omega}_{H_{rot}} + \underbrace{\frac{1}{2}\frac{\partial\alpha}{\partial t}[\tilde{\omega}X + \tilde{X}\omega]}_{H_{vib\text{-}rot}} + \underbrace{\frac{1}{2}Y\left(\frac{\partial\alpha}{\partial t}\right)^2 + V(\alpha)}_{H_{vib}}$$

the vector X is defined by

$$X_g = \sum_{i=1}^{n} M_i g_i \frac{\partial g_i}{\partial \alpha}$$

g = a,b,c
n = number of atoms

the vector Y is defined by

$$Y_g = \sum_{i=1}^{n} M_i \left(\frac{\partial g_i}{\partial \alpha}\right)^2$$

Since, for the present, the interest is only in describing the microwave spectrum, H_{vib} may be dropped (provided that $\Delta E_{\pm}$ is introduced into the quantum mechanical Hamiltonian). The problem which remains is then to define an axis system such that the elements of X are all zero. This is equivalent to choosing the Eckart axis system (EAS) for the internal motion[39,40] (but the RAS is not necessarily the same as the EAS in the general case discussed by Pickett[27]). The consequence of eliminating $H_{vib\text{-}rot}$ in this way is that the instantaneous inertial tensor I may no longer be assumed to be diagonal. The resulting quantum mechanical Hamiltonian must therefore, in principle, include three product of inertia terms. A further simplification is however possible if a hybrid axis system can be chosen so as to exploit the desirable properties of both the Principal and the Eckart axis systems. This axis system (following Pickett) will be referred to (unrigorously) as the RAS.

For partially deuterated nitrosomethanes and acetaldehydes (near-prolate rotors), the only important torsion-rotation interactions occur through prolate type near degeneracies, therefore, although b and c axis coupling

occurs, only a axis coupling is important. The RAS is therefore chosen with its a-axis identical to the a principal axis, the principal axis system (PAS) and the RAS are then related by a rotation about the a-axis which minimises the Coriolis coupling. The resulting Hamiltonian has only one product of inertia term (identify $T_{bc} = \langle I_{bc}^{-1} \rangle$) and the residual coupling is folded into the state effective rotational constants.

The major approximation involved in using the RAS Hamiltonian as defined, lies in the assumption that the tunnelling co-ordinate is aperiodic. This is equivalent to saying that tunnelling gauche $\leftrightarrow$ gauche is much more important than tunnelling gauche $\leftrightarrow$ cis and is a good approximation except where there occur appropriate accidental $0_0 \leftrightarrow 0_{\pm}$ degeneracies. Descriptive failures of the Hamiltonian can therefore be associated with the sought after cis-gauche interactions.

Transformation of Parameters PAS $\leftrightarrow$ RAS

For hindered internal rotors, (+) and (-) state probability densities are only appreciably large in the regions of the gauche potential minima[20] (see Figure 5). Structural estimates of the PAS rotational constants can therefore be made in the usual way, on the assumption that the effective rotational constants for the gauche form are the averages of the effective rotational constants for molecules in the (+) and (-) states.

An algorithm for locating the Eckart axis system for large displacements of internal co-ordinates has been given by Pickett and Strauss[41]. This provides a method for estimating I^{-1} for this axis system if the structure of the molecule in its transition state (the trans form) is assumed. This in turn provides a means for estimating the necessary rotation PAS $\rightarrow$ RAS and hence T_{bc}.

Wavefunctions for the CXY_2 Internal Rotor.

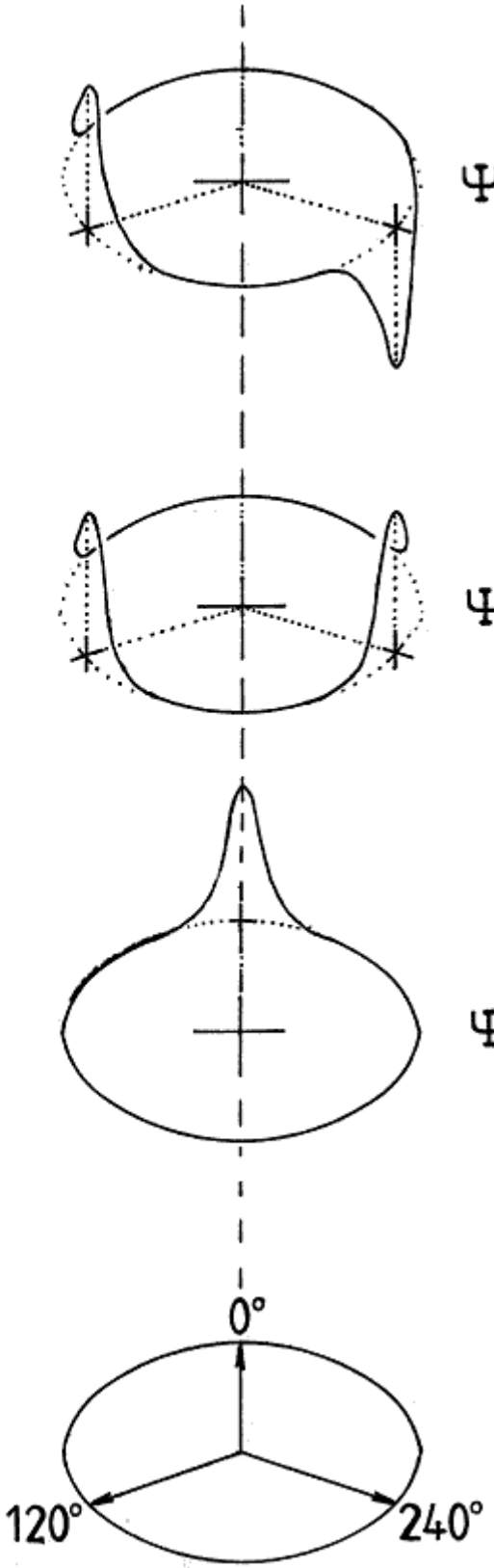

Figure 5

The inverse of the instantaneous inertial tensor in the RAS has the form;

$$I^{-1} = \begin{bmatrix} A_r & 0 & 0 \\ 0 & B_r & T_{bc} \\ 0 & T_{bc} & C_r \end{bmatrix}$$

hence;

$$A_p = A_r = A$$

$$B_p = \frac{(B_r + C_r)}{2} + \frac{1}{2}\sqrt{(B_r - C_r)^2 + 4T_{bc}^2}$$

$$C_p = \frac{(B_r + C_r)}{2} - \frac{1}{2}\sqrt{(B_r - C_r)^2 + 4T_{bc}^2}$$

where;

$$A = \frac{1}{2}(A_+ + A_-) = \frac{1}{2}(A_0 + A_1)$$

$$B_p = \frac{1}{2}(B_+ + B_-) \neq B_r = \frac{1}{2}(B_0 + B_1)$$

etc.

Subscripts r and p refer to RAS and PAS constants. The angle of rotation θ required to bring the RAS into the PAS is defined by

$$\left|\text{Tan } 2\theta\right| = \frac{2T_{bc}}{(B_r - C_r)}$$

also;

$$\left|\text{Sin } 2\theta\right| = \frac{2T_{bc}}{\sqrt{(B_r - C_r)^2 + 4T_{bc}^2}}$$

$$\text{Cos } 2\theta = \frac{(B_r - C_r)}{\sqrt{(B_r - C_r)^2 + 4T_{bc}^2}}$$

A complete set of parameters for the PAS Hamiltonian may be transformed into a complete set of parameters for the RAS Hamiltonian (and vice versa) from a knowledge of the matrix elements in each case. Matrix elements may be evaluated using Wang basis functions[42] and the usual four way factorisation of each J block results. The Wang block appropriate to a particular energy level is given by the parities of J, K_a and K_c + v (see Table 1).

Off-diagonal elements connecting states of the same parity but different v are as follows[27];

$\langle K^{\pm} | P_a | K^{\mp} \rangle = K$

$\langle 1^{\pm} | P_b P_c + P_c P_b | 1^{\mp} \rangle = \pm \frac{1}{2} J(J+1)$

The transformation can then be obtained by equating the analytical forms of the eigenvalues for the two different Hamiltonians. Only quadratic angular momentum terms are considered here, giving the following;

Equating the 1_{01} levels;

$$B_+ + C_+ = B_0 + C_0$$

$$B_- + C_- = B_1 + C_1$$

Equating the J = 1,2 K_a = 1 levels;

$$\left[J\,\frac{(J+1)}{2}\,\mathfrak{Z}_p \pm 2\delta_p \right]^2 + 4Q_a^2 = \left[J\frac{(J+1)}{2}\mathfrak{Z}_r \pm 2\delta_r \right]^2 + 4\left[J\frac{(J+1)}{2}\,T_{bc} \right]^2$$

upper or lower signs taken together.

Where

$$\mathfrak{Z}_p = B_p - C_p$$

$$\mathfrak{Z}_r = B_r - C_r$$

$$2\delta_p = \Delta E^{-}_{+} + \Delta A_p + \tfrac{1}{2}(\Delta B_p + \Delta C_p)$$

$$2\delta_r = \Delta E^{-}_{+} + \Delta A_r + \tfrac{1}{2}(\Delta B_r + \Delta C_r)$$

$$\Delta A_p = A_- - A_+$$

$$\Delta A_r = A_1 - A_0$$

$$\Delta B_r = B_1 - B_0 \quad \text{etc.}$$

Also, from the matrix diagonal sum (trace) rule;

$$\Delta B_p + \Delta C_p = \Delta B_r + \Delta C_r$$

Hence;

$$\mathfrak{Z}_p \delta_p = \mathfrak{Z}_r \delta_r$$

$$T_{bc} = \tfrac{1}{2}\sqrt{\mathfrak{Z}_p^2 - \mathfrak{Z}_r^2}$$

$$Q_a = \sqrt{\delta_r^2 - \delta_p^2}$$

Hence;

$$\mathfrak{Z}_p = \sqrt{4T_{bc}^2 + \mathfrak{Z}_r^2}$$

$$\delta_p = \frac{\mathfrak{Z}_r \ \delta_r}{\sqrt{4T_{bc}^2 + \mathfrak{Z}_r^2}}$$

$$Q_a = \frac{2\delta_r \ T_{bc}}{\sqrt{4T_{bc}^2 + \mathfrak{Z}_r^2}}$$

$$\Delta A_p = 2\delta_p - \Delta E_{\mp} - \tfrac{1}{2}(\Delta B_r + \Delta C_r)$$

$$A_- = A + \tfrac{1}{2}\,\Delta A_p$$

$$A_+ = A - \tfrac{1}{2}\,\Delta A_p \qquad \text{etc.}$$

TABLE 1

Wang Block Identification

K Parity		Sub block	
K_a	K_c for O_0 and O_+ $K_c + 1$ for O_-	Jeven	Jodd
Even	Even	E^+	E^-
Even	Odd	E^-	E^+
Odd	Even	O^+	O^-
Odd	Odd	O^-	O^+

MICROWAVE SPECTRUM AND ASSIGNMENT

Microwave spectra were studied in the range 7.9 - 42 GHz using klystron and BWO sources and a 3m X-band Stark cell (see Appendix 1). The parent species, CH_3NO, is a light, near-prolate rotor ($\kappa = -0.95$) with $\mu_a = 2.3D$ and $\mu_b = 0.5D$. The deuterium analogues are similar and spectra of all species are dominated by μ_a, Q-branch transitions. For the gauche-forms of CH_2DNO and CHD_2NO, μ_a Q-branch lines appear in pairs, usually situated within a few tens of MHz of each other and having the same intensities, Stark effects and hyperfine patterns. The μ_b lines, mainly R-branches, are somewhat weaker and more scattered by the effects of ro-torsional mixing. Despite the symmetry relaxation, the only μ_c lines observed in the gauche-form spectra were weak intersystem ($0_+ \leftrightarrow 0_-$) transitions arising as a result of intensity borrowing from the corresponding μ_b transition.

Gauche CH_2DNO

The (+) and (-) $1_{01} - 0_{00}$ transitions and the series $5_{14} - 5_{15}$ through to $8_{17} - 8_{18}$ had already been assigned[14] and measured[16,43]. The (PAS) rotational constants $B_p + C_p$ and $B_p - C_p$ were therefore known to reasonable accuracy. An estimate for the A rotational constant was made by substituting deuterium into the published CH_3NO structure[17]. The quadrupole coupling constants were estimated by taking a 2 : 1 weighted average of their values for CH_3NO and CD_3NO.

Work on the spectrum of gauche-CH_2DNO commenced with the measurement of the $2_{02} - 1_{01}$ transitions and the $9_{18} - 9_{19}$ transitions. The latter were located by extrapolating a plot of $\nu_{obs}/J(J+1)$ vs $J(J+1)$ for the already known members of the $K_a = 1$ Q-branch series. The $9_{18} - 9_{19}$ (+) transition turned out to be perturbed by a cis-gauche interaction (see later), but the quadrupole hyperfine structure agreed with calculation.

The $K_a = 1$ R-branch transitions were assigned next. The rigid rotor frequencies of the $2_{11} - 1_{10}$ (3B + C) and the $2_{12} - 1_{11}$ (B + 3C) were

estimated from the known rotational constants, but the observed transitions deviate strongly from this approximation. The least perturbed transitions were the $2_{12} - 1_{11}$ (+) and $2_{11} - 1_{10}$ (-) falling respectively 31 MHz above and below prediction and having Stark effects and quadrupole patterns similar to their rigid rotor counterparts. The $2_{12} - 1_{11}$ (-) and $2_{11} - 1_{10}$ (+) transitions were found to be 174 MHz above and below prediction with heavily perturbed quadrupole patterns (see later) and anomalous Stark effects. Due to an avoided crossing of M states, the $M_J = 1$ Stark lobes for these transitions were observed to turn around and proceed back towards the zero field line as the modulating voltage was increased. This peculiar behaviour, seen also in the mono-deutero species of acetaldehyde[44] and propylene[37], was rationalised on the basis of a near degeneracy between the 1_{10} (+) and 1_{11} (-) substates (see figure 6). Sufficient data were then available to solve for Q_a and for the (+) $\leftrightarrow$ (-) energy difference between the mid points of the $K_a = 1$ asymmetry doublets (2δ in the notation of ref. 37). This led to the prediction and assignment of two strong intersystem transitions; the 2_{11} (+) - 1_{11} (-) and the 2_{12} (-) - 1_{10} (+) (see Figure 6). A search was also made for the 2_{12} (+) - 1_{10} (-) transition but this proved to be too weak to be measured accurately.

Still without knowledge of the A rotational constants, the μ_a Q-branch $K_a = 2$ and $K_a = 3$ transitions were assigned. It was hoped that the small A dependence of these lines would be of some use. By this time also, the RAS Hamiltonian least-squares fitting program had been set up on the Bristol computer. The fit obtained (excluding the $9_{18} - 9_{19}$ (+)) was admirable, estimating the standard deviation of an observation to be ~0.1 MHz, but the A constants obtained were not accurate, being strongly correlated with the corresponding ΔK.

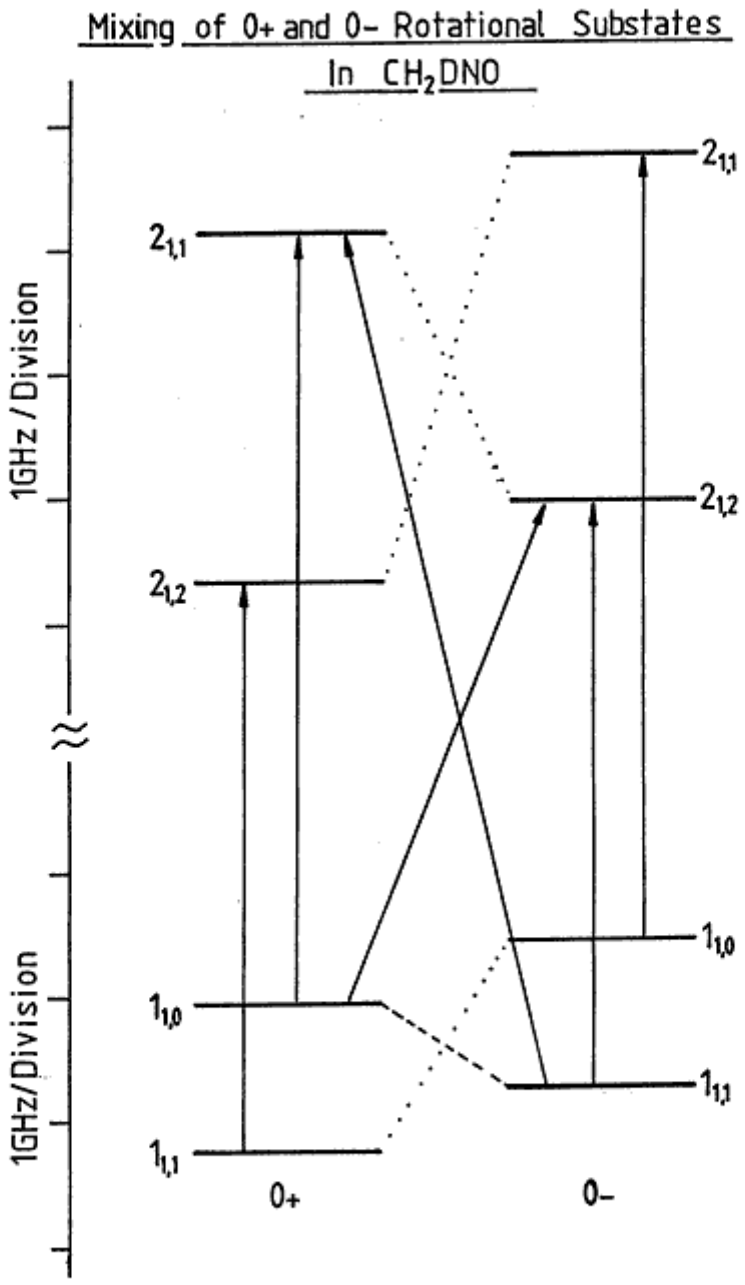

Figure 6

Solid arrows are observed transitions.

Broken lines indicate interactions through Q_a.

The 1_{10} (+) $\leftrightarrow$ 1_{11} (-) connection is particularly strong.

The determination of the A constants was eventually accomplished by assigning the μ_b $4_{04} - 3_{13}$ and $3_{03} - 2_{12}$ transitions. The $4_{04} - 3_{13}(-)$ transition was found by means of a BWO and Klystron search and confirmed via the $3_{03} - 2_{12}$ (-) transition. The $3_{03} - 2_{12}$ (+) transition, similar in appearance to its (-) counterpart, was found by a Klystron search and confirmed through the partially obscured $4_{04} - 3_{13}$ (+). Predictions based on the fitting of these data then led to the location of high J high K_a transitions necessary for the determination of the centrifugal distortion constants.

The data, fitted to the RAS Hamiltonian, are given at the end of the chapter. A few perturbed transitions, excluded from the fit, are discussed later under cis-gauche interactions. Determined constants are given in Table 2.

Gauche CHD_2NO

The (+) and (-) $1_{01} - 0_{00}$ transitions and the series $4_{13} - 4_{14}$ through to $8_{17} - 8_{18}$ had already been measured[16] giving B_p and C_p to reasonable accuracy. A and the quadrupole coupling constants were estimated as before. The data were then fitted directly to the RAS Hamiltonian.

The $2_{02} - 1_{01}$ transitions and $K_a = 2$ Q-branches attributable to gauche CHD_2NO were noticed during the course of the work on the monodeutero species. The $2_{12} - 1_{11}$ and the $2_{11} - 1_{10}$ transitions were found close to their rigid rotor frequencies, with quadrupole patterns for the (+) and (-) transitions overlapping in each case. The A rotational constants were determined from the μ_b $1_{10} - 1_{01}$ transitions. These assignments were immediately confirmed by prediction of the $2_{11} - 2_{02}$ transitions using the relationship

$(2_{11} - 1_{10}) + (1_{10} - 1_{01}) = (2_{11} - 2_{02}) + (2_{02} - 1_{01})$.

Determining $\Delta E_{\overline{+}}$ and extending the data set to high J proved to be more difficult. A period of extensive searching for (+) $\leftrightarrow$ (-) intersystem transitions produced no result and so further pure-rotational transitions

TABLE 2

Gauche-CH_2DNO Rotational Constants.

		RAS			PAS
$\Delta E_{\pm}$	/MHz	922.01	(19)		
T_{bc}	/MHz	306.31	(4)	Q_a /MHz	313.23 (9)
T_j	/KHz	2.37	(80)		
T_{k1}	/Hz	-0.058	(10)		
T_{k2}	/Hz	186	(20)		
A_0	/MHz	56 038.72	(9)	A_+ /MHz	56 161.80
B_0		10 439.57	(4)	B_+	10 560.81
C_0		9 780.72	(4)	C_+	9 659.69
A_1		56 037.84	(10)	A_-	55 914.78
B_1		10 437.55	(4)	B_-	10 558.81
C_1		9 781.04	(4)	C_-	9 660.02
ΔJ_0	/KHz	443.8	(1.4)		
ΔJK_0		-1 222	(8)		
ΔK_0		794	(7)		
δJ_0		-218.5	(9)		
δK_0		391	(3)		
ΔJ_1		451.1	(1.9)		
ΔJK_1		-1 232	(9)		
ΔK_1		796	(8)		
δJ_1		-222.0	(1.1)		
δK_1		392	(4)		

70 Transitions.

Standard deviation of fit 0.149 MHz

were measured in an attempt to uncorrelate ΔE^{-}_{+} from other parameters. This led to assignment and fitting problems. K_a = 2, 3 and 4 Q-branch transitions came in close spaced (+), (-) doublets of identical appearance and it was not clear which were (+) and which were (-). Various combinations were tried and all resulted in a poor fit. Similarly, high K_a R-branches could be located but did not fit well and could not be assigned unambiguously to (+) or (-). For some time, this gave rise to the view that the $0_0 \leftrightarrow 0_{\pm}$ energy difference might be small, thereby spoiling the RAS fit. This view was apparently corroborated by the relatively poor fit of the cis-CHD_2NO spectrum to the Watson Hamiltonian (see data section).

All fitting difficulties were eventually resolved by means of an RF pumping experiment (see Figure 7). Earlier attempts to pump the $2_{11}(-) - 2_{11}(+)$ energy difference whilst observing the $2_{11} - 1_{10}$ transitions had failed due to operational problems, but repeating the experiment whilst observing the $2_{11} - 2_{02}$ transitions led to an observable resonance at ~88 MHz in both cases. ΔE^{-}_{+} was then directly calculable from sum rules and its value was immediately confirmed by assignment of the weak μ_c intersystem transitions; $5_{15}(+) - 5_{05}(-)$, $5_{15}(-) - 5_{05}(+)$, $6_{16}(+) - 6_{06}(-)$ and $6_{16}(-) - 6_{06}(+)$. These new data made it immediately obvious that a number of cis-gauche perturbed transitions (see later) had been included in the earlier fit, distorting the parameter set. When these observations were excluded, all (+), (-) ambiguities disappeared and the assignment was rapidly completed.

Determined constants for gauche-CHD_2NO are given in Table 3. The final fit to the data is given at the end of the chapter.

CHD_2NO. Determination of $\Delta E_{\mp}$ by RF-Microwave Double Resonance.

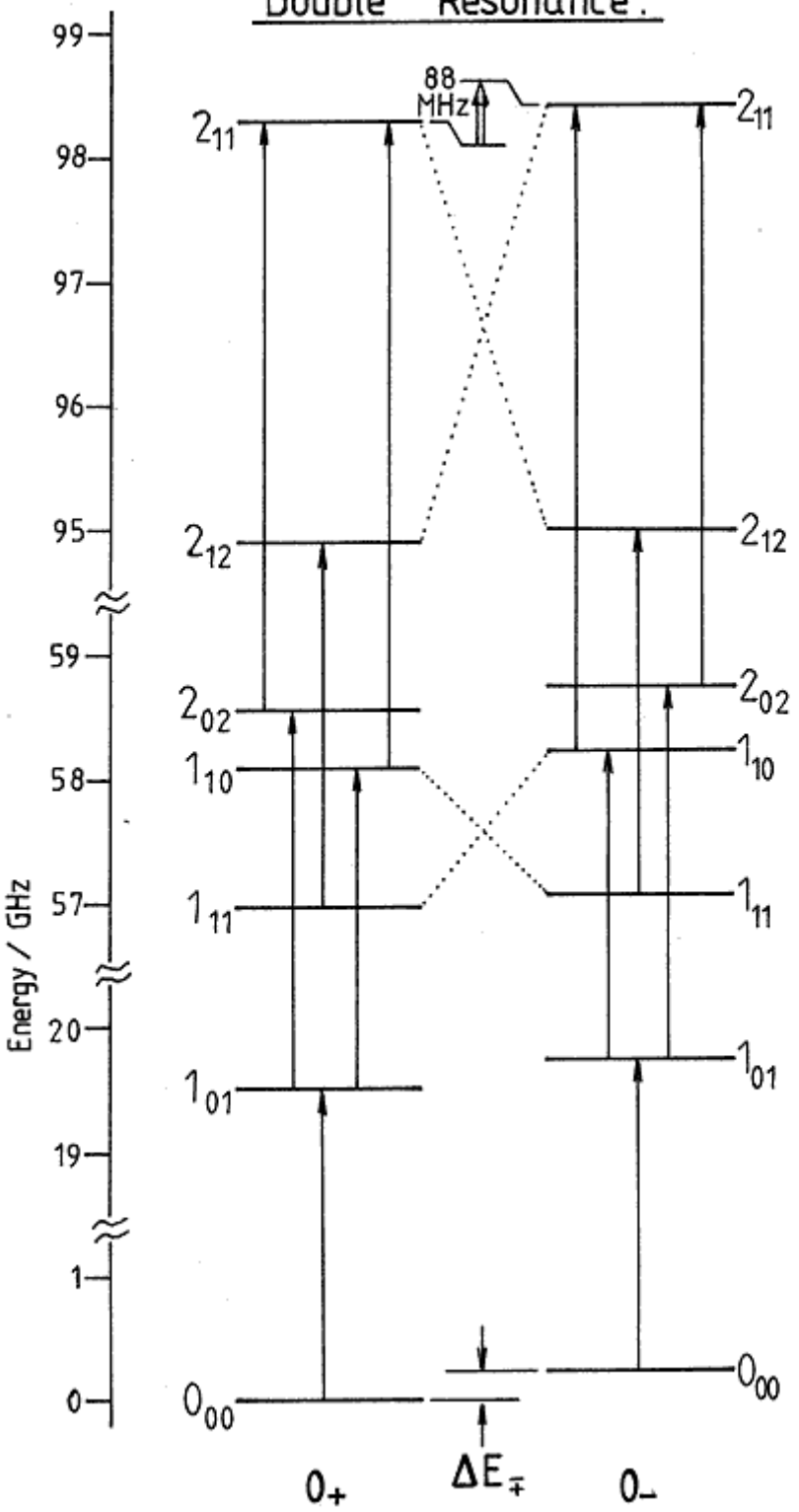

Figure 7

TABLE 3

Gauche-CHD_2NO Rotational Constants

	RAS		PAS	
ΔE^{-}_{+} /MHz	190.16 (14)			
T_{bc} /MHz	497.61 (10)	Q_a /MHz	83.44	(7)
T_j /MHz	3.9 (1.1)			
T_{k1} /Hz	-0.11 (5)			
T_{k2} /Hz	819 (163)			
A_0 /MHz	47 721.83 (4)	A_+ /MHz	47 771.55	
B_0	10 038.48 (18)	B_+	10 335.36	
C_0	9 499.67 (18)	C_+	9 202.96	
A_1	47 722.02 (4)	A_-	47 672.34	
B_1	10 037.28 (18)	B_-	10 334.15	
C_1	9 499.71 (18)	C_-	9 203.00	
ΔJ_0 /KHz	227.9 (1.3)			
ΔJK_0	-597 (4)			
ΔK_0	393 (2)			
δJ_0	-115.3 (5)			
δK_0	191.9 (1.0)			
ΔJ_1 /KHz	228.3 (1.0)			
ΔJK_1	-598 (4)			
ΔK_1	392 (2)			
δJ_1	-115.4 (6)			
δK_1	192.4 (1.0)			

72 Transitions

Standard deviation of fit = 0.106 MHz

NITROGEN-14 QUADRUPOLE COUPLING

Most of the microwave transitions of CH_2DNO and CHD_2NO show hyperfine structure due to ^{14}N (I = 1) quadrupole coupling and most of the quadrupole patterns can be fitted with the usual first order theory[45]. However, for the gauche species, certain patterns refuse to fit this scheme. This problem arises because the rigid-rotor wavefunctions implied by the usual treatment are not good state descriptions in the event of strong ro-torsional mixing. This is particularly true of transitions involving the highly perturbed $1_{10}(+)$ and $1_{11}(-)$ substates in CH_2DNO. Here the hyperfine components fall in a different order to that predicted by the rigid approximation, making it difficult to assign F quantum numbers or to determine hypothetical centres in this case, unless (+) ⇔ (-) mixing is taken into account.

Quadrupole Coupling Theory

Although internal angular momentum affects the mass distribution in the molecule, it does not physically couple with the overall angular momentum. In effect, internal rotation modulates the overall rotation velocity in such a way as to leave the total angular momentum unaffected. J is therefore a good quantum number in the first-order quadrupole coupling limit, so that only the coupling between $\underset{\sim}{J}$ and $\underset{\sim}{I}$ needs to be considered in calculating the quadrupole energy. The quadrupole energy expression therefore retains its usual form[42] in terms of q_J;

$$E_q = eQq_J \left[\frac{\frac{3}{4}C\,(C+1) - J\,(J+1)\,I\,(I+1)}{2J\,(2J-1)\,I\,(2I-1)} \right]$$

where $C = F(F+1) - J(J+1) - I(I+1)$

and $q_J = \left\langle \frac{\partial^2 V}{\partial Z^2} \right\rangle_{M_J = J}$ Z = space fixed axis

The effect of internal rotation arises in the evaluation of q_J. Although J is unaffected by internal motions, the expectation value of $\partial^2 V/\partial Z^2$ must now

be taken as the average over the torsion-rotation wavefunction. Hence;

$$q_J = \langle J,\tau,V,\ M_J = J \left| \frac{\partial^2 V}{\partial Z^2} \right| J,\tau,V,\ M_J = J\rangle.$$

Appropriate torsion-rotation wavefunctions can be constructed as linear combinations of rigid rotor basis functions. In the case of a two-fold near degeneracy this gives $\psi_{J\tau V} = C_1\ \psi_{J\tau} + C_2\ \psi_{J\tau'}$

where the C_n are eigenvector elements.

Hence;

$$q_J = C_1^{\,2}\ \langle J,\tau \left| \frac{\partial^2 V}{\partial Z^2} \right| J,\tau\rangle + C_2^{\,2}\langle J,\tau' \left| \frac{\partial^2 V}{\partial Z^2} \right| J,\tau'\rangle$$

$M_J = J$ throughout.

Each of the brackets in the above expression are amenable to the Bragg - Golden[45] treatment, so that the quadrupole energy expression, in first order, becomes;

$$E_Q = \frac{2Y\ (I,J,F)}{J(J+1)} \left[\left(C_1^2 \sum_g \chi_{gg} \langle J,\tau \left| P_g^{\,2} \right| J,\tau\rangle\right) + \left(C_2^{\,2} \sum_g \chi_{gg} \langle J,\tau' \left| P_g^2 \right| J,\tau'\rangle\right) \right]$$

$g = a, b, c$

where Y (I,J,F) is Casimir's function[42] and $\chi_{gg} = eQ\ \partial^2 V/\partial g^2$ expressed in the molecule PAS.

For practical evaluation of C_1 and C_2, all that is required is a knowledge of the energy difference between the unperturbed states and the overlap integral connecting them.[37]

Consider, for example, the $1_{10}(+)$ and $1_{11}(-)$ substates in CH_2DNO.

$$E_+^{(0)} = E^{(0)}(1_{10}^{(+)}) = A_+ + B_+$$

$$E_-^{(0)} = E^{(0)}(1_{11}^{(-)}) = A_- + C_- + \Delta E_{\pm}$$

$$\langle 1_{10}^{(+)} \left| Q_a\ P_a \right| 1_{11}^{(-)}\rangle = Q_a$$

hence

$$T^{-1} \begin{bmatrix} E_+^{(0)} & Q_a \\ Q_a & E_-^{(0)} \end{bmatrix} T = \begin{bmatrix} E_+^{(1)} & 0 \\ 0 & E_-^{(1)} \end{bmatrix}$$

Where $T = \begin{bmatrix} \cos\phi & -\sin\phi \\ \sin\phi & \cos\phi \end{bmatrix}$

and $\text{Tan } 2\phi = 2Q_a / (E_+^{(0)} - E_-^{(0)})$

the columns of T are the eigenvectors, hence;

$$E_Q\,(1_{10}^{(+)}) = Y\,[\cos^2\phi \sum \chi_{gg} \langle 1_{10} \mid P_g^2 \mid 1_{10} \rangle + \sin^2\phi \sum \chi_{gg} \langle 1_{11} \mid P_g^2 \mid 1_{11} \rangle]$$

$$E_Q\,(1_{11}^{(-)}) = Y\,[\cos^2\phi \sum \chi_{gg} \langle 1_{11} \mid P_g^2 \mid 1_{11} \rangle + \sin^2\phi \sum \chi_{gg} \langle 1_{10} \mid P_g^2 \mid 1_{10} \rangle]$$

which simplifies to;

$$E_Q\,(1_{10}^{(+)}) = Y\,[-\chi_{cc}\cos^2\phi \quad -\chi_{bb}\sin^2\phi\,]$$

$$E_Q\,(1_{11}^{(-)}) = Y\,[-\chi_{bb}\cos^2\phi \quad -\chi_{cc}\sin^2\phi\,]$$

Quadrupole Coupling Constants

Principal axis quadrupole coupling constants for gauche-CH_2DNO and gauche-CHD_2NO were determined by least-squares fitting, using the computer program described in Appendix 4. The program essentially makes use of spectroscopic line splittings and frequency derivatives of energy levels with respect to rotational constants, but expects its input data to be unperturbed by the effects of internal rotation. The data input to the program were therefore corrected, where necessary, using the theory outlined in the previous section. Energy denominators $(E_2^{(0)} - E_1^{(0)})$ required for the correction were obtained from unperturbed energy levels calculated using the PAS rotational constants. These constants, used also in calculating derivatives $(\partial E/\partial G,\ G = A,B,C)$, were obtained by transforming the RAS rotational constants (see Tables 2 and 3).

Details of the quadrupole data fitting and internal rotation corrections are given in the data section. Corrections were generally small or unnecessary, the $J = 1 \rightarrow 2$ transitions of gauche-CH_2DNO were not used in the fit because these are used in a test (next section) of the quadrupole-coupling/internal-rotation theory previously outlined. Determined quadrupole coupling constants are given in Table 4.

TABLE 4

Principal axis Quadrupole Coupling Constants /MHz

Species	χ_{aa}	χ_{bb}	χ_{cc}	$\chi_{bb} - \chi_{cc}$
Gauche CH_2DNO	0.45(26)	-5.97(13)	5.52(13)	-11.485(21)
Gauche CHD_2NO	0.78(6)	-6.09(3)	5.31 (3)	-11.393(15)

Perturbed Quadrupole Patterns

As mentioned earlier, the $J = 1 \rightarrow 2$, $K_a = 1$ quadrupole patterns of gauche CH_2DNO deviate considerably from those predicted by the rigid-rotor approximation. This is due maintly to an accidental near degeneracy (see Figure 6) of the $1_{10}(+)$ and $1_{11}(-)$ rotational substates. Calculation of the quadrupole patterns using the torsion-rotation wavefunctions described earlier, however, gives a perfectly satisfactory agreement with experiment.

Hypothetical line centres for the six $J = 1 \rightarrow 2$ transitions observed were obtained by least-squares fitting to the calculated pattern. Residuals, given in Table 5, are within experimental error except where identifiable experimental difficulties exist (see table). Figure 8 illustrates the difference between the quadrupole patterns, for the four most perturbed transitions, before and after introduction of the internal rotation perturbation. The spectra shown are actual oscilloscope traces recorded using the Sweep adapter described in Appendix 3. It should be noted however that the Stark modulation voltages given were chosen in an attempt to simultaneously present all of the hyperfine components, and do not necessarily correspond to the conditions used for the actual frequency measurements.

TABLE 5

CH_2DNO J = 1 → J = 2 K_a = 1 R Branches

Transition	F' - F	ν_{obs}/MHz	Fitting Weight	Obs-Calc./MHz	Comments
$2^+_{11} - 1^+_{10}$	2 - 2	41168.88	1	-0.043	
	2 - 1	41168.48	2	-0.027	
41167.40	3 - 2 } 1 - 0 }	41167.06	4	+0.038	
	1 - 1	41165.48	1	-0.059	
$2^-_{12} - 1^+_{10}$	1 - 0	39047.64	1	+0.113	(a)
	1 - 1	Shoulder on 3 - 2	0		
39045.38	3 - 2	39045.83	4	-0.004	
	2 - 2	39044.05	1	-0.104 }	(b)
	2 - 1	39043.65	2	+0.002 }	
$2^-_{12} - 1^-_{11}$	1 - 1	39713.40	1	+0.064	
	3 - 2 }				
39711.48	1 - 9 }	39711.68	4	-0.044	
	2 - 1	39710.79	2	+0.068	
	2 - 2	39710.03	1	-0.027	
$2^+_{11} - 1^-_{11}$	2 - 1	41835.60	0	+0.409	(c)
	2 - 2	41834.78	0	+0.253	(d)
	3 - 2 }				
41833.20	1 - 1 }	41832.62	4	-0.005	
	1 - 0	41830.67	1	+0.019	
$2^+_{12} - 1^+_{11}$	1 - 1	39572.67	1	-0.024	
	3 - 2 }				
39569.95	2 - 1 }	39570.05	6	+0.016	
	1 - 0 }				
	2 - 2 }	39568.38	2	-0.038	
$2^-_{11} - 1^-_{10}$	2 - 2	41305.96	1	-0.095	
	1 - 0	41305.27	1	+0.123	(e)
	2 - 1	41304.54	2	+0.008	
	3 - 2	41304.14	4	-0.013	
41304.32	1 - 1	41301.58	1	+0.006	

Comments:

(a) Partially resolved from CHD_2NO $2_{02} - 1_{01}$ on 39048.35

(b) Partially resolved

(c) Interfering line?

(d) Interfering line on 41834.05

(e) Interference from 2 - 2 Stark lobe.

Gauche – CH_2DNO J=1→2 Quadrupole Patterns.

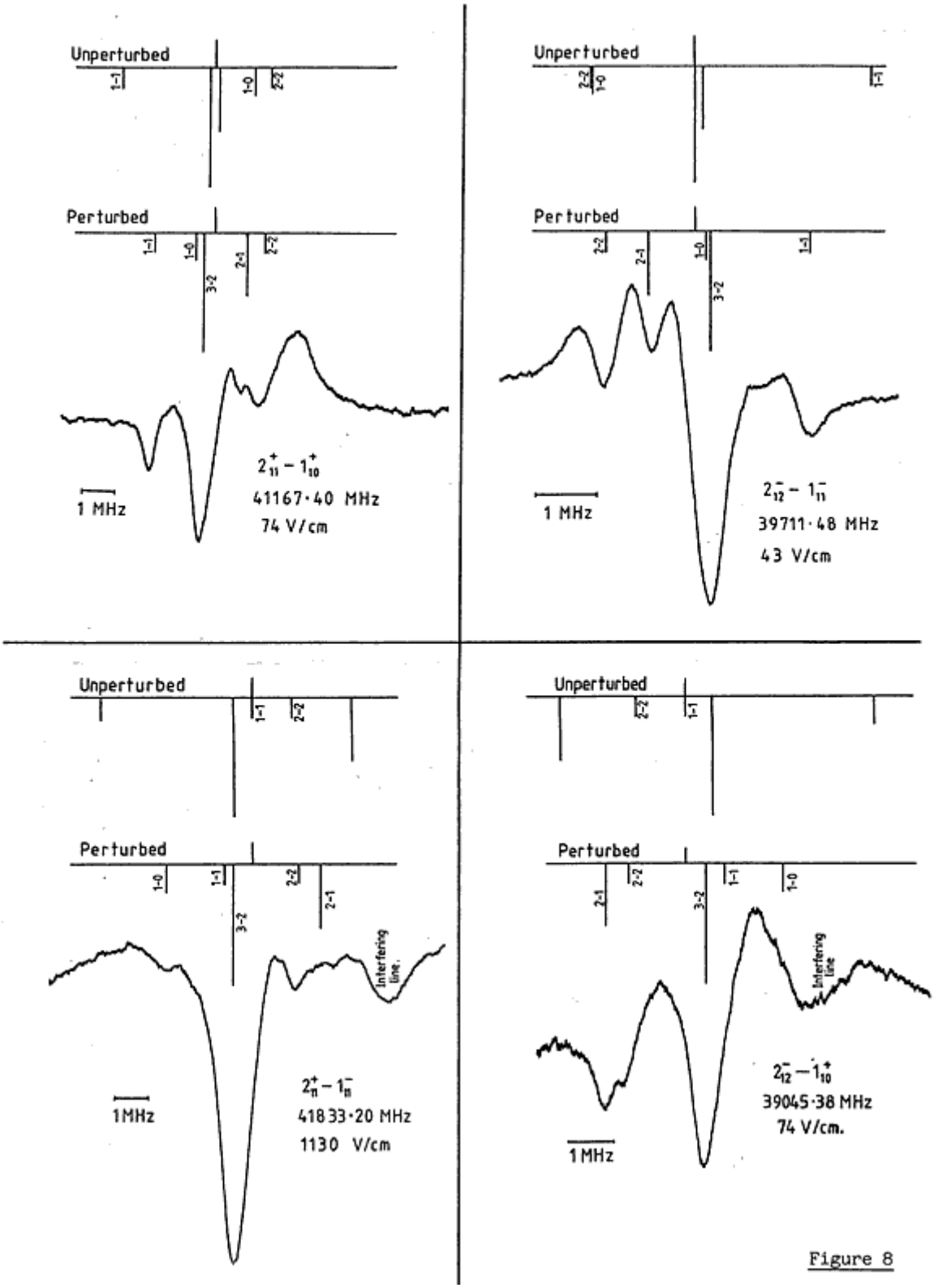

Figure 8

Further Work (Quadrupole Coupling)

It should be possible, in principle, to evaluate quadrupole coupling constants in the RAS or preferably the Eckart axis system (EAS). Then, since the rotation required to bring the EAS into the PAS is known from the off diagonal elements of the EAS inertial tensor, it would be possible, provided that the rotation is large enough, to determine the complete quadrupole tensor. Such an approach is similar to the method used to determine dipole moment orientation from IAM studies[46,47]. Evaluation of the EAS quadrupole coupling constants however requires expressions for the expectation values of the direction cosines of the quadrupole z-axis in the EAS. Such expressions are not yet available at the time of writing.

CIS-GAUCHE INTERACTIONS

For nitrosomethane, in a field-free environment, total angular momentum ($\underset{\sim}{F} = \underset{\sim}{J} + \underset{\sim}{I}$) is the only true constant of the motion. F and M_F are therefore good quantum numbers and the restriction $\Delta F = 0$ applies rigorously to the interaction of all close lying states. The predominant selection rule however, obtained in the first-order quadrupole coupling limit ($\underset{\sim}{J} + \underset{\sim}{I} \rightarrow \underset{\sim}{J}$) will be $\Delta J = 0$. In addition, parity is conserved, so that the restrictions $E^+, O^+ \leftrightarrow E^+, O^+$ and $E^-, O^- \leftrightarrow E^-, O^-$ also apply. (i.e. neglecting quadrupole coupling, the complete cis+gauche Hamiltonian only factors into two blocks.)

In order to determine the cis-gauche zero-point energy difference, it is necessary to overlap the 0_0 and $0_{\pm}$ torsion-rotation energy manifolds in such a way as to account for perturbed transitions on the basis of accidental near degeneracies. Ill-fitting lines however, need not always be due directly to $\Delta J = 0$ cis $\leftrightarrow$ gauche interactions. Possible reasons for poor residuals (obs-calc.) are as follows;

1) Direct, $\Delta J = 0$, cis-gauche Interaction.
   One of the levels involved in the transition lies close to another level of appropriate symmetry.
2) Indirect, $\Delta J = 0$, cis-gauche Interaction.
   A level in the same Wang block as a level involved in the transition lies close to another level of appropriate symmetry.
3) Second Order Quadrupole Interaction.
   $\Delta F = 0$, $\Delta J = \pm 1, \pm 2$ near degeneracy (which may be a cis-gauche interaction) causing shifts in individual hyperfine levels and leading to a poor estimate for the hypothetical line centre.
4) High Order Centrifugal Distortion.
   Descriptive failure of the Hamiltonian, particularly for high J, $\Delta K_a \neq 0$ transitions.

5) b and c axis coupling.

Descriptive failure of the RAS Hamiltonian due to a choice of axis system which does not fully cancel the torsion-rotation interaction.

For the purpose of calculating the rotational energy levels of cis-CH_2DNO and cis-CHD_2NO, the data of reference 17 were fitted to Watson's A-reduction Hamiltonian[38]. The computer program used was the same as that used for the gauche species (Appendix 7), but made to revert to a PAS program by setting all coupling parameters and (-) state parameters to zero. In addition, the cis data sets were expanded (see data section) and the already measured perturbed cis lines were re-checked. Transitions giving poor residuals were, of course, excluded from the fits.

CH_2DNO

Poor residuals for the transitions $15_{5,11} - 16_{4,12}$ and $15_{5,10} - 16_{4,13}$ and for the J = 17, 18 and 19, K_a = 3 series of cis-CH_2DNO were recognised as being due to cis-gauche interactions by Paul Turner[16]. The perturbation of the $15_5 - 16_4$ asymmetry doublet (see Table 6) is consistent with either the 15_5 or the 16_4 levels being pushed together by interaction with a more widely split doublet in the gauche species. An RF pumping experiment performed during the course of this work showed that both of the $15_5 - 16_4$ transitions are resonant at ~18.5 MHz, which is the calculated unperturbed 15_5 splitting. The perturbation therefore definitely occurs at the 16_4 levels.

The lowest J transition, in CH_2DNO, known to have a perturbation large enough to be due to a direct cis-gauche interaction, is the $9_{18}(+) - 9_{19}(+)$ of the gauche species. It follows that; either the $9_{18}(+)$ level (Wang block 0^-) is interacting with one of the nine J = 9 levels in E^- and 0^- in the cis species, or that the $9_{19}(+)$ level (Wang block 0^+) is interacting with one of the ten J = 9 levels in E^+ and 0^+ in the cis species. All of these 2J + 1 possibilities were investigated as follows:

TABLE 6

CH_2DNO Perturbed Transitions

(Abstracted from data section at end of chapter)

Cis Form

Transition	Obs-Calc./MHz	Notes
$^{12}_{2,11} - {}^{11}_{3,8}$	-1.05	(1)
$^{15}_{5,11} - {}^{16}_{4,12}$	31.48	(2)
$^{15}_{5,10} - {}^{16}_{4,13}$	-25.22	(2)
$^{17}_{3,14} - {}^{17}_{3,15}$	-1.06	
$^{18}_{3,15} - {}^{18}_{3,16}$	6.81	
$^{19}_{3,16} - {}^{19}_{3,17}$	17.05	
$^{23}_{4,19} - {}^{23}_{4,20}$	6.53	
$^{24}_{4,20} - {}^{24}_{4,21}$	11.53	
$^{25}_{4,21} - {}^{25}_{4,22}$	19.21	
$^{26}_{4,22} - {}^{26}_{4,23}$	30.61	

Gauche Form

$9^{(+)}_{18} - 9^{(+)}_{19}$	4.49	
$10^{(-)}_{1,10} - 9^{(-)}_{2,7}$	1.87	(3)

Notes

(1) The $^{12}_{2,10} - {}^{12}_{2,11}$ transition is unperturbed, therefore the $^{11}_{3,8}$ level is pushed up by 1.05 MHz.

(2) RF-microwave double resonance experiment (see text) shows the perturbation to occur at the 16_4 levels.

(3) Perturbation due to C axis coupling (see text).

Firstly, three of the cis levels, the 9_{27}, 9_{28} and 9_{19}, were eliminated, since transitions involving them are unperturbed. Secondly the cis 10_{28} - 9_{37} transition was measured, thus eliminating the 9_{37} level. After this, a simple computer program was written to overlap the calculated cis and gauche energy level manifolds. The program added a trial gauche-cis zero-point energy difference (one of the 15 remaining possibilities) on to all of the gauche energy levels, and then printed out the $\Delta J = 0$ near degeneracies of less than 50GHz. This method was used in order to ensure that the final scheme not only accounted for known perturbations, but also did not predict perturbations which were known not to occur. Only one scheme turned out to have the desired properties (see Figure 9), the $9_{18}(+)$ level lying slightly above the $9_{36}(0)$. It was thus established that the zero-point of gauche-CH_2DNO lies 335.7_4 GHz ($11.20\ cm^{-1}$) above that of the cis species.

As might be expected from the discussion earlier, not all of the perturbations encountered in the spectrum of CH_2DNO are attributable to cis-gauche interactions. One case in point is the +1.9 MHz residual of the $10_{1,10}(-)$ - $9_{27}(-)$ transition, which is probably due to c-axis coupling. At low J, the energy levels of the (+) state manifold lie below their (-) state counterparts, but overtake as J increases, eventually giving rise to b and c type (+) $\leftrightarrow$ (-) near degeneracies which are too close to be absorbed by adjustments in the rotational constants. The perturbation in question probably occurs through the connection $10_{1,10}(-) \leftrightarrow 10_{0,10}(+)$ (energy separation 26.83 GHz) arising from the interaction Hamiltonian

$$H_c = Q_c P_c + N_c (P_a P_b + p_b P_a).$$

CH_2DNO Gauche–Cis Interactions. $\Delta E_{g-c} = 11{\cdot}20\ cm^{-1}$

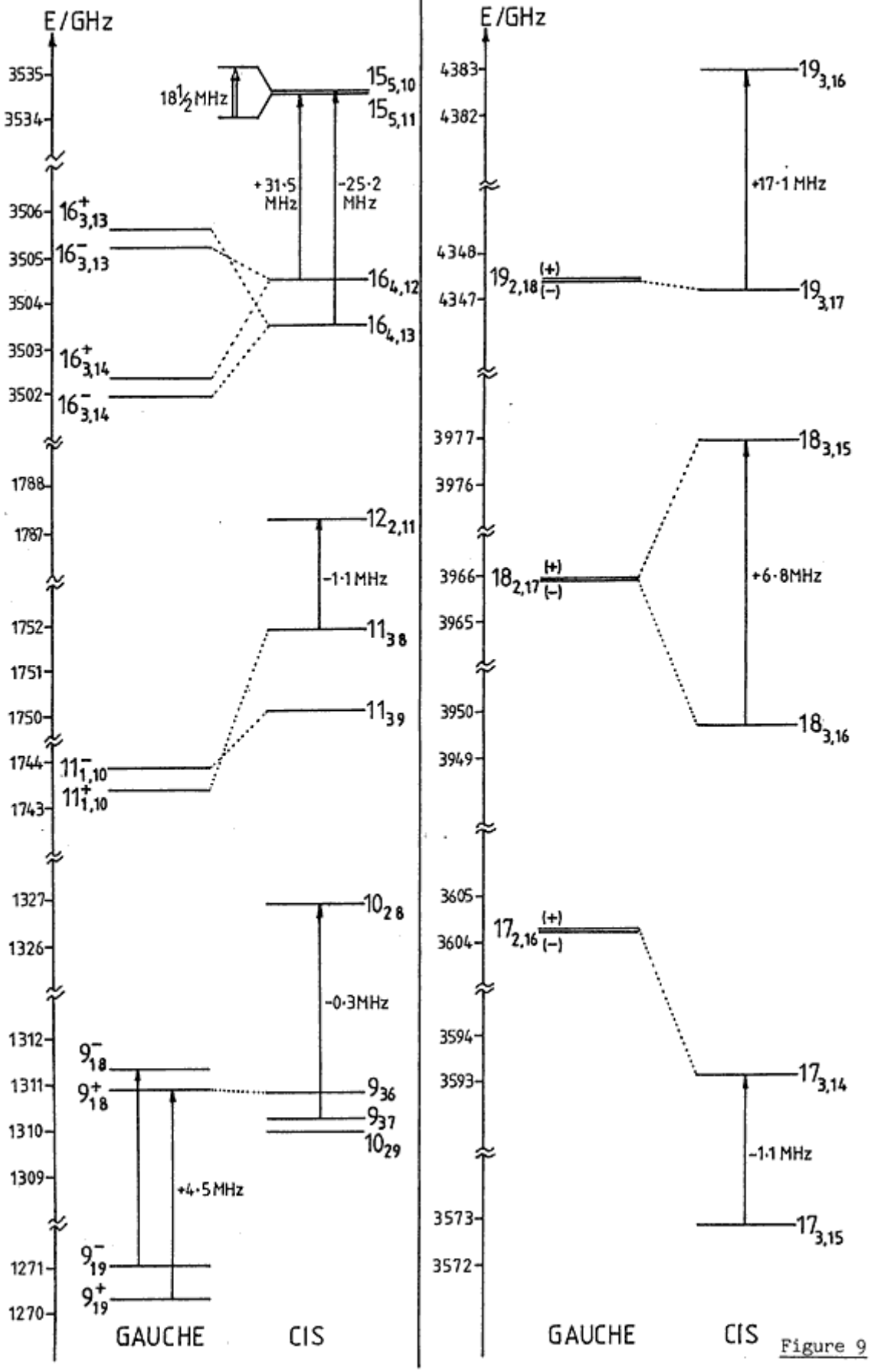

Figure 9

$\underline{CHD_2NO}$

If the potential function $V(\alpha)$ is considered to undergo an incremental change for each successive isotopic substitution at the methyl group (see next section), then the gauche potential minima in CHD_2NO should be expected to be lowered in energy with respect to the cis, by an amount equal to the rise which occurs in CH_2DNO. To a crude first approximation therefore (i.e. neglecting kinetic effects), for CHD_2NO, ΔE_{c-g} (note reversal of subscripts) should be expected to be ~ 11.2 cm^{-1}.

The behaviour of the residuals of the cis and gauche CHD_2NO data sets (see data section) are certainly consistent with the view that the cis zero point energy lies above that of the gauche. The gauche data show an excellent fit up to J=17, whereas the cis data show a generally poor fit. This suggests that the high K_a, $O_{\pm}$ energy levels have become enmeshed with the low K_a, O_o levels in a way which is generally perturbing. Moreover, the $J > 18$, $K_a=3$, Q-branch transitions of the gauche form are perturbed, as are the $J > 18$, $K_a=2$ Q-branch transitions of cis, suggesting that these perturbations may be mutual.

The lowest J transitions in CHD_2NO having perturbations large enough to be due to direct cis-gauche interaction are the cis-8_{17}-8_{18} (-1.38 MHz) and the cis-8_{17}-7_{26} (-1.07 MHz). The 8_{17} level is evidently pushed down by $\sim$1.2 MHz. This again gives rise to 2J+1 possibilities for ΔE_{c-g}, many of which can be eliminated easily. Firstly, the $8_{17}(+)$, $8_{18}(-)$, $8_{27}(+)$ and $8_{26}(-)$ levels have well-fitting observations associated with them. Secondly, to set the cis-8_{17} level adjacent to the gauche J=8, K_a=6,7 or 8 levels makes ΔE_{c-g} so large as to leave no possibilities for perturbing any of the observed gauche levels. Careful computer searching then gave rise to the view that the cis-8_{17} level is best placed slightly below the $8_{36}(-)$ level, giving ΔE_{c-g} = 309.2 GHz (10.31 cm^{-1}).

Although there is little doubt that the proposed zero-point energy separation is correct, the resulting energy level scheme does not give as satisfactory an account of the data as in the monodeutero case. In particular, although the scheme predicts where most of the observed perturbations occur, it does not always account for the observed pattern of residuals. This applies especially to the gauche $J \gtrsim 18$ transitions. For some time, this gave rise to the view that the scheme had failed, and that the origin of the apparent shift of the cis-8_{17} level had some other cause. The possibilities here however are very limited: Both the $8_{17} - 8_{18}$ and $8_{17} - 7_{26}$ have normal quadrupole patterns. The $8_{17} - 8_{18}$ transition is unlikely to exhibit the effects of high-order centrifugal distortion. The possibility that the 8_{18} and 7_{26} levels are both pushed up by identical amounts was also investigated and rejected. Moreover, the $8_{35} - 9_{28}$ has been observed, so that an indirect perturbation via a close degeneracy at 8_{35} is ruled out. All of this leads to the conclusion that the perturbation at 8_{17} is a genuine cis-gauche interaction, which in turn indicates that some of the interaction effects elsewhere in the energy manifold have been absorbed into rotational and centrifugal distortion constants. This is not very surprising, since to eliminate from the fits all of the transitions made suspect on the basis of $\Delta E_{c-g} = 309.2$ GHz, would reduce the data set to a size inadequate for determination of all of the distortion constants. It therefore follows that the high J energy levels calculated for CHD_2NO are not necessarily accurate.

In fact, there is a variety of ways in which the cis and gauche data sets can be fitted. For example, in fitting the gauche-CHD_2NO data, the $^{11}_{29} - ^{10}_{38}(+)$, $^{11}_{2,10} - ^{10}_{37}(+)$ and $^{12}_{2,11} - ^{11}_{38}(+)$ transitions were omitted. These transitions, however, can be fitted at the expense of being unable to fit any of the data above J=17. The rotational and centrifugal distortion constants resulting from this alternative strategy are given in Table 7. They are not grossly different from those in Table 3, but

TABLE 7

Gauche CHD_2NO Rotational Constants (Reduced Axis System) obtained by fitting all data up to J=17

$\Delta E_{\pm}$ /MHz	190.60	(16)
T_{bc} /MHz	497.32	(10)
T_j /KHz	13.8	(1.5)
T_{k1} /Hz	0.5	(1)
T_{k2} /Hz	235	(304)

	v=0	v=1
A/MHz	47721.81 (4)	47722.04 (4)
B	10039.03 (20)	10037.81 (20)
C	9499.15 (20)	9499.16 (20)
Δ_J/KHz	220.5 (1.7)	222.4 (1.2)
Δ_{JK}	-574 (5)	-580 (4)
Δ_K	393 (2)	396 (2)
δ_J	-120.2 (6)	-121.2 (9)
δ_K	195.2 (1.0)	197.2 (1.0)

67 Transitions

Standard deviation of fit 0.096 MHz

illustrate the uncertainties which occur from a somewhat arbitrary choice of data set. The fit given in the data section was in fact chosen because it involves the greatest number of transitions and produces similar distortion constants for both (+) and (-) states.

It is nevertheless apparent, by examination of the (+) ↔ (-) splittings in Table 8, that the K_a=3 Q-branch series of gauche-CHD_2NO is perturbed. This perturbation is predicted to occur when ΔE_{c-g} = 309.2 GHz even if the actual residuals do not obey the pattern expected. Moreover, none of the other trial zero-point separations give rise to a perturbation in this series. The difficulties encountered, therefore, arise as a consequence of making a least-squares data adjustment under unfavourable circumstances.

Figure 10 shows the overlap of the calculated cis and gauche energy manifolds.

TABLE 8

Gauche-CHD_2NO K_a=3 Q-Branch Transitions

Transition		Observed Frequency/MHz	± Splitting/MHz
$16_{3,13} - 16_{3,14}$	(+)	8819.72	6.56
	(-)	8813.16	
$17_{3,14}$ 0 $17_{3,15}$	(+)	12291.32	7.36
	(-)	12283.96	
$18_{3,15} - 18_{3,16}$	(+)	16706.03	8.46
	(-)	16697.57	
$19_{3,16} - 19_{3,17}$	(+)	22184.92	3.46
	(-)	22181.46	
$20_{3,17} - 20_{3,18}$	(+)	28831.73	5.83
	(-)	28825.90	
$21_{3,18} - 21_{3,19}$	(+)	36721.22	2.26
	(-)	36718.96	

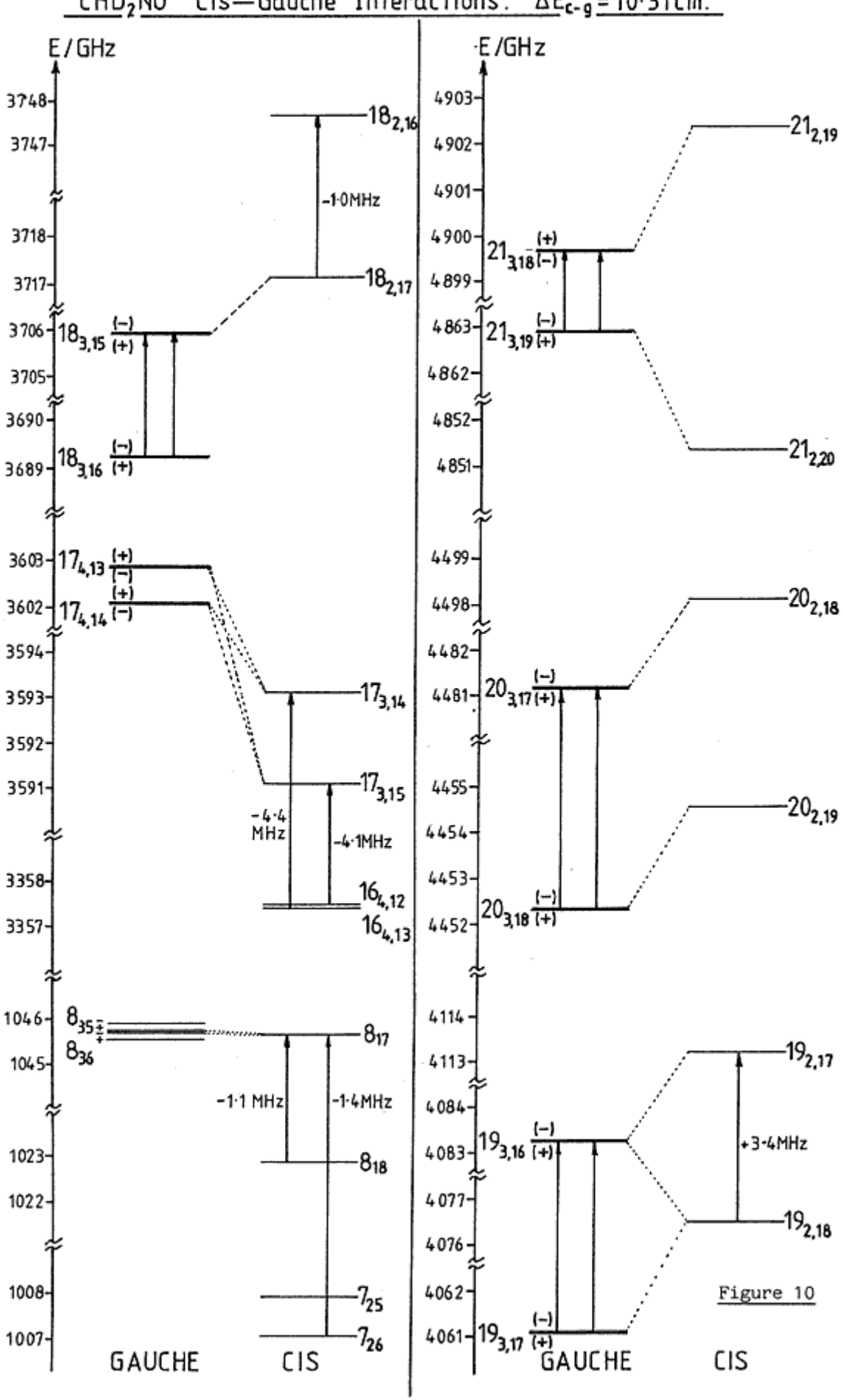
CHD2NO Cis—Gauche Interactions. ΔEc-g = 10·31cm.-1
E/GHz
3748
3747
3718
3717
3706
3705
3690
3689
3603
3602
3594
3593
3592
3591
3358
3357
1046
1045
1023
1022
1008
1007
18 2,16
18 2,17
-1·0MHz
18 3,15 (−) (+)
18 3,16 (−) (+)
17 4,13 (+) (−)
17 4,14 (+) (−)
17 3,14
17 3,15
-4·4 MHz
-4·1MHz
16 4,12
16 4,13
8 35 ± ±
8 36
8 17
-1·1 MHz
-1·4MHz
8 18
7 25
7 26
GAUCHE
CIS
E/GHz
4903
4902
4901
4900
4899
4863
4862
4852
4851
4499
4498
4482
4481
4455
4454
4453
4452
4114
4113
4084
4083
4077
4076
4062
4061
21 2,19
21 3,18 (+) (−)
21 3,19 (−) (+)
21 2,20
20 2,18
20 3,17 (−) (+)
20 2,19
20 3,18 (−) (+)
19 2,17
19 3,16 (−) (+)
+3·4MHz
19 2,18
19 3,17 (−) (+)
GAUCHE
CIS

Figure 10

INTERNAL ROTATION ANALYSIS

Incremental Change in the Potential Function With Deuterium Substitution

The potential function for internal rotation is conventionally expressed as a series expansion;

$$V(\alpha) = \tfrac{1}{2} \sum_{n} V_n \, (1-\cos n\alpha)$$

which, for a molecule with a three-fold symmetric internal rotor, contains only terms where n is a multiple of 3. Moreover, if the series is considered to converge for $n > 6$, V_3 corresponds to the effective barrier height.

If the barrier is considered to arise purely as a consequence of the α dependence of the total electronic energy, partial deuteration of a $-CH_3$ internal rotor should not be expected to reduce the symmetry of the potential. The symmetry is, however, effectively reduced, as is evident from this and other work. One way to treat deuterium substitution is to assume that the effective potential undergoes an incremental change with each successive isotopic substitution. This approach, which is based on an idea originally put forward by Walker and Quade[48], was first applied to the acetaldehyde data[26] by Thorvald Pedersen[49]. Using the mono-deutero species torsional energy spacings, $\Delta E_{\pm}$ and ΔE_{g-c}, Pedersen was able to predict the same quantities for the di-deutero species. His predicted $\Delta E_{\pm}$ for CHD_2CHO was in good agreement with the experimental quantity[26], but there was no experimental result available for comparison with the predicted ΔE_{g-c} (see later work). The method will now be tested again using the more complete partially-deuterated nitrosomethane data.

Incremental change in the torsional potential with isotopic substitution corresponds to the postulate; that the effect of isotopic substitution at a given position in the methyl group is the same regardless of the state of substitution of the rest of the methyl group, which may be formalised as follows:

Firstly, it will be convenient to ascribe a value of α to each hydrogen or deuterium atom in the methyl group, so that in nitrosomethane a hydrogen having α=0 is in the cis position, a hydrogen having α=120 is in a gauche position and so on. Then, split the total energy of the molecule, so that there are three energies (denoted E^H_α or E^D_α) associated with the locations of the H or D atoms, plus an energy E_0 for the ground-state geometry or $E^\ddagger$ for the transition state (top of the barrier) geometry. The total energy of CH_3NO in the ground state, for example, then becomes;

$$E_{tot}\ (\alpha=0) = E_0 + E^H_0 + 2E^H_{120}$$

and in the transition state;

$$E_{tot}(\alpha= 60) = E^\ddagger + 2E^H_{60} + E^H_{180}$$

(Note that, by symmetry, $E^H_{120} = E^H_{240}$ etc.).

It is now possible to relate the V_n coefficients of the potential expansion to the differences in energy between conformers.

Let the number of primes attached to a V_n coefficient represent the number of deuterium atoms in the methyl group of the species to which it relates. Then note that, by symmetry;

$$V_1 = V_2 = V_4 = V_5 = 0 \qquad (\text{for } CH_3\text{-})$$
$$V'''_1 = V'''_2 = V'''_4 = V'''_5 = 0 \qquad (\text{for } CD_3\text{-})$$

(It will be assumed that potential coefficients for n > 6 are zero).

Also let $V_f = E^\ddagger - E_0$.

Then, by considering all possible methyl isotopic variants, the following eight expressions are easily obtained;

1) $V_3 = V_f + 2E^H_{60} + E^H_{180} - E^H_0 - 2E^H_{120}$

2) $V'''_3 = V_f + 2E^D_{60} + E^D_{180} - E^D_0 - 2E^D_{120}$

3) $\frac{1}{4}(V'_1 + V'_5) + \frac{3}{4}(V'_2 + V'_4) + V'_3 = V_f + E^H_{60} + E^D_{60} + E^H_{180} - E^D_0 - 2E^H_{120}$

4) $\frac{1}{4}(V''_1 + V''_5) + \frac{3}{4}(V''_2 + V''_4) + V''_3 = V_f + E^D_{60} + E^H_{60} + E^D_{180} - E^H_0 - 2E^D_{120}$

5) $\frac{3}{4}(V'_1 + V'_2 + V'_4 + V'_5) = (E^H_0 - E^D_0) + (E^D_{120} - E^H_{120})$

6) $\frac{3}{4}(V''_1 + V''_2 + V''_4 + V''_5) = (E^D_0 - E^H_0) + (E^H_{120} - E^D_{120})$

$$7)\quad V_1' + V_3' + V_5' = V_f + 2E_{60}^H + E_{180}^D - E_0^D - 2E_{120}^H$$

$$8)\quad V_1'' + V_3'' + V_5'' = V_f + 2E_{60}^D + E_{180}^H - E_0^H - 2E_{120}^D$$

from which, after some manipulation, the following may be extracted;

$$a)\quad V_3 - V_3' = V_3' - V_3'' = V_3'' - V_3'''$$

$$b1)\quad V_1' + V_5' = -(V_1'' + V_5'')$$

$$b2)\quad V_2' + V_4' = -(V_2'' + V_4'')$$

which raises the following points:

If the potential for internal rotation undergoes an incremental change for each successive isotopic substitution;

a) The V_3 coefficient for a partially deuterated species is the substitution weighted average of the V_3 coefficients for the $-CH_3$ and $-CD_3$ species.

b) The energy differences between cis and gauche potential minima are equal and opposite for $-CH_2D$ and $-CHD_2$ species.

In the original derivation by Pedersen[49], the potential series was assumed to be truncated at n=3. By retaining the series up to n=6 it can also be seen that; in respect of establishing the cis-gauche potential difference, there is unit correlation between V_1 and V_5 and also between V_2 and V_4. Note also that V_6 makes no contribution to the energies at the turning points provided that they occur at 60° intervals (i.e. provided that V_3 is the dominant term).

Internal Rotation in Nitrosomethane

In order to test the hypothesis in the preceeding section, it is necessary to make use of CH_3NO and CD_3NO data. Infrared torsional fundamentals for these species have not been observed and there has been no microwave analysis of torsionally excited states. The V_6 contribution to the potential in each case is therefore unknown. Van Eijck[50] has, however, recently re-analysed all of the available data eliminating some earlier approximations to obtain (in cm^{-1});

$V_3 = 405.3$ (2)

$V_3''' = 390.0$ (3)

from which it is expected;

$V_3' = 400.2$

$V_3'' = 395.1$

Internal Rotation Constants

The internal rotation (F) constants for CH_3NO and CD_3NO are also derived from the parameters of the IAM fits[50]. These F constants, which appear in Table 9, were used as a guide in arriving at a structure from which to calculate F constants for CH_2DNO and CHD_2NO. The structure used was as published[17], but with the methyl group constrained to be symmetric about the internal rotation (z) axis and adjusted to reproduce the IAM value for I_α (I_α = 3.253(3) uÅ² for CH_3NO and 6.497(1) uÅ² for CD_3NO)[50]. The z-axis is not co-incident with the C-N bond and is defined such that the methyl group is tilted slightly away from the oxygen atom. F constants were evaluated from the methyl end of the molecule, using ground state moments of inertia. The computer program given in Appendix 5 was used for this purpose. Van Eijck[50] has also calculated F constants, from structure, for the cis partially deuterated species, and these appear in Table 9 for comparison with those obtained here.

For the partially deuterated species, F is a function of α. For these species therefore, F was also computed, purely from structure, at intervals of 30°. $F(\alpha)$, in both cases, underwent one cycle of smooth change in 360°. A Fourier series, adequate to reproduce F in the regions of maximum probability for the torsional oscillation, may therefore, in both cases, have the form;

$$F(\alpha) = F_0 + F_1 \cos \alpha.$$

For CH_2DNO (see Table 9); $F'(\alpha=0^\circ) = 6.7267\ cm^{-1}$, $F'(\alpha=120°) = 6.3246\ cm^{-1}$.

TABLE 9

Nitrosomethane Structure Used For Calculation of Internal Rotation Constants (Bond lengths /Å Angles/Degrees)

r(C-H)	1.0980
r(C-D)	1.0977
r(C-N)	1.4800
r(N=O)	1.2114
$H\widehat{C}Z$	109.15
$N\widehat{C}Z$(tilt)	1.07
$C\widehat{N}O$	113.2

Internal Rotation Constant F/cm^{-1}

Species	This Work	Van Eijck[50]
CH_3NO	7.7130	7.7130
CD_3NO	5.0176	5.0272
cis-CH_2DNO	6.7267	6.735
gauche-CH_2DNO	6.3246	-
cis-CHD_2NO	5.4475	5.431
gauche-CHD_2NO	5.6968	-

Reproducing these values with the above expression requires (in cm^{-1});

$F_0' = 6.4586$

$F_1' = 0.2681$

Similarly, for CHD_2NO; F"(0°) = 5.4475cm^{-1}, F"(120°) = 5.6968 cm^{-1}. Hence;

$F_0'' = 5.6137$

$F_1'' = -0.1662$

Data Adjustment

For the purpose of fitting the nitrosomethane torsional data, the computer program given in Appendix 6 was used. Energy levels were calculated using the Hamiltonian;

$$H = -\frac{d}{d\alpha}(F_0 + F_1\cos\alpha)\frac{d}{d\alpha} + \tfrac{1}{2}\sum_n V_n(1 - \cos n\alpha)$$

expanded in a free-rotor basis and diagonalised numerically. 40 basis functions gave sufficient accuracy.

Taking the derived parameters V_3', F_0' and F_1', the CH_2DNO torsional data; $\Delta E_{-+}' = 922.01(19)$ MHz and $\Delta E_{g-c}' = 11.20(1)cm^{-1}$, were fitted to V_1' and V_2' yielding (in cm^{-1});

$V_1' = -17.0063$

$V_2' = 38.3669$

(two parameters for two data constitutes a numerical solution, not a least-squares fit, but a spurious degree of freedom for the fit was generated by giving $E(0_-) - E(0_0) = \Delta E_{-+} + \Delta E_{g-c}$ to the program, along with the independent data).

Assuming $V_1'' = -V_1'$ and $V_2'' = -V_2'$, and using the derived parameters V_3'', F_0'' and F_1'', then gave rise to the following predictions;

$\Delta E_{-+}'' = 170.15$ (cf 190.16(14) observed)MHz.

$\Delta E_{g-c}'' = -13.04$ (cf -10.31 observed)cm^{-1}.

Fitting the CHD_2NO data gave (in cm^{-1});

$V_1'' = 14.4353$ (cf $V_1' \simeq -17.0$)

$V_2'' = -31.8544$ (cf $V_2' \simeq 38.4$)

Thus, the pattern of coefficients is quite well predicted by the incremental theory when the potential is truncated for $n > 3$. The theory actually states that the cis-gauche potential differences will be equal and opposite for $-CH_2D$ and $-CHD_2$ species. From the Fourier expansion;

$$\Delta V_{g-c} = V(120°) - V(0°) = \tfrac{3}{4}(V_1+V_2+V_4+V_5)$$

Hence, in the present approximation;

$\Delta V'_{g-c} = 16.02\ cm^{-1}$

$\Delta V''_{g-c} = -13.06\ cm^{-1}$

The Effect of V_6

When the barrier to internal rotation, for a molecule with a three-fold symmetric internal rotor, is determined solely from microwave data for the torsional ground-state, the derived value for V_3 contains a contribution due to the neglect of V_6 and higher terms in the potential. This limitation on the accuracy of V_3 has to be accepted because V_3 and V_6 always remain correlated in the absence of data for torsionally excited states. Such is the position for nitrosomethane. There is however, good reason to believe that nitrosomethane will have V_6 in the region $\sim$-5 to $\sim$-20 cm^{-1}. This follows because experimental V_6 determinations for comparable molecules appear always to fall in this region[11,12,51,52] (see also Chapter 4). Furthermore, the contribution to the effective V_6 from the interaction between internal rotation and other vibrations, calculated in the harmonic approximation[6], appears always to be negative and $\sim$-5 cm^{-1} for acetaldehyde and isovalent species. It is therefore important to assess the consequence of neglecting V_6 when applying the potential increment theory.

The parameter which comes out of the microwave analysis of ground-state torsional splittings, and which is invariant with respect to V_6, is the scaling factor for the A-E splittings Δ_0, defined such that;

$$-\Delta_0 = \nu(OE-0A)$$

Van Eijck[50], in his re-analysis of the CH_3NO and CD_3NO data, did not state Δ_0 explicitly, but it can easily be calculated from V_3 and F using the torsional Hamiltonian. The results are as follows:

	CH_3NO	CD_3NO
F/cm^{-1}	7.7130	5.0272
V_3/cm^{-1}	405.3	389.96
$-\Delta_0$/MHz	2142.98	239.05

These Δ_0 values agree, within three standard deviations, with those obtained by Turner and Cox[17] ($-\Delta_0$ = 2149.3(9.9) MHz for CH_3NO and 240.8(8) MHz for CD_3NO). Now, by taking Δ_0 and F it is possible to calculate V_3 for various assumed values of V_6. These results are given in Table 10 (numerical solutions were again obtained by least-squares fitting, a spurious degree of freedom for the fit being generated by observing that the E-state is doubly degenerate).

V_3' and V_3'' may now be calculated for assumed values of V_6, by taking the weighted average of V_3 and V_3''' as before. This, of course, requires that V_6 is invariant with isotopic substitution, which is only a good assumption with regard to the electronic contribution to V_6. Nevertheless, as soon as the first calculation involving V_6 is performed, it is immediately apparent that this assumption has no consequence in the potential increment theory.

A calculation was performed with $V_6' = V_6'' = -6\ cm^{-1}$. The appropriate weighted averages of V_3 and V_3''' (calculated from the quantities in Table 10) are thus (in cm^{-1});

V_3' = 404.361

V_3'' = 399.439

Using the derived values of F_0', F_1', V_3' and V_6' and fitting $\Delta E_{\pm}'$ and $\Delta E_{g-c}'$ as before gave;

V_1' = -16.9127 (cf -17.0063)

V_2' = 38.2782 (cf 38.3669)

TABLE 10

Variation of V_3 With Respect to V_6 (all units are cm^{-1})

	CH_3NO	CD_3NO
F	7.7130	5.0272
$-\Delta_0$	0.07148219	0.00797400

V_6	V_3	V_3'''
0	405.300	389.960
-2	406.627	391.478
-4	407.955	392.998
-6	409.283	394.517
-8	410.611	396.038
-10	411.940	397.559
-12	413.269	399.081
-14	414.598	400.604
-16	415.927	402.128
-18	417.257	403.652
-20	418.587	405.176

Values obtained previously with V_6=0 are given in brackets. Thus V_1' and V_2' are hardly affected by the inclusion of V_6. Furthermore, by taking F_0'', F_1'', V_3'' and V_6'' and $V_1'' = -V_1'$ and $V_2'' = -V_2'$ as before, the following predictions were obtained;

$\Delta E_{+}''$ = 170.22 (cf 170.15) MHz

$\Delta E_{g-c}''$ = -13.05 (cf -13.04) cm^{-1}

Then, fitting to the observed $\Delta E_{+}''$ and $\Delta E_{g-c}''$ gave (in cm^{-1});

V_1'' = 14.3892 (cf 14.4353)

V_2'' = -31.8000 (cf -31.8544)

It may be concluded that neglect of the V_6 contribution to the potential has no significant effect on the determination of V_1 and V_2 coefficients from torsional ground-state data, provided that the V_6 contribution is folded into the effective V_3.

The Effect of V_4 and V_5

Since there are four data ($\Delta E_{+}'$, $\Delta E_{g-c}'$, $\Delta E_{+}''$ and $\Delta E_{g-c}''$) and eight parameters (V_1', V_2', V_4', V_5' and V_1'', V_2'', V_4'', V_5'') and only two combination rules, i.e.:

$$V_1' + V_5' = -(V_1'' + V_5'')$$

and

$$V_2' + V_4' = -(V_2'' + V_4'') ,$$

there exist, in principle, a family of solutions which satisfy the requirements of the potential increment theory. The question remains as to whether any of these solutions are physically reasonable.

Table 11 shows how V_1' and V_2' change with the inclusion of assumed values for V_4' and V_5'. Shown also are the predicted values of $\Delta E_{+}''$ and $\Delta E_{g-c}''$ using the arbitrary additional constraint; $V_4'' = -V_4'$ and $V_5'' = -V_5'$. With this constraint the system shows no tendency to converge on the observed $\Delta E_{g-c}''$ for $V_{n\neq3} \ll V_3$. Moreover, the constraint is not physically unreasonable if the substitution effects are to be equal and opposite for the two isotopic species. It seems sensible to conclude that the discrepancy between $\Delta V_{g-c}'$

TABLE 11

The Effect of V_4' and V_5'

V_1'	V_2'	Assumed V_4'	Assumed V_5'	Predicted $\Delta E''_+$/MHz	Predicted $\Delta E''_{g-c}$
-17.0063	38.3669	0	0	169.89	-13.042
-17.6428	44.9173	0	-10	172.93	-12.567
-22.3233	36.1397	+10	0	174.45	-12.623
-22.9370	42.7770	+10	-10	176.94	-12.299
-28.3124	40.8290	+20	-10	179.75	-12.186
-33.7666	39.0701	+30	-10	181.38	-12.218
-34.3229	45.8798	+30	-20	183.11	-12.216
Target Values ⟶				190.16(14)	-10.31(1)

and $-\Delta V''_{g-c}$ arises out of approximations inherent in the potential increment theory or in the derivation of the fixed parameters used in its application.

Scaling of V_1 and V_2

One notable property of the V_1 and V_2 coefficients determined earlier, using a potential series truncated at n=3, is that the following relationship is obeyed to a good approximation;

$$V''_1 = -c\ V'_1$$
$$V''_2 = -c\ V'_2$$

where c is a scaling factor.

This suggests the possibility of predicting $\Delta E''_{c-g}$ by using $\Delta E''_{+}$ to find the scaling factor.

Starting with $V'_1 = -17.0063\ cm^{-1}$ and $V'_2 = 38.3669$ as determined from the CH_2DNO data, use of c = 0.833 in the above relationship fits $\Delta E''_{+}$ and predicts;

$$\Delta E''_{c-g} = 10.58 \text{ (cf 10.31 observed) } cm^{-1}.$$

Given the difficulties inherent in the calculation of the fixed parameters which were used, this is a very good prediction. It is also interesting because it suggests a means of refining Pedersen's earlier prediction[49] for the unknown $\Delta E''_{g-c}$ of acetaldehyde.

INTERNAL ROTATION IN ACETALDEHYDE

The microwave spectra of the gauche partially-deuterated acetaldehydes were studied by Turner Cox and Hardy[26] giving:

$\Delta E_{+}^{'}$ = 804.5 (1) MHz

$\Delta E_{g-c}^{'}$ = 15.55 cm^{-1}

$\Delta E_{+}^{''}$ = 183.6 (1) MHz

It was not possible to determine $\Delta E_{g-c}^{''}$ because no definite cis-gauche perturbations were observed in the spectrum of CHD_2CHO. The purpose of this section is to use the potential increment approach, in conjunction with the most up-to-date information available, to predict $\Delta E_{c-g}^{''}$ and compare it with the known experimental data.

Species of acetaldehyde with a symmetric internal rotor have been subjected to a number of barrier determinations[11,12,21,50,52,53,54,55], with interest directed mostly towards CH_3CHO. Only Far-Infrared data and IAM studies involving direct diagonalisation of the torsion-rotation Hamiltonian will be considered here.

Direct diagonalisation IAM studies of CH_3CHO have been published by Bauder and Günthard[12] and Van Eijck[50] and it is difficult to choose between them. Bauder and Günthard restricted their data set to $J \leqslant 3$ and reported $F = 7.6408\ cm^{-1}$ and $-\Delta_0 = 2070.025$ MHz. Van Eijck appears to have fitted more data and reports $V_3 = 401.0\ (1.7)\ cm^{-1}$. In this case, F, calculated from the IAM parameters, is $7.6405\ cm^{-1}$. A recent IAM study including v=1 data, by Petty and Baker[52], is yet to be published at the time of writing.

The most detailed analysis of the Far-Infrared spectrum of CH_3CHO is that of Hollenstein and Winther[54]. These authors report the following transition frequencies (in cm^{-1});

ν(1A-0A) = 143.75 (10)

ν(1E-0E) = 142.03

ν(2A-1A) = 114.41 (10)

These data were therefore combined with the microwave Δ_0 of Bauder and GÜnthard and subjected to a weighted non-linear least-squares fit to the Hamiltonian;

$$H = -F\frac{\partial^2}{\partial\alpha^2} + \frac{V}{2}3(1-\cos 3\alpha) + \frac{V}{2}6\ (1-\cos 6\alpha)$$

Details of the fit, including calculated energy levels, are given in Table 12. Weighting coefficients are $1/\sigma^2$ for the observation in question. Δ_0 was assumed to have σ = 2 MHz. m is the limiting free-rotor quantum number (see also Appendix 6). The determined parameters are (in cm^{-1});

$F = 7.6441$

$V_3 = 416.6$

$V_6 = -18.6$

The F value obtained is comparable to the IAM results (q.v.). The V_3 and V_6 results are similar to those obtained recently by Crighton and Bell[55], who fitted the Far-Infrared data of Hollenstein and Winther[54], but not Δ_0, and used an F constant of 7.8588 cm^{-1} calculated from the structure reported by Iijima and Tsuchiya[56]. Crighton and Bell used an unusual definition of $V(\alpha)$, but after this is taken into account, their results correspond to;

V_3 = 415.0 (1.1) cm^{-1} and V_6 = -22.3 (1.7) cm^{-1}.

At this point, it is appropriate to comment on the physical significance of the V_6 term. Quade[6] has calculated the contribution to the effective V_6 term from the interaction between internal rotation and other vibrations. In the harmonic approximation he finds the contribution to be -4.72 cm^{-1} for CH_3CHO and -5.50 cm^{-1} for CH_3CDO. Ab-initio calculations performed by Crighton and Bell[57], using structures in which the methyl group is constrained to be symmetric, indicate that the electronic contribution to V_6 is ~+1 cm^{-1}. There remains the possibility that a three-fold dependence of the internal rotation constant has been folded into the V_6 term[10] (see also Chapter 4). The data can indeed be fitted with the following parameters (in cm^{-1});

TABLE 12

CH3CHO Acetaldehyde.
Torsional Potential Program VFIT
3 Fold Dominated Potential

40 Basis Functions

	mu	ml	Obs	Obs-Calc	Weight
0E- 0A	1	0	0.06904860	0.00000015	0.22471E+09
1E- 0E	2	1	142.03000000	0.01816181	100.00
1A- 0A	-3	0	143.75000000	-0.01774130	100.00
2A- 1A	3	-3	114.41000000	-0.00044826	100.00

E.S.D. of an Observation = 0.25393980/Sqrt(Weight)

Estimated Parameters		E.S.D.
F0	7.64413625	0.00083004
V3	416.63175029	0.08135572
V6	-18.59500421	0.06808352

Correlation Coefficients.

F0	V3	V6
1.0000		
0.7986	1.0000	
-0.4131	-0.8124	1.0000

Energy Levels

Iml	Odd (Sin) Wfn.	Even (Cos) Wfn.
0		74.44323882
1	74.51228727	74.51228727
2	216.52412544	216.52412544
3	218.21098010	332.62142835
4	346.09925732	346.09925732
5	429.18893529	429.18893529
6	487.36962477	506.58643621
7	589.83894404	589.83894404
8	700.21439767	700.21439767
9	827.32738413	827.57195170
10	970.83442997	970.83442997

F_0 = 7.706

F_3 = -1.08

V_3 = 422.7

V_6 = -4.72 (assumed)

but the F_3 term obtained is far too large to be physically reasonable. It must therefore be concluded that the potential determination will benefit from additional data and possibly the inclusion of even higher terms in the potential expansion such as[52] V_9.

Calculation of V_3' and V_3'' for Acetaldehyde

Since the V_6 term is expected to have no significant effect on the determination of V_1 and V_2 coefficients for the partially deuterated species, the most straightforward procedure is to start with V_3 and V_3''' coefficients which already have the V_6 contribution folded into them. For CH_3CHO, taking F = 7.6441 cm^{-1} from the fit given earlier, and Bauder and Günthard's $-\Delta_0$ = 2070.025 MHz, gives;

V_3 = 404.25 cm^{-1}

For CD_3CHO, V_3 from the IAM fit of Van Eijck[50] is already in the appropriate form. Hence;

V_3''' = 392.1 (5.0) cm^{-1}

The weighted averages are (in cm^{-1});

V_3' = 400.2

V_3'' = 396.1

Internal Rotation Constants

The F constant from the fit to the CH_3CHO torsional data was used as a guide in arriving at a structure from which to calculate F constants for CH_2DCHO and CHD_2CHO. The structure used was that published by Nösberger, Bauder and Günthard[58] but with the methyl group constrained to be symmetric about the C-C bond. F constants were evaluated from the methyl end of the molecule using effective moments of inertia. For $-CH_3$ and $-CD_3$ species,

rotational constants were obtained from reference 50. For the partially deuterated species, the data of references 22 and 26 were fitted to appropriate A-reduction Hamiltonians and the rotational constants were used after correction for centrifugal distortion[38]. In the case of the gauche forms, effective rotational constants were taken to be the average of those for (+) and (-) states after transformation into the PAS. F constants for the cis forms of CH_2DCHO and CHD_2CHO have also been calculated, from structure, by Van Eijck[50]. These are given in Table 13 for comparison with those obtained here. F constants for CH_3CHO and CD_3CHO calculated from Van Eijck's IAM parameters are also given.

$F(\alpha)$, for both partially deuterated species, again undergoes one cycle of smooth change in 360°. Using the quantities in Table 13 therefore gives (in cm^{-1}), for CH_2DCHO;

$F_0' = 6.3934$

$F_1' = 0.2364$

and for CHD_2CHO;

$F_0'' = 5.5588$

$F_1'' = -0.1515$

These coefficients are in good agreement with those obtained from a much earlier calculation by Knopp and Quade[59].

Data Adjustment

The procedure used was identical to that given earlier for nitrosomethane.

Taking the derived parameters V_3', F_0' and F_1', the CH_2DCHO torsional data; $\Delta E_{+}' = 804.5$ (1) MHz and $\Delta E_{g-c}' = 15.55\ cm^{-1}$, were fitted to V_1' and V_2' yielding (in cm^{-1});

$V_1' = -8.0178$

$V_2' = 34.4919$

TABLE 13

Acetaldehyde Structure used for Calculation of Internal Rotation Constants

Bond lengths /Å	Angles/Degrees
$r(C\text{-}H_{Me})$, $r(C\text{-}D_{Me})$	1.0966
$r(C\text{-}C)$	1.5005
$r(C{=}O)$	1.2038
$r(C\text{-}H_{ald})$	1.1237
$C\text{-}\hat{C}\text{-}H_{Me}$	109.47
$C\text{-}\hat{C}{=}O$	124.72
$C\text{-}\hat{C}\text{-}H_{ald}$	113.93

Internal Rotation Constant /cm^{-1}

Species	This Work	Van Eijck[50]
CH_3CHO	7.6441	7.6405
CD_3CHO	4.9740	4.9380
cis-CH_2DCHO	6.6298	6.679
gauche-CH_2DCHO	6.2752	-
cis-CHD_2CHO	5.4073	5.434
gauche-CHD_2CHO	5.6345	-

Assuming $V_1'' = -V_1'$ and $V_2'' = -V_2'$, and using the derived parameters V_3'', F_0'' and F_1'', gave the prediction;

$\Delta E_{+}'' = 175.08$ (cf 183.6 (1) observed) MHz

$\Delta E_{g-c}'' = -16.93\ cm^{-1}$.

Assuming $V_1'' = -cV_1'$ and $V_2'' = -cV_2'$, and adjusting c to fit $\Delta E_{+}''$ gave;

$c = 0.915$

$\Delta E_{g-c}'' = -15.37\ cm^{-1}$.

In order to test these predictions, the microwave data for cis[22] and gauche[26] CHD_2CHO were fitted to appropriate Hamiltonians and the resulting constants used to calculate rotational energy levels. These energy manifolds were searched for co-incidences, using assumed values for ΔE_{c-g}. Degeneracies closer than 2 cm^{-1} were printed and examined in each case.

$\Delta E_{c-g}'' = 16.93\ cm^{-1}$ (507.7 GHz) predicted one close degeneracy in the range $J = 0 \rightarrow 20$; $18_{2,17}$(cis) with $18_{4,15}$(+). The cis $18_{2,16} - 18_{2,17}$ is unperturbed, so that this scheme fails. Reducing $\Delta E_{c-g}''$ has the property of moving this K_a=2(cis), K_a=4(gauche) degeneracy to lower J.

$\Delta E_{c-g}'' = 15.37\ cm^{-1}$ (460.7 GHz) predicted close degeneracies at; $14_{2,12}$(cis) $\leftrightarrow$ $14_{4,10}$(+) and $14_{4,11}$(-), also; $12_{2,11}$(cis) $\leftrightarrow$ 12_{49}(+) and 12_{48}(-). The cis $14_{2,12} - 14_{2,13}$ is unperturbed, so that this scheme fails also. There is, however, a poor residual, in the cis data set, for the $10_{1,10} - 9_{27}$ transition (+0.44 MHz). This residual could not be eliminated by the inclusion of sextic distortion constants, whereas poor residuals for the higher J ΔK_a=1 transitions could be so eliminated. This suggests a further small reduction in $\Delta E_{c-g}''$ to place suitable gauche K_a=4 levels slightly above the cis 9_{27}. Such a scheme gives; $\Delta E_{c-g}''$ = 442.4 GHz (14.76 cm^{-1}) and, as is required, predicts there to be no other perturbations in the observed data set. Perturbations are predicted to occur at J=14, K_a=7 and J=23, K_a=5 and J=27, K_a=4 in the cis spectrum, bearing in mind that these levels are not likely to have been calculated very accurately.

These levels are also not associated with transitions occurring in the frequency range covered at Bristol, and cannot easily be observed. The calculated K doubling at J=27, K_a=4 is, for example, only ~2300 MHz.

$\Delta E''_{c-g}$ = 14.76 cm $^{-1}$ for CHD_2CHO must, at this stage, be regarded as a tentative assignment, although it agrees closely with prediction. Taken with the derived parameters, F''_0, F''_1, V''_3 and the observation; $\Delta E''_+$ = 183.6(1)MHz, it gives (in cm^{-1});

V''_1 = 7.9261

V''_2 = -31.3045

The collected results of these investigations, for nitrosomethane and acetaldehyde, are given in Table 14.

TABLE 14

Internal Rotation Parameters[a]

Species	ΔE_+ /MHz	ΔE_{g-c}	F_0	F_1	V_1	V_2	V_3	ΔV_{g-c}
CH_2DNO	922.01(19)	11.20	6.4586	0.2681	-17.01	38.37	400.2	16.02
CHD_2NO	190.16(14)	-10.31	5.6137	-0.1662	14.44	-31.85	395.1	-13.06
CH_2DCHO	804.5 (1)	15.55	6.3934	0.2364	-8.02	34.49	400.2	19.86
CHD_2CHO	183.6 (1)	-14.76	5.5588	-0.1515	7.93	-31.30	396.1	-17.53

(a) all quantities in cm^{-1} except where indicated.

DISCUSSION

Apart from acetaldehyde[26] and nitrosomethane, there have been only two other determinations of conformer zero-point energy differences in partially deuterated methyl species. These were in methylamine[60], CH_2DNH_2, and methanol[61,62], CH_2DOH/D and CHD_2OH/D. The asymmetric mass distribution of the internal rotor in these species, gives rise to an α dependence of effective moment of inertia for the torsion, even if the rest of the molecule is considered to be rigid. This α dependence contributes to the energy difference between torsional substates, but in all cases it is insufficient to explain the measured energy difference. It follows, given the Born-Oppenheimer separation of electronic and vibrational energies, that contributions to the energy of the torsional oscillation occur through interactions between the torsion and other modes of vibration. These interactions manifest themselves as modifications to $F(\alpha)$ or $V(\alpha)$, as a result of any α dependence in the coupling of the torsion with other vibrations, or as a consequence of any α dependence of the zero-point energy of the other vibrations[48]. These two mechanisms will be discussed in turn:

Potential Effects

Consider a molecule in which the torsion is frozen. Then, for a given (fixed) value of α, the complete vibrational Hamiltonian may be constructed in terms of isolated vibrational modes and then transformed into the appropriate molecular basis. The Hamiltonian for an isolated vibration is;

$$H_x^{(0)} = \frac{P_x^2}{2m_x^*} + V_x$$

where m_x^* is the reduced mass and V_x is the potential function. V_x depends on the complete electronic wavefunction and so is dependent on the positions of all nuclei, but an appropriate average over all vibrations will be assumed to exist.

Transformation into the molecular basis requires introduction of the coupling between vibrations (which occurs through the kinetic energy);

$$T^{-1}\begin{bmatrix} H_1^{(0)} & & H_{xx'} \\ & H_2^{(0)} & \\ H_{xx'} & & H_n^{(0)} \end{bmatrix} T = \begin{bmatrix} H_1 & & 0 \\ & H_2 & \\ 0 & & H_n \end{bmatrix}$$

then, since the vibrational quantum number v is a good quantum number for the ground state, a v=0 matrix may be constructed with the zero-point energies of the various modes as its diagonal entries. The trace of this matrix is the total zero-point energy and is invariant with respect to transformation of basis. Therefore, within the Born-Oppenheimer approximation, any zero-point energy difference between <u>isolated</u> conformers must arise through an α dependence of the potentials, and hence force-constants, of all or some of the vibrations. In this respect, there will be a small contribution due to a slight change in the average geometry, but the major contribution will be due to any α dependence of the methyl group stretching and bending force constants.

The effective potential for internal rotation, on the assumption of no coupling between torsion and other vibrations, may then be constructed as follows;

$$V(\alpha) = E_{el}(\alpha) + E_{zp}(\alpha)$$

where E_{el} is the total electronic energy, and E_{zp} is the total zero-point energy excluding the torsion. Now, within the Born-Oppenheimer approximation, $E_{el}(\alpha)$ is three-fold symmetric; therefore, any difference within the minima of the effective potential is the zero-point energy difference between the hypothetical isolated conformers.

The above is the physical basis for the incremental potential theory given earlier. The assumptions inherent in that theory are therefore;

1) that the Born-Oppenheimer (electronic/vibrational) separation is valid.

2) that the slight changes in the reduced masses of the various vibrations, on going from one isotopic species to another, can be neglected.

3) that there is no coupling between the torsion and other vibrations.

The third assumption is by far the worst and results in a breakdown of the incremental approach in the event of a vibrational contribution to the torsional kinetic energy.

Kinetic Effects

The torsional eigenvalue spacings at v=0 are not equivalent to isolated conformer zero-point energy differences, firstly because of the α dependence of the rigid top-rigid frame internal rotation constant (q.v.), and secondly because of tunnelling, which causes the isolated conformer description to break down. The addition of the torsion, however, completes the total vibrational Hamiltonian, so that the sum of the v=0 torsional eigenvalues is equal to the sum of the conformer zero-point energies, provided that each conformer zero-point energy is taken as the sum over all vibrations including the torsion. The zero-point energy differences between isolated torsionless conformers may therefore be obtained by correcting for the torsion, i.e. by taking the differences between the minima in the effective torsional potential, but only if there is no coupling between torsion and other vibrations. The effect of coupling is to alter the distribution of energy between the torsion and other modes and hence to modify the rate of tunnelling. This is equivalent to a vibrational contribution to the effective moment of inertia of the torsion and hence to $F(\alpha)$. Furthermore, this contribution may be strongly α dependent. The molecules under consideration have C_s (mirror symmetric) forms, in which only A'' vibrations may couple with torsion in the normal-coordinate description, and C_1 (asymmetric) forms in which all vibrations may couple with torsion[63]. The degree of coupling will also be expected to change for different isotopic species, which places

a limitation on the applicability of the potential increment theory. This limitation occurs because the potential and the kinetic contributions to the torsion, from other vibrations, cannot be distinguished using torsional data alone, i.e. changes in $F(\alpha)$ may be modelled by changes in $V(\alpha)$ and vice versa[6,10,59]. The result that the rule $V_1' = -V_1''$ and $V_2' = V_2''$, was only obeyed approximately in the investigations given earlier, is therefore probably due mainly to a pseudo-potential contribution from the coupling between torsion and other vibrations. It is remarkable, however, that the incremental approach was so successful, especially with the inclusion of the scaling factor c. This may indicate that a substantial cancellation of coupling effects can be expected, with c representing a correction for the differences in coupling between the $-CH_2D$ and $-CHD_2$ species in each case.

Methylamine

The first determination of a conformer zero-point energy difference, for a partially deuterated species, was that in CH_2DNH_2. In this case, Tamagake and Tsuboi[60] determined the trans-gauche energy separation, ΔE_{tg}, from variations in microwave inversion splittings. There are two large-amplitude internal degrees of freedom in this molecule; rotation about the C-N bond and inversion at the nitrogen atom, and these two processes allow alternative paths between minima in the potential energy surface. The investigators were therefore able to calculate ΔE_{tg} from the spectroscopic inversion parameters, and subsequently to confirm it precisely by identifying perturbations due to trans $\leftrightarrow$ gauche interactions. They reported $\Delta E_{tg} = 7.060\ cm^{-1}$ and combining this with other microwave and far-infrared[63] torsional data, calculated a set of torsional parameters. They noted a considerable difference between their fitted $F(\alpha)$ and its counterpart calculated from structure, and attributed this change to coupling between torsion and other vibrations. This interpretation may, however, require some modification, as will be shown.

McKean and co-workers[23] have made extensive use of isolated C-H stretching frequencies to determine properties of C-H bonds. Their work is based on the idea that the stretching frequency of a C-H bond, observed free from Fermi Resonance, corresponds closely to that of an isolated oscillator. In this approximation, the C-H stretching force constant may be deduced directly. These isolated C-H stretching frequencies might also relate usefully to conformer zero-point energy differences as described above.

If the isolated C-H bond is assumed to be a harmonic oscillator, its absorption frequency is given by;

$$\nu(\text{C-H}) = \frac{1}{2\pi}\sqrt{\frac{k}{m^*}}$$

where k is the average force constant.

The zero-point energy is;

$$\langle 0 \left| H^{(0)}_{\text{C-H}} \right| 0 \rangle = \frac{\hbar}{2}\sqrt{\frac{k}{m^*}} = \tfrac{1}{2}h\nu(\text{C-H})$$

If the rest of the molecule is assumed rigid, as required for the oscillator to be isolated;

$$m^* = \frac{m_H\,(M-m_H)}{M}$$

where M is the molecular mass and m_H is the hydrogen atomic mass.

Isolated C-D stretching frequencies cannot be observed for the type of molecule under consideration here, but a hypothetical isolated C-D stretching frequency, on the assumption that the force-constant is unaffected by substitution, is given by;

$$\nu(\text{C-D}) = \nu(\text{C-H})\sqrt{\frac{m^*_H}{m^*_D}} = \nu(\text{C-H})\sqrt{\frac{m_H\,(M-m_H)}{m_D\,(M-m_D)}}$$

This provides a simple method, for estimating the C-H stretching contribution to the conformer zero-point energy difference in partially deuterated methyl species, by observing the difference between C-H stretching frequencies in different rotamers, and by observing that;

$$E^H_\alpha \simeq \tfrac{1}{2}\nu_\alpha(\text{C-H}) \quad \text{etc.}$$

in equations 5 and 6 of the potential increment theory given earlier (page 55).

Hence, in the absence of torsion-vibration coupling;

$$\Delta V'_{gt} \simeq \tfrac{1}{2}[\nu_t(C\text{-}H)-\nu_t(C\text{-}D)+\nu_g(C\text{-}D)-\nu_g(C\text{-}H)]$$

$$\simeq \tfrac{1}{2}\left[1-\sqrt{\frac{m^*_H}{m^*_D}}\right](\nu_t(C\text{-}H)-\nu_g(C\text{-}H))$$

Similarly;

$$\Delta V''_{gt} \simeq -\tfrac{1}{2}\left[1-\sqrt{\frac{m^*_H}{m^*_D}}\right](\nu_t(C\text{-}H)-\nu_g(C\text{-}H))$$

where, by definition;

$$\Delta V_{gt} = -\Delta V_{tg} = \frac{3}{4}(V_1+V_2)$$

For CHD_2NH_2, McKean and Ellis[64] report (in cm^{-1});

$\nu_g(C\text{-}H)$ = 2955.5(5) (gauche form)

$\nu_t(C\text{-}H)$ = 2880.0(5) (trans form)

which give;

$$\Delta V''_{tg} = -10.63 \text{ cm}^{-1}$$

Applying a small correction to the observed $\nu(C\text{-}H)$ frequencies for the change in reduced mass on going $CHD_2 - CH_2D$ gives;

$$\Delta V'_{tg} \simeq +10.62 \text{ cm}^{-1}$$

This is in favourable qualitative agreement with ΔE_{tg} = 7.06 cm^{-1}, but not in agreement with the reported internal-rotation parameters. Tamagake and Tsuboi[60] give (for V'_6 = 0, in cm^{-1});

V'_1 = 37.815

V'_2 = -26.006

hence;

$$\Delta V'_{tg} = -8.86 \text{ cm}^{-1}.$$

It follows from these potential parameters that although the trans zero-point lies above the gauche, the trans potential minimum lies below the gauche. This artefact can be traced to their large value of F_2 = 2.3 cm^{-1}.

As mentioned before, kinetic energy parameters may give rise to pseudo-potential effects and vice-versa. The simultaneous determination of $F(\alpha)$ and $V(\alpha)$ is therefore, at best, unreliable. Their torsional data, corrected for nitrogen inversion effects, were therefore re-analysed with the coefficients of $F(\alpha)$ held constant at the rigid top-rigid frame values[63]. This gave (in cm^{-1});

$$V_1' = 6.10$$

$$V_2' = -16.45$$

hence;

$$\Delta V_{tg}' = 7.76 \text{ cm}^{-1}$$

This compares very favourably with the quantity calculated from the C-H stretching force constants, bearing in mind that torsion-vibration coupling and any α dependence of C-H bending force constants have been neglected. It appears to indicate in this case that the observed ΔE_{tg} arises mainly from the α dependence of the C-H stretching force constants.

Methanol

Conformer zero-point energy differences in the partially deuterated methanol species were investigated by Serrallach, Meyer and Günthard[61] during the course of an extensive valence force-field refinement. These authors initially adjusted force-constants from the vibrational fundamentals of the four symmetrically substituted species, CH_3OH/D and CD_3OH/D, and found, in the vibrational potential function, that significant deviation from local C_{3v} symmetry of the methyl group was required in order to reproduce the observed methyl C-H/D stretching frequencies. This initial force field predicted the fundamentals of the four partially deuterated species, CH_2DOH/D and CHD_2OH/D, with good accuracy, the partially deuterated data being used for subsequent refinement, and also enabled the conformer zero-point energy differences to be calculated. They predicted the trans form

to be more stable than the gauche in the $-CH_2D$ species, and the reverse in the $-CHD_2$ species, the differences being ± 9 cm^{-1} for -OH species and ± 10 cm^{-1} for -OD species. These predictions were approximately confirmed by study of rotamer interconversion rates in low-temperature inert-gas matrices[62]. The results were held to be consistent with the methyl in-plane (trans) C-H stretching force-constant being greater than the out of plane (gauche) force constants. This is also directly evident from the CHD_2 species (i.e. ~isolated) methyl stretching frequencies which were reported (in cm^{-1});

	CHD_2OH	CHD_2OD
ν_t (C-H)	2978.8	2980.2
ν_g (C-H)	2919.3	2919.5

Note, incidentally, that the trans-gauche splitting of ν(C-H) is in the opposite sense to that found for methylamine (lone-pair trans effect[64]).

Nitrosomethane and Acetaldehyde

McKean[23] has reported the methyl C-H stretching frequencies of CHD_2CHO as (in cm^{-1});

ν_c(C-H) = 3002

ν_g(C-H) = 2945

Using these data, as before, gives a contribution to $\Delta V'_{g-c}$ of +8.12 cm^{-1}. This is in good agreement with an estimate of +8.33 cm^{-1} obtained from a more complete normal co-ordinate analysis[26]. It is also in agreement with the direction of shift obtained from the microwave analysis of CH_2DCHO data ($\Delta E'_{g-c}$ = 15.55 cm^{-1}). The C-H stretching contribution is, of course, not expected to account completely for the observed torsional spacing, but it is probably the main single contributor. Moreover, the same situation should be expected to prevail in nitrosomethane since there is some

indication that, in general, for a $-CH_3$ group adjacent to a double bond, the C-H bond in the plane of the double bond is stronger than the out of plane bond[23].

Concluding Remarks

It is clear that a major contribution to the conformer zero-point energy differences, in molecules with a partially deuterated methyl group, is attributable to asymmetry in the C-H stretching force-constants. Such a conclusion is consistent with the observation that isolated C-H stretching frequencies differ between conformers of the same molecule[23] and is also a further indication that, in general, the methyl group does not possess C_{3v} symmetry, but has only the symmetry of the molecule as a whole. This asymmetry, in the case of acetaldehyde, has also been predicted by the high-level ab-initio calculations of Pulay[24]. Furthermore, the ordering of the torsional eigenvalues in partially deuterated species is dictated by the resulting vibrational contribution, unless changes in torsion-vibration coupling, or the α dependence of the internal rotation constant, make contributions which offset this effect.

The observation that the symmetry of the methyl group is affected by its environment relates also to the extramolecular surroundings. McPhail, Snyder and Strauss[65] have made solid-state variable-temperature studies of the splitting of the asymmetric stretching vibrations of the $-CH_3$ terminus in long-chain alkanes. The stretching frequencies, and hence force-constants, were found to exhibit an apparent cos 5α dependence in the region of the torsional minimum, this being attributable, at least in part, to inter-molecular effects. Such environmental effects also relate to other systems. For example, by freezing out the 180° flipping motion of weakly bound HOD in the crystalline hydrates $NaClO_4.H_2O$ and $LiI.3H_2O$, two distinct O-D stretching frequencies are observed[66]. Similarly it has been shown that

NH_3D^+ ions, in NH_4ClO_4 crystals, have four possible orientations of the N-D bond at low temperatures, two of which are degenerate[67].

CH_2DNO AND CHD_2NO DATA

Raw data and details of least-squares data adjustments are given in the following pages.

Hypothetical line centres for gauche-CH_2DNO (Table 15) and gauche-CHD_2NO (Table 21) were fitted to the Hamiltonian given on page 21, using the computer program given in Appendix 7. Hypothetical centres for the cis-forms (Tables 19 and 25), obtained mainly from reference 17, were fitted to the v=0 part of the same Hamiltonian. Additions to the cis-data sets, made during the course of this work, are given in Tables 20 and 26.

Individual hyperfine components and residuals from the quadrupole fit are given in Tables 16 (for CH_2DNO) and 22 (for CHD_2NO). F is the total angular momentum quantum number. $\Delta F = \pm 1$ transitions are labelled $F' \leftarrow F$, $\Delta F = 0$ transitions are labelled with a single F (i.e. implying $F \leftarrow F$). Where two quadrupole components overlap, the frequency is taken to be the intensity weighted average of the two. Relative intensities of quadrupole hyperfine components were obtained from reference 42. The anomalous $J=1 \rightarrow 2$ hyperfine patterns of gauche-CH_2DNO have already been given on page 40.

State mixing parameters, which were used to correct the observed quadrupole splittings for the effects of internal rotation (see pages 36 - 38 for details) are given in Tables 17 and 23. After correction, splittings were fitted to χ_{aa} and $(\chi_{bb} - \chi_{cc})$ (Tables 18 and 24) using the computer program given in Appendix 4. $\langle P_a^2 \rangle$, $\langle P_b^2 \rangle$ and $\langle P_c^2 \rangle$ values were obtained from rigid-rotor calculations, using the effective PAS rotational constants which appear in Tables 2 and 3 (pages 32 and 35). (+) and (-) states were treated separately for this purpose.

The unresolvable effects of deuterium (I=1) quadrupole coupling were neglected throughout.

TABLE 15

Gauche Mono-deutero Nitrosomethane. CH2DNO.

A REDUCTION REPRESENTATION IIR

UPPER LEVEL				LOWER LEVEL							V=0 CHAR	
V	J	Ka	Kc	V	J	Ka	Kc	OBS/MHz	OBS-CALC	WEIGHT	%U	%L
1	1	0	1	- 1	0	0	0	20218.55	-0.010		0	- 0
0	1	0	1	- 0	0	0	0	20220.32	0.060		100	- 100
0	2	1	2	- 0	1	1	1	39569.95	0.148		92	- 97
1	2	1	1	- 1	1	1	0	41304.32	-0.012		8	- 3
1	2	0	2	- 1	1	0	1	40423.68	0.051		0	- 0
0	2	0	2	- 0	1	0	1	40427.20	0.166		100	- 100
0	2	1	1	- 1	1	1	1	41167.40	-0.082		75	- 30
0	2	1	1	- 0	1	1	0	41833.20	-0.196		75	- 70
1	2	1	2	- 1	1	1	1	39045.38	0.005		25	- 30
1	2	1	2	- 0	1	1	0	39711.48	0.190		25	- 70
1	3	0	3	- 1	2	1	2	16179.07	0.046		0	- 25
0	3	0	3	- 0	2	1	2	15924.02	0.014		100	- 92
0	4	0	4	- 0	3	1	3	37358.67	-0.084		100	- 90
1	4	0	4	- 1	3	1	3	37593.41	-0.030		0	- 18
0	4	1	3	- 0	4	1	4	9030.72	-0.133		84	- 89
1	4	1	3	- 1	4	1	4	9007.73	-0.044		11	- 16
1	5	1	4	- 1	5	1	5	13491.17	-0.019		12	- 15
0	5	1	4	- 0	5	1	5	13525.69	0.011		85	- 88
1	6	1	5	- 1	6	1	6	18871.83	0.002		12	- 15
0	6	1	5	- 0	6	1	6	18919.87	-0.037		85	- 88
1	6	1	6	- 0	6	0	6	37978.18	-0.208		15	- 100
0	7	1	6	- 0	6	2	5	15967.30	-0.673	0.000	86	- 86
0	7	1	6	- 0	7	1	7	25207.33	-0.069		86	- 87
1	7	1	6	- 1	7	1	7	25143.58	-0.021		13	- 14
1	8	1	7	- 1	8	1	8	32298.76	-0.028		13	- 14
0	8	1	7	- 0	8	1	8	32380.51	0.127		86	- 87
0	8	1	7	- 0	7	2	6	39548.32	-0.199		86	- 75
1	8	1	7	- 0	7	2	5	40081.81	0.068		13	- 71
0	9	1	8	- 0	9	1	9	40432.47	4.485	0.000	86	- 87
1	9	1	8	- 1	9	1	9	40326.66	0.095		13	- 14
1	10	1	10	- 1	9	2	7	34800.21	1.873	0.000	14	- 36
0	11	2	9	- 0	11	2	10	9102.56	-0.054		51	- 57
1	11	2	9	- 1	11	2	10	9108.34	-0.090		40	- 51
0	12	2	10	- 0	12	2	11	12519.98	-0.038		53	- 56
1	12	2	10	- 1	12	2	11	12526.68	-0.095		41	- 50
0	13	2	11	- 0	13	2	12	16734.62	-0.023		55	- 55
1	13	2	12	- 1	12	3	10	28332.95	-0.013		49	- 18
0	13	2	12	- 1	12	3	9	27973.83	0.108		55	- 5
0	13	4	10	- 0	14	3	11	35481.11	-0.003		100	- 59
1	13	4	9	- 1	14	3	12	37392.38	0.088		0	- 41
0	13	4	9	- 0	14	3	12	37094.40	-0.007		100	- 90
1	13	4	10	- 1	14	3	11	35784.18	-0.041		0	- 11
1	13	2	11	- 1	13	2	12	16741.80	-0.109		41	- 49
0	14	2	12	- 0	14	2	13	21807.26	0.067		56	- 55
0	14	4	11	- 0	15	3	12	14391.69	-2.741	0.000	100	- 68
0	14	4	10	- 0	15	3	13	16708.72	-3.163	0.000	100	- 87
1	14	4	10	- 1	15	3	13	16977.14	0.086		0	- 31
1	14	4	11	- 1	15	3	12	14666.90	-0.127		0	- 14
1	14	2	12	- 1	14	2	13	21814.20	-0.098		41	- 48
0	15	2	13	- 0	15	2	14	27783.72	0.144		57	- 54
1	15	2	13	- 1	15	2	14	27789.62	-0.006		40	- 48
0	16	2	14	- 0	16	2	15	34694.78	0.063		59	- 54
1	16	2	14	- 1	16	2	15	34698.65	0.013		40	- 48

TABLE 15 (cont/d)

UPPER LEVEL V J Ka Kc		LOWER LEVEL V J Ka Kc	OBS/MHz	OBS-CALC	WEIGHT	V=0 CHAR %U	%L
0 17 3 15	-	0 16 4 12	23931.65	1.816	0.000	83 -	99
1 17 3 15	-	1 16 4 12	23708.70	-0.182		24 -	1
1 17 3 14	-	1 16 4 13	28376.46	0.168		18 -	1
0 17 3 14	-	0 16 4 13	28610.84	-0.022		74 -	99
0 19 3 16	-	0 19 3 17	8516.03	-0.031		75 -	81
1 19 3 16	-	1 19 3 17	8495.17	0.007		22 -	22
0 20 3 17	-	0 20 3 18	11317.25	0.009		74 -	80
1 20 3 17	-	1 20 3 18	11291.91	0.003		23 -	22
0 21 3 18	-	0 21 3 19	14782.93	0.024		74 -	80
1 21 3 18	-	1 21 3 19	14753.02	-0.024		25 -	22
1 22 4 19	-	1 21 5 16	35511.40	-9.164	0.000	3 -	1
0 22 4 18	-	0 21 5 17	36998.40	27.042	0.000	97 -	99
1 22 4 18	-	1 21 5 17	36951.78	-9.933	0.000	3 -	2
1 22 3 19	-	1 22 3 20	18963.76	-0.104		27 -	22
0 22 3 19	-	0 22 3 20	18998.13	0.034		72 -	79
0 22 4 19	-	0 21 5 16	35553.15	27.870	0.000	97 -	98
0 23 3 20	-	0 23 3 21	24042.26	0.131		71 -	79
1 23 3 20	-	1 23 3 21	24003.89	-0.065		29 -	22
0 24 3 21	-	0 24 3 22	29985.46	0.057		69 -	78
1 24 3 21	-	1 24 3 22	29943.83	-0.151		31 -	22
0 25 3 22	-	0 25 3 23	36885.80	-0.048		67 -	78
1 25 3 22	-	1 25 3 23	36842.16	0.066		32 -	22
0 28 4 24	-	0 28 4 25	8866.35	0.409		91 -	94
1 28 4 24	-	1 28 4 25	8851.22	0.242		9 -	6
0 29 4 25	-	0 29 4 26	11479.27	-0.435		90 -	93
1 29 4 25	-	1 29 4 26	11463.11	-0.302		11 -	7
1 30 4 26	-	1 30 4 27	14672.11	0.210		12 -	8

Parameter	Value	E.S.D.
DE/MHz	922.008347	0.193892
Txz/MHz	306.309407	0.038356
Tj/KHz	2.367001	0.798601
Tk1/KHz	-0.000058	0.000010
Tk2/KHz	-0.186310	0.019902
X0/MHz	9780.723283	0.040245
Y0/MHz	56038.716350	0.094162
Z0/MHz	10439.568946	0.040912
X1/MHz	9781.038728	0.039704
Y1/MHz	56037.841299	0.102322
Z1/MHz	10437.553551	0.042478
DJ0/KHz	443.808742	1.425225
DJK0/KHz	-1221.981659	8.095396
DK0/KHz	793.642359	6.835300
dJ0/KHz	-218.451724	0.886524
dK0/KHz	390.712437	3.320968
DJ1/KHz	451.072583	1.915322
DJK1/KHz	-1232.032436	9.477156
DK1/KHz	795.595322	7.708544
dJ1/KHz	-222.043415	1.076902
dK1/KHz	392.286146	3.742169

Weighted S.D. of Fit 0.148955 MHz

TABLE 16

Transitions Showing Resolvable Hyperfine Structure

Gauche-CH_2DNO R-Branch

(For discussion of J = 1 → 2 Transitions see text)

Transition	F′← F	Obs/MHz	Relative to Hyp.Cent/MHz	Obs-Calc	χ/MHz
$3^+_{03} - 2^+_{12}$	3,2 - 2	15925.54	1.52	0.098	-6.09 (16)
	4,3 - 3	15923.54	-0.48	-0.072	Weak line
	2 - 1	15922.60	-1.42	-0.007	
$3^-_{03} - 2^-_{12}$	3,2 - 2	16180.58	1.51	0.088	-6.05 (16)
	4,3 - 3	16178.58	-0.49	-0.082	Weak line
	2 - 1	16177.69	-1.38	0.033	
$4^+_{04} - 3^+_{13}$	4,3 - 3	37360.01	1.34	-0.006	-5.36 (16)
	5,4 - 4	37358.23	-0.44	0.008	
	3 - 2	37357.59	-1.08	-0.002	
$4^-_{04} - 3^-_{13}$	4,3 - 3	37594.65	1.24	-0.106	-4.97 (16)
	5,4 - 4	37593.00	-0.41	0.038	Partially
	3 - 2	37592.40	-0.01	0.068	resolved
$7^+_{16} - 6^+_{25}$	7 - 6	15968.63	1.33	-0.073	-5.31 (19)
	8 - 7, 6 - 5	15966.64	-0.66	0.039	Weak line
$8^+_{17} - 7^+_{26}$	8 - 7	39549.66	1.34	-0.041	-5.36 (19)
	9 - 8, 7 - 6	39547.65	-0.67	0.019	
$8^-_{17} - 7^-_{26}$	8 - 7	-			
	9 - 8, 7 - 6	40081.14	-0.67	0	
$10^-_{1,10} - 9^-_{27}$	9 - 8	34801.43	1.22	0.001	+8.29 (16)
	11 - 10	34801.09	0.88	-0.027	
	10 - 9	34798.14	-2.07	0.025	
$13^+_{2,12} - 12^-_{39}$	12 - 11, 14 - 13	27974.01	+0.18	0	
	13 - 12	27973.5			
$13^-_{2,12} - 12^+_{39}$	12 - 11, 14 - 13	28333.10	0.15	-0.034	
	13 - 12	28332.66	-0.29	0.078	

Cont/d

TABLE 16 Cont/d

Gauche-CH_2DNO Q-Branch

Transition	F	Obs/MHz	Relative to Hyp.Cent/MHz	Obs-Calc	χ/MHz
$4^+_{13} - 4^+_{14}$	4	9033.53	2.81	-0.060	-11.24 (16)
	5	9029.70	-1.02	0.024	
	3	9028.71	-2.01	0.040	
$4^-_{13} - 4^-_{14}$	4	9010.58	2.85	-0.020	-11.38 (16)
	5	9006.67	-1.06	-0.016	
	3	9005.73	-2.00	0.050	
$5^+_{14} - 5^+_{15}$	5	13528.55	2.86	-0.009	-11.47 (16)
	6	13524.54	-1.15	-0.047	
	4	13523.81	-1.88	0.033	
$5^-_{14} - 5^-_{15}$ (JH)	5	13494.07	2.90	0.031	-11.61 (16)
	6	13490.04	-1.13	-0.027	
	4	13489.24	-1.93	-0.017	
$6^+_{15} - 6^+_{16}$ (JH)	6	18922.74	2.87	0.003	-11.47 (16)
	7	18918.74	-1.13	0.017	
	5	18918.03	-1.84	-0.016	
$6^-_{15} - 6^-_{16}$ (JH)	6	18874.73	2.90	0.033	-11.59 (16)
	7	18870.68	-1.15	-0.003	
	5	18869.98	-1.85	-0.026	
$6^-_{16} - 6^+_{06}$	7, 5	37978.83	0.65	0.039	+5.23 (19)
	6	37976.87	-1.31	-0.087	weak
$7^+_{16} - 7^+_{17}$ (JH)	7	25210.20	2.87	0.007	-11.48 (16)
	8	25206.14	-1.19	-0.011	
	6	25205.57	-1.76	0.002	
$7^-_{16} - 7^-_{17}$ (JH)	7	25146.44	2.86	-0.003	-11.43 (16)
	8	25142.41	-1.17	0.009	
	6	25141.82	-1.76	0.002	
$8^+_{17} - 8^+_{18}$ (JH)	8	32383.36	2.85	-0.006	-11.41 (16)
	9	32379.30	-1.21	-0.007	
	7	32378.80	-1.71	0.004	
$8^-_{17} - 8^-_{18}$ (JH)	8	32301.62	2.86	0.004	-11.45 (16)
	9	32297.56	-1.20	0.003	
	7	32297.03	-1.73	-0.016	
$9^+_{18} - 9^+_{19}$	9	40435.31	2.84	-0.008	-11.38 (16)
	10	40431.26	-1.21	0.010	
	8	40430.78	-1.69	-0.015	
$9^-_{18} - 9^-_{19}$	9	40329.50	2.84	-0.007	-11.36 (16)
	10	40325.44	-1.22	0.000	
	8	40324.99	-1.67	0.005	
$11^+_{29} - 11^+_{2,10}$	11	9103.39	0.83	-0.009	-3.31 (19)
	10,12	9102.15	-0.41	0.009	
$11^-_{29} - 11^-_{2,10}$	11	9109.16	0.82	-0.021	-3.28 (19)
	10,12	9107.93	-0.41	0.011	
$12^+_{2,10} - 12^+_{2,11}$	12	12520.95	0.97	0.005	-3.87 (19)
	11,13	12519.50	-0.48	0.003	
$12^-_{2,10} - 12^-_{2,11}$	12	12527.65	0.97	0.003	-3.87 (19)
	11,13	12526.20	-0.48	0.004	

Cont/d

TABLE 16 Cont/d

Gauche-CH_2DNO Q-Branch

Transition	F	Obs/MHz	Relative to Hyp.Cent/MHz	Obs-Calc	χ/MHz
$13^{+}_{2,11} - 13^{+}_{2,12}$	13 12,14	16735.72 16734.07	1.10 -0.55	0.012 -0.006	-4.40 (19)
$13^{-}_{2,11} - 13^{-}_{2,12}$	13 12,14	16742.90 16741.25	1.10 -0.55	0.010 -0.005	-4.40 (19)
$14^{+}_{2,12} - 14^{+}_{2,13}$	14 13,15	21808.45 21806.66	1.19 -0.60	-0.017 0.004	-4.77 (19)
$14^{-}_{2,12} - 14^{-}_{2,13}$	14 13,15	21815.40 21813.60	+1.20 -0.60	-0.009 0.005	-4.80 (19)
$15^{+}_{2,13} - 15^{+}_{2,14}$	15 14,16	27785.07 27783.04	1.35 -0.68	0.032 -0.021	-5.41 (19)
$15^{-}_{2,13} - 15^{-}_{2,14}$	15 14,16	27790.94 27788.96	1.32 -0.66	0.000 0.000	-5.28 (19)
$16^{+}_{2,14} - 16^{+}_{2,15}$	16 15,17	34696.22 34694.06	1.44 -0.72	0.020 -0.010	-5.76 (19)
$16^{-}_{2,14} - 16^{-}_{2,15}$	16 15,17	34700.11 34697.92	1.46 -0.73	0.037 -0.019	-5.84 (19)
$19^{-}_{3,16} - 19^{-}_{3,17}$	19 18,20	8516.42 8515.84	+0.39 -0.19	-0.014 0.013	
$19^{+}_{3,16} - 19^{+}_{3,17}$	19 18,20	8495.56 8494.98	+0.39 -0.19	-0.012 0.012	
$20^{-}_{3,17} - 20^{-}_{3,18}$	20 19,21	11317.71 11317.02	0.46 -0.23	-0.020 0.011	
$20^{+}_{3,17} - 20^{+}_{3,18}$	20 19,21	11292.40 11291.66	0.49 -0.25	0.012 -0.011	
$21^{-}_{3,18} - 21^{-}_{3,19}$	21 20,22	14783.46 14782.66	0.53 -0.27	-0.032 0.012	
$21^{+}_{3,18} - 21^{+}_{3,19}$	21 20,22	14753.57 14752.74	0.55 -0.28	-0.010 0.001	
$22^{-}_{3,19} - 22^{-}_{3,20}$	22 21,23	18998.78 18997.80	0.65 -0.33	0.001 -0.005	
$22^{+}_{3,19} - 22^{+}_{3,20}$	22 21,23	18964.38 18963.45	0.62 -0.31	-0.026 0.014	
$23^{-}_{3,20} - 23^{-}_{3,21}$	23 22,24	24043.01 24041.89	0.75 -0.37	0.012 0.000	
$23^{+}_{3,20} - 23^{+}_{3,21}$	23 22,24	24004.63 24003.52	0.74 -0.37	0.005 -0.002	
$24^{-}_{3,21} - 24^{-}_{3,22}$	24 23,25	29986.31 29985.04	0.85 -0.42	0.022 -0.005	
$24^{+}_{3,21} - 24^{+}_{3,22}$	24 23,25	29944.69 29943.40	0.86 -0.43	0.035 -0.017	
$25^{-}_{3,22} - 25^{-}_{3,23}$	25 24,26	36886.77 36885.32	0.97 -0.48	0.052 -0.020	
$25^{+}_{3,22} - 25^{+}_{3,23}$	25 24,26	36843.09 36841.70	0.93 -0.46	0.015 -0.001	

Note: (JH) obtained from Ref. 43.

TABLE 17

State Mixing Parameters CH_2DNO Q_a = 313.22 MHz

ψ_1	ψ_2	$\lvert E_1^\circ - E_2^\circ \rvert$ /MHz	Ø/°	Cos^2 Ø	Sin^2 Ø
1^+_{10}	1^-_{11}	225.8	35.09	0.6695	0.3305
1^-_{10}	1^+_{11}	1574.1	10.85	0.9646	0.0354
2^+_{11}	2^-_{12}	2029.1	8.58	0.9778	0.0222
2^-_{11}	2^+_{12}	3370.6	5.26	0.9916	0.0084
3^+_{12}	3^-_{13}	4733.8	3.77	0.9957	0.0043
3^-_{12}	3^+_{13}	6065.3	2.95	0.9974	0.0026
4^+_{13}	4^-_{14}	8339.6	2.15	0.9986	0.0014
4^-_{13}	4^+_{14}	9657.7	1.86	0.9990	0.0010
5^+_{14}	5^-_{15}	12845.2	1.40	0.9994	0.0006
5^-_{14}	5^+_{15}	14146.5	1.27	0.9995	0.0005
6^+_{15}	6^-_{16}	18248.2	0.98	0.9997	0.0003
6^-_{15}	6^+_{16}	19529.3	0.92	0.9997	0.0003
7^+_{16}	7^-_{17}	24544.4	0.73	0.9998	0.0002
7^-_{16}	7^+_{17}	25802.0	0.69	0.9999	0.0001
8^+_{17}	8^-_{18}	31727.0	0.57	0.9999	0.0001
8^-_{17}	8^+_{18}	32957.6	0.54	0.9999	0.0001
9^+_{18}	9^-_{19}	39785.9	0.45	0.9999	0.0001
9^-_{18}	9^+_{19}	40986.1	0.44	0.9999	0.0001
$10^-_{1.10}$	10^+_{19}	48706.8	0.37	1.0000	0.0000
6^+_{25}	6^-_{24}	823.7	18.63	0.8980	0.1020
7^+_{26}	7^-_{25}	1543.2	11.05	0.9633	0.0367
9^-_{27}	9^+_{28}	4136.1	4.31	0.9944	0.0056
$11^+_{2,10}$	11^-_{29}	8880.6	2.02	0.9988	0.0012
$11^-_{2,10}$	11^+_{29}	9228.2	1.94	0.9989	0.0011
$12^+_{2,11}$	$12^-_{2,10}$	12282.9	1.46	0.9994	0.0006
$12^-_{2,11}$	$12^+_{2,10}$	12672.1	1.42	0.9994	0.0006

Cont/d

TABLE 17 (Cont/d)

State Mixing Parameters CH_2DNO Q_a = 313.22 MHz

ψ_1	ψ_2	$\lvert E_2^o - E_1^o \rvert$ /MHz	ø/°	$\cos^2$ ø	$\sin^2$ ø
$13^+_{2,12}$	$13^-_{2,11}$	16475.8	1.09	0.9996	0.0004
$13^-_{2,12}$	$13^+_{2,11}$	16910.7	1.06	0.9997	0.0003
$14^+_{2,13}$	$14^-_{2,12}$	21521.2	0.83	0.9998	0.0002
$14^-_{2,13}$	$14^+_{2,12}$	22006.5	0.82	0.9998	0.0002
$15^+_{2,14}$	$15^-_{2,13}$	27466.0	0.65	0.9999	0.0001
$15^-_{2,14}$	$15^+_{2,13}$	28006.5	0.64	0.9999	0.0001
$16^+_{2,15}$	$16^-_{2,14}$	34341.6	0.52	0.9999	0.0001
$16^-_{2,15}$	$16^+_{2,14}$	34942.7	0.51	0.9999	0.0001

TABLE 18

Program Chi.

Quadrupole data - g-CH_2DNO.

Number of observations = 32

J						Obs/MHz	Res/MHz	Weight
2+	1	2-	3+	0	3	-6.19000	-0.50123	0.00000
2-	1	2-	3-	0	3	-6.31000	-0.62202	0.00000
3+	1	3-	4+	0	4	-5.39000	-0.00410	1.00000
3-	1	3-	4-	0	4	-5.02000	0.36459	0.00000
4+	1	3-	4+	1	4	-11.27000	0.21161	1.00000
4-	1	3-	4-	1	4	-11.41000	0.07160	1.00000
5+	1	4-	5+	1	5	-11.49000	-0.01379	1.00000
5-	1	4-	5-	1	5	-11.63000	-0.15384	1.00000
6+	1	5-	6+	1	6	-11.48000	-0.01368	1.00000
6-	1	5-	6-	1	6	-11.60000	-0.13378	1.00000
6-	1	6-	6+	0	6	5.23000	0.33680	0.00000
6+	2	5-	7+	1	6	-5.43000	0.18194	0.00000
7+	1	6-	7+	1	7	-11.48000	-0.02987	1.00000
7-	1	6-	7-	1	7	-11.43000	0.01994	1.00000
7+	2	6-	8+	1	7	-5.42000	0.10371	0.70914
8+	1	7-	8+	1	8	-11.41000	0.01553	1.00000
8-	1	7-	8-	1	8	-11.45000	-0.02480	1.00000
9+	1	8-	9+	1	9	-11.38000	0.01015	1.00000
9-	1	8-	9-	1	9	-11.36000	0.02962	1.00000
9-	2	7-10-		1	10	8.28000	-0.10172	1.00000
11+	2	9-11+		2	10	-3.31000	0.04678	0.70914
11-	2	9-11-		2	10	-3.28000	0.08466	0.70914
12+	2	10-12+		2	11	-3.87000	-0.01097	0.70914
12-	2	10-12-		2	11	-3.87000	-0.00244	0.70914
13+	2	11-13+		2	12	-4.40000	-0.04751	0.70914
13-	2	11-13-		2	12	-4.40000	-0.03856	0.70914
14+	2	12-14+		2	13	-4.77000	0.05635	0.70914
14-	2	12-14-		2	13	-4.80000	0.03549	0.70914
15+	2	13-15+		2	14	-5.41000	-0.13834	0.70914
15-	2	13-15-		2	14	-5.28000	0.00075	0.70914
16+	2	14-16+		2	15	-5.76000	-0.07824	0.70914
16-	2	14-16-		2	15	-5.84000	-0.14940	0.70914

E.S.D. of an Observation/MHz = 0.07981/sqrt(Weight)

Chiaa =	0.45442	MHz	esd	0.26156
Chibb-Chicc =	-11.48486	MHz	esd	0.02127
Chibb =	-5.96964	MHz	esd	0.13121
Chicc =	5.51522	MHz	esd	0.13121

TABLE 19

Cis Mono-deutero Nitrosomethane, s-CH2DNO.

A REDUCTION REPRESENTATION IIR

UPPER LEVEL J	Ka	Kc		LOWER LEVEL J	Ka	Kc	OBS/MHz	OBS-CALC	WEIGHT
1	0	1	-	0	0	0	20887.31	-0.027	
1	1	0	-	1	0	1	41705.62	0.007	
2	0	2	-	1	0	1	41736.97	-0.034	
2	1	2	-	1	1	1	40344.36	-0.025	
3	1	2	-	3	1	3	8578.52	0.037	
3	2	2	-	4	1	3	32370.86	-0.154	
3	0	3	-	2	1	2	23628.32	-0.117	
4	1	3	-	4	1	4	14293.66	-0.007	
4	2	2	-	5	1	5	30040.87	0.084	
5	1	4	-	5	1	5	21428.82	0.038	
6	1	5	-	6	1	6	29971.26	0.021	
7	3	5	-	8	2	6	32015.09	0.206	
7	3	4	-	8	2	7	39682.10	0.078	
7	1	6	-	7	1	7	39899.29	-0.079	
8	3	5	-	9	2	8	19999.49	-0.092	
9	1	9	-	8	2	6	23716.29	-0.035	
9	2	7	-	9	2	8	11598.16	-0.021	
10	2	8	-	10	2	9	16931.61	-0.059	
10	2	8	-	9	3	7	16661.80	-0.327	0.000
10	1	10	-	9	2	7	32794.89	-0.035	
11	1	11	-	10	2	8	39779.55	0.043	
11	4	7	-	12	3	10	34678.52	0.091	
11	4	8	-	12	3	9	31676.51	-0.072	
11	2	9	-	11	2	10	23660.25	-0.058	
12	2	11	-	11	3	8	35404.69	-1.046	0.000
12	2	10	-	12	2	11	31861.46	-0.019	
13	2	11	-	13	2	12	41570.43	0.074	
15	3	12	-	14	4	11	38642.06	0.237	
15	5	11	-	16	4	12	30064.19	31.480	0.000
15	5	10	-	16	4	13	31032.66	-25.221	0.000
15	3	13	-	14	4	10	27946.90	0.185	
15	3	12	-	15	3	13	10339.50	-0.019	
16	3	13	-	16	3	14	14689.25	-0.044	
17	3	14	-	17	3	15	20278.80	-1.056	0.000
18	4	15	-	17	5	12	12133.27	0.024	
18	3	15	-	18	3	16	27273.83	6.811	0.000
18	4	14	-	17	5	13	14690.82	0.229	
19	4	16	-	18	5	13	33758.06	-0.349	
19	4	15	-	18	5	14	37632.99	-0.207	
19	6	14	-	20	5	15	27701.19	-0.000	
19	6	13	-	20	5	16	28026.86	-0.062	
19	3	16	-	19	3	17	35790.83	17.047	0.000
22	5	18	-	21	6	15	15596.87	-0.002	
22	5	17	-	21	6	16	16424.30	-0.216	
22	4	18	-	22	4	19	11191.05	-0.003	
23	5	19	-	22	6	16	37544.82	0.142	
23	4	19	-	23	4	20	15420.03	6.533	0.000
23	5	18	-	22	6	17	38819.50	0.091	
24	4	20	-	24	4	21	20818.63	11.532	0.000
25	4	21	-	25	4	22	27568.25	19.213	0.000
26	4	22	-	26	4	23	35828.96	30.606	0.000

Table 19 (cont/d)

Parameter	Value	E.S.D.
X/MHz	9729.113808	0.016168
Y/MHz	51434.831547	0.072564
Z/MHz	11158.256217	0.019133
DJ/KHz	227.939324	0.648483
DJK/KHz	-612.156829	4.594572
DK/KHz	398.045981	3.970959
dJ/KHz	-110.401884	0.388188
dK/KHz	194.708118	1.947767
HJ/Hz	1.031511	0.592809
HJK/Hz	-1.393108	2.414325
HKJ/Hz	-1.153422	2.358022
HK/Hz	1.128219	0.647459

Weighted S.D. of Fit 0.138488 MHz.

DETERMINABLE ROT. CONSTS./MHz

9728.788918 51434.843882 11158.712096

TABLE 20

Cis - CH_2DNO Additions to existing data set[17]

Transition	F' - F	Obs/MHz	Hyp.Cent/MHz
$1_{10} - 1_{01}$	1 - 2,1,0 2 - 2,1 0 - 1	41706.92 41705.38 41702.89	41705.62
$2_{02} - 1_{01}$	all	41736.97	
$2_{12} - 1_{11}$	1 - 1 3 - 2} 2 - 1} 2 - 2} 1 - 0}	40347.12 40344.48 40342.75	40344.36
$7_{16} - 7_{17}$	7 - 7 8 - 8 6 - 6	39902.13 39898.14 39897.53	39899.29
$10_{28} - 9_{37}$	10 - 9 11 - 10} 9 - 8}	16662.65 16661.38	16661.80
$13_{2,11} - 13_{2,12}$	13 - 13 14 - 14} 12 - 12}	41571.96 41569.66	41570.43
$22_{5,17} - 21_{6,16}$	all	16424.30	
$22_{5,18} - 21_{6,15}$	all	15596.87	
$22_{4,18} - 22_{4,19}$	22 - 22 21 - 21} 23 - 23}	11191.37 11190.89	11191.05
$23_{4,19} - 23_{4,20}$	23 - 23 22 - 22} 24 - 24}	15420.42 15419.84	15420.03
$23_{5,18} - 22_{6,17}$	all	38819.50	
$23_{5,19} - 22_{6,16}$	all	37544.82	
$24_{4,20} - 24_{4,21}$	24 - 24 23 - 23} 25 - 25}	20819.11 20818.39	20818.63
$25_{4,21} - 25_{4,22}$	25 - 25 24 - 24} 26 - 26}	27568.84 27567.96	27568.25
$26_{4,22} - 26_{4,23}$	26 - 26 25 - 25} 27 - 27}	35829.62 35828.63	35828.96

TABLE 21

Gauche Di-deutero Nitrosomethane. CHD2NO.

A REDUCTION REPRESENTATION IIR

UPPER LEVEL					LOWER LEVEL						V=0 CHAR	
V	J	Ka	Kc		V	J	Ka	Kc	OBS/MHz	OBS-CALC	WEIGHT	%U - %L
1	1	0	1	-	1	0	0	0	19537.070	0.113		0 - 0
0	1	1	0	-	0	1	0	1	38574.720	-0.064		67 - 100
1	1	1	0	-	1	1	0	1	38474.460	-0.095		20 - 0
0	1	0	1	-	0	0	0	0	19538.120	-0.002		100 - 100
1	2	1	2	-	1	1	1	1	37947.530	0.026		28 - 33
0	2	1	2	-	0	1	1	1	37946.590	0.065		76 - 80
0	2	0	2	-	0	1	0	1	39050.730	0.027		100 - 100
1	2	0	2	-	1	1	0	1	39048.350	-0.009		0 - 0
0	2	1	1	-	0	2	0	2	39727.020	-0.006		72 - 100
1	2	1	1	-	1	2	0	2	39627.620	-0.031		24 - 0
0	2	1	1	-	0	1	1	0	40202.970	0.025		72 - 67
1	2	1	1	-	1	1	1	0	40201.480	0.025		24 - 20
1	3	1	2	-	1	3	0	3	41409.030	0.003		25 - 0
0	3	0	3	-	0	2	1	2	22186.460	0.071		100 - 76
1	3	0	3	-	1	2	1	2	22278.550	0.042		0 - 28
0	3	1	2	-	0	3	0	3	41508.320	0.006		73 - 100
0	4	1	3	-	0	4	1	4	11321.670	-0.049		73 - 74
1	4	1	3	-	1	4	1	4	11309.650	0.091		26 - 27
0	5	1	4	-	0	5	1	5	16974.710	-0.027		73 - 74
0	5	1	5	-	1	5	0	5	30040.020	-0.117		74 - 0
1	5	1	5	-	0	5	0	5	30303.800	0.016		27 - 100
1	5	1	4	-	1	5	1	5	16956.750	0.025		26 - 27
1	6	1	5	-	1	6	1	6	23722.230	0.020		26 - 27
0	6	1	5	-	0	6	1	6	23747.100	0.048		73 - 74
1	6	1	6	-	0	6	0	6	27584.290	0.043		27 - 99
0	6	1	6	-	1	6	0	6	27328.090	0.112		74 - 1
0	7	3	5	-	0	8	2	6	29410.920	-0.125		100 - 74
1	7	3	4	-	1	8	2	7	34725.230	-0.065		0 - 24
1	7	1	6	-	0	6	2	5	38263.640	-0.086		26 - 80
1	7	1	6	-	1	7	1	7	31593.420	-0.077		26 - 27
0	7	1	6	-	0	7	1	7	31626.040	-0.008		73 - 74
0	7	1	6	-	1	6	2	5	38112.640	0.072		73 - 26
0	7	3	4	-	0	8	2	7	34646.890	0.075		100 - 78
1	7	3	5	-	1	8	2	6	29493.270	0.073		0 - 24
1	8	1	7	-	1	8	1	8	40550.480	-0.092		26 - 27
0	8	1	7	-	0	8	1	8	40591.730	0.128		73 - 74
1	9	1	9	-	0	8	2	6	30343.510	-0.125		27 - 74
0	9	1	9	-	1	8	2	6	30172.450	-0.023		73 - 24
0	9	2	7	-	0	9	2	8	7980.100	0.109		73 - 78
1	9	2	7	-	1	9	2	8	7975.100	-0.131		26 - 23
0	10	2	8	-	0	10	2	9	11721.020	0.153		72 - 78
1	10	2	8	-	1	10	2	9	11714.790	-0.146		27 - 23
1	11	2	9	-	1	11	2	10	16487.640	-0.219		29 - 23
0	11	2	9	-	0	11	2	10	16494.830	0.106		70 - 78
0	11	4	7	-	0	12	3	10	29952.150	0.038		98 - 98
1	11	4	7	-	1	12	3	10	29975.290	0.131		1 - 2
1	11	4	8	-	1	12	3	9	28239.220	-0.075		2 - 2
0	11	4	8	-	0	12	3	9	28213.840	-0.048		99 - 97
0	11	2	9	-	0	10	3	8	37511.090	-0.730	0.000	70 - 99
0	11	2	10	-	0	10	3	7	20414.700	-0.715	0.000	78 - 99
1	11	2	10	-	1	10	3	7	20357.720	0.039		23 - 1
1	11	2	9	-	1	10	3	8	37446.190	-0.062		29 - 1
0	12	2	10	-	0	12	2	11	22384.410	0.118		68 - 78
0	12	2	11	-	0	11	3	8	37828.910	-1.190	0.000	78 - 98
1	12	2	11	-	1	11	3	8	37781.230	0.060		23 - 2
1	12	2	10	-	1	12	2	11	22376.760	-0.125		31 - 23

TABLE 21 (cont/d)

1 13	2 11	-	1 13	2 12	29435.780	-0.116		33	-	22
0 13	2 11	-	0 13	2 12	29443.370	0.001		66	-	78
0 14	2 12	-	0 14	2 13	37696.720	-0.077		64	-	78
1 14	2 12	-	1 14	2 13	37689.870	0.147		36	-	22
0 15	3 12	-	0 14	4 11	35253.290	-0.042		94	-	86
1 15	3 12	-	0 14	4 10	35296.210	0.023		6	-	56
0 15	3 13	-	1 14	4 11	28894.840	-0.030		97	-	44
1 15	3 13	-	1 14	4 10	28943.570	0.077		3	-	14
0 16	3 13	-	0 16	3 14	8819.720	-0.144		92	-	96
1 16	3 13	-	1 16	3 14	8813.160	0.053		8	-	4
1 17	3 14	-	1 17	3 15	12283.960	0.272		10	-	5
0 17	3 14	-	0 17	3 15	12291.320	-0.140		90	-	95
0 18	3 15	-	0 18	3 16	16706.030	-0.651	0.000	88	-	94
1 18	3 15	-	1 18	3 16	16697.570	-0.544	0.000	12	-	6
1 19	3 16	-	1 19	3 17	22181.460	4.772	0.000	15	-	7
0 19	3 16	-	0 19	3 17	22184.920	-0.914	0.000	85	-	93
1 20	3 17	-	1 20	3 18	28825.900	3.803	0.000	18	-	8
0 20	3 17	-	0 20	3 18	28831.730	-0.024		82	-	92
0 21	3 18	-	0 21	3 19	36721.220	1.618	0.000	79	-	91
1 21	3 18	-	1 21	3 19	36718.960	9.789	0.000	21	-	9
0 23	4 19	-	0 23	4 20	8086.040	-0.001		66	-	66
1 23	4 19	-	1 23	4 20	8085.730	0.875	0.000	34	-	34
0 24	4 20	-	0 24	4 21	11039.380	0.111		65	-	66
1 24	4 20	-	1 24	4 21	11037.880	-0.009		35	-	34
0 25	4 21	-	0 25	4 22	14806.940	1.293	0.000	64	-	65
1 25	4 21	-	1 25	4 22	14803.610	-0.026		36	-	35
0 26	4 22	-	0 26	4 23	19523.850	1.317	0.000	63	-	65
1 26	4 22	-	1 26	4 23	19518.010	-0.934	0.000	37	-	35
0 27	4 23	-	0 27	4 24	25321.140	1.620	0.000	62	-	64
1 27	4 23	-	1 27	4 24	25312.050	-0.560	0.000	38	-	36
0 28	4 24	-	0 28	4 25	32317.190	-0.006		61	-	64
1 28	4 24	-	1 28	4 25	32304.090	-0.008		39	-	36
0 29	4 25	-	0 29	4 26	40609.990	-2.879	0.000	60	-	63
1 29	4 25	-	1 29	4 26	40592.340	3.088	0.000	40	-	37

Parameter	Value	E.S.D.
DE/MHz	190.162144	0.144025
Txz/MHz	497.607175	0.098044
Tj/KHz	3.937725	1.104512
Tk1/KHz	-0.000114	0.000048
Tk2/KHz	0.819009	0.163159
X0/MHz	9499.671979	0.182030
Y0/MHz	47721.833673	0.041697
Z0/MHz	10038.483751	0.181160
X1/MHz	9499.712668	0.182720
Y1/MHz	47722.024842	0.040010
Z1/MHz	10037.276485	0.181089
DJ0/KHz	227.866646	1.286739
DJK0/KHz	-596.577966	4.315134
DK0/KHz	392.626669	2.083727
dJ0/KHz	-115.320781	0.519403
dK0/KHz	191.943451	1.017846
DJ1/KHz	228.331803	1.013890
DJK1/KHz	-598.041244	3.603630
DK1/KHz	392.272831	2.067612
dJ1/KHz	-115.432606	0.637038
dK1/KHz	192.372702	0.976697
HJK0/Hz	-0.523023	0.189655
HJK1/Hz	-0.263173	0.184521

Weighted S.D. of Fit: 0.106312 MHz.

TABLE 22

Gauche-CHD_2NO P- and R-Branch

Transition	F' - F	Obs/MHz	Relative to Hyp.Cent/MHz	Obs-Calc	χ/MHz
$2^+_{11} - 1^+_{10}$	2 - 2	40204.66	1.69	-0.097	χ_{110}= -5.22 (9)
	1 - 0	40204.06	1.09	-0.041	
	2 - 1	40203.15	0.18	-0.015	Interference from
	3 - 2	40202.83	-0.14	0.030	$2^-_{11} - 1^-_{10}$
	1 - 1	40200.15	-2.82	0.028	
$2^-_{11} - 1^-_{10}$	2 - 2	-		Obscured by	
	1 - 0	-		$2^+_{11} - 1^+_{10}$	
	2 - 1	40201.63	0.15	-0.045	
	3 - 2	40201.36	-0.12	0.050	
	1 - 1	40198.60	-2.88	-0.032	
$2^+_{12} - 1^+_{11}$	1 - 1	37949.39	2.80	-0.048	
	2 - 2, 2 - 1	37946.71	0.12	0.003	
	2 - 2, 1 - 0	37944.93	-1.66	0.020	
$2^-_{12} - 1^-_{11}$	1 - 1	37950.34	2.81	-0.038	
	3 - 2, 2 - 1	37947.64	0.11	-0.007	
	2 - 2, 1 - 0	37945.91	-1.62	0.060	
$3^+_{03} - 2^+_{12}$	3,2 - 2	22187.86	1.40	0.002	Interference from
	4,3,2 - 3	22186.03	-0.43	-0.030	$19_{3,16} - 19_{3,17}$(-)
	2 - 1	22185.11	-1.35		
$3^-_{03} - 2^-_{12}$	3,2 - 2	22279.95	1.40	0.002	
	4,3,2 - 3	22278.14	-0.41	-0.011	
	2 - 1	22277.18	-1.37	0.028	
$7^+_{16} - 6^+_{25}$	7 - 6	38113.99	1.35	-0.027	-5.41 (19)
	8 - 7, 6 - 5	38111.96	-0.68	0.009	
$7^-_{16} - 6^-_{25}$	7 - 6	38265.01	1.37	-0.007	-5.47 (19)
	8 - 7, 6 - 5	38262.96	-0.68	0.009	
$7^+_{35} - 8^+_{26}$	8 - 9, 6 - 7	29493.54	0.27	-0.022	
	7 - 8	29492.72	-0.55	0.034	
$7^-_{35} - 8^-_{26}$	8 - 9, 6 - 7	29411.19	0.27	-0.023	
	7 - 8	29410.38	-0.54	0.045	
$9^+_{19} - 8^+_{26}$	8 - 7, 10 - 9	30173.59	+1.14	0.044	
	9 - 8	30170.17	-2.28	-0.087	
$9^-_{19} - 8^-_{26}$	8 - 7	30344.81	1.30	0.000	8.78 (19)
	10 - 9	30344.42	0.91	-0.025	
	9 - 8	30341.30	-2.21	0.014	

Cont/d

TABLE 22 (cont/d)

Gauche-CHD_2NO P- and R- Branch

Transition	F' - F	Obs/MHz	Relative to Hyp.Cent/MHz	Obs-Calc	χ/MHz
$11^+_{29} - 10^+_{38}$	11 - 10	37447.03	0.84	-0.019	-3.36 (19)
	12 - 11 10 - 9	37445.77	-0.42	0.010	
$11^-_{29} - 10^-_{38}$	11 - 10	37511.96	0.87	0.010	-3.47 (19)
	12 - 11 10 - 9	37510.66	-0.43	0.000	
$12^+_{2,11} - 11^+_{38}$	13 - 12 11 - 10	37781.47	0.24	0.004	
	12 - 11	37780.76	-0.47	0.003	
$12^-_{2,11} - 11^-_{38}$	13 - 12 11 - 10	37829.15	0.24	0.003	
	12 - 11	37828.44	-0.47	0.004	
	Q-Branch μ_b and μ_c (Intersystem)				
$1^+_{10} - 1^+_{01}$	1-2,1,0	38576.02	1.30	-0.125	
	2-2,1	38574.50	-0.22	0.065	Interfering line
	0-1	38571.99	-2.73	0.118	38572.24
$1^-_{10} - 1^-_{01}$	1-2,1,0	38475.80	1.34	-0.085	Interfering line
	2-2,1	38474.23	-0.23	0.055	38476.47
	0-1	38471.60	-2.86	-0.012	
$2^+_{11} - 2^+_{02}$	2-1,2,3	39728.44	1.42	0.051	
	3-3,2	39726.62	-0.40	-0.009	
	1-1,2	39725.61	-1.41	-0.041	
$2^-_{11} - 2^-_{02}$	2-1,2,3	39629.04	1.42	0.051	
	3-3,2	39627.21	-0.41	-0.019	Interfering line
	1-1,2	39626.21	-1.41	-0.041	39627.65
$3^+_{12} - 3^+_{03}$	3	41509.80	1.48	0.012	
	4	41507.84	-0.48	0.009	
	2	41507.13	-1.19	-0.016	
$3^-_{12} - 3^-_{03}$	3	41410.53	1.50	0.032	
	4	41408.57	-0.46	0.029	
	3	41407.75	-1.28	-0.106	
$5^-_{15} - 5^+_{05}$	6,4	30304.41	0.61	0.007	+4.85 (19)
	5	30302.59	-1.21	0.003	
$5^+_{15} - 5^-_{05}$	6,4	30040.53	0.51	-0.093	Interference from
	5	30038.99	-1.03	0.176	cis CH_2DNO $4_{22} - 5_{15}$
$6^-_{16} - 6^+_{06}$	7,5	27584.84	0.55	-0.004	+4.40 (19)
	6	27583.19	-1.10	0.008	
$6^+_{16} - 6^-_{06}$	7,5	27328.64	0.55	-0.004	+4.40 (19)
	6	27326.99	-1.10	0.007	

Cont/d

TABLE 22 (Cont/d)

Gauche-CHD_2NO Q-Branch μ_a

Transition	F	Obs/MHz	Relative to Hyp.Cent/MHz	Obs-Calc	χ/MHz
4^+_{13} - 4^+_{14}	4	11324.53	2.86	0.014	11.44 (16)
	5	11320.62	-1.05	-0.015	
(PT)	3	11319.64	-2.03	0.003	
4^-_{13} - 4^-_{14}	4	11312.47	2.82	-0.026	-11.31 (16)
	5	11308.61	-1.04	-0.005	
(PT)	3	11307.63	-2.02	0.013	
5^+_{14} - 5^+_{15}	5	16977.55	2.84	-0.023	-11.38 (16)
	6	16973.62	-1.09	0.004	
(PT)	4	16972.80	-1.91	-0.014	
5^-_{14} - 5^-_{15}	5	16959.60	2.85	0.007	-11.39 (16)
	6	16955.66	-1.09	0.004	
(PT)	4	16954.85	-1.90	-0.004	
6^+_{15} - 6^+_{16}	6	23749.93	2.83	-0.008	-11.33 (16)
	7	23745.99	-1.11	0.025	
(PT)	5	23745.27	-1.83	-0.024	
6^-_{16} - 6^-_{16}	6	23725.09	2.86	0.022	-11.45 (16)
	7	23721.08	-1.15	-0.015	
(PT)	5	23720.41	-1.82	-0.014	
7^+_{16} - 7^+_{17}	7	31628.87	2.83	0.002	-11.32 (16)
	8	31624.88	-1.16	0.005	
(PT)	6	31624.29	-1.75	-0.009	
7^-_{16} - 7^-_{17}	7	31596.24	2.82	-0.008	-11.30 (16)
	8	31592.26	-1.16	0.005	
(PT)	6	31591.67	-1.75	-0.010	
8^+_{17} - 8^+_{18}	8	40594.54	2.81	-0.004	-11.23 (16)
	9	40590.58	-1.15	0.035	
(PT)	7	40590.02	-1.71	-0.021	
8^-_{17} - 8^-_{18}	8	40553.29	2.81	-0.004	-11.25 (16)
	9	40549.31	-1.17	0.015	
(PT)	7	40548.77	-1.71	-0.022	
9^+_{27} - 9^+_{28}	9	7975.95	0.85	-0.004	-3.40 (19)
	8,10	7974.67	-0.43	-0.003	
9^-_{27} - 9^-_{28}	9	7980.95	0.85	-0.005	-3.40 (19)
	8,10	7979.68	-0.42	0.008	
10^+_{28} - 10^+_{29}	10	11715.78	0.99	-0.017	-3.98 (19)
	9,11	11714.29	-0.50	0.004	
10^-_{28} - 10^-_{29}	10	11722.05	1.03	0.021	-4.09 (19)
	9,11	11720.51	-0.51	-0.006	

Cont/d

TABLE 22(Cont/d)

Gauche-CHD_2NO Q-Branch μ_a

Transition	F	Obs/MHz	Relative to Hyp.Cent/MHz	Obs-Calc	χ/MHz
$11^+_{29} - 11^+_{2,10}$	11	16488.82	1.18	0.024	-4.72 (19)
	10,12	16487.05	-0.59	-0.012	
$11^-_{29} - 11^-_{2,10}$	11	16496.00	1.17	0.013	-4.67 (19)
	10,12	16494.25	-0.58	-0.002	
$12^+_{2,10} - 12^+_{2,11}$	12	22378.03	1.27	-0.024	-5.09 (19)
	11,13	22376.12	-0.64	0.007	
$12^-_{2,10} - 12^-_{2,11}$	12	22385.73	1.32	0.024	-5.28 (19)
	11,13	22383.75	-0.66	-0.012	
$13^+_{2,11} - 13^+_{2,12}$	13	29437.19	1.41	-0.010	-5.63 (19)
	12,14	29435.08	-0.70	0.010	
$13^-_{2,11} - 13^-_{2,12}$	13	29444.83	1.46	0.039	-5.84 (19)
	12,14	29442.64	-0.73	-0.020	
$14^+_{2,12} - 14^+_{2,13}$	14	37691.36	1.49	-0.040	-5.97 (19)
	13,15	37689.12	-0.75	0.015	
$14^-_{2,12} - 14^-_{2,13}$	14	37698.26	1.54	0.009	-6.16 (19)
	13,15	37695.95	-0.77	-0.005	
$16^+_{3,13} - 16^+_{3,14}$	16	8813.61	0.45	-0.009	
	15,17	8812.94	-0.22	0.010	
$16^-_{3,13} - 16^-_{3,14}$	16	8820.17	0.45	-0.010	
	15,17	8819.50	-0.22	0.010	
$17^+_{3,14} - 17^+_{3,15}$	17	12284.55	0.59	0.031	
	16,18	12283.66	-0.30	-0.021	
$17^-_{3,14} - 17^-_{3,15}$	17	12291.85	0.53	-0.03	
	16,18	12291.06	-0.26	0.02	
$18^+_{3,15} - 18^+_{3,16}$	18	16698.22	0.65	-0.015	
	17,19	16697.24	-0.33	0.003	
$18^-_{3,15} - 18^-_{3,16}$	18	16706.69	0.66	-0.006	
	17,19	16705.70	-0.33	0.003	
$19^+_{3,16} - 19^+_{3,17}$	19	22182.25	0.79	0.015	
	18,20	22181.07	-0.39	-0.003	
$19^-_{3,16} - 19^-_{3,17}$	19	22185.72	0.80	0.023	
	18,20	22184.52	-0.40	-0.012	
$20^+_{3,17} - 20^+_{3,18}$	20	28826.74	0.84	-0.045	
	19,21	28825.48	-0.42	0.023	
$20^-_{3,17} - 20^-_{3,18}$	20	28832.60	0.87	-0.017	
	19,21	28831.29	-0.44	0.004	

Cont/d

TABLE 22(Cont/d)

Gauche-CHD_2NO Q-Branch μ_a

Transition	F	Obs/MHz	Relative to Hyp.Cent/MHz	Obs-Calc
$25^+_{4,21} - 25^+_{4,22}$	25	-		
	24,26	14803.40	-0.21	0
$25^-_{4,21} - 25^-_{4,22}$	25	-		
	24,26	14806.73	-0.21	0
$26^+_{4,22} - 26^+_{4,23}$	26	19518.48	0.47	-0.023
	25,27	19517.78	-0.23	0.017
$26^-_{4,22} - 26^-_{4,23}$	26	19524.35	0.50	0.006
	25,27	19523.60	-0.25	-0.003
$27^+_{4,23} - 27^+_{4,24}$	27	25312.63	0.58	0.001
	26,28	25311.76	-0.29	0.000
$27^-_{4,23} - 27^-_{4,24}$	27	25321.71	0.57	-0.011
	26,28	25320.85	-0.29	0.001
$28^+_{4,24} - 28^+_{4,25}$	28	32304.74	0.65	-0.019
	27,29	32303.77	-0.32	0.015
$28^-_{4,24} - 28^-_{4,25}$	28	32317.84	0.65	-0.021
	27,29	32316.87	-0.32	0.016
$29^+_{4,25} - 29^+_{4,26}$	29	40593.10	0.76	0.000
	28,30	40591.96	-0.38	0.000
$29^-_{4,25} - 29^-_{4,26}$	29	40610.75	0.76	-0.002
	28,30	40609.61	-0.38	0.001

Note

(PT) obtained from Ref. 16

TABLE 23

State Mixing Parameters CHD_2NO Q_a = 83.443 MHz

ψ_1	ψ_2	$\lvert E_1^o - E_2^o \rvert$/MHz	∅	$\cos^2$ ∅	$\sin^2$ ∅
1^+_{10}	1^-_{11}	1041.9	4.55°	0.9937	0.0063
1^-_{10}	1^+_{11}	1222.4	3.89°	0.9954	0.0046
2^+_{11}	2^-_{12}	3308.1	1.44°	0.9994	0.0006
2^-_{11}	2^+_{12}	3484.0	1.37°	0.9994	0.0006
6^+_{25}	6^-_{24}	1523.4	3.13°	0.9970	0.0030
6^-_{25}	6^+_{24}	1979.1	2.41°	0.9982	0.0018
8^+_{27}	8^-_{26}	4901.5	0.98°	0.9997	0.0003
8^-_{27}	8^+_{26}	5389.5	0.89°	0.9998	0.0002
10^+_{38}	10^-_{37}	160.5	23.06°	0.8466	0.1534
10^-_{38}	10^+_{37}	1353.5	3.51°	0.9962	0.0038

TABLE 24

Program Chi.

Quadrupole data - g-CHD2NO.

Number of observations = 31

J						Obs/MHz	Res/MHz	Weight
1	1	0	level			-5.29200	0.01441	1.00000
5-	1	5-	5+	0	5	4.85000	0.02401	0.24622
6-	1	6-	6+	0	6	4.40000	-0.03150	0.24622
6+	1	6-	6-	0	6	4.40000	-0.02862	0.24622
6+	2	5-	7+	1	6	-5.42000	0.08696	0.24622
6-	2	5-	7-	1	6	-5.47000	0.03634	0.24622
8-	2	6-	9-	1	9	8.78000	0.00201	0.34722
10+	3	8-	11+	2	9	-3.41000	0.02699	0.24622
10-	3	8-	11-	2	9	-3.47000	-0.02988	0.24622
4+	1	3-	4+	1	4	-11.44000	-0.05401	0.34722
4-	1	3-	4-	1	4	-11.31000	0.07597	0.34722
5+	1	4-	5+	1	5	-11.38000	-0.00645	0.34722
5-	1	4-	5-	1	5	-11.39000	-0.01651	0.34722
6+	1	5-	6+	1	6	-11.33000	0.02083	0.34722
6-	1	5-	6-	1	6	-11.45000	-0.09929	0.34722
7+	1	6-	7+	1	7	-11.32000	-0.00628	0.34722
7-	1	6-	7-	1	7	-11.30000	0.01348	0.34722
8+	1	7-	8+	1	8	-11.23000	0.02751	0.34722
8-	1	7-	8-	1	8	-11.25000	0.00711	0.34722
9+	2	7-	9+	2	8	-3.40000	0.01531	0.24622
9-	2	7-	9-	2	8	-3.40000	0.01958	0.24622
10+	2	8-	10+	2	9	-3.98000	0.04958	0.24622
10-	2	8-	10-	2	9	-4.09000	-0.05577	0.24622
11+	2	9-	11+	2	10	-4.72000	-0.09696	0.24622
11-	2	9-	11-	2	10	-4.67000	-0.04211	0.24622
12+	2	10-	12+	2	11	-5.09000	0.08739	0.24622
12-	2	10-	12-	2	11	-5.28000	-0.09776	0.24622
13+	2	11-	13+	2	12	-5.63000	0.04934	0.24622
13-	2	11-	13-	2	12	-5.84000	-0.15598	0.24622
14+	2	12-	14+	2	13	-5.97000	0.15097	0.24622
14-	2	12-	14-	2	13	-6.16000	-0.03467	0.24622

E.S.D. of an Observation/MHz = 0.03293/sqrt(Weight)

Chiaa =	0.78065	MHz	esd	0.06082
Chibb-Chicc =	-11.39347	MHz	esd	0.01533
Chibb =	-6.08706	MHz	esd	0.03136
Chicc =	5.30641	MHz	esd	0.03136

TABLE 25

Cis Di-deutero Nitrosomethane. s-CHD2NO.

A REDUCTION REPRESENTATION IIR

UPPER LEVEL J	Ka	Kc		LOWER LEVEL J	Ka	Kc	OBS/MHz	OBS-CALC	WEIGHT
1	0	1	-	0	0	0	18999.190	-0.081	
1	1	0	-	1	0	1	41823.580	-0.323	0.000
2	0	2	-	1	0	1	37990.910	-0.119	
2	1	2	-	1	1	1	37362.220	0.018	
2	1	1	-	1	1	0	38633.390	0.242	0.000
3	0	3	-	2	1	2	16408.260	0.082	
4	2	2	-	5	1	5	34435.480	-0.398	0.000
4	2	3	-	5	1	4	24795.540	-0.583	0.000
4	0	4	-	3	1	3	36291.920	0.003	
5	1	4	-	5	1	5	9529.660	-0.015	
5	2	3	-	6	1	6	17527.700	-0.250	0.000
6	1	5	-	6	1	6	13338.440	-0.004	
7	1	6	-	6	2	5	17225.250	0.125	
7	1	6	-	7	1	7	17778.380	0.124	
8	3	6	-	9	2	7	34669.550	0.063	
8	3	5	-	9	2	8	37085.690	0.046	
8	1	7	-	7	2	6	38669.300	-1.379	0.000
8	1	7	-	8	1	8	22844.820	-1.068	0.000
9	3	7	-	10	2	8	14791.540	0.577	0.000
9	3	6	-	10	2	9	18405.550	0.534	0.000
9	1	9	-	8	2	6	30329.150	-0.525	0.000
9	1	8	-	9	1	9	28536.440	-0.166	
10	1	9	-	10	1	10	34843.670	-0.086	
11	1	10	-	11	1	11	41758.440	0.118	
12	2	11	-	11	3	8	18573.090	-1.431	0.000
12	2	10	-	11	3	9	25809.500	-1.618	0.000
13	2	11	-	13	2	12	9527.970	0.013	
13	4	10	-	14	3	11	23072.780	0.034	
13	4	9	-	14	3	12	23736.380	-0.020	
14	2	12	-	14	2	13	12512.710	-0.039	
15	2	13	-	15	2	14	16074.690	0.027	
16	2	14	-	16	2	15	20250.000	0.024	
17	5	13	-	18	4	14	30053.390	-0.096	
17	5	12	-	18	4	15	30159.530	0.040	
17	3	15	-	16	4	12	33657.030	-4.055	0.000
17	3	14	-	16	4	13	35719.910	-4.431	0.000
17	2	15	-	17	2	16	25066.400	-0.031	
18	2	16	-	18	2	17	30542.130	-0.978	0.000
18	5	13	-	19	4	16	10913.250	0.023	
18	5	14	-	19	4	15	10750.890	0.004	
19	2	17	-	19	2	18	36694.200	3.417	0.000
20	4	17	-	19	5	14	8361.590	0.009	
20	4	16	-	19	5	15	8604.690	-0.019	
21	4	17	-	20	5	16	28021.780	-0.063	
21	4	18	-	20	5	15	27665.070	0.064	
22	3	19	-	22	3	20	8764.530	-0.032	
23	3	20	-	23	3	21	11210.960	0.005	
24	3	21	-	24	3	22	14149.530	0.088	
25	3	22	-	25	3	23	17633.360	0.018	
26	3	23	-	26	3	24	21712.330	-0.072	
27	3	24	-	27	3	25	26430.570	-0.443	0.000
28	3	25	-	28	3	26	31832.300	5.624	0.000
29	3	26	-	29	3	27	37928.850	0.009	

TABLE 25 (cont/d)

Parameter	Value	E.S.D.
X/MHz	9182.187641	0.011922
Y/MHz	51006.419173	0.055499
Z/MHz	9817.123364	0.013843
DJ/KHz	230.548523	1.105425
DJK/KHz	-496.143226	8.204344
DK/KHz	274.093553	6.896589
dJ/KHz	-112.415764	0.676432
dK/KHz	142.657320	3.402391
HJ/Hz	-0.297412	0.066559
HJK/Hz	1.247274	0.362178
HKJ/Hz	-1.335169	0.445340
HK/Hz	0.346258	0.149395

Weighted S.D. of Fit 0.081776 MHz.

DETERMINABLE ROT. CONSTS./MHz

9182.092112 51006.444610 9817.584461

TABLE 26

Cis-CHD_2NO Additions to Existing Data Set[17]

Transition	$F' - F$	Obs/MHz	Hyp.Cent/MHz
$1_{10} - 1_{01}$	1 - 2,1,0 2 - 2,1 0 - 1	41824.93 41823.34 41820.75	41823.58
$4_{23} - 5_{14}$	5 - 6 3 - 4 4 - 5	24796.29 24794.05	24795.54
$11_{1,10} - 11_{1,11}$	11 - 11 12 - 12 10 - 10	41761.29 41757.17 41756.83	41758.44
$22_{3,19} - 22_{3,20}$	22 - 22 23 - 23 21 - 21	8764.92 8764.33	8764.53
$23_{3,20} - 23_{3,21}$	23 - 23 22 - 22 24 - 24	11211.45 11210.71	11210.96
$24_{3,21} - 24_{3,22}$	24 - 24 23 - 23 25 - 25	14150.11 14149.24	14149.53
$25_{3,22} - 25_{3,23}$	25 - 25 24 - 24 26 - 26	17634.03 17633.02	17633.36
$26_{3,23} - 26_{3,24}$	26 - 26 25 - 25 27 - 27	21713.00 21711.99	21712.33
$27_{3,24} - 27_{3,25}$	27 - 27 26 - 26 28 - 28	26431.33 26430.19	26430.57
$28_{3,25} - 28_{3,26}$	28 - 28 27 - 27 29 - 29	31833.27 31831.82	31832.30
$29_{3,26} - 29_{3,27}$	29 - 29 28 - 28 30 - 30	37929.82 37928.36	37928.85

CHAPTER 3

CHLORODIFLUOROACETALDEHYDE

Introduction

The decision to study chlorodifluoroacetaldehyde arose out of an interest in the isoelectronic molecule chlorodifluoronitrosomethane. There have been several unsuccessful attempts to assign the microwave spectrum of the nitroso compound, one by Dr. Kelvin Tyler's group at Glasgow University, one by Judith Hardy at Bristol University[25] and one by this author. The structural and conformational analogies between nitroso compounds and their corresponding aldehydes have proved useful in the past, in work carried out at Bristol and elsewhere. ClF_2CCHO was, therefore, expected to provide a good model basis for a solution of the ClF_2CNO problem. For this reason, the discussion here will develop around comparison between these and related aldehydes and nitroso compounds, despite their chemical dissimilarity.

Chlorodifluoronitrosomethane is a fascinating compound, if only for aesthetic reasons. It is a dark blue gas, this colour being due to an absorption centred at 660 nm (red), associated with the $n \rightarrow \pi^*$ transition of the nitrosyl group[68] . All free nitroso compounds show some colouration, but the perhalo- compounds exhibit it dramatically because they do not exist preferentially as colourless dimers.

The chemistry of perhalonitrosomethanes is dominated by processes involving free radicals. Perhalonitrosomethanes probably play a minor role in the stratospheric photochemistry of freons[69] , ClF_2CNO being formed from CCl_2F_2 (freon 12) and NO;

$$CCl_2F_2 \xrightarrow{h\nu} CF_2Cl^{\cdot} + Cl^{\cdot}$$

$$CF_2Cl^{\cdot} + NO \longrightarrow ClF_2CNO$$

The fate of the chlorine atom from the first reaction has been of some concern to ecologists [70,71].

$$Cl^{\cdot} + O_3 \longrightarrow ClO^{\cdot} + O_2$$

$$ClO^{\cdot} + O: \longrightarrow Cl^{\cdot} + O_2$$

Although perhalonitrosomethanes do not dimerise in the way that CH_3NO does, they do form compounds of empirical formula $C_2X_6N_2O_2$ on exposure to light. These are not strictly dimers but are sometimes referred to as such. Mason[72] has shown that photolysis of CF_3NO with red light produces the N-nitritoamine $(CF_3)_2N\text{-}O\text{-}NO$, a pale orange compound. A variety of other products are possible also, especially with light of shorter wavelengths. Chlorodifluoronitrosomethane no doubt exhibits similar behaviour. It is very unstable to light, forming an orange-brown liquid, which can present difficulties in handling and purification. This impurity is probably $(CF_2Cl)_2NONO$ and other products of a radical process analogous to that proposed by Mason for CF_3NO.

$$ClF_2CNO \xrightarrow{h\nu} ClF_2C^{\cdot} + NO$$

$$ClF_2CNO + ClF_2C^{\cdot} \longrightarrow (ClF_2C)_2NO^{\cdot}$$

$$(ClF_2C)_2NO^{\cdot} + NO \longrightarrow (ClF_2C)_2N\text{-}O\text{-}NO$$

Radical processes might also form the basis of a chemical preparation. CF_3NO has been prepared by photolysis of CF_3I and NO in the presence of mercury[73]. The sample of ClF_2CNO used in this work, supplied by Dr. Josef Pfab of Heriot-Watt University, was however prepared by reduction of the corresponding nitro compound[74].

The infrared[74] and photoelectron[75] spectra of ClF_2CNO have been reported by Pfab et al. Interpretation of these, and of the electronic spectrum[68], has however been hampered by a lack of knowledge of the ground state structure of the molecule and its rotational isomerism. CF_3NO is now known to change conformation from eclipsed to staggered upon electronic excitation[76]. ClF_2CNO probably behaves in the same way but with the added complexity that it can exhibit rotational isomerism in either case. Identification of the

preferred ground state conformers of ClF_2CNO would therefore facilitate the analysis, for which reason a study of the microwave spectrum was undertaken.

Initial modelling for the microwave spectrum of ClF_2CNO was carried out by Judith Hardy[25] on the basis of the microwave structure[77] of CF_3NO. It seemed likely that the molecule would exist in cis or gauche forms (Figure 1) and that the spectrum might be complicated by gauche - gauche tunnelling, or that the molecule may have a low barrier to internal rotation. The latter suggestion, made on the basis of the richness of the ClF_2CNO spectrum, would indicate a breakdown of the localised conformer approach and added difficulty in the analysis.

The suggested 'plausible' structure for ClF_2CNO, in the cis form, is reproduced in reference 74 . It remains plausible except, as will be seen from this work, the predominant rotamer is expected to be the gauche. Also, the precise structure of CF_3NO, on which it is based, is still not established in detail. An electron diffraction study[78] indicates that the C-N bond may be unusually long, and microwave $^{13}CF_3NO$ data are needed to unequivocally locate the carbon atom in the molecular frame. Further discussion of the CF_3NO structure, although not in this context, is given in Chapter 4.

Initial attempts by this author to assign the spectrum of ClF_2CNO were based on minor variants of the structure already proposed. The spectrum is indeed very rich, but not particularly strong. A simple bond moment calculation based on CF_3NO (μ = 0.18D)[77] and CF_3Cl (μ = 0.50D)[79] indicates that the total dipole moment is probably $\sim$0.5D in the approximate direction of the C-Cl bond (Cl $\rightarrowtail$ C). Care is therefore needed to eliminate impurities such as[80] COF_2 and the photolytic products. Radio frequency - microwave double resonance was used to try to locate mutually resonant pairs of asymmetry doublets, but emphasis was placed mainly on the cis form ($\kappa \sim 0.5$), which was thought, at the time, to be the most probable. Many double resonances were found, but none were assigned on this basis. With hindsight,

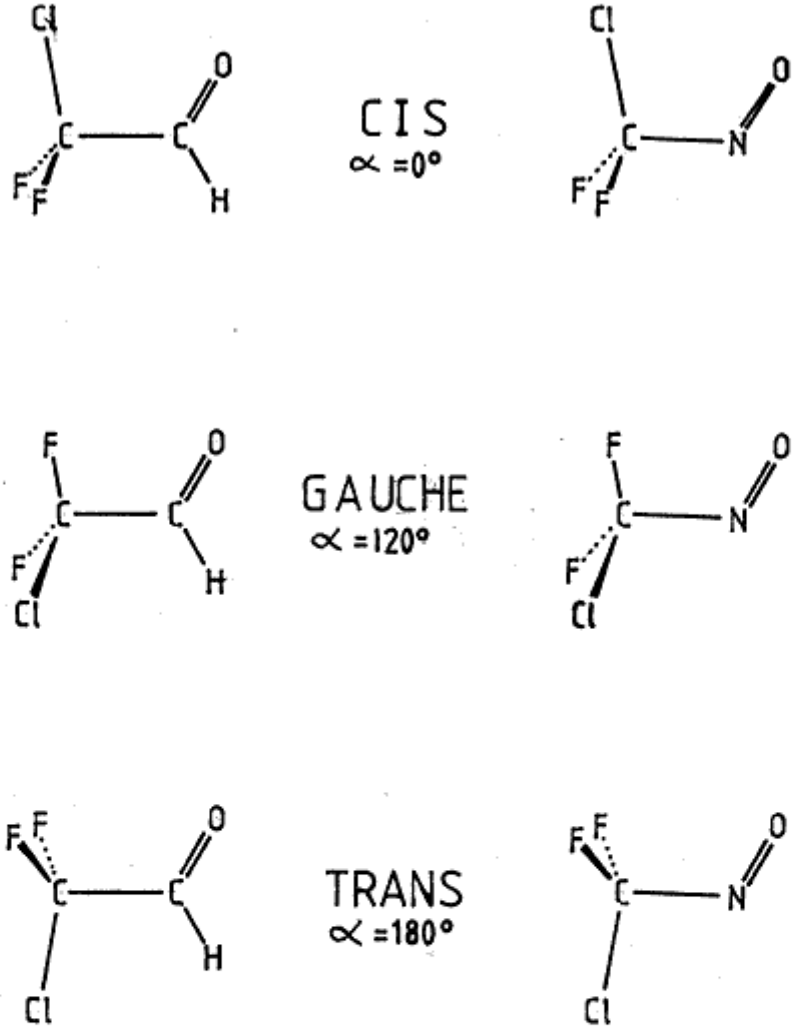

Figure 1

Rotamer Definitions for ClF_2CCHO and ClF_2CNO.

the spectrum is reminiscent of the gauche form ($K \sim -0.7$). It contains certain groups of first order lines similar to those due to gauche-ClF_2CCHO, but this could not be known at the time. It was not until assignment of the ClF_2CNO spectrum seemed a very distant prospect that study of the corresponding aldehyde became an attractive idea.

Chlorodifluoroacetaldehyde has received little attention in the literature to date. A 1959 patent[81] describes its preparation, by catalytic hydrogenation of ClF_2CCOCl, and puts forward its properties as a dehydrating agent. ClF_2CCHO, in common with the other perhaloaldehydes, reacts with water to form a geminal diol or 'aldehyde hydrate'.

$$ClF_2CCHO \xrightarrow{H_2O} ClF_2CCH(OH)_2$$

This particular hydration reaction is facile enough to dissociate water from HCl. Other interest[82,83] has been shown in the polymerisation of ClF_2CCHO, by opening of the C=O double bond, to form chains of the type;

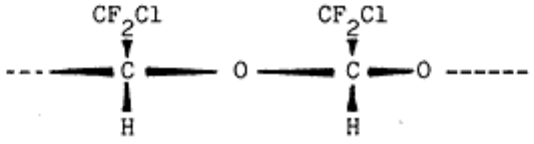

PREPARATION AND PROPERTIES OF ClF_2CCHO

The familiar scheme for the interconversion between primary alcohols and acids leaves the aldehyde apparently inaccessible in the middle.

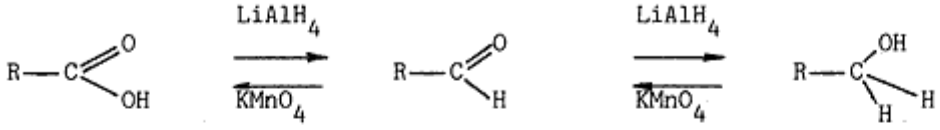

The problem of how to stop at the aldehyde when reducing the acid has however been solved, at least in the case of perhaloaldehydes, by the technique of "inverse addition" (of the lithium aluminium hydride) [84,85]. In this method, $LiAlH_4$ is added to the acid slowly and in just sufficient quantity to produce the aldehyde. Yields of around 70% can be obtained. A synthesis of ClF_2CCHO based on this method is given by Yamada, Campbell and Vogl [82]. This involves $LiAlH_4$ reduction of the methyl ester ClF_2CO_2Me at -78% and a work-up via the hemiacetal.

In this work, ClF_2CCHO was prepared by $LiAlH_4$ reduction of the anhydrous acid ClF_2CCO_2H at 0°C and a work up via the aldehyde hydrate.

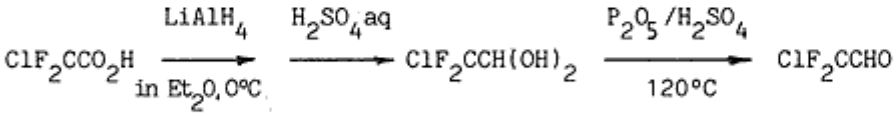

The $LiAlH_4$ reduction proceeds as follows;

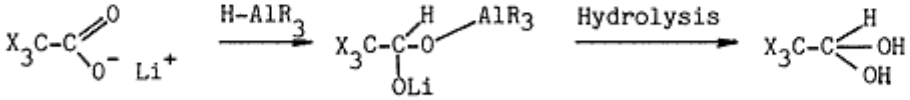

One half mole of $LiAlH_4$ is sufficient to reduce one mole of acid to the aldehyde. The use of sulphuric acid for the hydrolysis avoids the production of aluminium hydroxide sludge.

Experimental

$LiAlH_4$ (0.8g) was slurried in 30 ml of either and added to 5g of ClF_2CCO_2H (Aldrich 98%) in 40 ml of ether at 0°C. The apparatus was maintained under a dry nitrogen atmosphere and the nitrogen stream was bubbled through the

dropping funnel to maintain the $LiAlH_4$ slurry. Ether was Na dried and 10% more $LiAlH_4$ than calculated from stoichiometry was allowed to remove residual water. The addition, which resulted in vigorous effervescence, was performed drop by drop over a period of one hour. The resulting metal complex was then hydrolysed with 10 ml of 6M sulphuric acid. The ether and water fractions were separated. The water fraction was washed with further small portions of ether and then discarded. The combined ether fractions were dried with anhydrous $MgSO_4$. Ether was then removed from the reaction product by distillation.

A fraction boiling in the range 95-105°C was taken to be the aldehyde hydrate (bpt. 104-106°C). Attempts to dehydrate this product however, by warming it in vacuo with P_2O_5 and conc. H_2SO_4, apparently failed to liberate the free aldehyde. The production of a white solid, possibly poly-ClF_2CCHO was observed, but there was no significant rise in the vapour pressure of the mixture. Steps were therefore taken to establish if the starting material was in fact the aldehyde hydrate.

The thin-film infrared spectrum showed a broad absorption at 3400 cm^{-1} consistent with O-H stretching. The 60MHz n m r spectrum in $CDCl_3$ solution showed a broad peak at δ = 4.44 ppm and a strong impurity spectrum due to diethyl ether. The presence of a large amount of ether was surprising in view of the great difference between its boiling point (34.6°C) and that of the product. The product was submitted for mass spectroscopy, but the recorded mass spectrum proved to be highly misleading. In order to interpret the fragmentation pattern it was necessary to re-assign all peaks above m/e = 100 to the next lowest integer. This was not done until the whole preparation had been repeated.

In the second preparation, no attempt was made to isolate the aldehyde hydrate. After removal of ether by distillation, the dehydrating mixture of P_2O_5 in conc. H_2SO_4 was dropped directly into the crude product. The

free aldehyde (bpt. 17.8°C) evolved easily with an oil bath temperature between 95 and 120°C, and was collected in a receiver cooled to -70°C. The alleged aldehyde hydrate from the first attempted preparation was also dehydrated in this way to yield a second batch of aldehyde. Both samples were transferred to a vacuum frame to be separated from the air and were then stored at liquid nitrogen temperature. It was concluded that, since dehydration took place at a temperature about the boiling point of $ClF_2CCH(OH)_2$, refluxing at atmospheric pressure had served to keep the reactants in contact.

The mass spectrum of the aldehyde hydrate, suitably re-interpreted, showed m/e peaks at 428, 354, 280, 206 and 132, each with a ^{37}Cl satellite two units above. This corresponds to the repeated loss of 74 units ($C_2H_5OC_2H_5$=74) indicating that the hydrate forms an ether complex. This explains the presence of ether in the sample as determined from the n m r spectrum. The most abundant etherate complex was at m/e = 280, i.e. $ClF_2CCH(OH)_2.2(C_2H_5)_2O$. The parent ion $ClF_2CCH(OH)_2^+$ was very weak, the ion due to the free aldehyde at m/e = 114 (116 for ^{37}Cl) being eight times stronger. This indicates elimination of H_2O in the ionisation region, either as a result of the ionisation process, or due to a shift in the $ClF_2CCH(OH)_2 \rightleftharpoons ClF_2CCHO + H_2O$ equilibrium at low pressure. The ionisation energy was not reported.

The deuterium analogue ClF_2CCDO was prepared by reacting ClF_2CCO_2H with $LiAlD_4$ (Aldrich 98 atom % D). All other chemicals used were normal hydrogen species and no exchange occurred. The H species could not be detected in the microwave spectrum of the D species, indicating better than 98% isotopic purity.

Gas phase I.R. spectra of ClF_2CCHO and ClF_2CCDO were recorded from 650 to 4000 cm^{-1}. The carbonyl stretching absorption of ClF_2CCHO occurred at 1775 cm^{-1}, that of ClF_2CCDO at 1763 cm^{-1}. An absorption at 2855 cm^{-1}, moving to 2159 cm^{-1} on deuteration was obviously the C-H stretching mode.

The compounds prepared as described were ready for use. Microwave spectra were checked for the presence of diethyl ether and none was found. No other obvious impurities were detected.

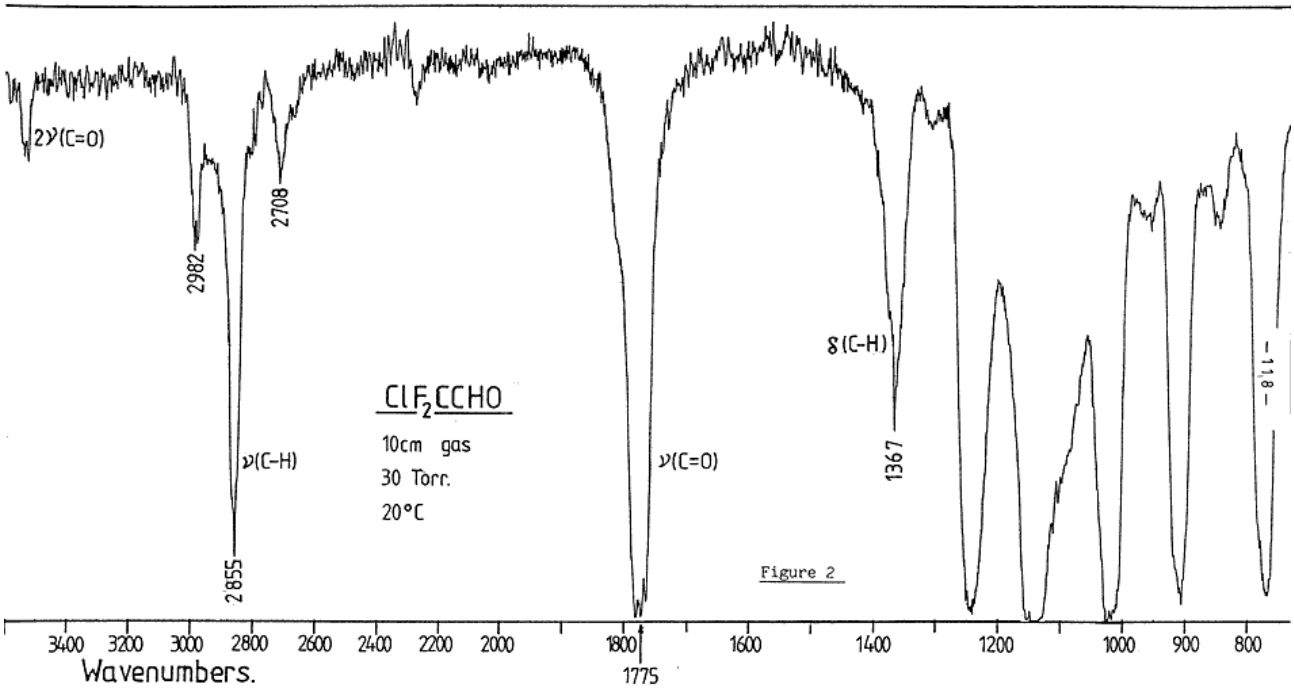

Figure 2

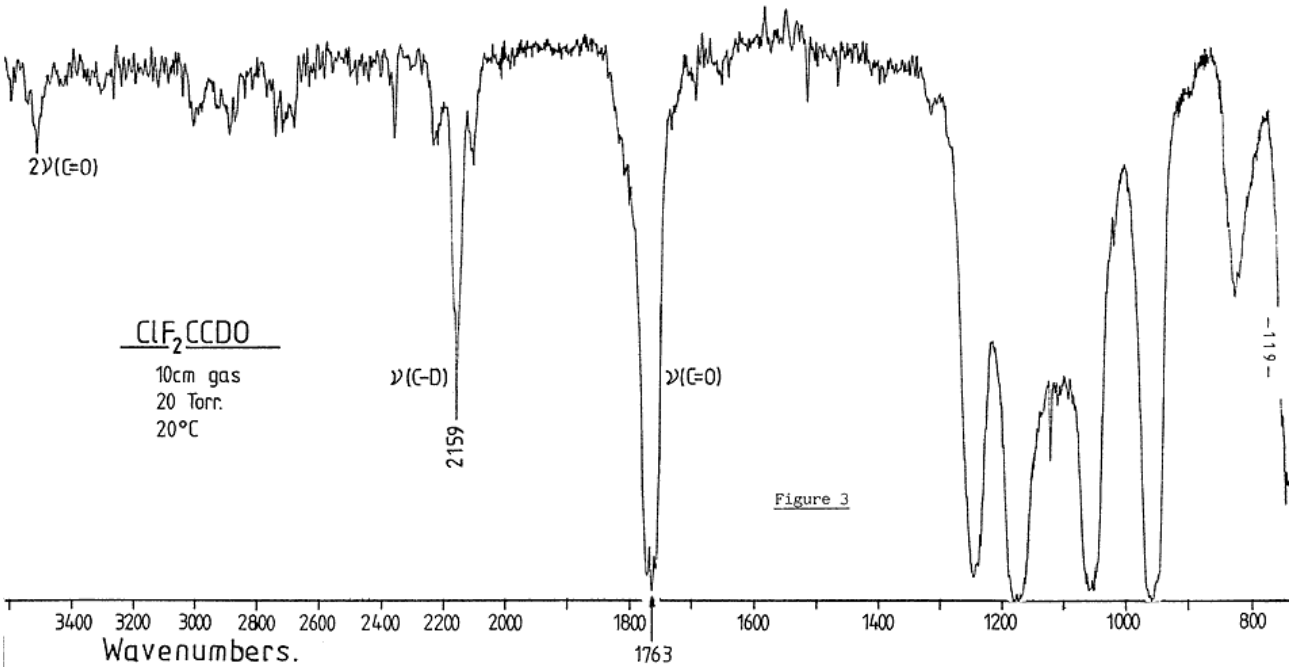

Figure 3

ASSIGNMENT OF GAUCHE - ClF_2CCHO

Initial estimates for the rotational constants of ClF_2CCHO were made on the basis of the structure of fluoral given by Woods[86]. This structure was refined to some extent, by fitting to the rotational constants[87] and incorporation of other data. This matter is discussed further in Chapter 4. Substitution of chlorine into the fluoral structure, with the C-Cl bond length taken from trifluoromethyl chloride[79] then gave rise to the basic model. There was however, no available reliable way to decide which would be the preferred conformer, although forms with a halogen eclipsing the oxygen atom (cis or gauche) were thought to be the most likely.

Chlorodifluoroacetaldehyde proved to be a good candidate for microwave spectroscopy. It has more than adequate vapour pressure for study at dry ice temperature and appeared to be almost indefinitely stable in the waveguide. A strong rich spectrum was observed in the 18 to 40 GHz region, with pressures between 0.01 and 0.05 Torr in the 3m X-band cell.

Initial searches were made using a K-band (18 - 26.5 GHz) BWO sweep, with either Stark modulation or radio-frequency (RF) double-resonance modulation. RF pumping was attempted at frequencies corresponding to asymmetry splittings calculated for model cis ($\kappa \sim 0.16$) and gauche ($\kappa = -0.65$) structures, but although many double resonances were seen, none could be assigned at this stage. Instead, it was soon realised that the spectrum showed a clear repeat unit, having band heads at intervals approximating to 2A-(B + C) for a near prolate asymmetric top. The interval might conceivably have been (A + B)-2C for a near oblate top but this was thought to be highly unlikely. Rotational constants were estimated for all conformers between cis and trans at 30° intervals, and only the model cis form had positive kappa, and not very positive at that. The cis form could not therefore be expected to give tightly grouped bunches of lines and so it was decided that the predominant spectrum should be interpreted

as belonging to gauche - $^{35}ClF_2CCHO$ (chlorine natural abundances are 75.53% for ^{35}Cl and 24.47% for ^{37}Cl).

The pattern seen is shown in Figure 4. It is due to Q-branches ($\Delta J = 0$) of the type $\Delta Ka = 1$. Such transitions may have intensity as a result of a finite μ_b or μ_c, both of which were expected to be active in the gauche form, whereas cis or trans forms have $\mu_c = 0$ by symmetry. In a given bunch, all lines have the same change in Ka. On the high frequency side of the bunch (at the band head) lies the transition with J = Ka upper. This is the lowest value of J for the band. As J increases, so does the intensity, and the lines move progressively to low frequency. Lines close to the band head do not show resolvable asymmetry doubling and have first order Stark effects on account of the near degeneracy between pairs of levels connected by μa. Further away from the band head asymmetry doubling occurs and Stark effects become second order (Figure 5). The centres of doublets can then be said to progress downwards in frequency, but the upper members of such pairs actually turn around and start to rise in frequency with increasing J (Figure 6). The fall off in intensity as J rises is due mainly to the need for higher and higher modulating voltages as the interacting levels move apart.

A detailed analysis of the Ka = 7→8 band structure was undertaken next. The rate at which lines split away from the band head with increasing J is a function of the asymmetry of the molecule and therefore provides a means for determining Kappa. The analysis turned out to be far simpler than expected. Since the fluoral spectrum exhibits A-E splitting due to internal rotation[87], it was thought that ClF_2CCHO might show gauche - gauche tunnelling. No such complexity was found, moreover many of the absorption lines were clearly resolved, so that it was possible to assign the $8_8 \leftarrow 8_7$ right at the band head. As soon as this was done, assignment of J to the emanating lines was straightforward.

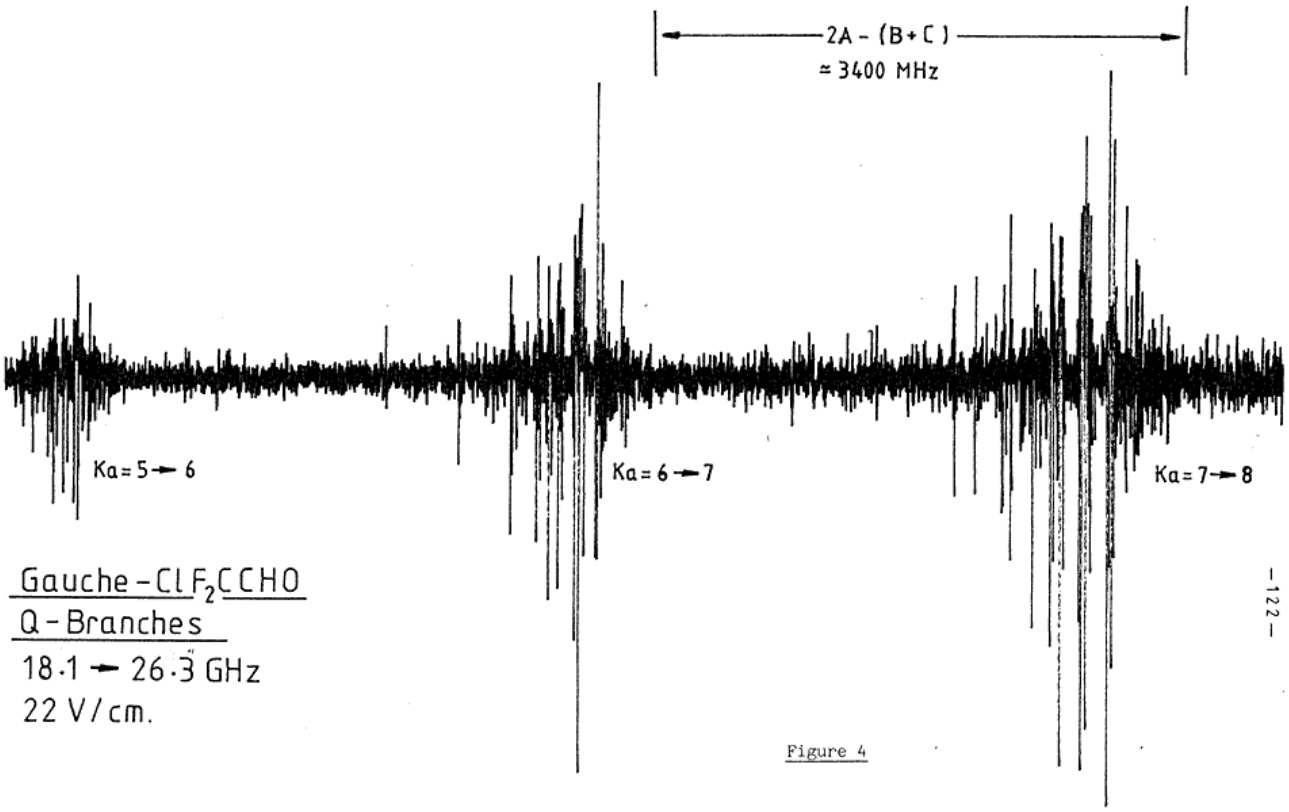

Figure 4

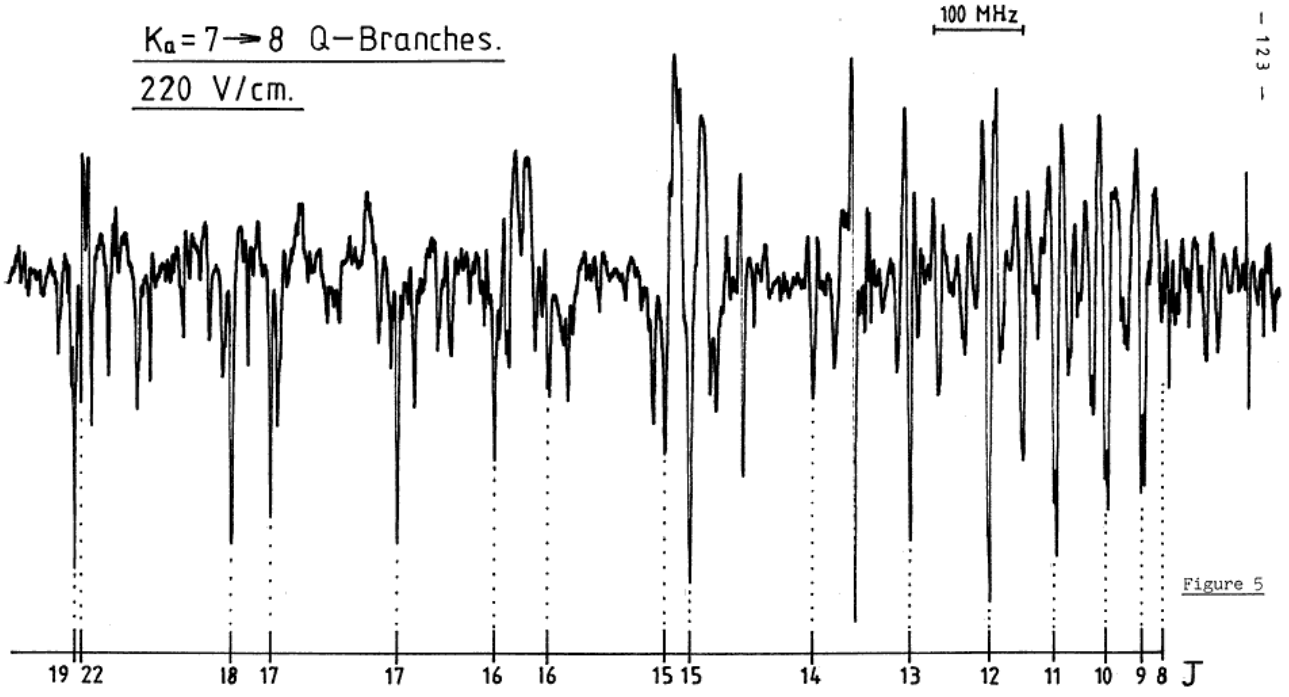

Figure 5

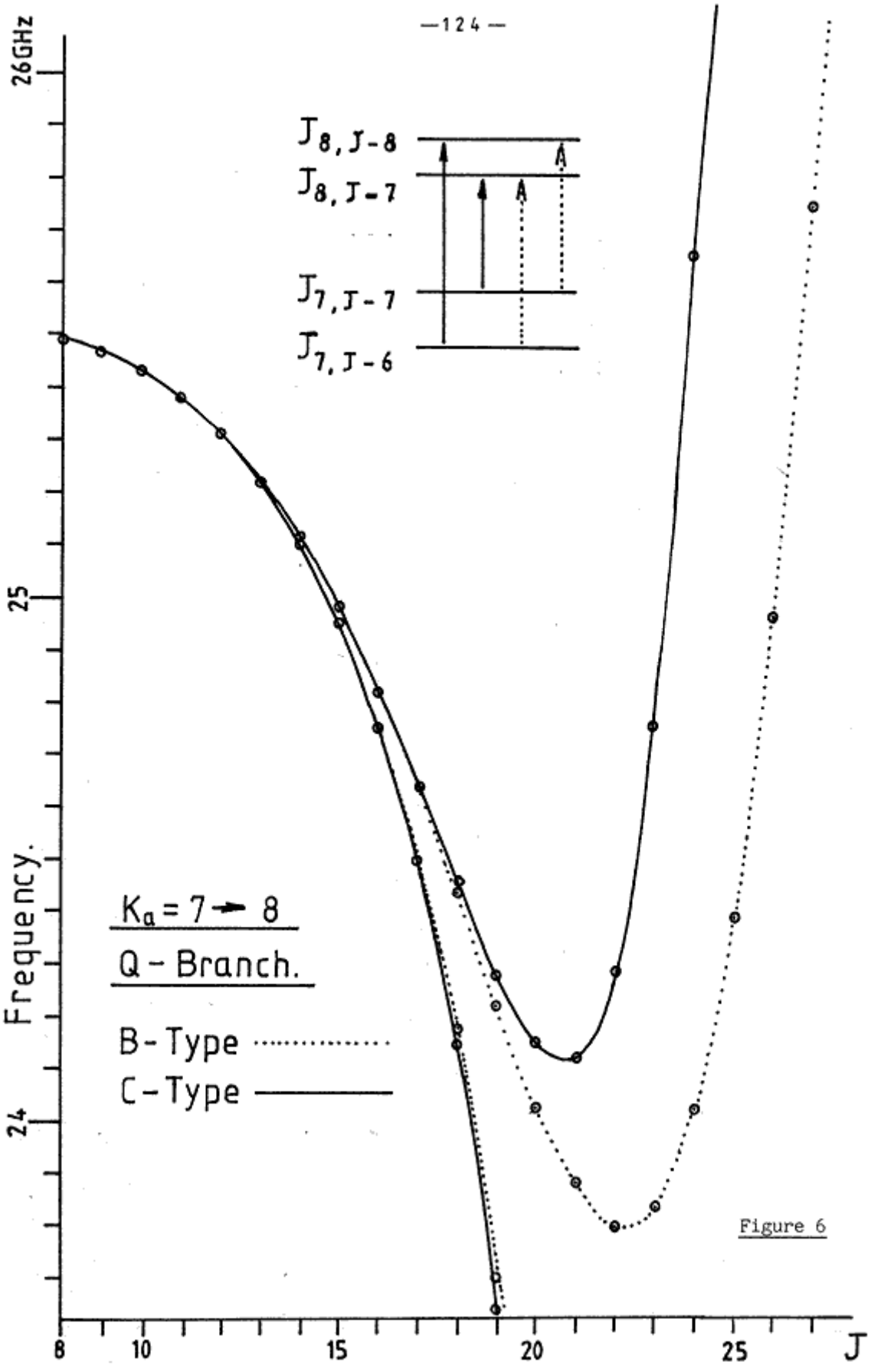
26GHz
25
24
Frequency.
$J_{8,J-8}$
$J_{8,J-7}$
$J_{7,J-7}$
$J_{7,J-6}$
A
A
$K_a = 7 \rightarrow 8$
Q - Branch.
B - Type
C - Type
8
10
15
20
25
J

Figure 6

To confirm the gauche assignment, or at least to banish the possibility that the spectrum was due to a trans form ($\kappa \sim -0.84$) the predominant dipole component turned out to be μ_c. A rough relative intensity measurement showed the μ_c, $16_{8,8} \leftarrow 16_{7,10}$ transition to be 8.75 times stronger than the μ_b, $16_{8,9} \leftarrow 16_{7,10}$ transition. This indicates that $\mu_c/\mu_b \simeq 3$. A bond moment calculation based on fluoral (μ_a=0.15D, μ_b=1.64D)[87] and CF_3Cl (μ=0.5D)[79] gave μ_a=0.74D, μ_b=0.42D and μ_c=1.53D which is in fair agreement with experiment.

Most of the lines in the ClF_2CCHO spectrum show resolvable hyperfine structure due to chlorine quadrupole coupling, the Q-branches being no exception (see Figure 7). Quadrupole splitting was initially modelled by assuming the quadrupole tensor to lie along the C-Cl bond direction and to be the same as in CF_3Cl (eQq = -77.902 MHz)[88]. Hence, χ_{zz} = -77.90 MHz and $\chi_{xx} = \chi_{yy}$ = 38.95 MHz. Rotation of this tensor into the intertial axis system was facilitated by observing that the C-Cl bond in gauche ClF_2CCHO lies almost exactly in the a, b plane. The bond was therefore assumed to lie in the plane, hence $\chi_{xx} = \chi_{cc}$ = 38.95 MHz and if θ is the angle between the C-Cl bond and the a-axis;

$$\chi_{aa} = \chi_{zz} \cos^2\theta + \chi_{yy} \sin^2\theta$$

$$\chi_{bb} = \chi_{yy} \cos^2\theta + \chi_{zz} \sin^2\theta$$

taking θ = 37.65° from the trial structure gave χ_{aa} = -34.31 MHz and χ_{bb} = -4.64 MHz which is in fair agreement with the observed (see Table 5 and later discussion). The predicted constants permitted straightforward assignment of F quantum numbers to hyperfine components. The constants were then refined in the reduction of transitions to hypothetical centres, by means of first-order perturbation theory, so that they were fairly well known by the time that attempts were made to assign R-branch transitions.

The R-branch (ΔJ = +1) transitions in gauche - ClF_2CCHO presented more of a search problem than expected. Predictions were made by adjusting the trial structure to reproduce the Q-branch data, but although μ_c, R-branches were expected to be strong, they were not obvious features of the spectrum.

$K_a = 7 \rightarrow 8$ Q-Branches Showing Quadrupole Splitting.
220 V/cm. Vibrational Satellites due to C—C Torsion.

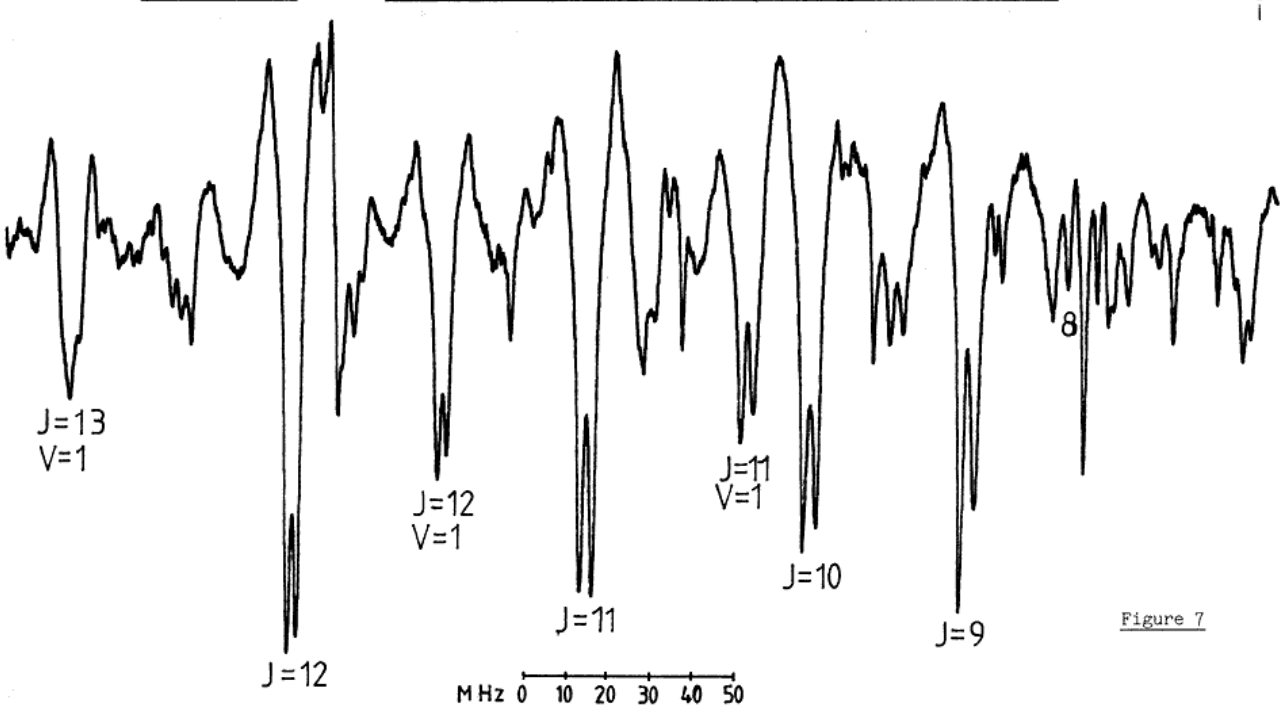

Figure 7

This is partly due to the difference between Stark effects for Q- and R-branch transitions. For a $\Delta M_J = 0$ spectrometer, the relative intensities of the different M_J components are[89] ;

For Q branches $I_{MJ} \propto M_J^2$

For P or R branches $I_{MJ} \propto (J + 1)^2 - M_J^2$ (J = J lower)

where $M_J = J, J-1, \ldots\ldots, 1, 0$.

For a Q-branch, the most easily modulated Stark component ($M_J = \pm J$) is also the most intense, whereas for an R-branch the strongest component ($M_J = 0$) tends to remain superimposed on the zero field line. To compound this difficulty, most of the R-branches in the region studied have large quadrupole splittings to spread their intensity.

The first R-branches to be assigned were the μ_c, $3_{30} \leftarrow 2_{20}$ and $3_{31} \leftarrow 2_{21}$. There were identified by pumping the $2_{20} \leftarrow 2_{21}$ at 48 MHz and scanning the region 21.5 - 22.5 GHz (see Figure 8). The transitions occur in a particularly dense part of the Ka = 6 → 7 Q-branch band and so were not measured accurately. Instead, their frequencies were estimated and successfully used to predict other R-branches more conveniently placed.

During the course of work on the ground state spectrum of gauche-$^{35}ClF_2CCHO$ a wide variety of transitions were measured enabling quartic centrifugal distortion constants to be determined. The trial structure, adjusted to fit the observed rotational constants was then used to predict rotational constants for $^{37}ClF_2CCHO$ and $^{35}ClF_2CCDO$. Spectra of these species were assigned without difficulty on the basis of quadrupole patterns and Stark effects. Quadrupole splittings in the ^{37}Cl spectrum were consistent with the chlorine quadrupole moment ratio[42]. The observed quadrupole coupling constants for $^{35}ClF_2CCDO$ were determined to be significantly different from those of $^{35}ClF_2CCHO$.

After completion of the experimental work described here, the microwave spectrum of the oxygen-18 species $^{35}ClF_2CCH^{18}O$ was studied by Dr. A Peter Cox

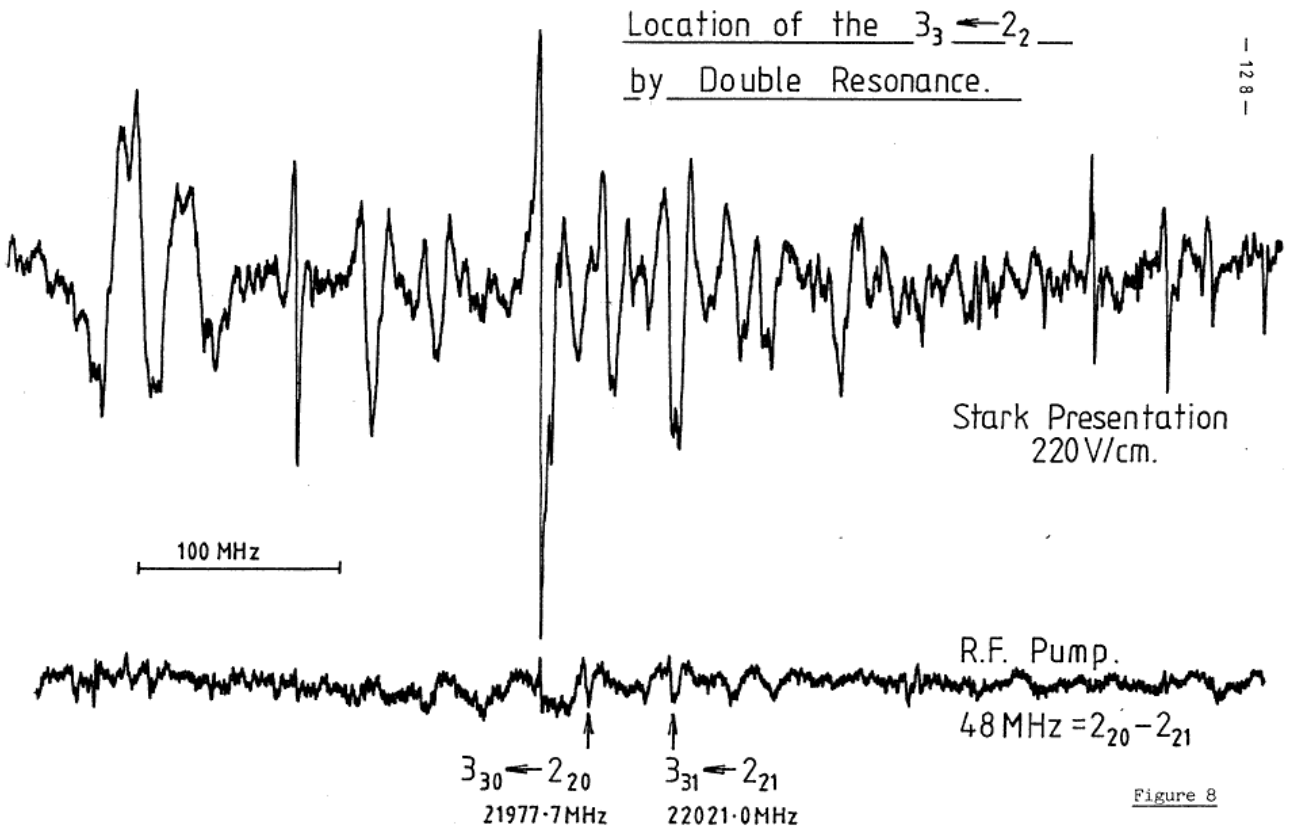

Figure 8

and Jeremy Randell.[90] These workers kindly made their results available to the author. The spectrum of this species was obtained by hydrating the parent compound with a large excess of ^{18}O water. It was found that the aldehyde hydrate dissociated on entering the spectrometer cell at low pressure. This explains the attenuation of the parent ion in the mass spectrum of $ClF_2CCH(OH)_2$ as described earlier, it also places some doubt on the general utility of the aldehyde as a dehydrating agent. At the time of this study, the structure of the molecule was sufficiently well known to predict the ^{18}O species rotational constants to within 1 MHz. Accurate rotational and quadrupole coupling constants determined from the study are used in the data analysis which follows.

Collected ground state rotational constants for all species of chlorodifluoroacetaldehyde so far studied are given in Table 1. Full details of the data employed in their determination are given in the data section at the end of the chapter.

TABLE 1

Ground-State Rotational Constants/MHz and Centrifugal Distortion Constants/KHz*.

	$^{35}ClF_2CCHO$	$^{37}ClF_2CCHO$	$^{35}ClF_2CCDO$	$^{35}ClF_2CCH^{18}O$
A_o	3 950.572 (9)	3 918.392 (25)	3 854.286 (8)	3 918.404 (21)
B_o	2 405.923 (10)	2 361.761 (26)	2 360.676 (8)	2 306.155 (22)
C_o	2 075.369 (10)	2 033.773 (35)	2 061.007 (9)	1 992.339 (24)
Δ_J	1.05 (14)	0.84 (65)	0.88 (11)	0.36 (37)
Δ_{JK}	-3.47 (3)	-3.76 (10)	-2.70 (3)	-2.66 (6)
Δ_K	8.46 (6)	8.79 (26)	6.96 (6)	7.56 (10)
δ_J	0.355 (3)	0.365 (6)	0.290 (3)	0.340 (6)
δ_K	1.08 (7)	0.80 (20)	0.42 (9)	0.89 (15)
Transitions	53	25	37	19

*A-reduction (I^r representation); errors = 1σ from least squares fit.

STRUCTURE OF GAUCHE ClF_2CCHO

Ground state rotational constants, corrected for centrifugal distortion, and effective moments of inertia for the various isotopic species are reproduced in Table 2. Inspection of the planarity relationships ($I_A + I_B - I_C$) immediately reveals that both the chlorine and the oxygen atoms lie close to or in the a, b plane. In fact, the Kraitchman procedure[91] yields imaginary c co-ordinates for these atoms (see Table 4) this being attributable to zero-point vibrational effects.

Actual determination of the structure made use of the method of Nösberger Bauder and Günthard[58] . This involves least-squares fitting of the isotopic moments of inertia to the molecular valence co-ordinates. If there are isotopic substitution data for every atom in the molecule, the structure determined by least-squares fitting is similar to the r_s (Kraitchman) structure. The least-squares method, however, permits full use of all of the available data, and automatically places the origin of the principal axes at the centre of mass. It is also the obvious choice where there are limited data, provided it is recognised that computed structural parameters can become seriously contaminated by zero-point effects in these circumstances.

Gauche-chlorodifluoroacetaldehyde is a totally asymmetric species having 3N-6 = 15 internal degrees of freedom. There are twelve independent moments of inertia available. Assumptions therefore have to be made in order to generate surplus degrees of freedom for the fit (observations minus parameters) and to allow for vibrational averaging. Two assumptions can be made readily;

(i) The C-CHO fragment is planar due to sp^2 hybridisation of the aldehyde carbon atom.

TABLE 2

Rotational Constants/MHz and Effective Moments of Inertia/uÅ^2

	$^{35}ClF_2CCHO$	$^{37}ClF_2CCHO$	$^{35}ClF_2CCDO$	$^{35}ClF_2CCH^{18}O$
Ao	3 950.574 (9)	3 918.394 (25)	3 854.287 (8)	3 918.404 (21)
Bo	2 405.918 (10)	2 361.757 (28)	2 360.674 (8)	2 306.150 (22)
Co	2 075.371 (10)	2 033.774 (35)	2 061.007 (9)	1 992.340 (24)
Kappa	-0.64745	-0.65194	-0.66579	-0.67414
I_A	127.9255 (3)	128.9761 (8)	131.1213 (3)	128.9757 (7)
I_B	210.0566 (9)	213.9843 (25)	214.0825 (7)	219.1440 (21)
I_C	243.5126 (12)	248.4932 (43)	245.2097 (11)	253.6610 (31)
$I_A + I_B - I_C$	94.4965 (15)	94.4672 (50)	99.9940 (13)	94.4587 (38)

Errors (in brackets) are one standard deviation.

(ii) McKean[23] has demonstrated a correlation between bond lengths and stretching frequencies for isolated C-H bonds. He gives the emperical relationship;

r_o /Å = 1.402 - 0.0001035 [ν(C-H) is /cm^{-1}]

since, for ClF_2CCHO ν(C-H) = 2855 cm^{-1},

this gives r_o(C-H) = 1.106_5 Å .

Further assumptions then made in order to cope with insufficient data are as follows;

(iii) Both C-F bond lengths are the same.

(iv) Both C-$\hat{C}$-F angles are the same.

(v) Both projections of Cl-$\hat{C}$-F angles onto a plane perpendicular to the C-C bond (denoted ϕ_{F-C-Cl}) are the same.

Three possible sets of structural parameters, obtained by least-squares fitting, are given in Table 3. Case (1) employs only the constraints given above, Case (2) also constrains both projections of F-$\hat{C}$-C angles onto a plane perpendicular to the C-Cl bond (denoted ϕ_{F-C-C}) to be 120°, and Case (3) constrains r(C-F) to be 1.345 Å as in[92] CF_2Cl_2. In each case also, an allowance has been made for shrinkage of the C-H bond by 0.0041 Å on deuteration (by analogy with formaldehyde[93]). This was done by adjusting the ClF_2CCDO moments of inertia to compensate for such a change, the required shifts being obtained from a structure close to the final one in each case. The quantity σ_{fit} is defined by;

$$\sigma_{fit} = \sqrt{\sum_i \frac{\left(I_i^{obs} - I_i^{calc} \right)^2}{n_I - n_P}}$$

I = moment of inertia

n_I = number of moments of inertia used (= 12)

n_P = number of variable parameters in the fit.

TABLE 3

STRUCTURE OF GAUCHE-ClF_2CCHO

Parameter	Case (1)	Case (2)	Case (3)
r (C-Cl)	1.749 (18)	1.740 (18)	1.749 (21)
r (C-F)	1.363 (12)	1.349 (7)	1.345 (assumed)
r (C-C)	1.498 (30)	1.538 (8)	1.535 (27)
r (C=O)	1.196 (5)	1.190 (4)	1.189 (6)
r (C-H)	1.1065	1.1065	1.1065
C-$\hat{C}$-O	124.82 (23)	124.75 (26)	124.63 (25)
C-$\hat{C}$-H	114.93 (48)	114.53 (47)	114.57 (81)
C-$\hat{C}$-Cl	110.63 (97)	109.43 (55)	109.24 (24)
C-$\hat{C}$-F	110.3 (1.3)	-	109.1 (1.4)
Ø (F-C-Cl)	121.42 (81)	-	120.83 (91)
F-$\hat{C}$-Cl	-	110.90 (84)	-
Ø (F-C-C)	-	120.0 (assumed)	-
α	109.42 (16)	109.44 (19)	109.51 (24)
$\sigma_{fit}/\mu\text{Å}^2$	0.0076	0.0218	0.1016

Notes: Bond lengths/Å Angles/Degrees

Structure (1) fits all of the available moments of inertia practically to within experimental error. It is therefore immediately suspect because it has absorbed all of the contribution from zero-point vibrational effects. It is also unsatisfactory because the C-F bonds are long compared with other molecules [79,92] and the C-C bond is too short. These two parameters must, of needs, be correlated in the absence of ^{13}C data for the methyl group carbon atom. Attempts to avoid this difficulty led to the additional constraints used in structures (2) and (3).

Both (2) and (3) are acceptable working structures. They are also arguably the same, since all parameters agree within their uncertainties. Table 4 gives the principal axis co-ordinates of the atoms in structure (3), for comparison with the Kraitchman co-ordinates for Cl, H and O given in the same table. Note that discrepancies between the least-squares structure co-ordinates and the Kraitchman co-ordinates, for the H atom, are mainly due to the shrinkage correction.

TABLE 4

Gauche ClF_2CCHO

Principal Axis Co-ordinates / Å

Atom	a	b	c
C_{Me}	-0.02231	-0.31945	-0.01938
Cl	-1.40508	0.75031	0.01437
F	0.28095	-0.73422	1.22361
F	-0.28304	-1.40019	-0.77639
C_{al}	1.18196	0.42895	-0.60819
H	1.10817	0.63867	-1.69213
O	2.13450	0.77246	0.01492

Kraitchman Co-ordinates / Å

Atom	|a|	|b|	|c|
Cl	1.40574	0.74929	0.0239i
H	1.10896	0.63603	1.68407
O	2.13471	0.77149	0.0552i

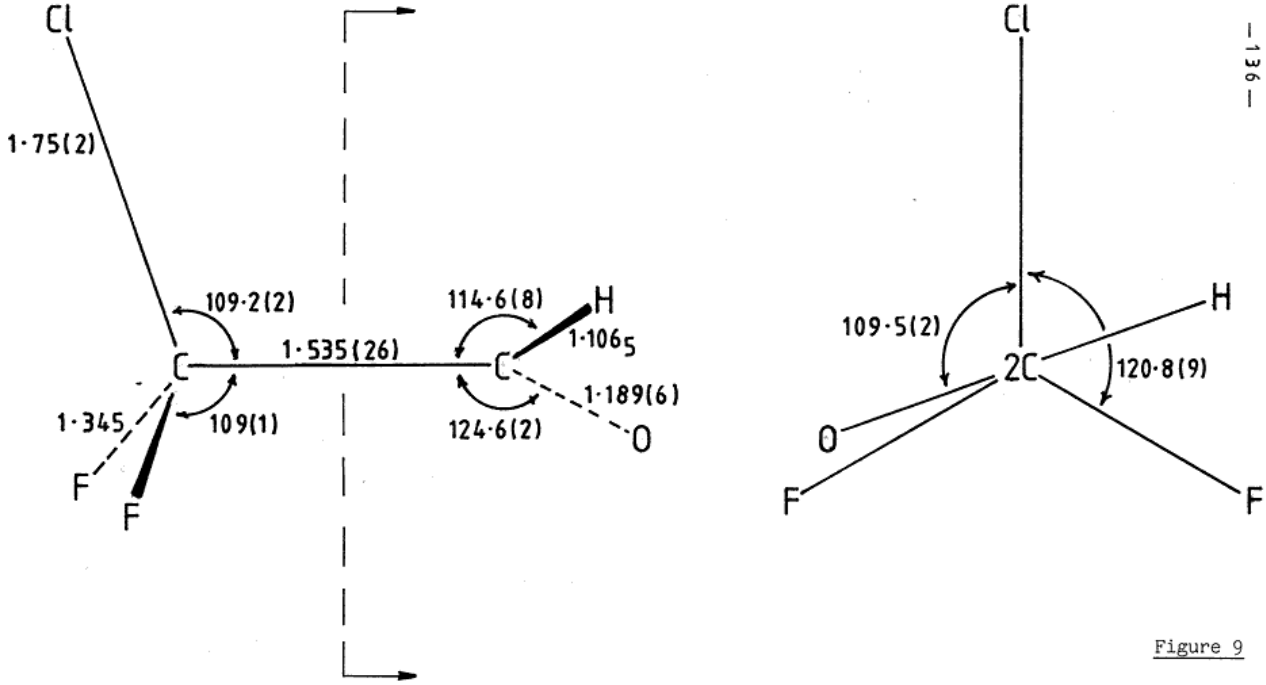

Figure 9

Structure of Gauche Chlorodifluoroacetaldehyde.

Certain features of the structure are well determined from the fit, notably the C=O bond length and α, the preferred conformational angle. The r(C=O) value obtained (1.190 A) is shorter than that of acetaldehyde (1.207 A)[56] and of formaldehyde (1.207 A)[93] . This is consistent with an increase of the C=O stretching frequency compared to that of acetaldehyde[94] (1775 cf 1743 cm^{-1}). The determined value for α (109.5°) is considerably different from the expected value of 120° for a gauche molecule. It is also a very important parameter to be carried through into the internal rotation analysis which follows later. For this reason, the possibility of its value being an artefact was carefully investigated. All of the isotopic data were re-fitted with α as a constant. It was then found that α could not be changed from 109.5° without serious degradation of the fit and unacceptable bond length changes. This follows because there are isotopic substitution data for both Cl and O. The Cl-O non-bonded distance is therefore well determined. This, in combination with the centre-of-mass requirements, imposes considerable constraint on the possible value of α.

^{35}Cl QUADRUPOLE COUPLING IN GAUCHE - ClF_2CCHO

Quadrupole coupling constants for the main, oxygen-18 and deuterium species of gauche-chlorodifluoroacetaldehyde were determined from spectroscopic line splittings using the method given in Appendix 4. Least-squares fits to the data are given at the end of this chapter. The results are summarised in Table 5.

It has already been established from the structure (see Table 4) that the C-Cl bond for the main species lies almost exactly in the a, b plane. The same is also true of the ^{18}O and D species. Inspection of the quadrupole coupling constants (Table 5) reveals that χ_{cc} is invariant with isotopic substitution. This implies that the z-axis of the quadrupole coupling tensor also lies in the a, b plane. It follows that the only non-zero off diagonal coupling constant, for any of the three isotopic species, will be χ_{ab}. Use of this accidental planarity relationship permits complete determination of the quadrupole coupling tensor.

Isotopic substitution gives rise to a rotation, $\delta\theta$, in the orientation of the quadrupole tensor with respect to the molecular principal axes;

$$R^{-1}\begin{bmatrix}\chi_{aa} & \chi_{ab} & 0\\ \chi_{ab} & \chi_{bb} & 0\\ 0 & 0 & \chi_{cc}\end{bmatrix} R = \begin{bmatrix}\chi'_{aa} & \chi'_{ab} & 0\\ \chi'_{ab} & \chi'_{bb} & 0\\ 0 & 0 & \chi_{cc}\end{bmatrix}$$

where;

$$R = \begin{bmatrix}\cos\delta\theta & -\sin\delta\theta & 0\\ \sin\delta\theta & \cos\delta\theta & 0\\ 0 & 0 & 1\end{bmatrix}$$

hence;

$$\chi'_{aa} = \chi_{aa}\cos^2\delta\theta + \chi_{bb}\sin^2\delta\theta + \chi_{ab}\sin 2\delta\theta$$

$$\chi'_{bb} = \chi_{aa}\sin^2\delta\theta + \chi_{bb}\cos^2\delta\theta - \chi_{ab}\sin 2\delta\theta$$

TABLE 5

GAUCHE-CHLORODIFLUOROACETALDEHYDE

Chlorine -35 Quadrupole Coupling Constants/MHz

	main species	D	^{18}O
χ_{aa}	-34.175 (109)	-33.141 (91)	-30.965 (175)
χ_{bb}	- 2.441 (74)	- 3.415 (68)	- 5.796 (85)
χ_{cc}	36.616 (74)	36.556 (68)	36.761 (85)
χ_{ab}	51 (5)		
χ_{xx}	36.6 (2)		
χ_{yy}	35.1 (40)		
χ_{zz}	-71.7 (40)		
$\theta_{a,C-Cl}$	36.4 (7)° (structural 36.7)°		

and hence;

$$\chi_{ab} = \frac{(\chi'_{aa} - \chi'_{bb}) - (\chi_{aa} - \chi_{bb}) \cos 2\delta\theta}{2 \sin 2\delta\theta}$$

The parameter $\delta\theta$ can be estimated from the shift, on isotopic substitution, of the angle between the a-axis and the C-Cl bond axis (denoted $\theta_{a,C-Cl}$). $\theta_{a,C-Cl}$, determined from structure, for each of the three isotopic species, is as follows;

Species	$\theta_{a,C-Cl}$/Degrees
ClF_2CCHO	36.731
ClF_2CCDO	37.177
$ClF_2CCH^{18}O$	38.795

Two independent determinations of χ_{ab} are possible with these data. χ_{ab} given in Table 5 is the weighted average, greater weight being given to the ^{18}O substitution because the shift, $\delta\theta$, is larger. Diagonalisation of the main species quadrupole tensor then gives the coupling constants in the quadrupole principal axis system and also gives the orientation of the tensor with respect to the molecule principal axes.

Results, given in Table 5, show that, within experimental error, the quadrupole tensor lies along the C-Cl bond direction and is cylindrically symmetric. This implies that the amount of π character in the C-Cl bond is small.

Determination of the principal coupling constants allows an estimate of the ionic character of the C-Cl bond to be made. Chlorine valence electrons have a principal quantum number n = 3, so that s, p and d electrons may be involved in the bonding. Only p electrons will be considered here since s electrons give no field gradient at the chlorine nucleus, and the effect of d electrons cannot be independently determined. Orbital overlap, charge screening and hybridisation effects will also be neglected, giving a particularly simple expression[42] for χ_{zz} in terms of the p orbital populations n_x, n_y and n_z, and the atomic quadrupole coupling constant $2b = eQq_{310}$

$$\chi_{zz} = 2b \left[n_z - \frac{(n_x + n_y)}{2} \right]$$

Jaccarino and King[95] give b = 54.873(5) MHz for ^{35}Cl. Assuming $n_x = n_y = 2$ gives n_z = 1.35(4) electrons. The chlorine atom in gauche-ClF_2CCHO therefore has a formal charge of -0.35e.

Electron withdrawing substituents at the carbon atom might be expected to affect the ionic character of the C-Cl bond. It is therefore interesting to compare the ClF_2CCHO quadrupole coupling constants with those of methyl chloride (eQq = -74.7434(15) MHz)[96] , trifluoromethyl chloride (eQq = -77.902(30) MHz)[88] and chloroacetaldehyde[97] . The complete quadrupole tensor for chloroacetaldehyde has not been determined, but on the assumption of a cylindrically symmetric field gradient at the chlorine nucleus, for the cis form (where the C-Cl bond lies in the a, b plane) $\chi_{zz} = -2\chi_{cc} = -72.48$MHz. If the electron withdrawing effect of the fluorine atoms were important for ClF_2CCHO, χ_{zz} might be expected to approach the eQq value of CF_3Cl. Instead it is convergent with $-2\chi_{cc}$ for cis-ClH_2CCHO. It must therefore be concluded, on the basis of the quadrupole coupling, that the two aldehydes have very similar C-Cl bonds.

Second-Order Quadrupole Coupling in Gauche -ClF_2CCDO

The 13_{85}-13_{77} and 13_{86}-13_{76} transitions in ClF_2CCDO are predicted, by first-order theory, to be split by the quadrupole. In fact, both transitions show an unresolved singlet at the hypothetical centre frequency. Inspection of the calculated energy levels reveals that the $14_{5,10}$ level lies only 29.3 MHz away from the 13_8 levels (K doubling at 13_8 is 0.06 MHz). The effect is therefore due to second-order quadrupole coupling.

Selection rules for the second-order quadrupole interaction are given by Schwendeman[98] . The interaction $13_{86} \leftrightarrow 14_{5,10}$ ($E^- \leftrightarrow 0^+$) is allowed via χ_{ab}, but the interaction $13_{85} \leftrightarrow 14_{5,10}$ ($E^+ \leftrightarrow 0^+$) is only normally

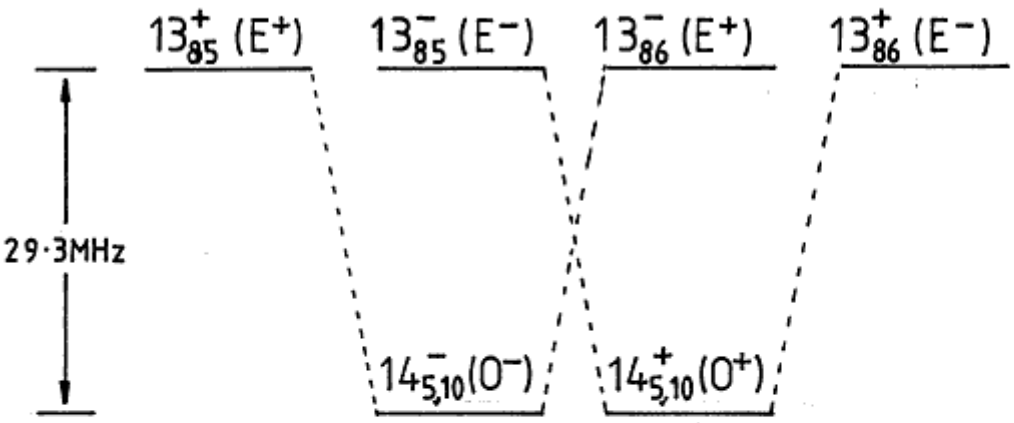

Figure 10

Gauche- ClF_2CCDO. Second Order Quadrupole Interaction Via χ_{ab}.

Energy Level Diagram.

allowed via χ_{ac}. From the results of the previous section, it is already known that, for ClF_2CCDO, $\chi_{ab} \simeq 53$ MHz and $\chi_{ac} \simeq 0$. Moreover, both transitions show identical perturbations. The normal selection rules are therefore violated. The only sensible conclusion to be drawn from this is that all of the energy levels involved are ($\pm$) doubly degenerate.

Except for the success of the localised conformer approach used in deriving the structure, it has not yet been revealed whether gauche-chlorodifluoroacetaldehyde has a low barrier to internal rotation, in which case the 0_+ and 0_- torsional states will be well separated, or a high barrier, in which case the 0_+ and 0_- states will be degenerate. The second-order quadrupole interaction is therefore direct evidence; that the observed spectrum belongs to a high-barrier molecule in the gauche form. As soon as the parities of the wavefunctions, with respect to inversion of the molecular c co-ordinates, are considered, the quadrupole interaction can be explained. It corresponds to $E^{\pm} \leftrightarrow 0^{\mp}$ via χ_{ab}, so that the 13^-_{85} state interacts with the $14^+_{5,10}$ and so on. Full details of the interactions are given in Figure 10.

VIBRATIONALLY EXCITED STATES

In addition to the ground-state data, the microwave spectrum of gauche-chlorodifluoroacetaldehyde has been analysed out to $\underline{v}$=3 in the torsional mode. A complete assignment is available up to $\underline{v}$=2 (see data section), but no R-branches were assigned for $\underline{v}$=3, so that only A-(B+C)/2 and Kappa are known in this case.

A plot of rotational constants vs torsional state, for the gauche form, is given in Figure 11. The graphs are shown extrapolated back to $\underline{v}= -\frac{1}{2}$ using the relationship;

$$B_e = B_v + \alpha'(v+\tfrac{1}{2}) + \beta(v+\tfrac{1}{2})^2$$

where B_e is the torsionless rotational constant. Simultaneous solution of the above equation for v=0, 1 and 2 gives;

$$B_e = \frac{15}{8}B_0 - \frac{10}{8}B_1 + \frac{3}{8}B_2$$

The torsionless rotational constants for gauche-chlorodifluoroacetaldehyde, determined in this way are (in MHz);

A_e = 3946.9

B_e = 2404.2

C_e = 2075.5

These constants were not used in the structure determination because there are insufficient data to perform the same extrapolation for all isotopic species used. In view of the assumptions necessary to define a complete structure, this will make an insignificant contribution to the structural error.

The variation of the rotational constants with torsional state is found to be smooth. This is consistent with ClF_2CCHO being a high-barrier molecule, since molecules with a low barrier to inversion tend to show a zig-zag pattern in this respect [97,99]. In addition, none of the transitions

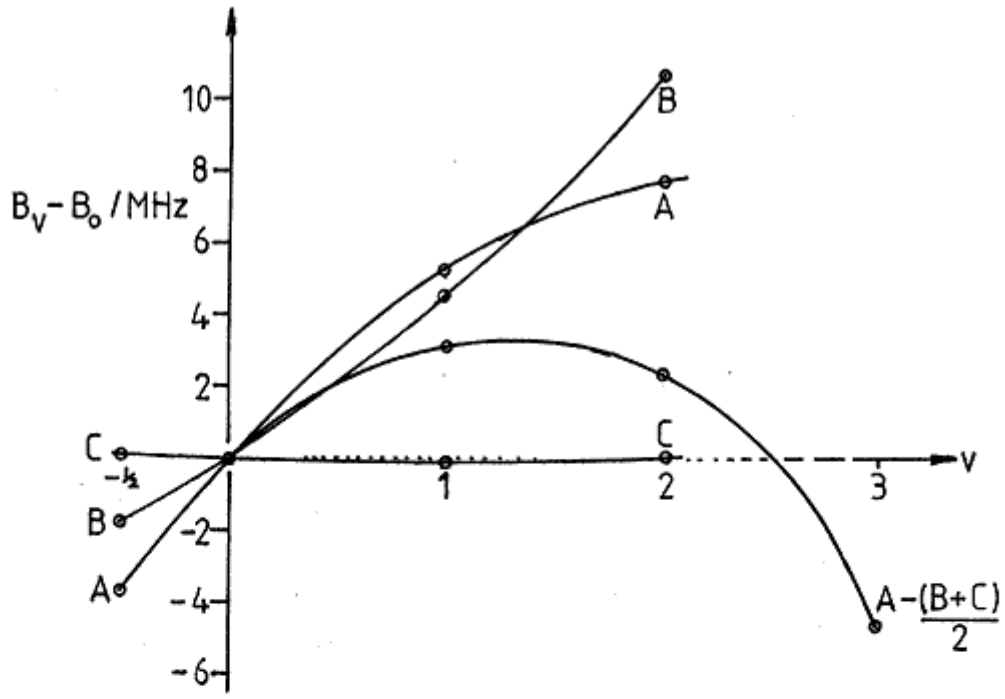

Variation of Rotational Constants with Torsional State (Relative to v=0).

Variation of κ with Torsional State.

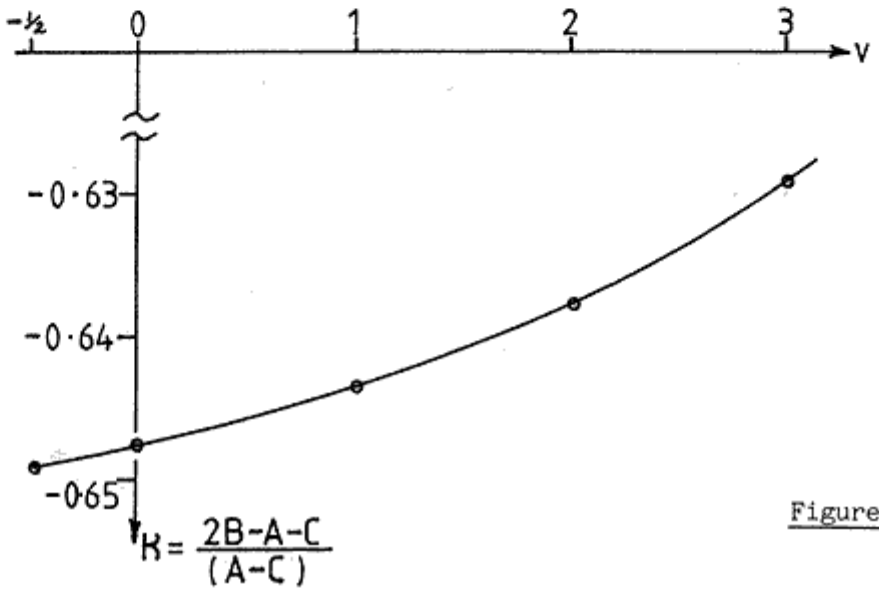

Figure 11

observed for torsionally excited states showed any sign of gauche-gauche doubling. Most of the transitions were μ_c type. It has been pointed out by Hirota[100], that for a molecule which inverts about the c-axis, the μ_c selection rule within a given $\underline{v}$ requires a change of inversion parity. μ_c transitions therefore show a splitting of twice the (+) ↔ (-) energy difference (ΔE_{+}^{-}). The spectrometer resolution being ~0.5 MHz, this implies that even for the $\underline{v}$=3 state, $\Delta E_{+}^{-} \lesssim 0.25$ MHz.

Figure 12 shows a group of excited state and chlorine-37 satellite lines due to the $17_{7,11}$-$17_{6,11}$ transition of gauche-ClF_2CCHO. The recording was made at dry-ice temperature. A careful comparison of the ground-state and $\underline{v}$=1 torsional-state relative intensities established the $\underline{v}$=0↠1 energy difference to be 95(5) cm^{-1}.

A line at 19839.7 MHz has been assigned to a $17_{7,11}$- $17_{6,11}$ transition on the basis of its Stark effect. Unlike other lines in the group, however, this line shows a splitting of 0.7 MHz. Its relative intensity indicates that it probably belongs to the C-Cl bending mode 250 cm^{-1} above the ground state (see FTIR spectrum later). This suggests that excitation of the bending vibration lowers the internal-rotation barrier sufficiently to allow observable gauche-gauche tunnelling.

The estimated torsional fundamental frequency $\nu(1 \leftarrow 0) \sim 95$ cm^{-1} falls in the range observable by Far-Infrared spectroscopy. The Fourier-Transform (FTIR) spectra of ClF_2CCHO and ClF_2CCDO were measured by Dr. Peter Goggin, using a Nicolet 7199A instrument. Spectra, shown in Figures 13 and 14, were recorded at room temperature using vapour samples in a 10 cm cell with polythene windows. Unfortunately, it is not possible to assign the torsional fundamental unambiguously in either of these spectra. The FTIR spectrum of ClF_2CCHO shows a small peak at 96.2 cm^{-1} as a high frequency shoulder on a group of strong absorptions. These strong absorptions do not appear to be artifacts, and are probably comprised mostly of torsional hot transitions attributable to the gauche form and also to an unidentified high energy form of the molecule (see next section).

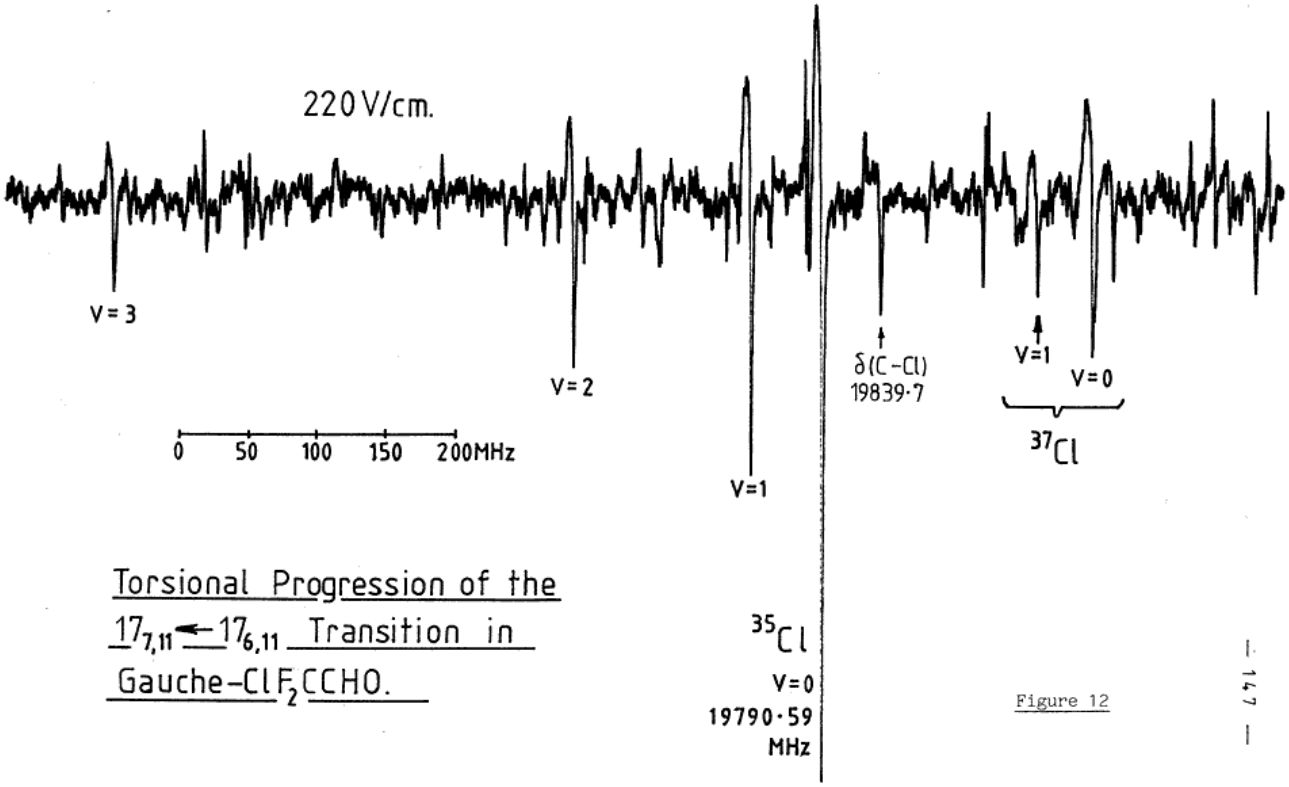

Torsional Progression of the $17_{7,11} \leftarrow 17_{6,11}$ Transition in Gauche-ClF_2CCHO.

Figure 12

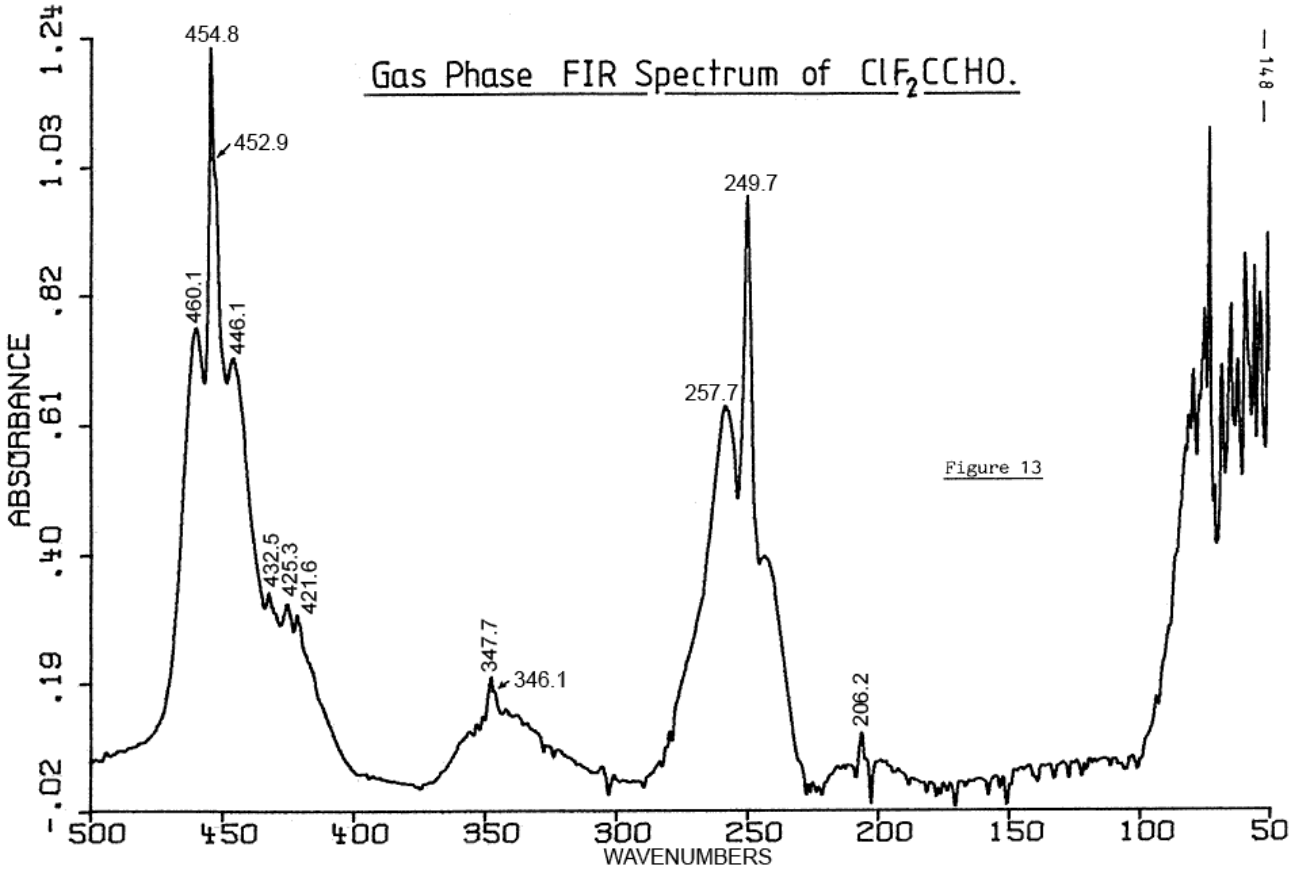

Figure 13

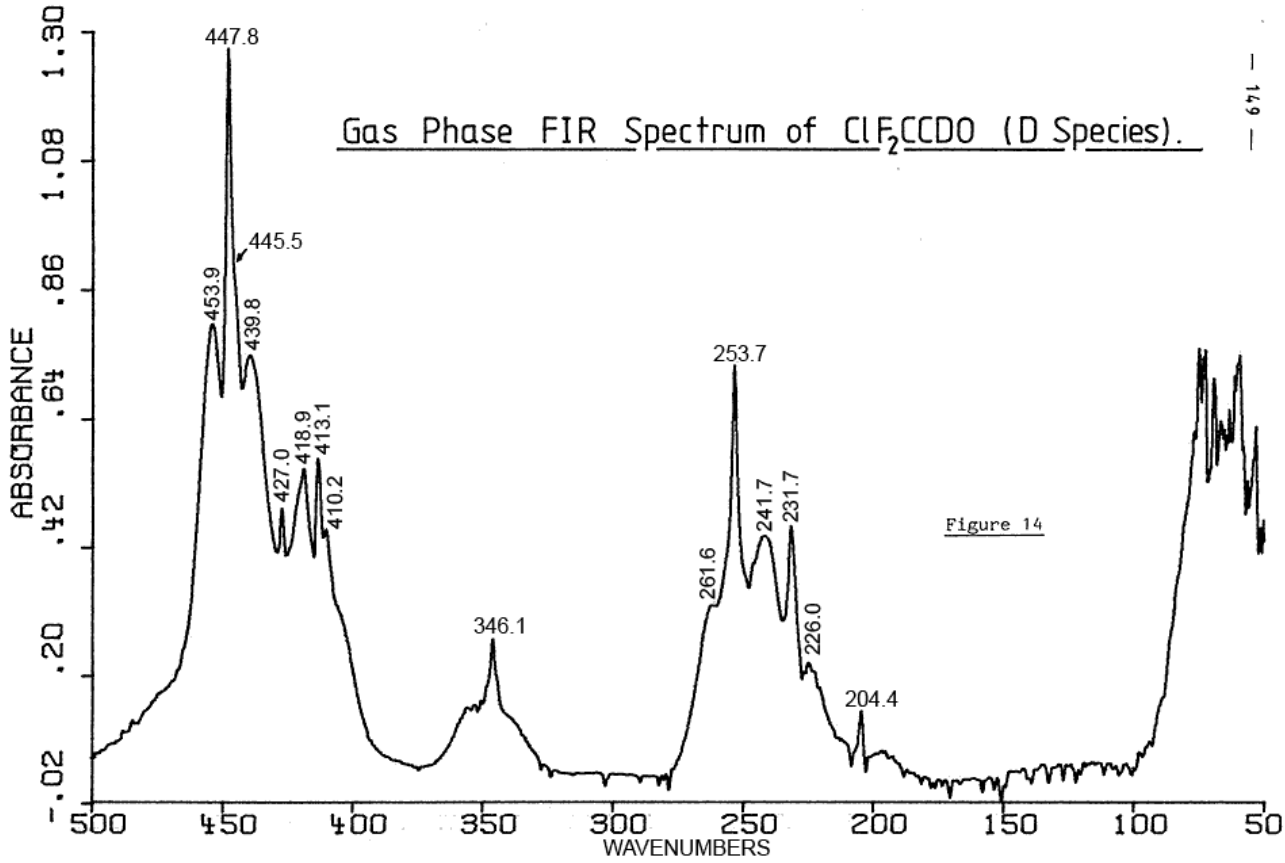
Gas Phase FIR Spectrum of ClF2CCDO (D Species).
ABSORBANCE
-.02
.20
.42
.64
.86
1.08
1.30
447.8
445.5
453.9
439.8
427.0
418.9
413.1
410.2
346.1
253.7
261.6
241.7
231.7
226.0
204.4
500
450
400
350
300
250
200
150
100
50
WAVENUMBERS

Figure 14

HIGH ENERGY FORM OF CHLORODIFLUOROACETALDEHYDE

During work on the microwave spectra of ClF_2CCHO and ClF_2CCDO, a large number of lines were encountered which could not be attributed to the gauche form. These lines are, with few exceptions, all very similar in appearance. They are characterised by a small splitting (1.0~1.7 MHz) and a slow, high-frequency Stark effect, requiring 1~2 KV/cm for full modulation. They are therefore suggestive of a species having few rotational degeneracies. They almost certainly do not arise from impurities in the samples, for two reasons. Firstly, the main and deuterium species line frequencies are all different, so that an impurity would have had to have been carried through from the $LiAlH_4/LiAlD_4$ stage of the preparation. Secondly, the species responsible behaves as if it is in thermal equilibrium with the gauche form. The relationship between the two species is therefore isomeric, rotameric or chemical. There is no obvious mode of chemical rearrangement for ClF_2CCHO. The spectrum is also not due to the aldehyde-hydrate because addition of water to the spectrometer attenuates the unknown and the gauche-form spectra to the same extent. It is therefore most probable that the unknown lines originate from an alternative rotameric form of ClF_2CCHO.

There is also some evidence for an alternative rotameric form of the molecule in the FTIR spectrum. Gauche-gauche splitting of the $17_{7,11}$-$17_{6,11}$ transition of the molecule in the lowest (250 cm^{-1}) bending mode (q.v.) indicates a coupling between this vibration and the torsion. One way of interpreting the difference between the main and deuterium species FTIR spectra in the 250 cm^{-1} region would be to assume that there are two distinct rotamers and that the effect of deuterium substitution on the coupling between C-Cl deformation and other vibrations is much greater in one than in the other. The main species FTIR spectrum (Figure 13) shows a strong

absorption at 250 cm^{-1} and an enhanced R-branch at 258 cm^{-1} which may hide another transition. The deuterium species FTIR spectrum (Figure 14) shows a strong absorption at 254 cm^{-1} and a weaker transition at 232 cm^{-1}. Deuterium substitution therefore apparently shifts the weaker transition from 258 cm^{-1} to 232 cm^{-1}. This effect may be due to the conformational dependence of the coupling between the various modes of vibration.

It was thought originally that the 'non-gauche' microwave transitions would be readily assignable to a cis form of chlorodifluoroacetaldehyde. The molecule chloroacetaldehyde has a cis form, of higher energy than a trans form (trans being the average configuration. ClH_2CCHO has energy minima in the gauche positions and a low inversion barrier) [97,101]. It was therefore reasonable to expect that ClF_2CCHO would also have a high energy cis form.

Modelling for the rotational constants of cis-ClF_2CCHO was carried out on the basis of a modified gauche structure, with some allowance for opening up of the Cl-$\hat{C}$-C and C-$\hat{C}$-O angles to accommodate chlorine in the eclipsed position. An estimate for the Cl-O non-bonded distance was made by fitting the cis-chloroacetaldehyde rotational constants[97] to an assumed structure. This suggested that the Cl-$\hat{C}$-C angle should be opened up to ~112° and the C-$\hat{C}$-O angle to ~126°. Cis-ClF_2CCHO rotational constants predicted on this basis are (in MHz);

A = 3364

B = 2849

C = 2130

giving Kappa = 0.165. The cis-conformer is therefore expected to be highly asymmetric, with a consequent lack of rotational degeneracies. Furthermore, a plot of Kappa versus internal-rotation angle (Figure 15), indicates that only structures close to the cis form would give rise to the more obvious characteristics of the observed spectrum.

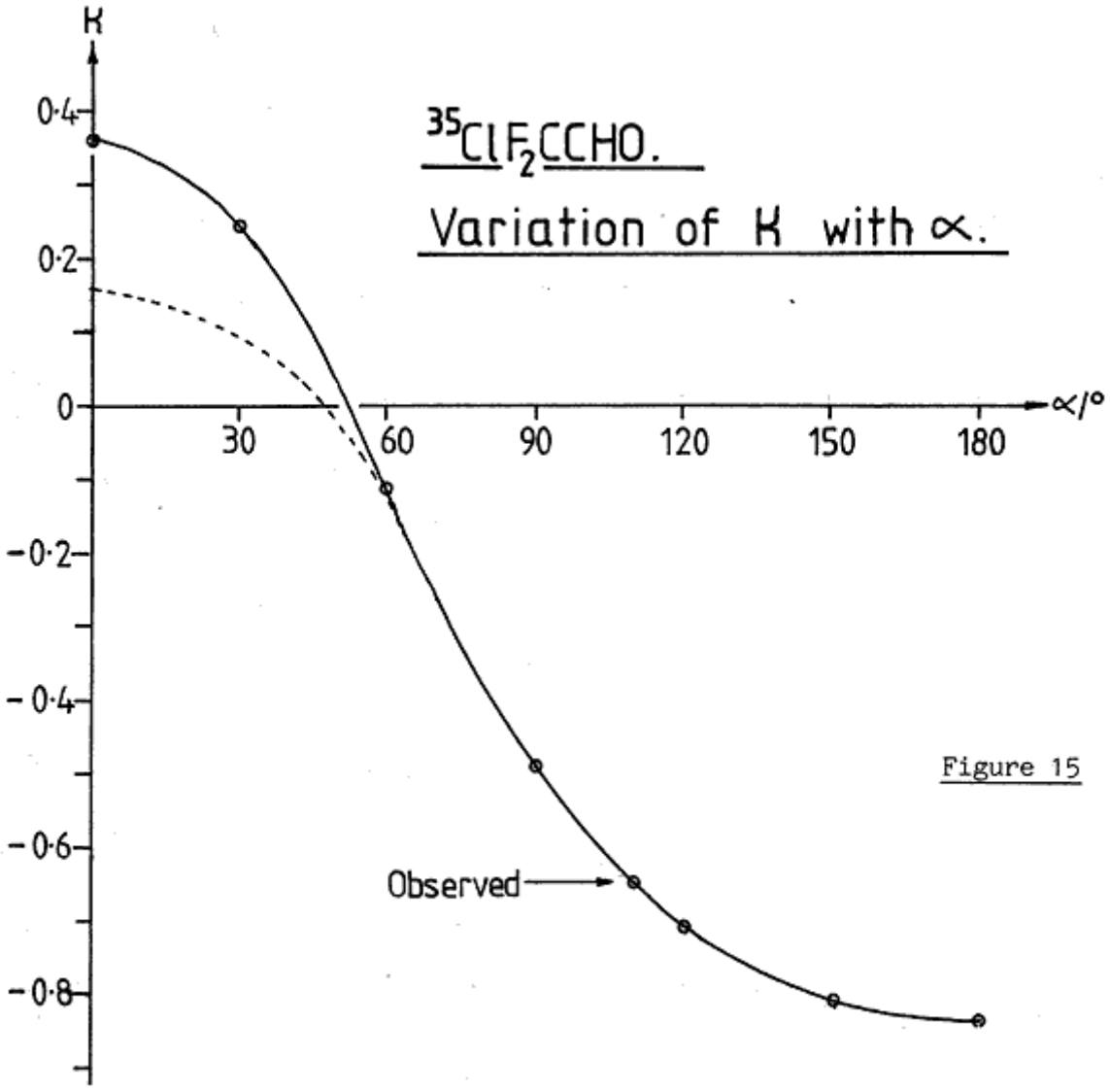

$^{35}ClF_2CCHO$.

Variation of K with ∝.

Figure 15

------Result of opening out the C-Ĉ-Cl and C-Ĉ-O angles to accomodate chlorine in the cis position.

After performing a number of broad scans, using modulating voltages of ~2KV/cm, it was noted that some of the non-gauche lines formed clearly identifiable series. Moreover, once four members of a series had been identified, it was possible to predict the rest in a stepwise manner by taking successive differences (see data section). Assignment seemed inevitable, until it became apparent that the series could not be accounted for using asymmetric rotor theory.

Two series occurring in the spectrum of ClF_2CCHO are shown in Figures 16 and 17. These, and also a series occurring in the spectrum of ClF_2CCDO, are shown plotted against an arbitrary abscissa in Figure 18. On moving along a series, the lines show a steady decrease in intensity, until they disappear into the background noise at the high frequency end. The decrease in intensity is also associated with greater ease of modulation, suggesting that the weakest lines correspond to the lowest J values. It is here, however, that the utility of pure asymmetric rotor theory ends. As can be seen from Figure 16, the series around 24 GHz has a point of inflection, but the series around 19.5 GHz actually folds back on itself. To the author's knowledge, pure asymmetric rotor theory cannot be used to generate progressions of the latter type. It therefore seems probable that the observed lines correspond to ro-vibrational transitions. They are also, to some extent, reminiscent of a series of transitions seen in the microwave spectrum of propargyl mercaptan[102] . Propargyl mercaptan has a low gauche-gauche energy barrier and a (+) $\leftrightarrow$ (-) energy separation, ΔE_{+}^{-} of 0.23 cm^{-1}. Its spectrum therefore shows long series of μ_c-type (+) $\leftrightarrow$ (-) torsional transitions which are, in effect, vibrational transitions occurring in the microwave region.

Two of the anomalous ClF_2CCHO lines were selected for relative intensity measurements in comparison with lines from the gauche form. Since the lines chosen were unassigned, measurements were made at two temperatures. This

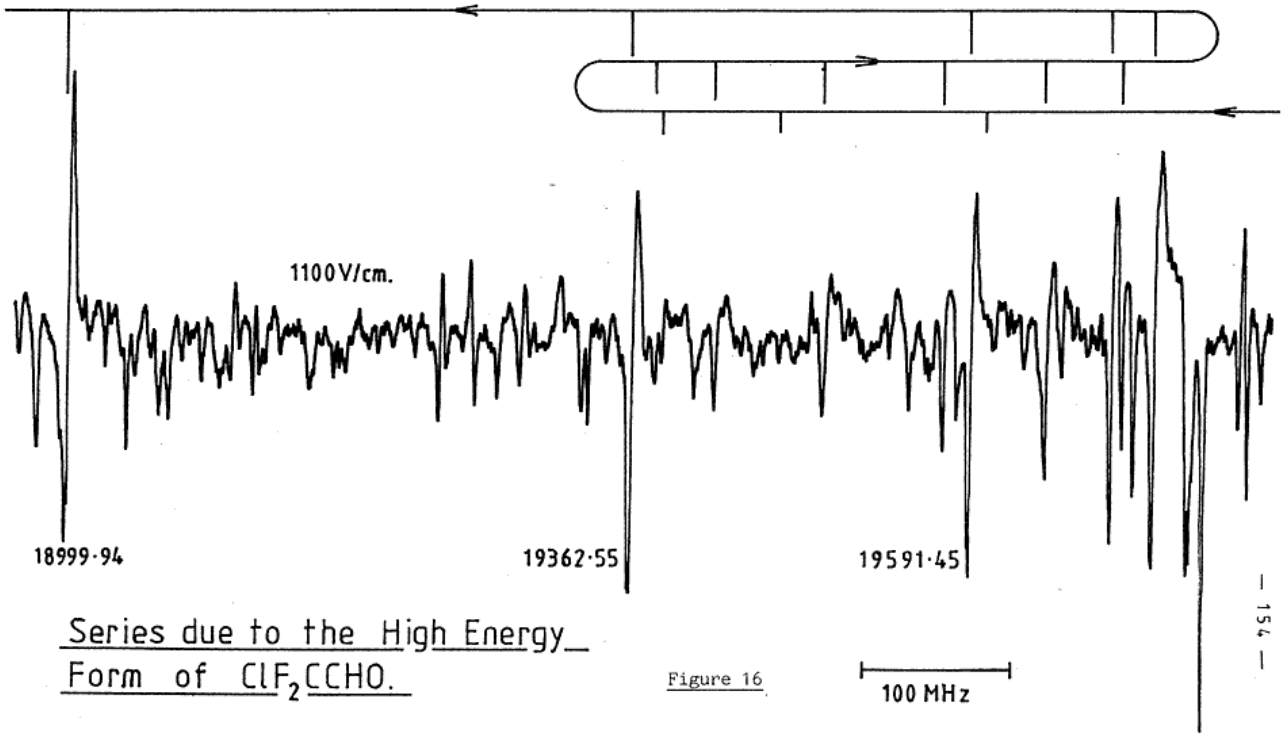

Series due to the High Energy Form of ClF_2CCHO.

Figure 16

has the effect of cancelling degeneracy and intensity factors, enabling the energy difference to be determined assuming that the two species are in thermal equilibrium.

The intensity of a line at 19747.27 MHz was compared with that of the gauche $17_{7,11}$-$17_{6,11}$ transition (19790.59 MHz) at 294 and 200K. This indicated the states responsible for the unknown line to lie 192(20) cm^{-1} above the (gauche) ground state. Similarly, a line at 23515.61 MHz was compared with the gauche - $30_{10,21}$-$30_{9,21}$ (23600.35 MHz) giving the energy difference to be 203(20) cm^{-1}. Both series therefore appear to belong to the same vibrational state.

It is interesting to note a small absorption in the FTIR spectrum of ClF_2CCHO (Figure 13) at 206 cm^{-1}. There is a corresponding absorption in the FTIR spectrum of ClF_2CCDO (Figure 14) at 204 cm^{-1}. It is possible that these correspond to direct transitions from the gauche ground state to the ground state of the unknown form.

The question as to the exact origin of the anomalous spectrum remains unanswered. It seems unlikely that the lines can come about as a result of accidental proximity of the 0_0 (cis) and $2_{\pm}$ (gauche) levels. $0 \rightarrow 2$ transitions are normally very weak, and an accidental degeneracy of this type would not be expected to be present in two different isotopic species. A more plausible explanation is that ClF_2CCHO cannot readily accommodate chlorine in the cis position. It may be that the methyl group is too crowded to allow the necessary opening of the $\overset{\wedge}{C\text{-}C\text{-}Cl}$ angle, so that a small hump appears in the internal rotation potential at $\alpha=0$. This could give rise to a slightly non-planar cis form, with the necessary low barrier to inversion. The anomalous series would then be μ_c type $(+) \leftrightarrow (-)$ transitions associated with the inversion process. Such an hypothesis might also account for many of the lines in the FTIR spectrum below 90 cm^{-1}, since a low barrier would give rise to many more close-lying states than would be expected for a conventional cis-form.

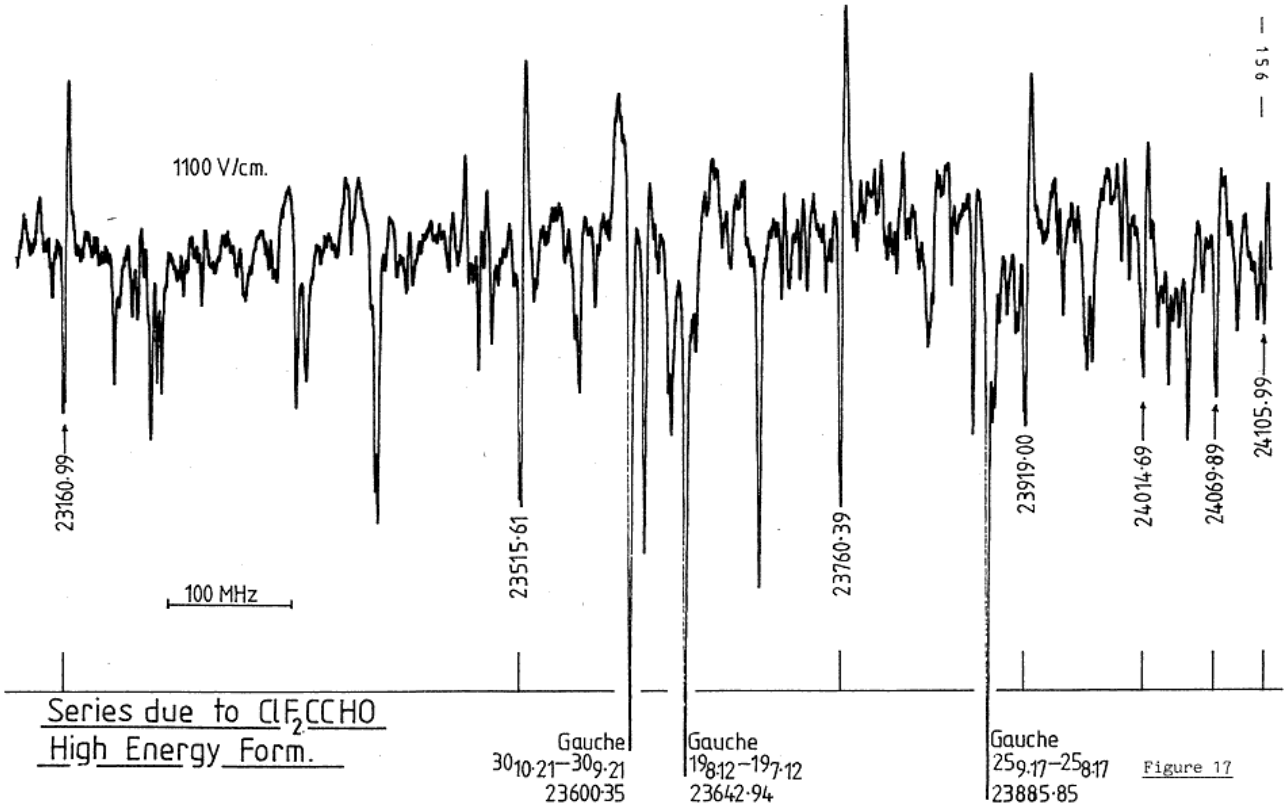
1100 V/cm.
23160·99
100 MHz
23515·61
23760·39
23919·00
24014·69
24069·89
24105·99
Series due to ClF2CCHO
High Energy Form.
Gauche
30 10·21 — 30 9·21
23600·35
Gauche
19 8·12 — 19 7·12
23642·94
Gauche
25 9·17 — 25 8·17
23885·85

Figure 17

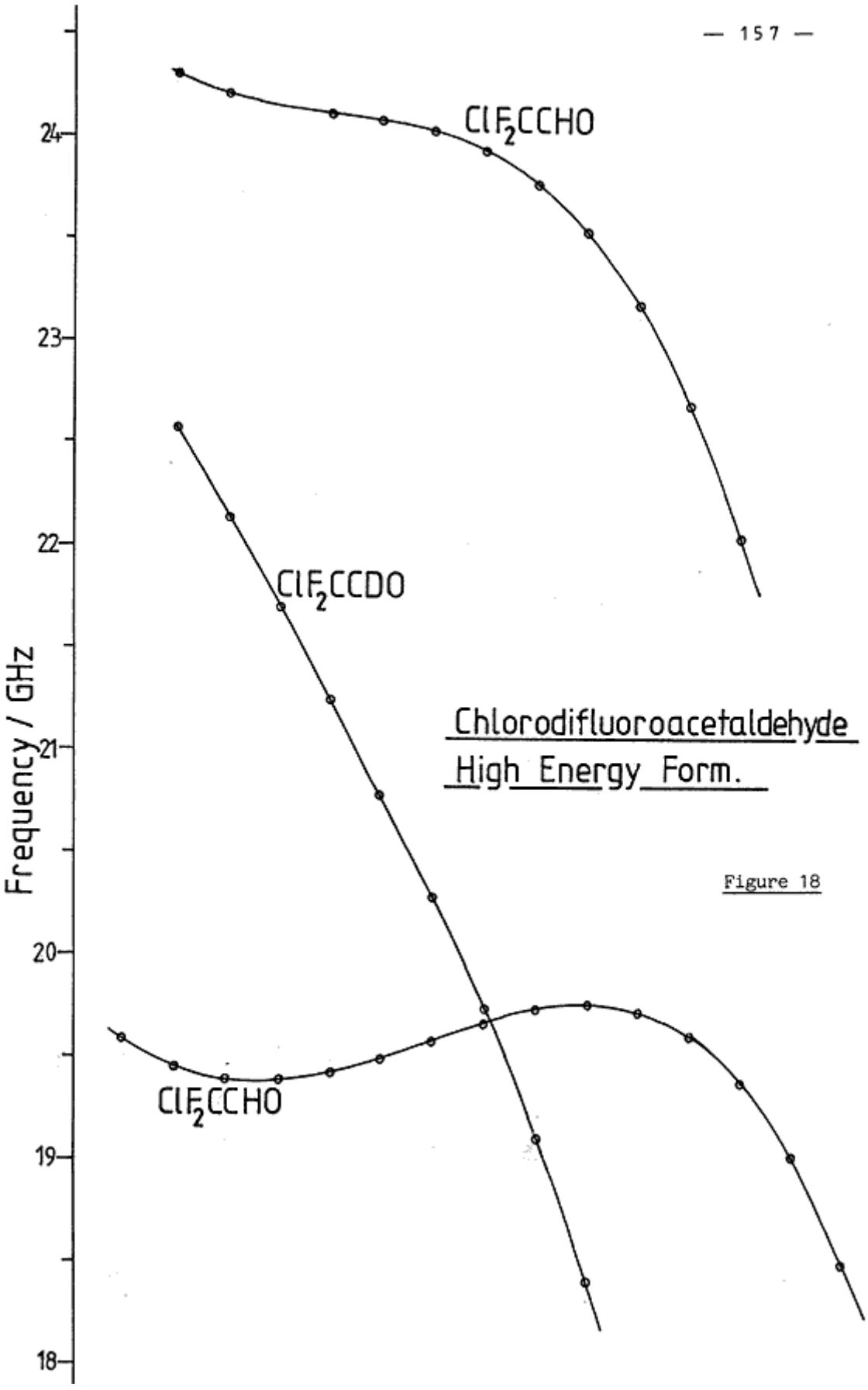

Chlorodifluoroacetaldehyde
High Energy Form.

Figure 18

CHLORODIFLUOROACETALDEHYDE: BARRIER TO INTERNAL ROTATION

Without data for the region of the cis potential minimum in ClF_2CCHO, it is impossible to determine a complete potential for internal rotation. Moreover, if the molecule does have a non-planar cis form, the potential function expressed as a Fourier series will be very complicated. For these reasons, a simplified model will be adopted here; that the cis form is localised at α=0 and lies 198(14) cm^{-1} above the gauche (as determined from the average of relative intensity measurements given earlier). It is then possible to make estimates for the barriers to conformer interconversion.

A plot of the internal rotation constant F as a function of alpha (determined using the method given in Appendix 5) is shown in Figure 19. It is clear, by inspection of the graph, that the best (simple) Fourier series for F is;

$$F(\alpha) = F_0 + F_2 \text{ Cos } 2\alpha .$$

From the structure (3) given earlier $F(109.5°) = 1.7473\ cm^{-1}$. Rotating the structure into the cis position and opening Cl-$\hat{C}$-C to 112° and C-$\hat{C}$-O to 126° gives $F(0°) = 2.0644\ cm^{-1}$. Reproduction of these values with the equation above requires the following Fourier coefficients;

$$F_0 = 1.886\ cm^{-1}$$

$$F_2 = 0.178\ cm^{-1}$$

These coefficients are used in the torsional Hamiltonian (see Appendix 6);

$$\hat{H} = \frac{-d}{d\alpha}(F_0 + F_2 \text{ Cos } 2\alpha)\frac{d}{d\alpha} + \tfrac{1}{2}\sum V_n(1-\text{Cos } n\alpha).$$

Potential coefficients (V_n) are chosen to reproduce the known energy spacings and the experimental conformational angle of the gauche form. Details of the potential calculation are given in Table 6, with a plot of the resulting function in Figure 20. From this it can be estimated that the barrier to gauche-gauche interconversion (trough to peak) is ~820 cm^{-1} and the barrier to gauche - cis interconversion is ~690 cm^{-1}. The gauche-gauche barrier, being consistent with experimental data should be reliable. It should be

noted, however, that the cis form in this model is hypothetical. The energy levels shown in the cis well of Figure 20 almost certainly do not correspond to those of the actual molecule. The gauche levels, on the other hand, are realistic.

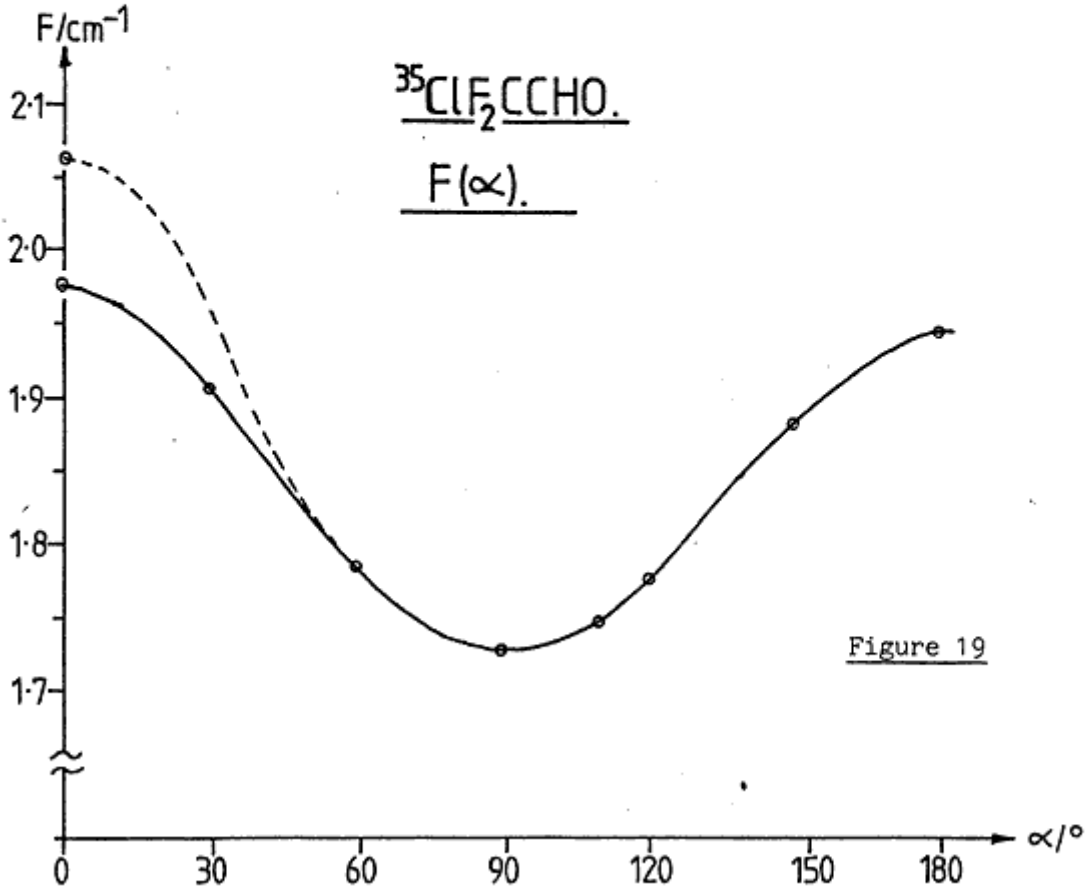

$^{35}ClF_2CCHO$.

F(∝).

Figure 19

– – – – –Result of opening out the Cl-C-C-O framework.

TABLE 6

Internal Rotation in 35-ClF2C-CHO.
Torsional Potential Program VFIT
3 Fold Dominated Potential

60 Basis Functions

	mu	ml	Obs	Obs-Calc	Weight
gauche	alpha	min	109.50000000	-0.13913521	1.0000
0- - 0+	-1	0	0.00000000	0.00000000	0.35942E+10
1- - 1+	-2	1	0.00000000	-0.00000000	0.35942E+10
2- - 2+	-3	2	0.00000000	-0.00000007	0.35942E+10
3- 3+	-4	4	0.00000000	-0.00000224	0.35942E+10
1+ - 0+	1	0	95.00000000	-0.03888647	0.10000E-01
1- - 0-	-2	-1	95.00000000	-0.03888647	0.10000E-01
1+ - 0-	1	-1	95.00000000	-0.03888647	0.10000E-01
1- - 0+	-2	0	95.00000000	-0.03888647	0.10000E-01
0o - 0+	3	0	198.00000000	-0.08340960	0.25000E-02
0o - 0-	3	-1	198.00000000	-0.08340960	0.25000E-02

E.S.D. of an Observation = 0.06460817/Sqrt(Weight)

Estimated Parameters		E.S.D.
F0	1.88600000	Const.
F2	0.17800000	Const.
V2	-349.86190430	1.09263735
V3	601.84117212	4.57320823
V4	129.00000000	Const.
V5	26.00000000	Const.

Energy Levels

State	E/cm^{-1}	$\Delta E_{\pm}$/MHz	State	E/cm^{-1}
$0_{\pm}$	-141.1	0	0_0	56.9
$1_{\pm}$	-46.0	0	1_0	166.9
$2_{\pm}$	46.1	0.002	2_0	268.2
$3_{\pm}$	134.9	0.07	3_0	359.6
$4_{\pm}$	219.9	1.5	4_0	437.3
$5_{\pm}$	300.8	20.1		
$6_{\pm}$	376.5	757.7		

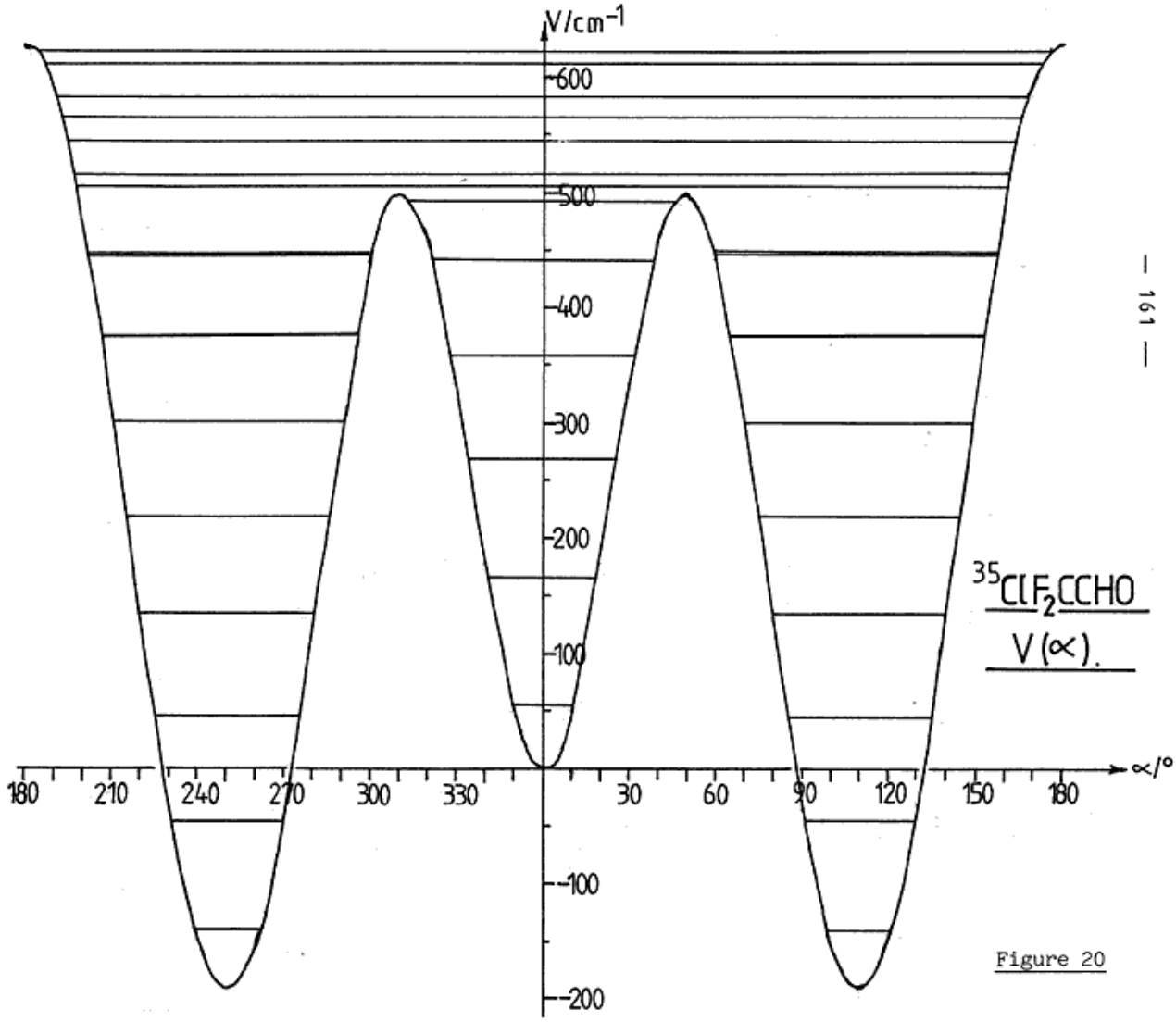
V/cm⁻¹
600
500
400
300
200
100
-100
-200
180
210
240
270
300
330
30
60
90
120
150
180
α/°
35ClF2CCHO
V(α).

Figure 20

DISCUSSION

In Chapter 1 it was mentioned that it would be useful to have some predictive theory, expressed in terms familiar to the chemist, to account for barriers to internal rotation. For the purpose of the present study, it is also of interest to predict the preferred ground-state conformation of ClF_2CNO so that its spectrum may be analysed. It is therefore instructive to make comparisons among a subset of small molecules where internal rotation occurs about a bond connecting an sp^2 to an sp^3 hybridised atom. This subset will however be restricted, since the primary concern is to compare aldehydes and nitroso-compounds.

To begin with, it is well known that the preferred conformation, in the sp^2 - sp^3 group, is nearly always one which has a bond attached to the sp^3 atom eclipsing the double bond. There are only two known exceptions to this rule; namely chloroacetaldehyde, CH_2ClCHO, and fluoroacetylfluoride, CH_2FCFO, both of which have forms with the methyl hetero-atom trans to the oxygen. Chloroacetaldehyde [97,101] is, however, not a true exception. The moments of inertia of the trans-form are not consistent with true planarity, and the rotational constants vary with torsional state in a zig-zag fashion indicating that the internal rotation potential has a small maximum at the trans position. The zig-zag behaviour comes about because of the alternating symmetry of the torsional wavefunctions. The odd functions have a node at the barrier position and are therefore relatively unaffected by it. Trans-CH_2ClCHO is therefore, in reality, a gauche-conformer with a low inversion barrier (60% of the zero point energy)[101] . It is still anomalous, however, because low barriers are very rare in the group of molecules under discussion.

Fluoroacetylfluoride[103] remains as a rule unto itself. The preferred conformation is with the fluorine cis to the oxygen, but the higher-energy trans-form poses a problem (the definitions of cis and trans adopted here are the reverse of those used in ref. 103). The moments of inertia of the

trans form are consistent with a planar geometry, although higher torsional states have not been assigned and so it is not clear whether the rotational constants will show a zig-zag behaviour. It is possible, therefore, that the molecule has a low gauche-gauche inversion barrier, but this is not very likely. It has been suggested instead that resonance is responsible for the anomaly[3]. The early CNDO/2 (complete neglect of differential overlap) ab-initio calculations of Pople and Gordon[104] suggest that fluorine is not only a strong σ electron acceptor, but also a weak π electron donor. It is possible therefore that fluoroacetyl fluoride has contributions from resonance structures such as;

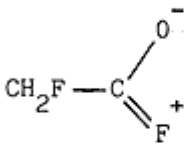

The exact nature of the potential energy surface in the region of the trans position would therefore be of considerable interest, but there has been no enthusiasm for the necessary experimental work. This is not surprising, however, because fluoroacetylfluoride is very toxic.

Some insight into why the sp^2-sp^3 internal rotors normally prefer the eclipsed confrmations has been given by LCAO-MO ab-initio calculations. Allen[105] proposed a division of the total electronic energy into attractive and repulsive components;

$$E_{el} = V_{ne} + (T_e + V_{nn} + V_{ee})$$

(The electron kinetic energy, T_e, being positive is grouped with the repulsive terms.) It was then found that the attractive and repulsive energies usually remained out of phase with respect to internal rotation. In ethane-like molecules (sp^3-sp^3) the repulsive term dominates in giving rise to the barrier and staggered conformations are preferred, but in the sp^3-sp^2 case, the attractive component helps to draw the rotating group into the eclipsed position. In acetaldehyde[105] and nitrosomethane[7] the barriers were found to be dominated by the attractive term, which led

Allen to propose an interaction somewhat like a weak hydrogen bond. It should be noted, however, that the methyl group staggers the nitrogen lone-pair in nitrosomethane, the aldehyde hydrogen atom in acetaldehyde, and the hydrogen atom on the central carbon in propene. Furthermore, the barrier in propene is actually dominated by the repulsive term[105], and an alternative energy component breakdown given by Liberles et al[106] suggests that, in this case it is predominantly due to an increase in the one-electron energy, $T_e + V_{ne}$. Nevertheless, it is legitimate to evoke attractive as well as repulsive contributions to the barrier, especially if a suitably placed electronegative atom is available.

Table 7 gives a list of effective barrier heights (V_3) in molecules with a symmetric sp^3-sp^2 internal rotor. The values given were all adjusted from microwave or combined microwave and optical data. One notable trend is that the alkene derivatives have considerably higher barriers than the aldehydes and nitroso- compounds. Liberles et al[106], on the basis of ab-initio calculations using standardised geometries, have suggested that the difference between acetaldehyde and propene is predominantly due to hyper-conjugation. The staggered (high energy) conformation in both molecules is apparently the most efficient for donation of methyl-hydrogen electron density into the π system. This molecular orbital is also anti-bonding across the sp^3-sp^2 C-C bond and is lowest in energy when the molecule is in its stable form. In acetaldehyde, however, the methyl C-H bonds are already polarised by the electron withdrawing effect of the oxygen atom. The change in electron density at the methyl group, on rotation into the high energy form, is therefore smaller in acetaldehyde than in propene. In fact, the change in acetaldehyde was calculated to be 59% of that in propene, which is also the ratio of the barrier heights (see Table 7). It remains to be seen, however, whether back-donation from fluorine p orbitals can similarly account for the barrier difference between fluoral and 3,3,3-trifluoropropene, but note that tri-fluoridation lowers the barriers in acetaldehyde and

TABLE 7

Symmetric Internal Rotors sp^3 - sp^2

Name	Formula	V_3/cm^{-1}	Refs.
Nitrosomethane	CH_3NO	405.3 (2)	50
Nitrosomethane-d_3	CD_3NO	390.0 (3)	50
Acetaldehyde	CH_3CHO	400.5 (2.4)	12
Acetaldehyde-d_3	CD_3CHO	397.5	11
Propene	$CH_3CH{=}CH_2$	682.9	11
Trifluornitrosomethane	CF_3NO	238 (2)	see Chapter 4
Fluoral	CF_3CHO	305 (26)	see Chapter 4
Fluoral-d	CF_3CDO	320 (26)	see Chapter 4
3,3,3-Trifluoropropene	$CF_3CH{=}CH_2$	1640 (800)	107

nitrosomethane and raises the barrier in propene. Schemes which evoke charge re-distribution during internal rotation to help account for the barrier, and inhibition of charge re-distribution, by suitable placement of electronegative substituents, as a barrier lowering agency, are therefore plausible. It would be of little value however to propose any complicated theory without a great deal of supportive evidence. Any single-factor theory of barrier heights is also obviously too simple.

Table 8 gives a collection of internal rotation data for molecules with an asymmetric internal rotor. The most striking trend is that, for all except two of the molecules, the preferred conformation can be deduced with a simple rule: if the molecule can place a hydrogen atom adjacent to an electronegative first-row atom (N,O,F) then this will take precedence. If not, the low-energy form will be the one with the smallest methyl substituent in the cis position. The two exceptions are fluoroacetyl fluoride (q.v.) and 3,3-difluoropropene. Note, however, that 2,3-difluoropropene, which is the iso-electronic analogue of fluoroacetylfluoride, is well behaved within the rule and is also unlikely to form resonance structures of the type suggested for fluoroacetylfluoride.

The rule stated, which is akin to evoking the competing effects of steric hindrance and Allen's weak hydrogen bond[105], is again too simple or it would have no exceptions. Nevertheless, it has sufficient predictive power to warrant consideration. It is therefore interesting to consider the CH_3 group V_3 barriers in nitrosoethane, propanal and 1-butene. These CH_3 groups rotate about a bond connecting sp^3 to sp^3 carbon and therefore almost certainly adopt the staggered conformation (this has been shown to be the case for propanal[108]). With the group cis to an oxygen atom, however, an attractive interaction would be expected to lower the energy of the eclipsed form. It would then be expected that, in propanal and nitrosoethane, the cis V_3 barrier would be lower than in the gauche, and in butene, the cis

TABLE 8

Asymmetric Internal Rotors sp^2-sp^3

Name	Formula	Stable Form	Metastable Form	$\Delta E/cm^{-1}$	Gauche $\alpha_{min}/°$	Gauche-gauche barrier/cm^{-1}	Stable→Metastable barrier/cm^{-1}	Refs.
Nitrosoethane	CH_3CH_2NO	cis	gauche	175(35)	125.5(5.0)	>230(45)	~635	25
Propanal	CH_3CH_2CHO	cis	gauche	420(52)	128.7	200(80)	750(100)	25,109,110
But-1-ene	$CH_3CH_2CH=CH_2$	gauche	cis	52(52)	119.9(3)	>605	-	111
3-Fluoropropene	$CH_2FCH=CH_2$	cis	gauche	58(23)	127(3)	520(40)	$1090\binom{+75}{-25}$	100,112
3-Chloropropene	$CH_2ClCH=CH_2$	gauche	cis		~122.4	$>>E_{0+}$		113
3-Bromopropene	$CH_2BrCH=CH_2$	gauche	-	-	~121.1	$>E_2$	-	114
3-Iodopropene	$CH_2ICH=CH_2$	gauche	-	-	~119.4	$>E_2$	-	115
Chloroacetaldehyde	CH_2ClCHO	Trans	cis			$\sim 0.6E_{0+}$		97,101
Glycolaldehyde	CH_2OHCHO	cis	-	-	-	-	-	116
3,3-Difluoropropene	$CHF_2CH=CH_2$	cis	gauche	260(80)	~120	~580	~600	117
Chlorodifluoronitrosomethane	CF_2ClNO	gauche	cis?	~180				See text.
Chlorodifluoroacetaldehyde	CF_2ClCHO	gauche	cis?	198(14)	109.5(2)	~820	~690	This work.
Fluoroacetylfluoride	CH_2FCFO	cis*	Trans*	318(35)	-	0		103
2,3-Difluoropropene	$CH_2FCF=CH_2$	cis	gauche	145(60)	~116.4	~955	1100	118

* Definitions altered from those in ref. 103 to be consistent with definitions used here.

V_3 barrier would be the same or higher than in the gauche. The evidence only partially supports this view (see Table 9). Propanal and butene behave as expected, but in nitrosoethane the cis and gauche V_3 barriers are practically the same.

TABLE 9

Name	Formula	V_3(cis)/cm^{-1}	V_3(gauche)/cm^{-1}	Refs.
Nitrosoethane	CH_3CH_2NO	878(31)	879(28)	25
Propanal	CH_3CH_2CHO	793.7(2.5)	$>V_3$(cis)*	119
But-1-ene	$CH_3CH_2CH{=}CH_2$	1396(4)	1105(14)	111

* Preliminary evidence (private communication. Dr. A.P. Cox).

It seems reasonable to conclude that short-range attractions and repulsions play a strong part in determining preferred conformations, but that any qualitative theory which relies solely on these effects will occasionally fail. The situation with regard to quantitative prediction is moreover worse. The conformer zero-point energy differences (ΔE) and interconversion barriers given in Table 8 show a fairly chaotic pattern. It will require a sophisticated theory to rationalise them all. This difficulty arises because of the delocalised nature of molecular orbitals and because of the smallness of the internal rotation barrier as a fraction of the total energy ($\sim 10^{-3}\%$)[5]. Nevertheless, the barrier does originate principally from the purely electronic part of the molecular energy, because ab-initio calculations which neglect nuclear kinetic energy generally predict barriers to internal rotation with good accuracy[4]. Moreover, such calculations usually neglect dispersion (VanderWaals type attraction) forces and relativistic effects without consequence, so that the origin of barriers to internal rotation is to be found within the self-consistent field (SCF, Hartree-Fock) approximation.

Returning now to the preferred conformation of chlorodifluoronitroso-methane, it is to be expected that the spectrum will arise from a stable gauche-form with a possible contribution from a high-energy cis- (or near-cis) form. Circumstantial evidence in support of this view is plentiful: A preference for gauche is to be expected on steric grounds, there is a close analogy between isoelectronic pairs of aldehydes and nitroso compounds (q.v.), and some features of the ClF_2CNO microwave spectrum are consistent with domination by the gauche form. Differences in appearance between the microwave spectra of ClF_2CNO and ClF_2CCHO must be expected as a consequence of the difference in dipole moments (the larger dipole moment of the aldehyde was one of the initial reasons for studying it as a model for ClF_2CNO). The aldehyde spectrum is dominated by the μ_c, whereas the nitroso compound is expected to have $\mu_c \simeq 0$. Bond moment calculations predict ClF_2CNO to have $\mu \simeq 0.5D$ in the approximate direction of the C-Cl bond, and the centre-of-mass requirements dictate, as they do in ClF_2CCHO, that the C-Cl bond will lie approximately in the a, b plane. Structure calculations based on CF_3NO (see Chapter 4), with a C-Cl bond length of 1.75 A and α=120° predict an angle between the a axis and the C-Cl bond axis of 31.7°. This predicts μ_a = 0.43D and μ_b = 0.26D. The rotational constants predicted for α=120° are A=4357, B=2447 and C=2159 MHz giving Kappa= -0.738, but there is no guarantee that this will correspond to the exact conformation adopted. Gauche-form conformational angles were included in Table 8 in the hope of seeing some pattern amongst various molecules, but none has emerged. This is partially because these angles are usually determined inaccurately by rotation of an assumed geometry to reproduce the observed rotational constants of only one isotopic species. Nevertheless, assignment of the microwave spectrum of gauche-ClF_2CNO should now be reasonably straightforward. There is also some evidence, from variable temperature studies of the visible spectrum[68], for the existence of a second form $\sim 180 cm^{-1}$ higher in energy than the stable form. This energy difference is remarkably similar to the $198(14) cm^{-1}$ difference between the two forms of ClF_2CCHO.

CHLORODIFLUOROACETALDEHYDE DATA

The following pages give raw data. Processed data appear in the text. Hypothetical line centres (Tables 10 - 18) were fitted to an asymmetric rotor Hamiltonian in Watson's A reduction in the I^r representation[38].

$$H^A = X^A P_X^2 + Y^A P_Y^2 + Z^A P_Z^2 - \Delta_J P^4 - \Delta_{JK} P^2 P_Z^2 - \Delta_K P_Z^4 - \delta_J [P^2, (P_x^2 - P_y^2)]_+ - \delta_K [P_z^2, (P_y^2)]_+$$

where $[A,B]_+ = AB + BA$

The effective rotational constants were obtained from the relationships[38];

$$A = Z^A + 2\Delta_J$$

$$B = X^A + 2\Delta_J + \Delta_{JK} - 2\delta_J - 2\delta_K$$

$$C = Y^A + 2\Delta_J + \Delta_{JK} + 2\delta_J + 2\delta_K$$

Observations (in MHz) given to two decimal places are assumed to have a standard deviation of 0.05 MHz. Those given to one decimal place have a standard deviation of 0.2 MHz and are therefore given 1/16th weight in the least-squares fit. Fitting weights are unity except where indicated.

Some asymmetry quartets could not be resolved. These appear in the data as a single transition labled with K_a only. For example, the $8_8 \leftarrow 8_7$ constitutes only a single observation but has intensity due to two asymmetry doublets, i.e. the C-type $8_{81} \leftarrow 8_{71}$ and $8_{80} \leftarrow 8_{72}$ and the B-type $8_{81} \leftarrow 8_{72}$ and $8_{80} \leftarrow 8_{71}$. In practice, the observation was put into the fit twice, each time with half weight, once as the $8_{81} \leftarrow 8_{71}$ and once as the $8_{80} \leftarrow 8_{72}$. The residuals (obs-calc) obtained were then averaged to obtain a residual for the $8_8 \leftarrow 8_7$. All unresolved pairs were treated similarly.

Some of the data sets for torsionally excited states (Tables 13, 15 and 16) contain no R-branch observations. In these cases, one rotational constant is assumed and therefore only A-(B+C)/2 and Kappa = (2B-A-C)/(A-C) (or some equivalent linear combinations) are determinable.

Following the tables of fits to hypothetical line centres are tables (19 and 20) of individual hyperfine components. Only transitions showing resolvable hyperfine structure are included in these tables. R-branches have the selection rule $\Delta F = +1$ and are labelled with $F_{UPPER} \leftarrow F_{LOWER}$. F takes on values J+I, J+I-1, ..., J-I where, for chlorine (35 and 37) I = 3/2. Q-branches have the selection rule $\Delta F = 0$ and are labelled with a single F per component. Where two Fs appear the transition contains two unresolved components and the frequency is taken to be the intensity weighted average of the two. Relative intensities of quadrupole hyperfine components have been taken from the tabulation by Gordy and Cook.[42] Where a component has been omitted, it was obscured by another line or too weak to measure accurately.

Quadrupole coupling constants have been obtained from the observed line splittings using the method given in Appendix 4. $\langle P_a^2 \rangle$, $\langle P_b^2 \rangle$ and $\langle P_c^2 \rangle$ values were obtained from the eigenvectors of the rigid rotor Hamiltonian.

$H = AP_a^2 + BP_b^2 + CP_c^2$

using the effective rotational constants determined from the centrifugal distortion fit. The quadrupole coupling constants determined (Tables 21 and 22) were then used to calculate quadrupole patterns and hence residuals. Residuals in Tables 19 and 20 are from the quadrupole fit only. Line splittings of less than 1 MHz were not used in the fit since the components were considered to be mutually interfering (spectrometer resolution ~0.5 MHz).

The effect of the deuterium (I=1) quadrupole coupling in ClF_2CCDO was too small to give rise to any observable hyperfine structure. It was therefore neglected.

A detailed analysis of quadrupole splitting in $^{37}ClF_2CCHO$ and in vibrational satellite spectra has not been attempted. The measured frequencies used in the calculation of hypothetical line centres for these data sets are included for the sake of completeness (Tables 23 and 24).

F numbers are given as a function of J and I, e.g. the column labelled J+I-1 contains transitions such that F'=J'+I-1 ← F=J+I-1.

The data for $^{35}ClF_2CCH^{18}O$ (Tables 25 and 26) were kindly supplied by Jeremy Randell and Dr. A. Peter Cox.[90]

Tables 27, 28 and 29 contain data for the high energy forms of ClF_2CCHO and ClF_2CCDO and show the patterns of successive differences mentioned previously.

TABLE 10.

Gauche-$^{35}ClF_2CCHO$. A-Reduction. I^r

Parameter	Value	E.S.D.
X/MHz	2405.922535	0.009726
Y/MHz	2075.369301	0.009935
Z/MHz	3950.571907	0.009275
DJ/KHz	1.045961	0.143666
DJK/KHz	-3.469874	0.031491
DK/KHz	8.456408	0.057233
dJ/KHz	0.354916	0.003087
dK/KHz	1.082089	0.071184
WEIGHTED S.D. OF FIT		0·061828 MHz

TABLE 10 Cont^{d}

Gauche- 35-ClF2CCHO

A REDUCTION REPRESENTATION IR

UPPER LEVEL					LOWER LEVEL					
V	J	Ka	Kc		V	J	Ka	Kc	OBS/MHz	OBS-CALC
0	3	2	2	-	0	2	1	2	19069.27	-0.100
0	4	3	2	-	0	3	2	2	26585.87	0.030
0	4	3	1	-	0	3	2	1	26384.00	-0.087
0	5	2	3	-	0	4	1	3	27287.16	0.025
0	5	1	4	-	0	4	0	4	26856.29	0.138
0	7	1	6	-	0	6	2	4	26963.31	-0.041
0	8	8		-	0	8	7		25496.92	0.007
0	9	8		-	0	9	7		25468.81	0.018
0	9	6	3	-	0	9	5	5	18535.84	-0.031
0	9	6	4	-	0	9	5	4	18514.21	0.088
0	10	8		-	0	10	7		25429.86	0.023
0	10	6	5	-	0	10	5	5	18383.08	-0.079
0	10	6	4	-	0	10	5	6	18447.11	0.046
0	11	8		-	0	11	7		25377.47	0.010
0	12	7	6	-	0	12	6	6	21749.33	-0.182
0	12	7	5	-	0	12	6	7	21774.62	0.065
0	12	8		-	0	12	7		25308.68	0.007
0	13	8	5	-	0	13	7	7	25221.65	0.035
0	13	7	6	-	0	13	6	8	21649.72	0.058
0	13	4	9	-	0	13	3	11	19109.66	0.046
0	13	8	6	-	0	13	7	6	25218.31	-0.072
0	14	7	7	-	0	14	6	9	21508.12	0.056
0	14	4	10	-	0	14	3	12	22137.07	-0.033
0	14	8	7	-	0	14	7	7	25102.53	-0.042
0	14	8	6	-	0	14	7	8	25112.05	-0.026
0	15	5	10	-	0	15	4	12	18959.74	0.037
0	16	8	9	-	0	16	7	10	24816.92	-0.105
0	16	8	8	-	0	16	7	9	24760.93	0.043
0	16	8	8	-	0	16	7	10	24820.51	0.095
0	16	7	10	-	0	16	6	10	20513.28	-0.044
0	16	7	9	-	0	16	6	11	21241.62	-0.002
0	16	8	9	-	0	16	7	9	24757.45	-0.046
0	17	7	11	-	0	17	6	11	19790.59	-0.048
0	17	8	10	-	0	17	7	11	24632.56	-0.012
0	17	8	10	-	0	17	7	10	24496.92	-0.037
0	17	8	9	-	0	17	7	11	24641.74	0.049
0	18	7	12	-	0	18	6	12	18770.11	-0.016
0	18	8	10	-	0	18	7	12	24452.71	0.037
0	19	8	12	-	0	19	7	12	23642.94	0.003
0	19	6	13	-	0	19	5	15	23238.13	-0.031
0	20	8	13	-	0	20	7	13	22939.24	-0.001
0	21	8	14	-	0	21	7	14	21954.25	0.010
0	22	8	15	-	0	22	7	15	20620.89	0.002
0	22	9	14	-	0	22	8	14	26767.21	-0.031
0	23	9	15	-	0	23	8	16	27003.75	0.025
0	23	9	15	-	0	23	8	15	26089.49	0.006
0	23	9	14	-	0	23	8	15	26189.40	0.042
0	23	9	14	-	0	23	8	16	27103.64	0.041
0	25	9	17	-	0	25	8	17	23885.85	0.075
0	25	8	17	-	0	25	7	19	27116.32	-0.024
0	26	10	17	-	0	26	9	17	29234.59	-0.039
0	26	9	18	-	0	26	8	18	22225.42	0.063
0	30	10	21	-	0	30	9	21	23600.35	-0.072

TABLE 11

Gauche- 35-ClF2CCHO V=1

A REDUCTION REPRESENTATION IR

UPPER LEVEL V	J	Ka	Kc		LOWER LEVEL V	J	Ka	Kc	OBS/MHz	OBS-CALC
1	4	2	2	-	1	3	1	2	22744.86	-0.020
1	4	3	2	-	1	3	2	2	26621.50	0.004
1	5	2	3	-	1	4	1	3	27327.86	0.018
1	7	1	6	-	1	6	2	4	26956.37	-0.003
1	8	8		-	1	8	7		25537.48	-0.057
1	15	8	7	-	1	15	7	9	25005.73	0.119
1	15	5	10	-	1	15	4	12	19176.50	0.012
1	16	8	8	-	1	16	7	10	24844.12	0.050
1	16	8	9	-	1	16	7	9	24775.50	-0.107
1	17	7	11	-	1	17	6	11	19731.08	-0.027
1	17	8	10	-	1	17	7	10	24504.86	-0.041
1	17	8	9	-	1	17	7	11	24662.21	0.036
1	17	6	11	-	1	17	5	13	19930.59	-0.003
1	18	8	10	-	1	18	7	12	24471.47	0.001
1	19	8	12	-	1	19	7	12	23611.51	0.014
1	20	9	11	-	1	20	8	13	27774.12	0.024
1	20	8	13	-	1	20	7	13	22872.59	0.011
1	21	7	14	-	1	21	6	16	23631.17	-0.030
1	22	9	13	-	1	22	8	15	27315.81	0.051
1	22	9	14	-	1	22	8	14	26731.94	-0.057
1	23	9	15	-	1	23	8	15	26018.22	-0.023
1	23	9	14	-	1	23	8	16	27124.24	0.021
1	25	9	17	-	1	25	8	17	23698.37	0.034
1	25	9	17	-	1	25	8	18	26637.02	-0.013
1	28	10	19	-	1	28	9	19	26975.04	-0.022

Parameter	Value	E.S.D.
X/MHz	2410.507136	0.006953
Y/MHz	2075.245754	0.007224
Z/MHz	3955.803116	0.006329
DJ/KHz	1.082455	0.094930
DJK/KHz	-3.674307	0.039224
DK/KHz	8.932165	0.058060
dJ/KHz	0.376842	0.003785
dK/KHz	1.158794	0.083918

WEIGHTED S.D. OF FIT 0.051728 MHz

TABLE 12

Gauche- 35-ClF2CCHO V=2

A REDUCTION REPRESENTATION IR

UPPER LEVEL V	J	Ka	Kc		LOWER LEVEL V	J	Ka	Kc	OBS/MHz	OBS-CALC
2	4	2	2	-	2	3	1	2	22771.94	-0.000
2	17	7	11	-	2	17	6	11	19581.83	-0.034
2	18	8	11	-	2	18	7	11	24049.22	0.049
2	19	8	12	-	2	19	7	12	23492.67	0.046
2	20	7	13	-	2	20	6	15	22558.54	-0.004
2	20	8	13	-	2	20	7	13	22702.34	-0.043
2	21	9	13	-	2	21	8	13	27152.48	-0.026
2	22	9	13	-	2	22	8	15	27259.51	0.024
2	23	9	14	-	2	23	8	16	27078.76	-0.022
2	24	9	15	-	2	24	8	17	27000.85	-0.093
2	25	9	16	-	2	25	8	18	27110.37	0.073
2	25	9	17	-	2	25	8	17	23342.55	0.033
2	30	10	21	-	2	30	9	21	22610.67	-0.005

Parameter	Value	E.S.D.
X/MHz	2416.531915	0.008521
Y/MHz	2075.372058	0.009100
Z/MHz	3958.243280	0.010640
DJ/KHz	1.078434	Const
DJK/KHz	-4.173941	0.153511
DK/KHz	9.904255	0.239743
dJ/KHz	0.404758	0.011499
dK/KHz	1.396315	0.247817

WEIGHTED S.D. OF FIT 0.063637 MHz

TABLE 13

Gauche- 35-ClF2CCHO V=3

A REDUCTION REPRESENTATION IR

UPPER LEVEL V	J	Ka	Kc		LOWER LEVEL V	J	Ka	Kc	OBS/MHz	OBS-CALC	WEIGHT
3	15	7	9	-	3	15	6	9	20758 (5)	0.792	0.000
3	16	7	10	-	3	16	6	10	20157 (5)	1.269	0.000
3	17	7	11	-	3	17	6	11	19280.65	0.017	
3	20	8	13	-	3	20	7	13	22355.59	-0.027	
3	21	9	13	-	3	21	8	13	26908.2	0.078	0.063
3	22	9	14	-	3	22	8	14	26296.3	0.035	0.063
3	25	9	17	-	3	25	8	17	22698.46	0.004	

Parameter	Value	E.S.D.
X/MHz	2424.100574	0.001563
Y/MHz	2075.400000	Const
Z/MHz	3954.957737	0.003416
DJ/KHz	1.078434	Const
DJK/KHz	-3.972750	Const
DK/KHz	5.411177	0.042389
dJ/KHz	0.424714	Const
dK/KHz	1.097544	Const

TABLE 14

Gauche- 35-ClF2CCDO

A REDUCTION REPRESENTATION IR

UPPER LEVEL V	J	Ka	Kc		LOWER LEVEL V	J	Ka	Kc	OBS/MHz	OBS-CALC	WEIGHT
0	3	2	2	-	0	2	1	2	18644.78	-0.008	
0	4	3	2	-	0	3	2	2	25999.49	-0.064	
0	5	2	3	-	0	4	1	3	26758.90	0.009	
0	5	1	4	-	0	4	0	4	26230.06	0.063	
0	6	1	5	-	0	5	1	4	27006.60	0.009	
0	7	2	5	-	0	6	3	3	24976.66	-0.013	
0	7	7		-	0	7	6		21250.22	-0.600	0.000
0	7	1	6	-	0	6	2	4	26841.50	-0.007	
0	9	7		-	0	9	6		21185.86	-0.005	
0	10	8		-	0	10	7		24464.44	-0.022	
0	11	8		-	0	11	7		22419.68	-0.019	
0	13	8	5	-	0	13	7	7	24286.41	-0.015	
0	13	8	6	-	0	13	7	6	24284.35	0.002	
0	14	7	7	-	0	14	6	9	20739.37	0.235	
0	14	5	10	-	0	14	4	10	10017.50	-0.078	
0	16	7	10	-	0	16	6	10	19967.38	-0.123	
0	16	5	11	-	0	16	4	13	19341.31	0.002	
0	17	6	11	-	0	17	5	13	18556.44	-0.006	
0	17	8	10	-	0	17	7	10	23687.25	-0.479	0.000
0	17	7	11	-	0	17	6	11	19401.15	-0.001	
0	18	6	12	-	0	18	5	14	19610.99	-0.009	
0	18	7	12	-	0	18	6	12	18595.09	0.049	
0	19	8	11	-	0	19	7	13	23435.36	0.081	
0	19	8	12	-	0	19	7	12	23015.45	-0.118	
0	19	6	13	-	0	19	5	15	21199.94	-0.052	
0	20	8	13	-	0	20	7	13	22473.47	0.013	
0	21	6	15	-	0	21	5	17	26181.03	0.008	
0	21	8	14	-	0	21	7	14	21715.55	-0.004	
0	22	9	13	-	0	22	8	15	26391.46	0.039	
0	22	9	14	-	0	22	8	15	26364.23	0.010	
0	22	9	14	-	0	22	8	14	26054.57	-0.111	
0	23	9	14	-	0	23	8	16	26186.06	0.014	
0	23	9	14	-	0	23	8	15	25597.21	0.078	
0	23	8	16	-	0	23	7	16	19303.41	0.061	
0	23	9	15	-	0	23	8	16	26126.95	-0.007	
0	23	9	15	-	0	23	8	15	25538.03	-0.013	
0	24	9	16	-	0	24	8	16	24833.13	-0.003	
0	25	9	17	-	0	25	8	17	23871.98	0.021	
0	26	10	17	-	0	26	9	17	28591.31	-0.019	
0	28	9	20	-	0	28	8	20	18942.88	-0.030	

PARAMETER	EST VALUE	E.S.D.
X/MHz	2360.677537	0.008426
Y/MHz	2061.008170	0.008773
Z/MHz	3854.285269	0.008020
DJ/KHz	0.898713	0.109442
DJK/KHz	-2.700518	0.033230
DK/KHz	6.943567	0.057816
dJ/KHz	0.289641	0.003007
dK/KHz	0.434864	0.090663

Weighted S.D. of Fit 0.067794 MHz.

TABLE 15

Gauche- 35-ClF2CCDO V=1

A REDUCTION REPRESENTATION IR

UPPER LEVEL V J Ka Kc		LOWER LEVEL V J Ka Kc	OBS/MHz	OBS-CALC
1 16 7 10	-	1 16 6 10	19943.24	-0.015
1 17 6 11	-	1 17 5 13	18685.50	0.030
1 17 7 11	-	1 17 6 11	19347.16	-0.000
1 18 6 12	-	1 18 5 14	19810.73	-0.021
1 18 7 12	-	1 18 6 12	18499.77	-0.003
1 21 8 14	-	1 21 7 14	21613.36	0.002
1 23 9 15	-	1 23 8 15	25476.79	0.036
1 23 8 16	-	1 23 7 16	19077.23	0.003
1 24 9 16	-	1 24 8 16	24728.12	-0.027
1 26 10 17	-	1 26 9 17	28528.55	-0.005
1 28 9 20	-	1 28 8 20	18541.22	0.001

Parameter	Value	E.S.D.
X/MHz	2365.442424	0.001955
Y/MHz	2060.992200	Const
Z/MHz	3859.339318	0.003594
DJ/KHz	0.882437	Const
DJK/KHz	-3.053948	0.006372
DK/KHz	7.729793	0.042783
dJ/KHz	0.289459	Const
dK/KHz	0.843848	0.031192

WEIGHTED S.D. OF FIT 0.024465 MHz

TABLE 16

Gauche- 35-ClF2CCDO V=2

A REDUCTION REPRESENTATION IR

UPPER LEVEL V J Ka Kc		LOWER LEVEL V J Ka Kc	OBS/MHz	OBS-CALC
2 16 7 10	-	2 16 6 10	19860.40	0.006
2 17 7 11	-	2 17 6 11	19223.80	-0.011
2 18 7 12	-	2 18 6 12	18320.96	0.005
2 21 8 14	-	2 21 7 14	21415.86	-0.000

Parameter	Value	E.S.D.
X/MHz	2371.122238	0.001238
Y/MHz	2060.992200	Const
Z/MHz	3861.755828	0.003395
DJ/KHz	0.882437	Const
DJK/KHz	-3.053948	Const
DK/KHz	5.922587	0.040588
dJ/KHz	0.289459	Const
dK/KHz	0.843848	Const

WEIGHTED S.D. OF FIT 0.013115 MHz

TABLE 17

Gauche- 37-ClF2CCHO

A REDUCTION REPRESENTATION IR

UPPER LEVEL V	J	Ka	Kc		LOWER LEVEL V	J	Ka	Kc	OBS/MHz	OBS-CALC
0	4	3	1	-	0	3	2	1	26096.07	-0.092
0	4	3	2	-	0	3	2	2	26294.25	0.092
0	5	2	3	-	0	4	1	3	26878.20	-0.000
0	11	8		-	0	11	7		25543.74	-0.028
0	16	8	8	-	0	16	7	10	24999.13	0.183
0	16	8	9	-	0	16	7	9	24941.21	-0.131
0	16	7	10	-	0	16	6	10	20711.31	0.001
0	17	8	9	-	0	17	7	11	24822.79	0.007
0	17	7	11	-	0	17	6	11	20019.36	-0.005
0	17	8	10	-	0	17	7	10	24690.08	-0.011
0	18	7	12	-	0	18	6	12	19039.74	0.017
0	18	8	10	-	0	18	7	12	24634.81	0.053
0	18	8	11	-	0	18	7	11	24348.22	-0.144
0	19	8	12	-	0	19	7	12	23872.75	0.051
0	20	8	12	-	0	20	7	14	24315.23	0.033
0	20	8	13	-	0	20	7	13	23202.30	0.043
0	21	8	13	-	0	21	7	15	24271.44	-0.001
0	21	8	14	-	0	21	7	14	22263.32	-0.003
0	22	9	14	-	0	22	8	14	27027.92	-0.050
0	22	8	14	-	0	22	7	16	24401.17	-0.011
0	22	9	13	-	0	22	8	15	27513.03	-0.004
0	23	8	15	-	0	23	7	17	24809.62	-0.050
0	23	8	16	-	0	23	7	16	19337.15	-0.018
0	23	9	15	-	0	23	8	15	26384.49	-0.017
0	23	9	14	-	0	23	8	16	27309.26	0.084

Parameter	Value	E.S.D.
X/MHz	2361.761132	0.027526
Y/MHz	2033.773337	0.034825
Z/MHz	3918.392328	0.025417
DJ/KHz	0.836362	0.647508
DJK/KHz	-3.764385	0.102083
DK/KHz	8.792626	0.262196
dJ/KHz	0.364750	0.005908
dK/KHz	0.796620	0.208341

WEIGHTED S.D. OF FIT 0.083341 MHz

TABLE 18

Gauche- 37-ClF2CCHO V=1

A REDUCTION REPRESENTATION IR

UPPER LEVEL V	J	Ka	Kc		LOWER LEVEL V	J	Ka	Kc	OBS/MHz	OBS-CALC	WEIGHT
1	4	3	2	-	1	3	2	2	26336.3	-0.000	0.063
1	16	7	10	-	1	16	6	10	20695.10	-0.013	
1	16	6	10	-	1	16	5	12	19044.7	-0.028	0.063
1	17	7	11	-	1	17	6	11	19973.03	0.011	
1	20	7	13	-	1	20	6	15	22412.6	0.069	0.063
1	21	8	14	-	1	21	7	14	22168.1	0.010	0.063
1	22	9	14	-	1	22	8	14	27006.78	0.007	
1	23	9	15	-	1	23	8	15	26331.13	-0.005	
1	24	9	15	-	1	24	8	17	27213.03	0.002	
1	25	9	16	-	1	25	8	18	27238.3	-0.066	0.063

Parameter	Value	E.S.D.
X/MHz	2366.857220	0.008046
Y/MHz	2034.350033	0.009045
Z/MHz	3924.589449	0.008129
DJ/KHz	0.836362	Const
DJK/KHz	-4.240697	0.020562
DK/KHz	9.764766	0.081224
dJ/KHz	0.364750	Const
dK/KHz	1.302408	0.030615

WEIGHTED S.D. OF FIT 0.021780 MHz

TABLE 19

TRANSITIONS SHOWING RESOLVABLE HYPERFINE STRUCTURE

$^{35}ClF_2CCHO$ R-Branch

Transition	F — F	Obs/MHz	Relative to hyp.cent./MHz	Obs-Calc	χ/MHz
$3_{22} - 2_{12}$	7/2 - 5/2	19075.84	6.57	0.031	$\chi_{322} = 0$
	5/2 - 3/2	19069.30	0.03	0.030	$\chi_{212} = \chi_{cc}$
	9/2 - 7/2	19066.63	-2.64	-0.025	$\chi_{212} = 36.84\ (21)$[a]
$4_{32} - 3_{22}$	9/2 - 7/2	26588.14	2.27	0.020	$\chi_{322} = 0$
	11/2 - 9/2	26584.57	-1.30	-0.014	$\chi_{432} = 14.28\ (28)$
$4_{31} - 3_{21}$	11/2 - 9/2) 5/2 - 3/2)	26383.19	-0.81	0	
$5_{23} - 4_{13}$	11/2 - 9/2	27288.32	1.16	-0.006	
	9/2 - 7/2	27287.59	0.43	-0.016	
	13/2 - 11/2	27286.56	-0.60	0.021	
	7/2 - 5/2	27285.82	-1.34	0.001	
$5_{14} - 4_{04}$	11/2 - 9/2	26861.09	4.86	0.026	-30.06 (21)
	9/2 - 7/2	26858.18	1.95	0.022	
	13/2 - 11/2	26853.60	-2.63	-0.008	
	7/2 - 5/2	26850.64	-5.59	-0.061	
$7_{16} - 6_{24}$	11/2 - 9/2	26966.13	2.82	-0.060	18.76 (21)
	17/2 - 15/2	26965.30	1.99	0.015	
	13/2 - 11/2	26961.46	-1.85	0.014	
	15/2 - 13/2	26960.59	-2.72	0.048	

(a) Error in χ value derived assuming 0.05 MHz standard deviation of an individual component (see Appendix 4) and used to give weighting factor in quadrupole fit (Table 21).

TABLE 19 (Cont/d)

$^{35}ClF_2CCHO$ Q -Branch

Transition	F	Obs/MHz	Relative to hyp.cent./MHz	Obs-Calc	χ/MHz
$8_8 - 8_7$	17/2	25499.92	3.00	0.026	-20.66 (21)
	15/2	25498.97	2.05	-0.005	
	19/2	25494.72	-2.20	-0.037	
	13/2	25493.84	-3.08	0.002	
$9_8 - 9_7$	19/2	25471.14	2.33	0.001	-16.18 (21)
	17/2	25470.45	1.64	-0.038	
	21/2	25467.09	-1.72	0.027	
	15/2	25466.41	-2.40	-0.002	
$9_{64} - 9_{54}$	19/2 17/2	18515.58	1.37	-0.018	-11.01 (28)
	21/2 15/2	18512.85	-1.36	0.029	
$9_{63} - 9_{55}$	19/2 17/2	18537.28	1.44	0.024	-11.58 (28)
	21/2 15/2	18534.41	-1.43	-0.014	
$10_{65} - 10_{55}$	21/2 19/2	18384.13	1.05	-0.009	- 8.46 (28)
	23/2 17/2	18382.03	-1.05	0.009	
$10_{64} - 10_{56}$	21/2 19/2	18448.22	1.11	-0.016	- 8.99 (28)
	23/2 17/2	18445.99	-1.12	0.006	
$10_8 - 10_7$	21/2 19/2	25431.50	1.64	-0.008	-13.22 (28)
	23/2 17/2	25428.22	-1.64	0.008	
$11_8 - 11_7$	23/2 21/2	25378.79	1.32	-0.033	-10.63 (28)
	25/2 19/2	25376.15	-1.32	0.033	
$12_8 - 12_7$	25/2 23/2	25309.77	1.09	-0.031	- 8.72 (28)
	27/2 21/2	25307.60	-1.08	0.041	
$12_{76} - 12_{66}$	25/2 23/2	21750.22	0.89	-0.010	- 7.15 (28)
	27/2 21/2	21748.44	-0.89	0.010	
$12_{75} - 12_{67}$	25/2 23/2	21775.51	0.89	-0.032	- 7.15 (28)
	27/2 21/2	21773.73	-0.89	0.032	
$13_{49} - 13_{3,11}$	27/2	19112.90	3.24	-0.044	-23.68 (21)
	25/2	19112.28	2.62	0.001	
	29/2	19106.95	-2.71	-0.041	
	23/2	19106.38	-3.28	0.054	
$13_{85} - 13_{77}$	27/2 25/2	25222.57	0.92	-0.016	- 7.44 (28)
	29/2 23/2	25220.72	-0.93	0.016	
$13_{86} - 13_{76}$	27/2 25/2	25219.23	0.92	-0.013	- 7.44 (28)
	29/2 23/2	25217.38	-0.93	0.003	
$13_{76} - 13_{68}$	27/2 25/2	21650.42	0.70	-0.061	
	29/2 23/2	21649.01	-0.71	0.051	

TABLE 19 (Cont/d)

$^{35}ClF_2CCHO$ Q-Branch (Cont/d)

Transition	F	Obs/MHz	Relative to hyp.cent./MHz	Obs-Calc	χ/MHz
$^{14}_{4,10} - {}^{14}_{3,12}$	29/2	22140.59	3.52	-0.016	-25.78 (21)
	27/2	22139.96	2.89	0.024	
	31/2	22134.15	-2.92	-0.008	
	25/2	22133.51	-3.56	0.022	
$^{14}_{86} - {}^{14}_{78}$	29/2 27/2	25112.85	0.80	0.016	-6.43 (28)
	31/2 25/2	25111.25	-0.80	-0.016	
$^{14}_{87} - {}^{14}_{77}$	29/2 27/2	25103.33	0.80	0.024	-6.47 (28)
	31/2 25/2	25101.72	-0.81	-0.034	
$^{14}_{77} - {}^{14}_{69}$	29/2 27/2	21508.73	0.61	-0.027	-4.92 (28)
	31/2 25/2	21507.50	-0.62	0.017	
$^{15}_{5,10} - {}^{15}_{4,12}$	31/2 29/2	18961.67	1.93	-0.008	-15.50 (28)
	33/2 27/2	18957.81	-1.93	0.008	
$^{16}_{88} - {}^{16}_{7,10}$	33/2 31/2	24821.04	0.53	-0.025	-4.28 (28)
	35/2 29/2	24819.97	-0.54	0.015	
$^{16}_{89} - {}^{16}_{7,10}$	33/2 31/2	24817.45	0.53	-0.022	-4.28 (28)
	35/2 29/2	24816.38	-0.54	0.012	
$^{16}_{88} - {}^{16}_{79}$	33/2 31/2	24761.39	0.46	-0.061	
	35/2 29/2	24760.47	-0.46	0.061	
$^{16}_{89} - {}^{16}_{79}$	33/2 31/2	24757.93	0.48	-0.038	
	35/2 29/2	24756.97	-0.48	0.038	
$^{16}_{79} - {}^{16}_{6,11}$	33/2 31/2	21242.09	0.47	-0.032	
	35/2 29/2	21241.15	-0.47	0.032	
$^{17}_{89} - {}^{17}_{7,11}$	35/2 33/2	24642.18	0.44	-0.031	
	37/2 31/2	24641.30	-0.44	0.031	
$^{17}_{8,10} - {}^{17}_{7,11}$	35/2 33/2	24632.99	0.43	-0.036	
	37/2 31/2	24632.13	-0.43	0.036	
$^{17}_{8,10} - {}^{17}_{7,10}$	35/2 33/2	24497.28	0.36	-0.038	
	37/2 31/2	24496.56	-0.36	0.038	
$^{18}_{7,12} - {}^{18}_{6,12}$	37/2 35/2	18770.37	0.26	-0.035	
	39/2 33/2	18769.84	-0.27	0.025	
$^{18}_{8,10} - {}^{18}_{7,12}$	37/2 35/2	24453.07	0.36	-0.049	
	39/2 33/2	24452.35	-0.36	0.049	
$^{19}_{6,13} - {}^{19}_{5,15}$	39/2 37/2	23239.87	1.74	-0.024	-13.92 (28)
	41/2 35/2	23236.39	-1.74	0.024	

TABLE 19 (Cont/d)

$^{35}ClF_2CCHO$ Q-Branch (Cont/d)

Transition	F	Obs/MHz	Relative to hyp.cent./MHz	Obs-Calc	χ/MHz
$^{21}_{8,14} - ^{21}_{7,14}$	45/2 39/2	21954.45	0.20	-0.036	
	43/2 41/2	21954.05	-0.20	0.036	
$^{22}_{8,15} - ^{22}_{7,15}$	47/2 41/2	20621.31	0.42	-0.019	
	45/2 43/2	20620.47	-0.42	0.019	
$^{23}_{9,14} - ^{23}_{8,16}$	47/2 45/2	27103.91	0.27	-0.007	
	49/2 43/2	27103.37	-0.27	0.007	
$^{23}_{9,15} - ^{23}_{8,16}$	47/2 45/2	27003.97	0.24	-0.002	
	49/2 43/2	27003.48	-0.25	-0.008	
$^{25}_{8,17} - ^{25}_{7,19}$	51/2 49/2	27117.35	1.03	-0.042	-8.28 (28)
	53/2 47/2	27115.28	-1.04	0.032	
$^{25}_{9,17} - ^{25}_{8,17}$	53/2 47/2	23886.24	0.39	0.031	
	51/2 49/2	23885.45	-0.40	-0.041	
$^{26}_{9,18} - ^{26}_{8,18}$	55/2 49/2	22225.88	0.46	-0.08	
	53/2 51/2	22224.96	-0.46	0.08	
$^{30}_{10,21} - ^{30}_{9,21}$	63/2 57/2	23600.92	0.57	-0.043	
	61/2 59/2	23599.78	-0.57	0.043	

TABLE 20

$^{35}ClF_2CCDO$ R-Branch

Transition	F — F	Obs/MHz	Relative to hyp.cent./MHz	Obs-Calc	χ/MHz
$3_{22} - 2_{12}$	7/2 - 5/2	18651.31	6.53	0.002	$\chi_{322} = 0$
	5/2 - 3/2	18644.66	-0.12	-0.120	$\chi_{212} = \chi_{cc}$
	9/2 - 7/2	18642.17	-2.61	0.001	
	3/2 - 1/2	18635.52	-9.26	-0.121	$\chi_{212} = 36.56\ (28)$ [a]
$4_{32} - 3_{22}$	11/2 - 9/2	26001.60	+2.11	-0.078	$\chi_{322} = 0$
	9/2 - 7/2	26000.53	1.04	0.057	
	13/2 - 11/2	25998.23	-1.26	-0.009	$\chi_{432} = -13.68\ (21)$
	7/2 - 5/2	25997.06	-2.43	0.026	
$5_{14} - 4_{04}$	11/2 - 9/2	26234.97	+4.91	0.014	-30.32 (21)
	13/2 - 11/2	26227.39	-2.67	0.000	
$5_{23} - 4_{13}$	11/2 - 9/2	26759.93	1.03	-0.018	
	9/2 - 7/2	26759.36	0.46	0.057	
	13/2 - 11/2	26758.28	-0.62	-0.060	
	7/2 - 5/2	26757.72	-1.18	0.025	
$6_{15} - 5_{14}$	15/2 - 13/2 9/2 - 7/2	27007.16	0.56	0.023	4.60 (28)
	11/2 - 9/2 13/2 - 11/2	27006.01	-0.59	-0.021	
$7_{25} - 6_{33}$	17/2 - 15/2 11/2 - 9/2	24977.14	0.48	0.003	
	15/2 - 13/2 13/2 - 11/2	24976.17	-0.49	-0.005	
$7_{16} - 6_{24}$	11/2 - 9/2	26844.27	2.77	-0.002	18.32 (21)
	17/2 - 15/2	26843.41	1.91	0.013	
	13/2 - 11/2	26839.73	-1.77	0.018	
	15/2 - 13/2	26838.79	-2.71	-0.046	

(a) See footnote to Table 19.
Quadrupole fit is given in Table 22.

TABLE 20 (Cont/d)

$^{35}ClF_2CCDO$ Q-Branch

Transition	F	Obs/MHz	Relative to hyp.cent//MHz	Obs-Calc	χ/MHz
$^{7}_{7} - ^{7}_{6}$	15/2	21253.35	3.13	-0.129	-22.08 (21)
	13/2	21252.45	2.23	0.099	
	17/2	21247.88	-2.34	-0.058	
	11/2	21246.88	-3.34	0.070	
$^{9}_{7} - ^{9}_{6}$	19/2 17/2	21187.48	1.62	-0.046	
	21/2 15/2	21184.23	-1.63	0.037	
$^{10}_{7} - ^{10}_{6}$	21/2 19/2	21134.12	1.35	0.005	-10.88 (28)
	23/2 17/2	21131/42	-1.35	-0.005	
$^{10}_{8} - ^{10}_{7}$	21/2 19/2	24466.04	1.60	0.003	-12.93 (28)
	23/2 17/2	24462.83	-1.61	-0.013	
$^{11}_{8} - ^{11}_{7}$	23/2 21/2	24420.99	1.31	-0.001	
	25/2 19/2	24418.37	-1.31	0.001	
$^{14}_{5,10} - ^{14}_{4,10}$	-	10018.36	0.86	- }	See Text
	-	10016.64	-0.86	- }	
$^{14}_{77} - ^{14}_{69}$	29/2 27/2	20739.90	0.53	-0.079	
	31/2 25/2	20738.84	-0.53	0.079	
$^{16}_{5,11} - ^{16}_{4,13}$	33/2 31/2	19343.47	2.16	-0.009	-17.32 (28)
	35/2 29/2	19339.14	-2.17	-0.001	
$^{17}_{6,11} - ^{17}_{5,13}$	35/2 33/2	18557.48	1.04	0.011	- 8.36 (28)
	37/2 31/2	18555.39	-1.05	-0.021	
$^{18}_{6,12} - ^{18}_{5,14}$	37/2 35/2	19612.31	1.32	0.014	-10.56 (28)
	39/2 33/2	19609.67	-1.32	-0.014	
$^{19}_{6,13} - ^{19}_{5,15}$	39/2 37/2	21201.54	1.60	-0.026	-12.84 (28)
	41/2 35/2	21198.33	-1.61	0.016	
$^{21}_{6,15} - ^{21}_{5,17}$	43/2 41/2	26183.24	2.21	-0.020	-17.68 (28)
	45/2 39/2	26178.82	-2.21	0.020	
$^{22}_{9,13} - ^{22}_{8,15}$	45/2 43/2	26391.70	0.24	-0.021	
	47/2 41/2	26391.22	-0.24	0.021	
$^{22}_{9,14} - ^{22}_{8,15}$	45/2 43/2	26364.46	0.23	-0.018	
	47/2 41/2	26363.99	-0.24	0.008	
$^{23}_{8,16} - ^{23}_{7,16}$	49/2 43/2	19303.94	0.53	-0.050	
	47/2 45/2	19302.88	-0.53	0.050	
$^{23}_{9,15} - ^{23}_{8,16}$	47/2 45/2	26127.17	0.22	0.003	
	49/2 43/2	26126.73	-0.22	-0.003	
$^{23}_{9,14} - ^{23}_{8,16}$	47/2 45/2	26186.27	0.21	-0.032	
	49/2 43/2	26185.85	-0.21	0.032	
$^{28}_{9,20} - ^{28}_{8,20}$	59/2 53/2	18943.64	0.76	-0.037	
	57/2 55/2	18942.11	-0.77	0.027	

TABLE 21

Program Chi.

Quadrupole data - 35ClF2CCHO

Number of observations = 28

J					Obs/MHz	Res/MHz	Weight
2	1	2 level			36.84000	0.22395	0.50000
4	3	2 level			-14.28000	-0.13795	0.50000
4	0	4-5	1	4	-30.06000	-0.23486	1.00000
6	2	4-7	1	6	18.76000	-0.21464	1.00000
8	8	- 8	7		-20.66000	-0.11364	1.00000
9	8	- 9	7		-16.18000	0.12315	1.00000
9	6	3- 9	5	5	-11.58000	-0.24849	0.50000
9	6	4- 9	5	4	-11.01000	0.09626	0.50000
10	6	4-10	5	6	-8.99000	0.01984	0.50000
10	6	5-10	5	5	-8.46000	0.01356	0.50000
10	8	-10	7		-13.22000	-0.03251	0.50000
11	8	-11	7		-10.63000	0.18973	0.50000
12	8	-12	7		-8.72000	0.24563	0.50000
12	7	6-12	6	6	-7.15000	0.04689	0.50000
12	7	5-12	6	7	-7.15000	0.22367	0.50000
13	8	5-13	7	7	-7.44000	0.04508	0.50000
13	8	6-13	7	6	-7.44000	0.02220	0.50000
13	7	6-13	6	8	-5.64000	0.44448	0.00000
13	4	9-13	3	11	-23.68000	0.13164	1.00000
14	7	7-14	6	9	-4.92000	0.17548	0.50000
14	8	6-14	7	8	-6.43000	-0.15931	0.50000
14	8	7-14	7	7	-6.47000	-0.25727	0.50000
14	4	10-14	3	12	-25.78000	0.01377	1.00000
15	5	10-15	4	12	-15.50000	0.00063	0.50000
16	8	8-16	7	10	-4.28000	0.15436	0.50000
16	8	9-16	7	10	-4.28000	0.13622	0.50000
19	6	13-19	5	15	-13.92000	0.19084	0.50000
25	8	17-25	7	19	-8.28000	0.29629	0.50000

E.S.D. of an Observation/MHz = 0.13233/sqrt(Weight)

Chiaa =	-34.17524	MHz	esd	0.10860
Chibb-Chicc =	-39.05686	MHz	esd	0.10113
Chibb =	-2.44081	MHz	esd	0.07420
Chicc =	36.61605	MHz	esd	0.07420

TABLE 22

Program Chi.

Quadrupole data - 35ClF2CCDO (Deuterium Sp.).

Number of observations = 17

J					Obs/MHz	Res/MHz	Weight
2	1	2 level			36.56000	0.00403	0.50000
4	3	2 level			-13.68000	0.07589	1.00000
4	0	4-5	1	4	-30.32000	-0.05485	0.50000
5	1	4-6	1	5	4.60000	0.14714	0.50000
6	2	4-7	1	6	18.32000	0.07820	1.00000
7	7	- 7	6		-22.08000	0.08381	1.00000
9	7	- 9	6		-13.12000	0.31978	0.00000
10	7	-10	6		-10.88000	-0.11966	0.50000
10	3	-10	7		-12.93000	-0.14919	0.50000
11	8	-11	7		-10.55000	-0.06530	0.50000
16	5	11-16	4	13	-17.32000	0.03429	0.50000
17	6	11-17	5	13	-8.36000	-0.12308	0.50000
18	6	12-18	5	14	-10.56000	-0.10732	0.50000
19	6	13-19	5	15	-12.84000	0.16688	0.50000
21	6	15-21	5	17	-17.68000	0.15482	0.50000
23	8	16-23	7	16	4.24000	-0.39811	0.00000
28	9	20-28	8	20	6.12000	-0.25396	0.00000

E.S.D. of an Observation/MHz = 0.08731/sqrt(Weight)

Chiaa	=	-33.14113 MHz	esd	0.09131
Chibb-Chicc	=	-39.97082 MHz	esd	0.10166
Chibb	=	-3.41485 MHz	esd	0.06832
Chicc	=	36.55597 MHz	esd	0.06832

TABLE 23

$^{37}ClF_2CCHO$ Obs/MHz

Transition \ F	J + I - 1	J - I + 1	J + I	J - I
$^{4}_{31} - ^{3}_{21}$	26096.79		26095.42	
$^{4}_{32} - ^{3}_{22}$	-	-	26293.23	-
$^{5}_{23} - ^{4}_{13}$	26878.85		26877.5	
$^{11}_{8} - ^{11}_{7}$	25544.88		25542.60	
$^{16}_{89} - ^{16}_{79}$	24941.58		24940.84	
$^{16}_{88} - ^{16}_{7,10}$	24999.70		24998.56	
$^{17}_{8,10} - ^{17}_{7,10}$	24690.42		24689.73	
$^{17}_{8,9} - ^{17}_{7,11}$	24823.21		24822.36	
$^{18}_{8,10} - ^{18}_{7,12}$	24635.15		24634.46	
$^{20}_{8,12} - ^{20}_{7,14}$	24315.52		24314.94	
$^{21}_{8,13} - ^{21}_{7,15}$	24271.76		24271.12	
$^{22}_{8,14} - ^{22}_{7,16}$	24401.52		24400.81	
$^{23}_{8,15} - ^{23}_{7,17}$	24810.11		24809.13	
$^{23}_{8,16} - ^{23}_{7,16}$	19337.49		19336.81	
$^{37}ClF_2CCHO$ V = 1				
$^{24}_{9,15} - ^{24}_{8,17}$	27213.23		27212.82	

TABLE 24

$^{35}ClF_2CCHO$ V = 1 Obs/MHz

Transition \ F	J + I - 1	J - I + 1	J + I	J - I
$^{4}_{22} - {}^{3}_{12}$	22745.81		22744.37	
$^{4}_{32} - {}^{3}_{22}$	26623.77	26622.44	26620.20	26618.98
$^{5}_{23} - {}^{4}_{13}$	27329.06	27328.29	-	-
$^{7}_{16} - {}^{6}_{24}$	26953.44	26954.50	26958.36	26959.27
$^{8}_{8} - {}^{8}_{7}$	25540.48	25539.56	25535.32	25534.33
$^{15}_{87} - {}^{15}_{79}$	25006.38		25005.08	
$^{16}_{88} - {}^{16}_{7,10}$	24844.69		24843.62	
$^{16}_{89} - {}^{16}_{79}$	24776.00		24775.00	
$^{17}_{89} - {}^{17}_{7,11}$	24662.68		24661.73	
$^{17}_{6,11} - {}^{17}_{5,13}$	19931.77		19929.41	
$^{17}_{8,10} - {}^{17}_{7,10}$	24505.21		24504.51	
$^{18}_{8,10} - {}^{18}_{7,12}$	24471.91		24471.02	
$^{20}_{9,11} - {}^{20}_{8,13}$	27774.45		27773.79	
$^{21}_{7,14} - {}^{21}_{6,16}$	23632.36		23629.98	
$^{22}_{9,13} - {}^{22}_{8,15}$	27316.04		27315.58	
$^{23}_{9,14} - {}^{23}_{8,16}$	27124.50		27123.98	
$^{25}_{9,17} - {}^{25}_{8,17}$	23698.40		23697.73	
$^{25}_{9,17} - {}^{25}_{8,18}$	26637.27		26636.76	
$^{28}_{10,19} - {}^{28}_{9,19}$	26975.23		26974.84	
$^{35}ClF_2CCHO$ V = 2				
$^{4}_{22} - {}^{3}_{12}$	22772.85	22772.15	22771.23	-
$^{18}_{8,11} - {}^{18}_{7,11}$	24049.48		24048.96	
$^{22}_{9,13} - {}^{22}_{8,15}$	27259.77		27259.25	
$^{23}_{9,14} - {}^{23}_{8,16}$	27079.02		27078.51	
$^{24}_{9,15} - {}^{24}_{8,17}$	27001.12		27000.58	
$^{25}_{9,16} - {}^{25}_{8,18}$	27110.54		27109.80	
$^{25}_{9,17} - {}^{25}_{8,17}$	23342.86		23342.24	
$^{30}_{10,21} - {}^{30}_{9,21}$	22611.29		22610.05	
$^{35}ClF_2CCDO$ V = 1				
$^{17}_{6,11} - {}^{17}_{5,13}$	18686.51		18684.48	
$^{18}_{6,12} - {}^{18}_{5,14}$	19812.06		19809.40	
$^{23}_{8,16} - {}^{23}_{7,16}$	19077.79		19076.66	
$^{28}_{9,20} - {}^{28}_{8,20}$	18541.98		18540.46	

TABLE 25

Gauche 35-ClF2CCH13-O V=0

A REDUCTION REPRESENTATION IR

UPPER LEVEL V	J	Ka	Kc		LOWER LEVEL V	J	Ka	Kc	OBS/MHz	OBS-CALC
0	5	4	2	-	0	4	3	2	33902.21	-0.100
0	5	5		-	0	4	4		37419.72	-0.005
0	5	4	1	-	0	4	3	1	33880.54	0.107
0	6	3	3	-	0	5	2	3	34133.68	-0.000
0	9	8		-	0	9	7		26379.84	0.117
0	11	8		-	0	11	7		26300.00	-0.116
0	13	6	8	-	0	13	5	8	18298.21	-0.029
0	17	7	11	-	0	17	6	11	21052.15	0.004
0	18	7	12	-	0	18	6	12	20263.85	-0.042
0	18	7	11	-	0	18	6	12	20435.79	0.059
0	19	8	12	-	0	19	7	12	24903.03	-0.029
0	20	8	13	-	0	20	7	13	24377.15	-0.008
0	21	7	14	-	0	21	6	16	23160.00	-0.056
0	22	7	15	-	0	22	6	17	24360.73	0.050
0	23	9	15	-	0	23	8	15	27690.43	0.068
0	24	8	16	-	0	24	7	18	25632.35	-0.024
0	25	9	17	-	0	25	8	17	26094.03	0.011
0	25	8	17	-	0	25	7	19	26511.63	0.014
0	28	11	18	-	0	28	10	18	34732.94	-0.025

Parameter	Value	E.S.D
XO/MHz	2306.154843	0.021927
YO/MHz	1992.339301	0.023643
ZO/MHz	3918.404089	0.021171
DJO/KHz	0.360367	0.373142
DJKO/KHz	-2.663146	0.061747
DKO/KHz	7.559732	0.099408
dJO/KHz	0.339973	0.006209
dKO/KHz	0.891580	0.147267

WEIGHTED S.D. OF FIT 0.084292 MHz

TABLE 26

Program Chi.

quadrupole data - 35ClF2CCHO (oxygen 18 sp).

Number of observations = 12

J						Obs/MHz	Res/MHz	Weight
4	3	2	level			-13.08000	0.04079	0.50000
3	0	3-	4	1	3	-30.96000	-0.08054	0.50000
4	0	4-	5	1	4	-31.78000	0.03421	1.00000
4	1	3-	5	2	3	-6.00000	-0.25662	0.00000
4	3	1-	5	4	1	-6.40000	0.30205	0.00000
4	3	2-	5	4	2	-7.40000	0.08142	0.50000
11	8	-11		7		-9.80000	-0.10073	0.50000
21	7	14-	21	7	15	-7.28000	-0.06995	0.50000
22	6	17-	22	7	15	-9.60000	-0.09683	0.50000
24	8	16-	24	7	18	-4.88000	0.14279	0.50000
25	8	17-	25	7	19	-6.72000	0.12564	0.50000
25	9	17-	25	8	17	2.52000	0.00394	0.50000

E.S.D. of an Observation/MHz = 0.06970/sqrt(Weight)

Chiaa =	-30.96513 MHz	esd	0.17540
Chibb-Chicc =	-42.55639 MHz	esd	0.08579
Chibb =	-5.79563 MHz	esd	0.09761
Chicc =	36.76076 MHz	esd	0.09761

TABLE 27

Series due to ClF_2CCHO High Energy Form /MHz

Splitting	Centre Freq.	1st Difference	2nd Difference	3rd Difference
1.0	19599.68			
		142.33		
1.0	19457.35		72.36	
		69.67		12.03
1.25	19387.68		60.33	
		9.34		13.77
1.28	19378.34		46.56	
		-37.22		14.41
1.23	19415.56		32.15	
		-69.37		15.78
1.32	19484.93		16.37	
		-85.74		15.71
1.40	19570.67		0.66	
		-85.08		20.15
1.44	19655.75		-19.49	
		-65.59		20.17
1.46	19721.34		-39.66	
		-25.93		21.90
1.46	19747.27		-61.56	
		35.63		23.00
1.56	19711.64		-84.56	
		120.19		24.15
1.60	19591.45		-108.71	
		228.90		25.00
1.60	19362.55		-133.71	
		362.61		25.45
1.63	18999.94		-159.16	
		521.77		
1.54	18478.17			

Decreasing Intensity

TABLE 28

Series due to ClF_2CCHO High Energy Form /MHz

Splitting	Centre Freq.	1st Difference	2nd Difference	3rd Difference
1.36	24297.63			
		96.94		
1.37	24200.69		39.37	
		57.57		18.93
-	obscured		20.44	
		37.13		19.41
1.45	24105.99		1.03	
		36.10		20.13
1.46	24069.89		-19.10	
		55.20		21.39
1.45	24014.69		-40.49	
		95.69		22.43
1.51	23919.00		-62.92	
		158.61		23.25
1.52	23760.39		-86.17	
		244.78		23.67
1.54	23515.61		-109.84	
		354.62		24.04
1.56	23160.99		-133.88	
		488.50		23.84
1.51	22672.49		-157.72	
		646.22		
1.47	22026.27			

Decreasing Intensity ↑

TABLE 29

Series due to ClF_2CCDO High Energy Form /MHz

Splitting	Centre Freq.	1st Difference	2nd Difference	3rd Difference
1.51	22567.20			
		444.15		
1.57	22123.05		7.42	
		436.73		14.32
1.57	21686.32		-6.90	
		443.63		14.70
1.56	21242.69		-21.60	
		465.23		15.23
1.68	20777.46		-36.83	
		502.06		15.48
1.68	20275.40		-52.31	
		554.37		16.07
1.69	19721.03		-68.38	
		622.75		16.45
1.72	19098.28		-84.83	
		707.58		
1.72	18390.70			

Decreasing Intensity ↑

CHAPTER 4

SOME CALCULATIONS ON INTERNAL ROTATION IN TRIFLUORONITROSOMETHANE AND TRIFLUOROACETALDEHYDE (FLUORAL)

For a molecule with a three-fold symmetric internal rotor, the simplest possible determination of V_3, the barrier to internal rotation, makes use of the Hamiltonian;

$$\hat{H} = -F\frac{d^2}{d\alpha^2} + \tfrac{1}{2}V_3(1 - \cos 3\alpha) \qquad \ldots.(1)$$

V_3 may be obtained from (1), provided that there is structural information to determine the internal rotation constant F, and given that the spacing between two torsional energy levels is known.

Torsional energy spacings may be obtained from microwave A-E splittings or from Far Infrared (FIR) or other optical data. Both of these methods are capable of yielding precise V_3 values, but unfortunately, if both methods are applied to the same molecule, the V_3 values obtained seldom agree. This has led a number of investigators to propose extensions to the Hamiltonian, to allow for non-rigidity of the molecule undergoing internal rotation, and to allow for terms of higher symmetry in the hindering potential. Such extensions have led to a satisfactory conclusion in the case of molecules where a methyl group is the internal rotor[11,12], but for molecules where the rotating group is of comparable mass to the frame, the discrepancy between microwave and optical V_3 determinations remains, and is particularly large.[46,76,120] For this reason, a re-investigation of the CF_3NO and CF_3CHO data has been undertaken here, permitting new conclusions to be drawn.

TRIFLUORONITROSOMETHANE

The most accurate and up-to-date investigations into the structure and internal rotation of CF_3NO are an Electron Diffraction study by Bauer and Andreassen[78], a Microwave study by Turner and Cox[16,77] and a Laser Induced Fluorescence (LIF) study by DeKoven, Fung, Hoffland, Levy and Spears[76]. The Infrared and Raman spectra have also been reported by Shurvell, Dass and Gordon[121].

The Microwave study of CF_3NO gave an accurate value for the ground state torsional splitting $-\Delta_0 = \nu(OE-OA) = 8.59(2)$ MHz, which when interpreted according to Hamiltonian (1) gave $V_3 = 269(17)$ cm^{-1}, using an internal rotation constant of 2.25 cm^{-1} as determined from the structure. This model predicts a torsional frequency $\nu(1E-0E)$ of $\sim$67 cm^{-1}, in clear disagreement with the optical results. Shurvell et al[121] had previously estimated the torsional frequency to be $\sim$50 cm^{-1} from an analysis of hot bands, but were unable to observe the torsional fundamental. After the microwave work, DeKoven et al[76] used supersonic nozzle expansion to obtain rotationally and vibrationally cold CF_3NO and studied the $A \leftarrow X$ $(n \rightarrow \pi^*)$ region. With much simplified spectra they were able to assign the torsional progressions and to report accurate torsional spacings up to $\underline{v}=5$ for the electronic ground state, giving $\nu(1E-0E) = 58(1)$ cm^{-1}. They then used the microwave structural data to calculate $F = 2.23(1)$ cm^{-1}, and using this constant in (1) reported that the derived V_3 value from the microwave work was unable to reproduce their spectra. This led them to propose that, although the microwave data were likely to be the best source of the parameter F, the LIF data were the best source of the barrier height V_3 because these data involved levels closest to the top of the barrier. On the basis of this argument they adopted $V_3 = 202(10)$ cm^{-1}, but by so doing had failed to address themselves to the raw microwave data. Their model predicts $\nu(OE-OA) = 46.5$ MHz (cf 8.59 MHz observed) and, moreover, does not fit the LIF data within experimental error. They obtained a much better fit by allowing both V_3 and F to vary, but chose not to attach any significance to this.

All of the available internal rotation data for CF_3NO have now been re-investigated using the Hamiltonian;

$$\hat{H} = -\frac{d}{d\alpha}(F_0 + F_3 \text{ Cos } 3\alpha)\frac{d}{d\alpha} - D_F^{(1)}\frac{d^4}{d\alpha^4} + \tfrac{1}{2}\sum_n V_n(1-\text{Cos } n\alpha) \qquad \ldots(2)$$

Energy levels were calculated using sine and cosine basis functions, following Lewis et al[122] (see also Appendix 6), and data were adjusted by the method of weighted non-linear least-squares fitting. Weighting is here essential owing to the large difference between microwave and optical experimental uncertainties. Weighting coefficients used were $1/\sigma^2$ for the observation in question.

Initial attempts were made to fit the ground state torsional splitting (0E-0A), and the LIF measurements of DeKoven et al[76] up to 5E, whilst holding F_0 close to the accepted value. Regardless of which other parameters of (2) were included, it was not possible to fit the data in this way. Conversely, as soon as F_0 was allowed to vary, it became possible to capture all of the data with a three parameter fit. Suitable parameter sets were either (F_0, V_3, V_6) or (F_0, F_3, V_3), with the following results:-

V_6 Fit /cm^{-1}	
F_0	1.9816 (79)
V_3	238.2 (3.0)
V_6	-5.7 (2.9)
σ_{fit}	0.986

F_3 Fit /cm^{-1}	
F_0	1.988 (13)
F_3	-0.189 (98)
V_3	239.1 (3.6)
σ_{fit}	0.996

σ_{fit} is the standard deviation of an observation of unit weight.

The equivalence between F_3 and V_6 is in keeping with the theoretical investigation by Lees[10], who showed that, to first order, the effect of F_n

is the same as that of V_{n+3} in Hamiltonians like (2). In fact, the V_6 fit is the better of the two and is here preferred, with the proviso that the effective V_6 term contains contributions from torsional flexing.

The surprising result of these calculation is that energy levels, calculated from either of the above parameter sets, accurately predict and confirm tentative assignments, made by DeKoven et al, for torsional spacings out to $\underline{v}$=8. These spacings were therefore estimated from the published spectra[76] and included, with generous uncertainties, into the fit. Full details of this are given in Table 1, where m is the limiting free-rotor quantum number. The determinable parameters are;

F_0 = 1.9822 (42)

V_3 = 238.4 (1.6)

V_6 = -5.8 (1.6)

with σ_{fit} = 0.582 cm^{-1}.

Finally, various ways of fitting the extended data set are given in Table 2. It is immediately clear that F_0 and V_3 are well determined quantities. The contribution of $D_F^{(1)}$ is determined to be negligible, which is taken to indicate that P^4 type centrifugal distortion is unimportant for this system. It was not possible to fit the data by including $D_F^{(1)}$ and constraining F_0 to an accepted structural value. The inclusion of V_9 and V_{12} terms is not justified by the data.

The fact that all of the internal rotation data for CF_3NO can be accounted for with a simple three parameter fit prompts investigation into possible uncertainties in the structurally determined value of F (from here on, F will be used to denote an internal rotation constant calculated from structure, and F_0 the constant determined from torsional data).

Three structures were explored;

1) Structure C from the electron diffraction work of Bauer and Andreassen[78] .

TABLE 1

Data For CF3NO.
Torsional Potential Program VFIT
3 Fold Dominated Potential

60 Basis Functions

	mu	ml	Obs	Obs-Calc	Weight
0E- 0A	1	0	0.00028646	0.00000000	0.22277E+13
1E- 0E	2	1	58.00000000	-0.37513747	1.0000
2E- 0E	4	1	112.00000000	-0.49735440	1.0000
3E- 0E	5	1	161.00000000	1.21177465	1.0000
4E- 0E	7	1	202.00000000	-1.39663718	.25000
5E- 0E	8	1	228.00000000	-2.27803380	.11111
5A- 0A	-9	0	257.00000000	-0.48472819	0.40000E-01
6A- 0A	9	0	261.00000000	0.42784462	0.40000E-01
6E- 0E	10	1	295.00000000	0.98331880	0.10000E-01
7E- 0E	11	1	337.00000000	3.20348232	0.10000E-01
7A- 0A	-12	0	378.00000000	-0.03643353	0.50000E-02
8A- 0A	12	0	378.00000000	-0.06992335	0.50000E-02

E.S.D. of an Observation = 0.58212128/Sqrt(Weight)

Estimated Parameters		E.S.D.
F0	1.98216791	0.00424084
V3	238.39529261	1.63829993
V6	-5.84634444	1.62686238

Correlation Coefficients.

F0	V3	V6
1.0000		
0.5737	1.0000	
-0.2630	-0.9406	1.0000

Energy Levels

Iml	Odd (Sin) Wfn.	Even (Cos) Wfn.
0		30.13676790
1	30.13705436	30.13705436
2	88.51219182	88.51219182
3	88.52451271	142.40500228
4	142.63440875	142.63440875
5	189.92527970	189.92527970
6	192.28087332	224.34022261
7	233.53369153	233.53369153
8	260.41508814	260.41508814
9	287.62149607	290.70892326
10	324.15373553	324.15373553
11	363.93357201	363.93357201
12	408.17320139	408.20669122
13	456.73772191	456.73772191
14	509.47329178	509.47329178
15	566.33300966	566.33313197
16	627.27533675	627.27533675
17	692.27148194	692.27148194
18	761.30122926	761.30122948
19	834.34982172	834.34982172
20	911.40628159	911.40628159

TABLE 2

F_0	F_3	$D_F^{(1)}$	V_3	V_6	V_9	V_{12}	σ_{fit}
1.9822(42)	-	-	238.4(1.6)	-5.8(1.6)	-	-	0.582
1.9894(66)	-0.194(55)	-	239.3(1.9)	-	-	-	0.588
1.9822(45)	-	0.0000(2)	238.3(2.9)	-5.8(1.8)	-	-	0.617
1.9768(41)	-	-	237.0(1.4)	-2.5(1.9)	-4.6(1.9)	-	0.470
1.9761(38)	-	-	236.1(1.5)	-1.0(2.1)	-7.2(2.7)	3.6(2.8)	0.451
1.9892(81)	-0.193(62)	0.0000(3)	239.2(3.3)	-	-	-	0.624

2) The microwave structure from the work of Turner and Cox[77].

3) A structure obtained by least-squares fitting the internal co-ordinates to the microwave data, using the method of Nösberger, Bauder and Günthard[58].

The details are given in Table 3 and Figure 1. The CF_3 group was assumed always to be symmetric about the z (internal rotation) axis. Bauer and Andreassen found their data to be best fitted when the average internal rotation angle α_{av}=21.8° (by definition, α=0 when fluorine eclipses oxygen). This may reflect the amplitude of the torsional oscillation, but since the top and frame are here assumed to be rigid, it makes no difference to the computed F.

There is, in fact, good agreement between the values of F calculated from the various structures, but all are greater than the F_0=1.982 cm^{-1} obtained earlier. This seems to indicate that the difference between F and F_0 is systematic, although the possibility that it arises simply out of structural uncertainty is not ruled out. Table 4 shows the effect of parameter increments on F. Structure 3) was used for this calculation because it gives F closest to F_0. It was found that F could be made to coincide with F_0 by reducing the tilt angle to 1.485°. After such a change, of course, the structure no longer reproduces the observed moments of inertia. To reproduce all of the observed rotational constants simultaneously, including F_0, requires complete re-derivation of the structure. This was not thought to be worthwhile, as will be seen from the discussion to follow.

An instantaneous value of F is given by;

$$F = \frac{h}{8\pi^2 I_{eff}}$$

where, for a symmetric internal rotor;

$$I_{eff} = I_\alpha \left[1 - \sum_{g=a,b,c} \lambda_{gz}^2 \frac{I_\alpha}{I_g}\right]$$

(Symbols are defined in Appendix 5).

TABLE 3

Structure of CF_3NO

Parameter	Electron Diffraction[78]	Microwave[77]	Microwave/ Least-Squares[(a)]
r(C-F)	1.3258(8)[(a)]	1.324 (5)	1.3258(assumed)
r(C-N)	1.5464(30)	1.512 (16)	1.5163(34)
r(N=O)	1.1967(15)	1.198 (4)	1.1912(34)
$C\widehat{-N=O}$	113.156 (415)	112.4 (3)	112.799 (262)
$N\widehat{-C}-Z$ (tilt)	4.372 (248)	4.76[(b)]	3.752 (318)
$F\widehat{-C}-Z$	108.984 (129)	109.14[(b)]	109.399 (187)
$F\widehat{-C}-F$	-	109.8 (4)	-
$F\widehat{-C}-N$ in plane	-	113.9 (1.0)	-
$F\widehat{-C}-N$ out of plane	-	107.5 (6)	-
α_{av}	21.8 (1.1)	0	0
θ_{az}	23.25	23.87[(c)]	24.56
F/cm^{-1}	2.1835	2.1653	2.1367

Notes

Bond lengths in Å. Angles in degrees.

(a) Errors in this column are 1σ from the least-squares fit.
(b) Calculated from the other quantities given.
(c) θ_{az} = 24.3° from the IAM fit

CF_3NO Structure.

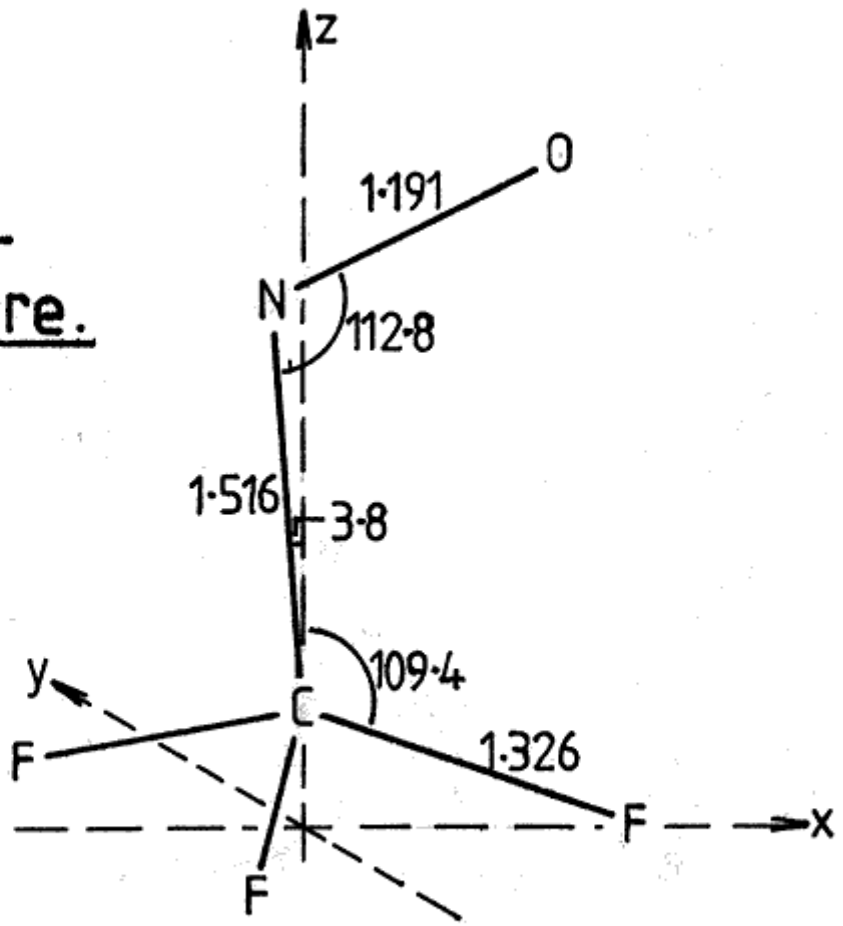

Bond lengths in Å.

Angles in degrees.

Figure 1

TABLE 4

CF_3NO

The Effect of Parameter Increments on F

Parameter	Increment/Å or /Deg	$\Delta F/cm^{-1}$
r(C-F)	+0.01 (a)	-0.0072
r(C-N)	+0.01	0.0021
r(N=O)	+0.01	-0.0301
N-$\hat{C}$-O	+1.0	0.0481
N-$\hat{C}$-Z(tilt)	+1.0	0.0703
F-$\hat{C}$-Z	-1.0 (a)	-0.0074
ϕ_{FCF} (b)	+2.0	-0.0065

Notes:

(a) All three quantities changed simultaneously.

(b) The angle between the projections of the out-of-plane C-F bonds on to the x,y plane, z being the internal rotation axis.

CF_3NO has an a,b plane of symmetry, so that the above reduces to;

$$I_{eff} = I_{\alpha} \left[1 - \frac{I_{\alpha}}{I_a} \cos^2\theta_{az} - \frac{I_{\alpha}}{I_b} \sin^2\theta_{az}\right] \quad ---(3)$$

θ_{az} is the angle between the a principal axis and the z axis.
Consideration of the quantities appearing in (3) reveals that uncertainty in θ_{az} will be the greatest contributor to uncertainty in F. This follows because the term $\frac{I_{\alpha}}{I_a} \cos^2\theta_{az}$ approaches 1 for the heavy top case, and the moments of inertia I_{α} and I_a are well determined from microwave data. If the CF_3 group is symmetric I_{α} is given by the planarity condition;

$$I_{\alpha} = I_a + I_b - I_c + \Delta$$

Turner and Cox[77] indicate that Δ, the inertial defect, for CF_3NO will be $\sim 0.1 u\text{Å}^2$, so that its neglect in the above expression, given that $I_{\alpha} \simeq 89.1 u\text{Å}^2$, is not sufficient to account for the difference between F and F_0. It is necessary to note however that F obtained from the microwave data applies to the ground state, whereas F_0 is the average over a number of torsional states. Such torsional averaging might show up in θ_{az} or in the moments of inertia, but in the latter case, some of the change ought to be modelled by centrifugal distortion terms. It has already been shown that $D_F^{(1)}$ does not help the fit (Table 2). Such a result is not surprising given that D_k (the coefficient of P_z^4) for CHF_3 is only 8.1 KHz ($2.7 \times 10^{-7} cm^{-1}$)[135].

Equation (3) may be re-arranged as follows;

$$\cos\theta_{az} = \sqrt{\frac{1 - \frac{I_{eff}}{I_{\alpha}} - \frac{I_{\alpha}}{I_b}}{\frac{I_{\alpha}}{I_a} - \frac{I_{\alpha}}{I_b}}}$$

By assuming that I_{α}, I_a and I_b are constants, obtained directly from the microwave analysis, the above expression may be used to calculate the value of θ_{az} (θ_{az}' say) which corresponds to F_0. For the purpose of comparison, moments obtained from structure 3) will be used.

I_{α} = 89.13099

I_a = 90.58957

I_b = 157.83388 ($u\mathring{A}^2$)

These give θ'_{az} = 25.78°. It is therefore found that a small change in θ_{az} of ~1.2° will bring F into co-incidence with F_0. Furthermore, the required shift corresponds to a rotation of the z axis towards the C-N bond where, in structure 3), $\theta_{a,C-N}$ = 28.31°. The significance of this is that the tilt angle ($\theta_{a,C-N}-\theta_{az}$) manifests itself as a difficulty in defining the exact direction of the internal rotation axis. Rotation of the CF_3 group must result in three identical minima, and yet the group cannot be symmetric because it does not exist in a symmetric environment. The measured tilt therefore reflects the complexity of the paths taken by the fluorine atoms when the CF_3 group executes a rotation about the C-N bond. It is, in effect, a means of reconciling the structural data with the requirement of the tunneling model, that there should be a single internal-rotation coordinate α. It therefore seems reasonable to evoke non-rigidity to explain, at least in part, the discrepancy between F_0 and F. It is then apparent that there would be a paradox in attempting to fit the structure to F_0.

The idea that the molecule possesses a symmetric group constrained to rotate about the z axis is one extreme view of the internal rotation process. The other extreme is that the molecule possesses an asymmetric group constrained to rotate about the C-N bond. In this case, equation (3) is no longer appropriate, but F may be calculated for an infinitesimal rotation using Pitzer's equation for a general asymmetric internal rotor[123] (see Appendix 5). The result of such a calculation is instructive. Using structure 3) gives F=1.9100 cm^{-1}. F_0 therefore appears to be bounded by the two extremes. It is also instructive to note that applying equation (3) to a system which has, in reality, a slightly asymmetric internal rotor, would require relaxation of the condition for direction cosines, such that;

$$\lambda^2_{az} + \lambda^2_{bz} + \lambda^2_{cz} \neq 1$$

FLUORAL

The microwave spectra of CF_3CHO and CF_3CDO were studied by Woods[87]. Both species were observed in their v=0 and 1 torsional states. For the H species, Woods reported V_3 = 309(26)cm^{-1} with F = 2.09cm^{-1}, which predicts a torsional frequency of ~76 cm^{-1}. Berney[120] recorded the gas-phase infrared spectrum of CF_3CHO and observed a band at 55 cm^{-1}, which he was unable to assign other than to the torsional mode, despite the microwave data. The same discrepancy appeared for CF_3CDO. Berney observed the torsional band at ~52 cm^{-1}, whereas Woods' data predict ~71 cm^{-1}. Thus, further consideration of the torsional data is required.

The structure of Fluoral is not fully determined. Woods had a working structure[86] based on his own data and the early Electron Diffraction results of Schwendeman[124], but he chose not to include it in his paper[87]. For the internal rotation calculation here, this structure was refined as follows; The rotational constants[87] extrapolated back to V=-½ give the CF_3 group moment of inertia I_α = 88.9351 uÅ².

Using the relationship;

$$C_F = \sqrt{I_\alpha / 4M_F}$$

(M_F = fluorine atomic mass) gives the fluorine out-of-plane distance C_F = 1.0818A. The electron diffraction r(C-F) = 1.332Å falls in the range found for other molecules[77,78,79,125]. Assuming this bond length gives $\widehat{F\text{-}C\text{-}Z}$ = 110.31°, and $\widehat{F\text{-}C\text{-}F}$ = 108.62° consistent with the electron diffraction value.

Berney[120] reported ν(C-H) = 2864 cm^{-1}. Using McKean's empirical correlation[23] this gives r_0(C-H) = 1.1056Å.

The electron diffraction r(C=O) = 1.204Å is virtually identical to that of acetaldehyde[56,58] and was therefore accepted.

TABLE 5

The Structure of CF_3CHO

Parameter	Electron Diffraction[124]	Microwave/ Least-Squares(a)
r(C-F)	1.332(7)	1.332
r(C-C)	1.54 (2)	1.527(22)
r(C=O)	1.204(14)	1.204
r(C-H)	-	1.1056
C-$\hat{C}$=O	121.8 (4.5)	123.91 (2.7)
C-$\hat{C}$-H	-	118.0
F-$\hat{C}$-F	108.7 (1)	(108.616)(b)
C-$\hat{C}$-Z(tilt)	-	2.01 (57)
F-$\hat{C}$-Z	-	110.3136

(a) Parameters without errors are constants in the fit.

(b) Determined from I_K and r(C-F). Included for comparison.

With the above constraints, the structure was fitted to the rotational constants of the two available isotopic species at V= -½. The C-H bond was constrained to bisect the C-$\widehat{C}$-O angle. The result is given in Table 5 and Figure 2. Internal rotation parameters derived from this structure are compared with Woods' values in Table 6.

TABLE 6

	This Work	Woods[87]
CF_3CHO θ_{az}/deg	20.97	21.63
F/cm^{-1}	2.1069	2.0942
CF_3CDO θ_{az}/deg	19.46	19.67(a)
F/cm^{-1}	1.7405	1.7681(a)

(a) Woods case I

For CF_3CHO, Woods reported ν(OE-OA) = 1.53 MHz and ν(1A-1E) = 75 MHz. Taken with Berney's observation ν(1-0) = 55 cm^{-1}, and using F_0 = 2.1(1) cm^{-1}, it was not possible to account for the data with any reasonable parameters in Hamiltonian (2). There are insufficient data for a least-squares fit, but (2) has a numerical solution. For CF_3CHO this is (in cm^{-1});

F_0 = 1.656

V_3 = 249.9

V_6 = -6.28

Even given the likely uncertainties in the structure and difficulties in defining a z axis, F_0 cannot be reconciled with F. Removal of the tilt gives F = 1.979 cm^{-1}. Use of $\theta_{a,c-c}$(22.99°) instead of θ_{az} in equation (3) gives F=1.882 cm^{-1}. Assuming the CF_3 group to be asymmetric, rotating about the C-C bond, and applying Pitzer's equation[123] gives F=1.991 cm^{-1}. On the basis of the CF_3NO work, F might therefore be expected to lie between 1.99 and 2.11 cm^{-1}. A re-appraisal of the raw data is obviously required.

CF_3CHO Structure.

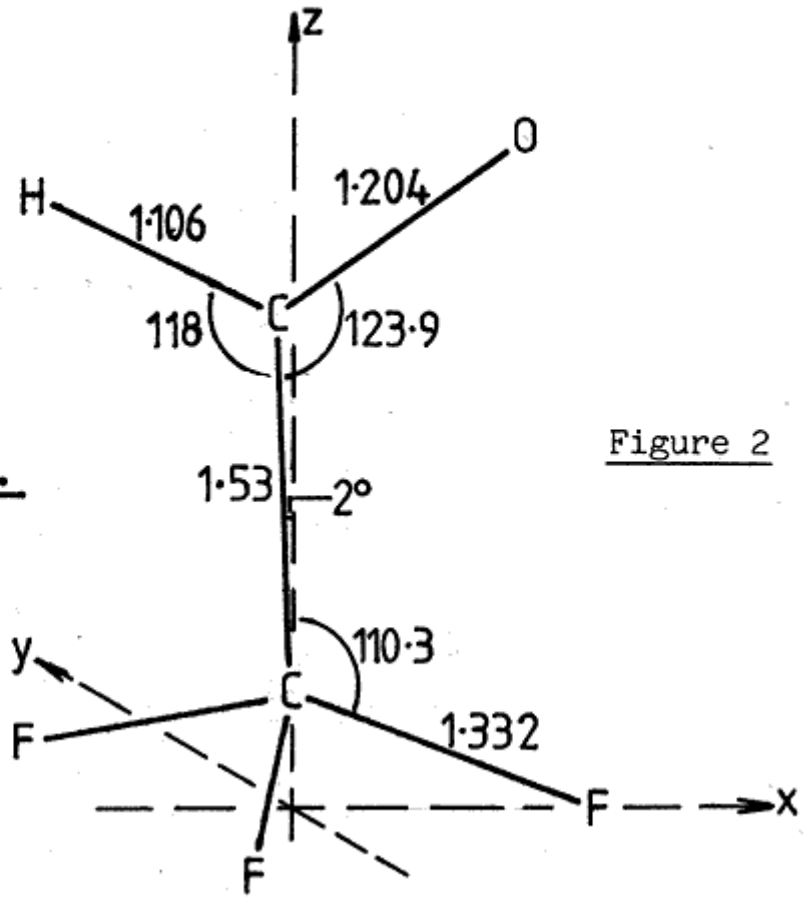

Figure 2

The torsional band in the far-infrared spectrum of CF_3CHO is reproduced in Figure 6 of reference 120. It is a broad feature covering ~30 cm^{-1}. Berney chose to identify a small dip in the band at 55 cm^{-1} as the torsional fundamental. There is no clearly identifiable dip in the corresponding band for CF_3CDO, for which reason Berney was much less certain of his assignment of 52 cm^{-1} for this species. In fact, the dip is almost certainly an artefact. Berney explored, and rejected, a number of reasons for why the given frequencies might be incorrect, but an important possibility, that most of the absorption profile might arise from torsional hot bands, was neglected. The anharmonicity of the torsional vibration is such that the first few hot bands split rapidly away to the low frequency side of the fundamental. Even if all of these bands had the same transition probability, they would misdirect the measurement of the fundamental, but a theoretical investigation by Pedersen[126] indicates that the transition moment for such a system can increase with torsional quantum number and thereby offset the adverse Boltzmann factor. Furthermore, Pedersen's investigations indicate the allowedness of the torsional Q-branch through higher terms in the torsion-rotation Hamiltonian. The assignment of the torsion frequency to a dip in the band profile is therefore not justified, and it is reasonable to expect that the fundamental will lie at the upper edge of the observed band.

For CF_3CHO, the intensity of the infrared torsion band starts to die away above ~66 cm^{-1}. Adopting $\nu(1\text{-}0)$ = 66(5) cm^{-1} and solving Hamiltonian (2) as before gives;

F_0 = 1.970 (142)

V_3 = 305.2 (25.4)

V_6 = -8.71 (1.16)

Hot transitions predicted by this model are given in Table 7. Berney recorded the torsion band at 34°C, but stated that its appearance remained essentially unchanged on going to dry ice temperature. Boltzmann factors

TABLE 7

TORSIONAL TRANSITIONS FOR CF_3CHO

Band	E States				A States			
	Line Freq/cm^{-1}	Lower Level cm^{-1}	Boltzmann Factor		Line Freq/cm^{-1}	Lower Level/cm^{-1}	Boltzmann Factor	
			34°C	-78°C			34°C	-78°C
1-0	66.0	33.86	1.0	1.0	66.0	33.86	1.0	1.0
2-1	62.1	99.86	0.73	0.61	62.1	99.86	0.73	0.61
3-2	56.8	161.98	0.55	0.39	57.6	161.93	0.55	0.39
4-3	51.7	218.79	0.42	0.26	46.4	219.49	0.42	0.25
5-4	34.3	270.46	0.33	0.17	58.0	256.86	0.34	0.18
6-5	57.0	304.80	0.28	0.14	10.0	323.87	0.26	0.12
7-6	38.0	361.79	0.22	0.09	108.7	333.93	0.25	0.11
8-7	90.5	399.79	0.18	0.07	0.2	442.63	0.15	0.05

given in the table indicate that such an observation is not inconsistent with the model.

For CF_3CDO Woods[87] observed ν(1A-1E) = 14.25 MHz but was unable to observe A-E splitting in the ground state. There are insufficient data for a three parameter solution to Hamiltonian (2). Calculations were therefore performed either with V_6=0 or V_6 assumed from the H species. Results are given in Table 8, firstly for ν(1-0) = 52 cm^{-1} as given by Berney, secondly for ν(1-0) = 63 cm^{-1}, this being the point above which the intensity of the CF_3CDO torsion band dies away. All models predict no observable ground state splitting, but it is again clear that F_0 can only be reconciled with structure if the torsional fundamental lies in the upper edge of the observed infrared band.

TABLE 8

CF_3CDO

ν(1-0)	F_0 (b)	V_3	V_6 (c)	Predicted ν(OE-OA)/MHz
52	1.360	249.4	0	0.23
52	1.400	260.3	-6.28	0.26
63(5)	1.628(121)	305.5(25.7)	0	0.23
63(5)	1.682(121)	320.6(25.7)	-8.7	0.26

(a) cm^{-1} except where indicated.

(b) F = 1.741 cm^{-1} for a symmetric CF_3 group rotating about the z axis.
F = 1.669 cm^{-1} for an asymmetric CF_3 group rotating about the C-C bond.

(c) Assumed value.

Finally, it is interesting to note that, for a number of molecules including CF_3CHO and CF_3CDO, Quade[6] has performed calculations to determine the contribution to the effective potential energy from the interaction of molecular vibrations with internal rotation. The important points arising from this study are as follows:

1) In the harmonic approximation, the only vibrational modes that interact with the internal rotation have displacements perpendicular to the molecular symmetry plane.

2) Mixing of the perpendicular vibrations with torsion, in the normal coordinate approximation, occurs through the kinetic energy.

3) A transformation to a new internal-rotation coordinate, $\alpha \longrightarrow \alpha'$, by means of a rotation in the molecular symmetry plane, separates the torsion from other vibrations in zeroth order in the kinetic energy. α', which does not have a simple structural definition, is the appropriate internal rotation coordinate for analysis of data using a model with an effective single degree of freedom.

4) After transformation, the interaction between torsion and other vibrations appears in the effective potential energy.

On this basis, Quade has calculated the contribution to the effective V_6 term (V_6') from molecular vibrations. Using the out-of-plane fundamentals reported by Berney[120] he obtains;

for CF_3CHO $\quad V_6' = -6.51\ cm^{-1}$

for CF_3CDO $\quad V_6' = -4.74\ cm^{-1}$

This result gives a surprisingly favourable comparison with $V_6 = -8.7(1.2) cm^{-1}$ for CF_3CHO which was obtained earlier, bearing in mind that, in addition to the vibrational contribution, the experimental V_6 term contains contributions from several sources: i.e. the equivalence between F_3 and V_6 (q.v.), F_3 being allowed by symmetry; the electronic contribution to V_6; and the effect of truncating the potential at V_6.

APPENDIX 1

THE SPECTROMETER

The microwave spectrometer used throughout this work was the instrument built at Bristol University under the direction of Dr. A.P. Cox. This spectrometer is a Hughes-Wilson (Stark modulation/Phase sensitive detection) instrument capable of operation in conjunction with Klystron or Backward Wave Oscillator (BWO) microwave sources. Klystrons were available covering the range 7.9 to 42.0 GHz. A K-band (18.0 - 26.5 GHz) and a Q-band (26.5 - 40.0 GHz) BWO were also available. In addition, Radio Frequency (RF) - microwave double resonance experiments were performed by injecting a radio signal at the Stark Electrode.

The spectrometer arrangement for Stark modulation, with a Klystron source, is given in Figure 1. The cell is a 3m length of stainless steel X-band waveguide with a mica window at each end providing a vacuum seal. The Stark electrode is an internal nickel septum, supported by PTFE insulating strips and arranged parallel to the broad face of the waveguide. It gives an electric field parallel to the plane of polarisation of the radiation and hence $\Delta M = 0$ selection rules. The effective electrode spacing was 0.459 cm, subject to slight variation depending on temperature and the state of contamination of the cell. The entire cell was surrounded by a lagged dry-ice trough.

Klystrons were used free running, with water cooling. Drift was not troublesome, being only a few MHz/hour after reaching thermal equilibrium. An attenuator or isolator was always placed at the output of the klystron to prevent the frequency pulling and mode hopping associated with reflected power. A D.C. heater supply was used to minimise 50 Hz frequency modulation. Frequency sweeping was accomplished by modulating the repeller voltage with the sawtooth X-deflector waveform from a cathode ray oscilloscope (CRO) as shown. X1 and X2 are direct connections to the deflector plates. XE is the

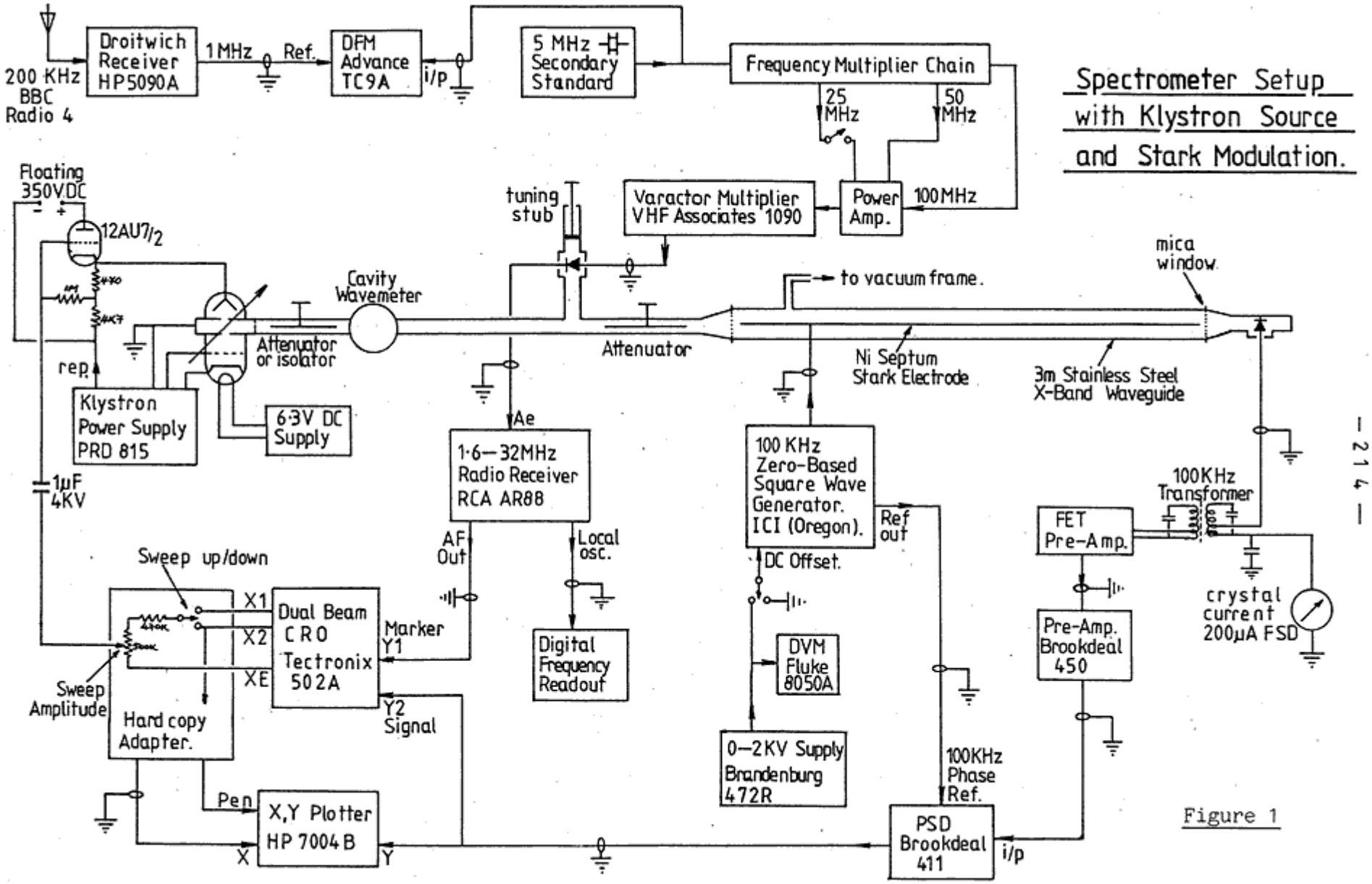

Spectrometer Setup with Klystron Source and Stark Modulation.

Figure 1

balance point for the X deflectors, i.e. the point in the EHT divider network about which X1 and X2 are always symmetric (it is not an earth connection!). Sweeps of up to 10 MHz (1.0 MHz/cm) could be achieved with good linearity, with a maximum sweep of ~25 MHz (2.5 MHz/cm) depending on the Klystron in use. Good linearity could also be maintained with sweeps as slow as 2s/cm. Prior to each frequency measurement, a check for constancy of Klystron output throughout the entire sweep was made by switching the Y2 input to display the voltage across the crystal current meter. This also provided a means for visualising the wavemeter dip and guageing its position relative to frequency markers at the Y1 input.

Frequency measurements were all made relative to the BBC 200 KHz standard transmission. 25, 50 and 100 MHz reference signals were converted into comb spectra (series of spikes, in the frequency domain, at exact multiples if an input frequency) and applied to a mixer arm. The tuning stub on this side arm relates only to the tuning of this section. The rectifier was a silicon point-contact diode. Mixing products were applied to an interpolation receiver which had its low impedance audio (headphone) output connected to the CRO at Y1. The effect of this arrangement is to produce a blip on the CRO trace when, at some point during a sweep, the difference between the Klystron frequency and an element of the comb spectrum is equal to the frequency to which the receiver is tuned. The origin of such a marker can be identified by noting its direction of movement relative to rotation of the receiver tuning control, or by elimination using the switch in the 25 MHz feed, the frequency already being known within ~5 MHz from the wavemeter reading. The receiver was used in its AM reception mode, with a 3dB bandwidth of ~6KHz. The digital readout attached to the receiver was designed and built by the author and is described in Appendix 2. Measurements were made by bringing frequency markers into co-incidence with absorption line maxima. This operation was always performed sweeping low→high and high→low, in order, by taking the average, to defeat the systemmatic lag

which results as a consequence of the detector time constant. Measurements were made using small sweeps of 0.2 ~ 0.5 MHz/cm at 2 sec/cm, i.e. 0.1 ~ 0.25 MHz/sec, with time constants of 0.3 or 1.0 sec depending on the strength of the line. In the spectrometer limited regime, this gave a repeatability of measurement of about ±0.02 MHz, with an estimated standard deviation, for such an observation, of about 0.05 MHz. Traces appearing on the CRO screen could be reproduced on an X,Y plotter using the hard-copy adapter. This unit was also designed and built by the author and is described in Appendix 3.

Stark modulation was accomplished by means of a zero-based square-wave generator operating at 100 KHz. Maximum output of this unit was 2 KV peak. Zero basing was accomplished by means of a (valve) clamping diode, the reference to this clamping system could also be connected to a D.C. supply, in order to make accurate Stark shift measurements. The 100 KHz drive signal, obtained from a 200 KHz crystal oscillator, was also supplied, via a variable phase-shift network, to the phase-sensitive detector (PSD). For very easily modulated absorption lines, more accurate zero basing was obtained by using a smaller unit (HP211A), capable of 0-60V output, locked to the large generator. The HP211A also has valve clamping, avoiding the 0.6V offset inherent with semiconductor devices.

Factors limiting the resolution of the spectrometer are as follows[127,128] (approximate constribution to line half-width at half-maximum in brackets);

1) Natural line width (~10^{-4}Hz) due to the background of thermal and zero-point[129] radiation.
2) Doppler effect (~40 KHz) due to the thermal spread of molecular velocities.
3) Wall collision broadening (~10 KHz) due to finite dimensions of the spectrometer cell.
4) Pressure (dipole-dipole or collision) broadening (~20 MHz/Torr), due to the finite time for which a molecule remains in a given state.

5) Power saturation effects, i.e. the tendency for the microwave radiation to equalise the populations of the upper and lower states.

6) Short term source instability (~200Hz), i.e. the bandwidth of the Klystron output.

7) Modulation sidebands (~200 KHz).

Pressure, power and modulation broadening are by far the most important factors. Moreover, power saturation tends to occur at the low pressures required for accurate frequency measurement and for the resolution of quadrupole hyperfine structure. Pressures were estimated using a priani guage. The crystal current was used as a measure of relative microwave power. Nominal pressures of 0.01~0.02 Torr and crystal currents of ~50μA were used during measurements. The choice of 100 KHz as the modulation frequency reflects the need for high sensitivity. The noise output of the detector crystal is inversely proportional to (modulation) frequency, hence resolution may be traded for an improvement in signal-to-noise ratio. The overall resolution of the instrument was ~0.5 MHz. The minimum absorption coefficient for a useable signal-to-noise ratio was about 10^{-9}/cm.

Figure 2 shows the spectrometer arrangement with a BWO, in a broad-band sweep unit, as the microwave source. No accurate line measurements were attempted with the spectrometer in this mode. Frequencies were estimated to ~5 MHz by manually tuning the BWO to the line of interest and then locating the wavemeter dip.

Figure 3 shows the spectrometer arrangement for RF-microwave double-resonance experiments. The 100 KHz square wave generator was used as the modulation source, but with the HP211A interposed to prevent accidental destruction of the balanced mixer. The RF amplifier was, in general, used without a terminating resistor, this being in order to maximise the RF voltage across the Stark electrode. The cell is almost purely reactive, all

Spectrometer Setup With BWO Source for Broad-Band Sweep.

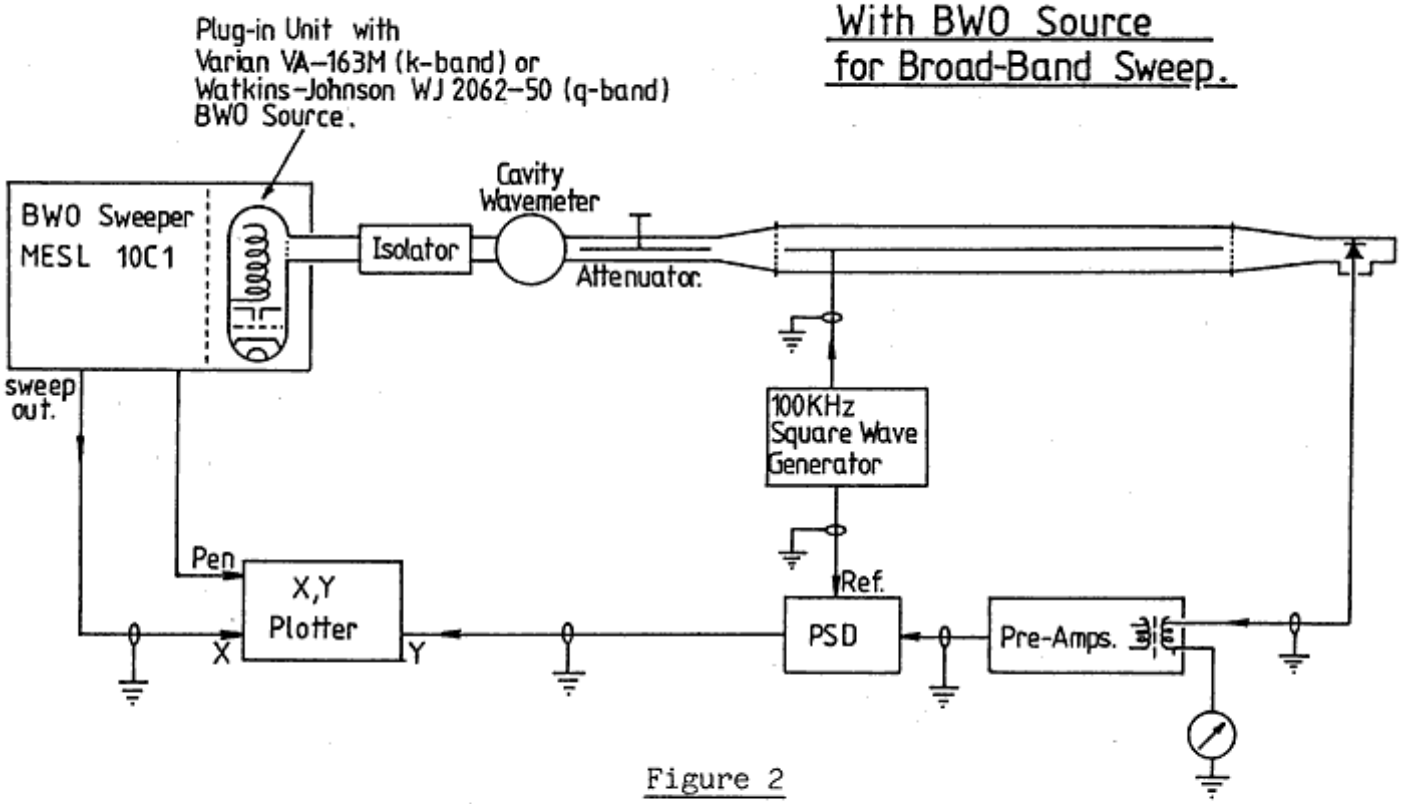

Figure 2

Spectrometer Setup for RF-Microwave Double-Resonance.

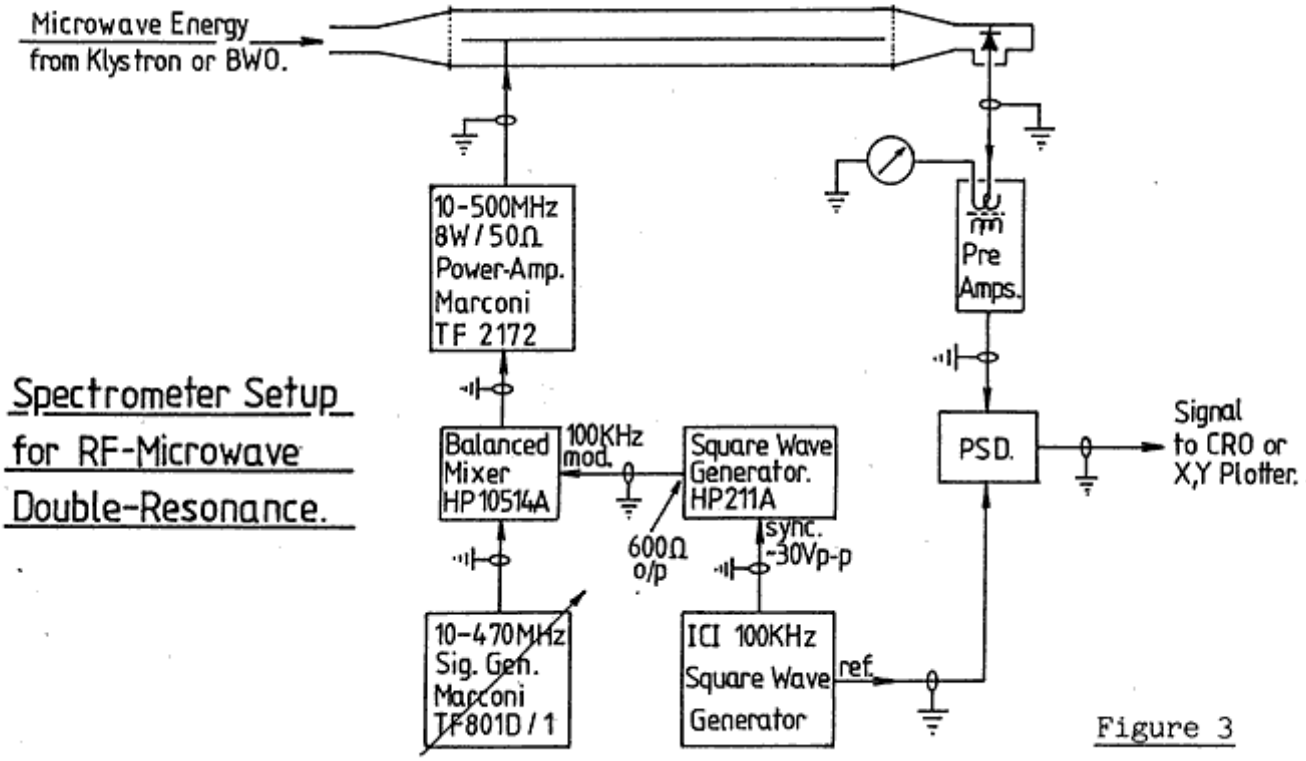

Figure 3

of the developed power being dissipated in the final amplifier. Survival of the amplifier in this regime is attributable to it having a valve output stage.

APPENDIX 2

DIGITAL FREQUENCY READOUT FOR A SINGLE CONVERSION SHORT-WAVE RADIO RECEIVER

The principle of operation of a single conversion superheterodyne radio receiver is shown in Figure 1. The desired input signal f_1 is mixed with a local oscillator signal f_0. This results in a signal having many frequency components, but notably the sum and difference of the two input signals. The intermediate frequency (IF) signal is obtained by applying the mixer output to a filter tuned to the frequency of the difference signal. This signal is then amplified and applied to a detector.

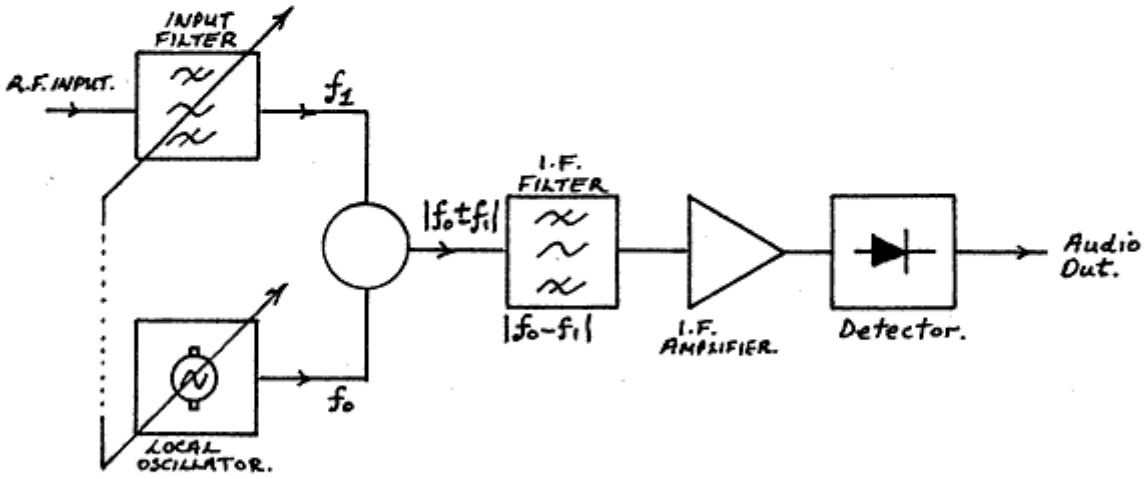

Single Conversion Superhet. Receiver.

Figure 1

There are two possible values for f_1 which satisfy the relationship $f_0 - f_1 = IF$, these are $f_1 = f_0 - IF$ and $f_1 = f_0 + IF$. The receiver therefore has an input filter to select whichever of these is required. Tuning of the receiver is accomplished by tuning the input filter and the local oscillator simultaneously, in such a way that $f_0 - f_1$ is a constant.

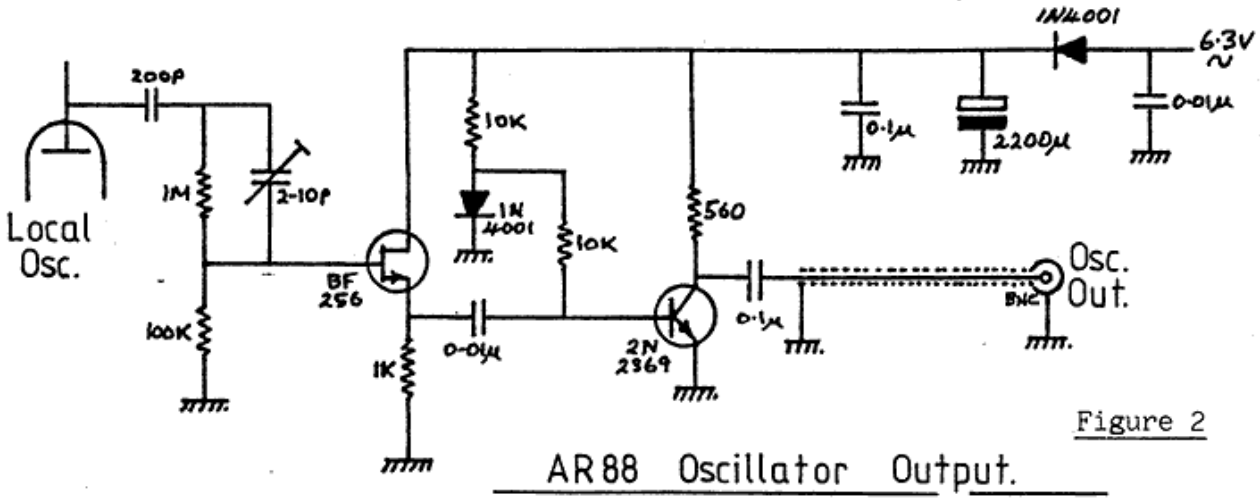

Figure 2

AR88 Oscillator Output.

A receiver in which $f_0 = f_1 + IF$ is said to operate with 'oscillator high', a receiver in which $f_0 = f_1 - IF$ is said to operate with 'oscillator low'. The oscillator low system has the disadvantage that at $f_1 = 2 \times IF$, $f_0 = IF$, therefore most general coverage single conversion receivers operate with oscillator high. To obtain a digital presentation of the input frequency to which such a receiver is tuned, it is therefore necessary to measure the frequency of the local oscillator and subtract from it the intermediate frequency before displaying the result.

In the Bristol laboratory, microwave frequency measurements are made by interpolation between components of 100, 50 or 25 MHz comb spectra. The interpolation receiver used is an R.C.A. model AR88, which is an oscillator high receiver having an IF of 455 KHz. Figure 2 above shows circuitry which has been included in the receiver in order to provide an oscillator output. This circuit is a non linear buffer amplifier, having a high input impedance, which takes energy directly from the anode of the oscillator valve. The adjustable capacitor provides some measure of control over the output waveform, it is best adjusted by experimenting with the receiver in conjunction with the digital counter and ensuring that satisfactory triggering occurs on all frequencies. It should be noted, however, that inclusion of the buffer

circuit necessitates complete retracking and alignment of the oscillator. The compensation trimmer should therefore only be adjusted prior to final receiver alignment. The circuit obtains its power by rectification of the receiver's 6.3 V heater supply. The rectifier and 220 µF smoothing capacitor are mounted in the power supply section of the receiver chassis, the remainder of the components are mounted inside the under-chassis oscillator compartment and as close as is practicable to the oscillator valve anode connection.

Figure 3 shows the circuit of the digital counter designed for use with the modified AR88 receiver or any similar receiver having an IF of less than 99.999 MHz. The least significant digit of the display is in ones of KHz. The counter does not explicitly perform a subtraction to obtain the true receiver frequency from the oscillator frequency - instead, the count register (5 x 74LS196) can be programmed by means of thumbwheel switches, so that it resets to a non-zero number before the start of each count. If, as is the case when used in conjunction with the AR88, the count register is reset to 99545, the first 455 pulses cause the register to contain 00000, since the one of 100 000's is lost in the overflow. Subsequent pulses increment the counter so that the result displayed at the end of the counting period is the oscillator frequency minus 455 KHz, i.e. the true receiver frequency. In general, to program the register correctly, for an oscillator high receiver;

Thumbwheel setting = 100 000 - IF in KHz.

For an oscillator low receiver, the thumbwheels are merely set to the IF.

Circuit Description

The frequency meter derives its timing waveforms from an internal 500 KHz crystal controlled clock oscillator. The output of this oscillator is divided by 250, in three 7490 integrated circuits, to provide a 2 KHz signal which is applied to the timing waveform generator. The operation of

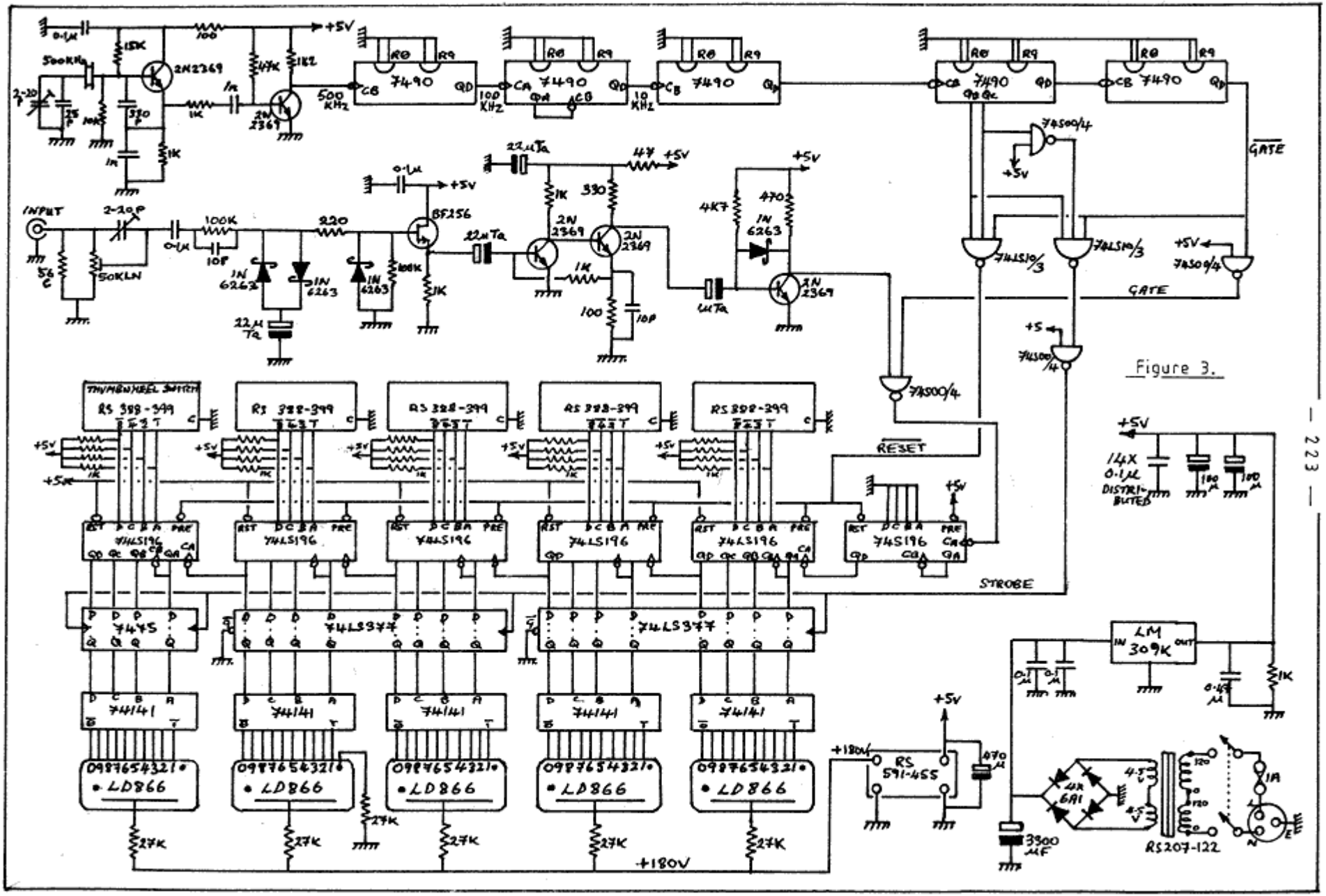
2N2369
7490
500 KHz
100 KHz
10 KHz
GATE
RESET
STROBE
INPUT
BF256
74LS196
74LS377
74145
74141
LD866
+180V
LM 309K
RS207-122

Figure 3.

the timing waveform generator is described in Figure 4. The Q outputs of the two quinary counters (shown in Figure 4) are gated together to produce the three housekeeping signals; 'gate', 'strobe' and 'reset'. The gate signal causes the amplified input signal to be applied, via the signal gate ($\frac{1}{4}$ x 74S00), to a 74S196 divide-by-ten circuit. The signal gate opens for 10 ms, during which time counting occurs, and then closes for 2.5 ms, during which time the strobe signal loads the display register (7475 and 2 x 74LS377) with the contents of the count register (5 x 74LS196), and then the reset signal loads the count register according to the thumbwheel switch settings. The display is therefore updated every 12.5 ms (80 Hz refreshment rate).

The 74S196 is a 100 MHz high speed counter which, in this circuit, since its status is never displayed, functions as a divide-by-ten pre-scaler. This circuit does however receive a reset signal, this signal being provided so that an ambiguity of ± 1 in the least significant digit, due to lack of phase coherence between gate signal and input signal, shows up in the status of this counter rather than in the counter which drives the least significant digit of the display. The frequency meter therefore measures to 0.1 KHz but only displays to 1KHz.

The input amplifier is a wide-band non-linear circuit. The input signal is limited, before amplification, to $\sim$400 mV peak-to-peak, by means of two 1N6263 Shottky diodes connected back to back. The final transistor in the amplifier chain is operated as a non-saturating switch, the Shottky diode between base and collector being present to prevent saturation, so that a rectangular waveform suitable for driving TTL circuitry is produced. The input to the amplifier is provided with two adjustments; input level and high frequency compensation. These are used to obtain satisfactory triggering of the counter on all frequencies covered, although below 50 MHz, HF compensation is unnecessary and the capacitor may be set to minimum.

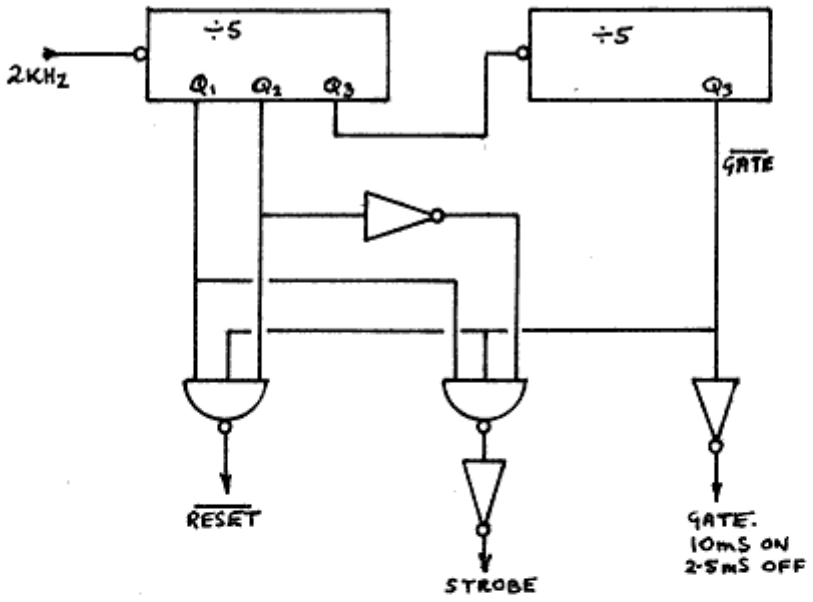

TIMING LOGIC.

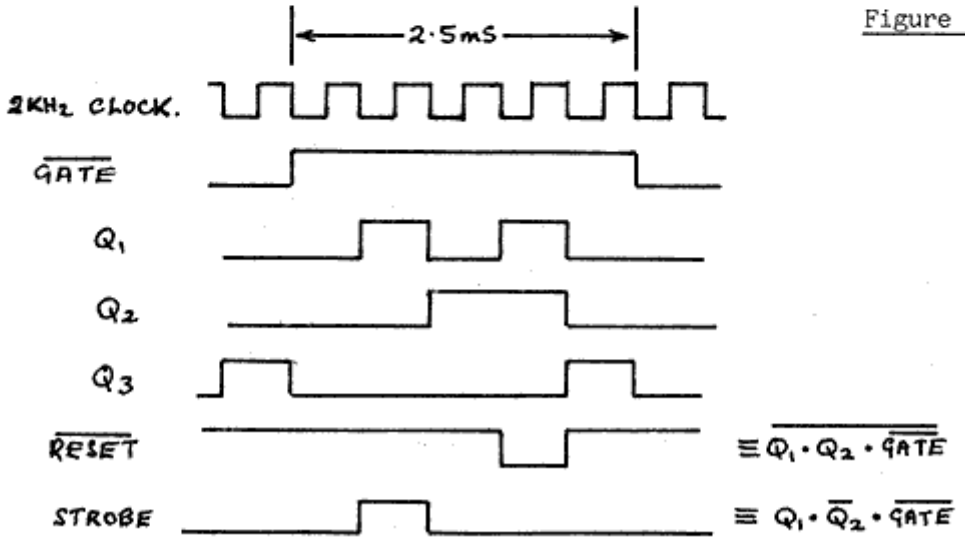

Figure 4

Accuracy of the Instrument

Microwave frequency measurements made in the Bristol laboratory are normally assumed to have an accuracy of ~50KHz. The digital frequency meter was therefore designed to have an accuracy at least an order of magnitude better than this. Error in the displayed frequency is primarily due to any discrepancy between the desired and the actual frequency of the reference oscillator: this error is given by;

Display Error = Input freq. x Fractional error in reference freq.

i.e. for oscillator high;

Display Error = (Display freq. + IF) x Fractional error in reference freq.

The crystal reference oscillator can be expected to have a short and long term stability of better than $\pm$20 ppm, which gives an accuracy of $\pm$ 0.6 KHz at an input frequency of 30 MHz.

The prototype counter suffers from rounding error in the last digit, since rounding up is not attempted in the event that the non displayed digit (tenths of KHz) is greater than 4. This problem may be overcome by pre-setting the 74S196 pre-scaler to binary five (0101) rather than re-setting it to zero as is presently done.

APPENDIX 3

HARD COPY ADAPTER

This unit was constructed in order to obtain permanent copies, on an X,Y plotter, of traces normally viewed on the spectrometer oscilloscope. Its circuit diagram is shown in the figure. A sweep signal is obtained by direct connection to the oscilloscope X2 plate. This provides a linear ramp moving from 140V to 240V (approx.) as the spot traverses the screen. Division of this signal by 100 in a resistor network, and addition of a nominal -1.4V back-off potential, provides a linear ramp of 0 → 1V at the input of the 741 operational amplifier. The gain control arrangement is such that the minimum gain of the amplifier is 1.0. The maximum usable output sweep is ~10V.

In order to use the hard copy adapter, the oscilloscope must be operated in the one-shot mode, i.e. the mode wherein pushing a button initiates a single sweep. The slowest sweep rate (5S/cm) is recommended. Pushing the pen-drop button, immediately prior to a sweep, sets a flip-flop (2 x BCY70) and causes a low impedance to appear across the pen control line (suitable for the HP7004B plotter). At the end of a sweep, the flyback is differentiated and used to reset the flip-flop, thus lifting the pen. The return of the chart recorder to the left hand margin is delayed, in order to give time for the pen to lift reliably. This delay is provided by the diode and 470μF capacitor at the chart X output.

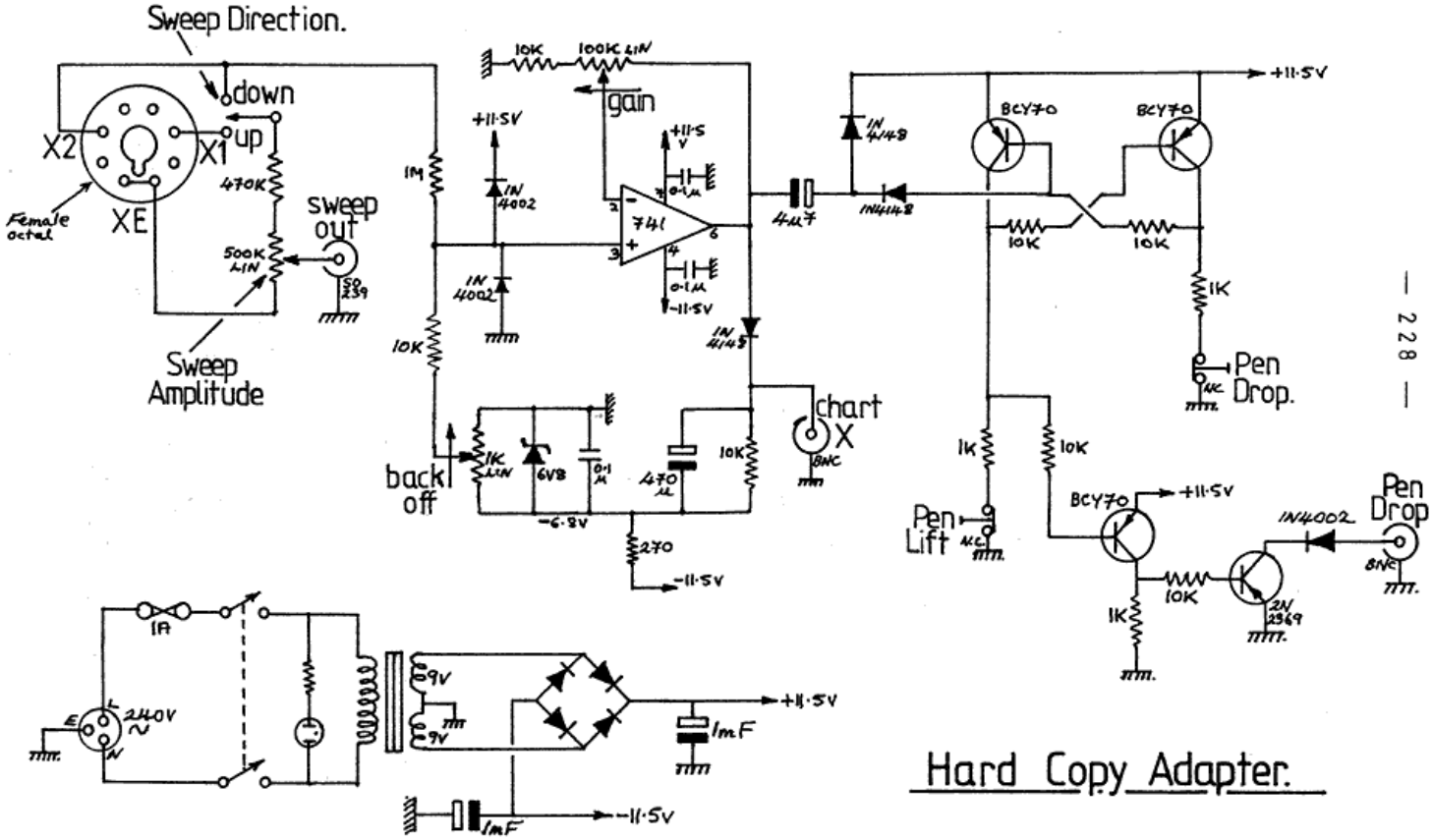
Sweep Direction.
down
up
X2
X1
XE
Female octal
470K
500K LIN
sweep out
Sweep Amplitude
10K
100K LIN
gain
+11·5V
1M
IN 4002
741
4µ7
IN 4148
BCY70
BCY70
10K
10K
1K
Pen Drop.
IN 4002
IN 4148
0·1µ
-11·5V
chart X
BNC
back off
1K LIN
6V8
0·1 µ
470 µ
10K
-6·8V
270
-11·5V
1K
10K
Pen Lift
BCY70
+11·5V
IN4002
Pen Drop
BNC
10K
2N 2369
1K
1A
240V
9V
9V
+11·5V
1mF
-11·5V
1mF
Hard Copy Adapter.

APPENDIX 4

EVALUATION OF QUADRUPOLE COUPLING CONSTANTS

The effect of a quadrupolar nucleus is to split observed spectroscopic lines into hyperfine components displaced about the hypothetical (unperturbed) line centre in such a way that the intensity weighted average of their frequencies gives (in the zero error limit) the frequency of the hypothetical centre[130].

First order quadrupole energies are given by;

$$E_q = \frac{2}{J\,(J+1)}(\chi_{aa}\langle P_a^2\rangle + \chi_{bb}\langle P_b^2\rangle + \chi_{cc}\langle P_c^2\rangle)Y(I,J,F)$$

where Y(I,J,F) is Casimir's function

and F takes on values J+I, J+I-1, ... , |J-I|.

Quadrupole shifts in the observed spectrum are given by

$$\Delta\nu_q = E'_q - E_q \quad \text{(in frequency units).}$$

Primed quantities refer to the upper state, unprimed quantities to the lower. Only transitions with the selection rule $\Delta F = \Delta J$ will be considered here, other transitions usually being of small intensity.

Q-Branches ($\Delta J=0$, $\Delta F=0$)

Since Y(I.J.F) is the same for both substates (for $\Delta F=0$ transitions)

$$\Delta\nu_q(\text{Q-branch}) = \frac{2}{J(J+1)}\left(\chi_{aa}\frac{\partial\nu}{\partial A} + \chi_{bb}\frac{\partial\nu}{\partial B} + \chi_{cc}\frac{\partial\nu}{\partial C}\right) Y(I,J,F)$$

where $\frac{\partial\nu}{\partial G} = \langle P'^2_g\rangle - \langle P^2_g\rangle$ $\qquad$ G = A,B,C; g = a,b,c

therefore, without knowledge of the hypothetical centre (which is not observable), by using the appropriate values of Casimir's function (tabulated in Reference 42) it is possible to extract, from the frequency differences between pairs of hyperfine components, estimates of a quantity here called;

$$\chi = \frac{2}{J(J+1)} \sum_{g=a,b,c} \chi_{gg} \frac{\partial \nu}{\partial G}$$

now $\chi_{aa} + \chi_{bb} + \chi_{cc} = 0$ (Laplace condition).

It is therefore possible to express E_q in terms of two parameters[131] χ_{aa} and $(\chi_{bb} - \chi_{cc})$.

Hence;

$$\chi = \frac{1}{J(J+1)} \left[\chi_{aa} \left(2 \frac{\partial \nu}{\partial A} - \frac{\partial \nu}{\partial B} - \frac{\partial \nu}{\partial C}\right) + (\chi_{bb} - \chi_{cc}) \left(\frac{\partial \nu}{\partial B} - \frac{\partial \nu}{\partial C}\right) \right]$$

and

$$\frac{J(J+1)\chi}{\left(\frac{\partial \nu}{\partial B} - \frac{\partial \nu}{\partial C}\right)} = \chi_{aa} \frac{\left(2 \frac{\partial \nu}{\partial A} - \frac{\partial \nu}{\partial B} - \frac{\partial \nu}{\partial C}\right)}{\left(\frac{\partial \nu}{\partial B} - \frac{\partial \nu}{\partial C}\right)} + (\chi_{bb} - \chi_{cc})$$

which can be used to determine the regression line, and hence χ_{aa}(slope) and $(\chi_{bb} - \chi_{cc})$ (Intercept) for a collection of χ values obtained from the observed line splittings.

It is not however sufficient to give unit statistical weight to the experimental quantities $J(J+1)\chi_{Obs}/(\frac{\partial \nu}{\partial B} - \frac{\partial \nu}{\partial C})$. In order to obtain the best estimates for χ_{aa} and $(\chi_{bb} - \chi_{cc})$, attention must be paid to the scaling of the uncertainties in χ's along with scaling of the χ's themselves.

Let $g = J(J+1) / (\frac{\partial \nu}{\partial B} - \frac{\partial \nu}{\partial C})$

and $y = g\chi$

and $x = (2 \frac{\partial \nu}{\partial A} - \frac{\partial \nu}{\partial B} - \frac{\partial \nu}{\partial C}) / (\frac{\partial \nu}{\partial B} - \frac{\partial \nu}{\partial C})$

The regression line then becomes

$$y = \chi_{aa} x + (\chi_{bb} - \chi_{cc}) \quad .$$

Let the uncertainty in χ_{obs} be U_χ

then the uncertainty in y_{obs}

$$U_y = g\, U_\chi$$

The statistical weight of a random variable is the reciprocal square of its uncertainty[132] . The correct weight for y_{obs} is therefore;

$$w = 1/(gU_\chi)^2$$

Solving for χ_{aa} and $\chi_{bb} - \chi_{cc}$

The residual e_i due to the i th observation y_i is defined by

$$y_i = \chi_{aa}\, x_i + (\chi_{bb} - \chi_{cc}) + e_i$$

Solving for the regression line is accomplished by minimising the weighted sum of the squares of the residuals, i.e. by imposing the conditions;

$$\frac{\partial \sum_i w_i e_i^2}{\partial \chi_{aa}} = 0 \quad , \quad \frac{\partial \sum_i w_i e_i^2}{\partial (\chi_{bb} - \chi_{cc})} = 0$$

which also imply $\sum_i w_i e_i = 0$

This yields;

$$\chi_{aa} = \frac{(\sum w_i)(\sum w_i x_i y_i) - (\sum w_i y_i)(\sum w_i x_i)}{(\sum w_i)(\sum w_i x_i^2) - (\sum w_i x_i)^2} \qquad .....(1)$$

and

$$\chi_{bb} - \chi_{cc} = \frac{(\sum w_i y_i) - \chi_{aa} \sum w_i x_i}{\sum w_i} \qquad .....(2)$$

It is also useful to express χ_{aa} in terms of $\chi_{bb} - \chi_{cc}$, permitting solution for one parameter while the other is held constant;

$$\chi_{aa} = \frac{(\sum w_i x_i y_i) - (\chi_{bb} - \chi_{cc}) \sum w_i x_i}{\sum w_i x_i^2} \qquad .....(3)$$

Error Analysis

The frequency derivatives $\partial\nu/\partial A$ etc. vary slowly as functions of the rotational constants A, B and C. Contributions to the residuals due to uncertainties in the rotational constants can therefore be neglected. The variance of an observation of unit weight can then be estimated from the weighted sum of the squares of the residuals divided by the number of degrees of freedom for the fit[133].

$$\sigma^2 = (\sum_i w_i' r_i^2)/(n - p)$$

where

$w' = 1/U_\chi^2$

n = effective number of observations.

p = number of parameters used in the fit.

$r = \chi_{obs} - \chi_{calc}$

and

$$\sigma'^2_i = \sigma^2/w_i'$$

Uncertainties in χ_{aa} and $\chi_{bb} - \chi_{cc}$

Provided that the errors in all observations included in the fit are truly random, the uncertainty of a parameter obtained from the fit can be estimated by summing the squares of the partial error contributions from each observation and taking the sqaure root[132] .

$$\sigma_p^2 = \sum_i (\sigma_i \, \partial p/\partial y_i)^2$$

For the case in point;

since $y_i = g_i \chi_i$ and $\sigma_i' = \sigma/\sqrt{w_i'}$

$$\sigma_i = g_i \sigma/\sqrt{w_i'}$$

Using the result and differentiating equations (1) and (2) yields;

$$\sigma_{\chi_{aa}} = \frac{\sigma}{D} \left(\sum [(\sum w_i) x_i \; - \; (\sum w_i \, x_i)]^2 w_i\right)^{\frac{1}{2}}$$

$$\sigma_{\chi_{bb}-\chi_{cc}} = \frac{\sigma}{D} \left(\sum [(\sum w_i \, x_i^2) - (\sum w_i \, x_i) \, x_i]^2 \, w_i\right)^{\frac{1}{2}}$$

where $D = (\sum w_i)(\sum w_i \, x_i^2) - (\sum w_i \, x_i)^2$

If only one parameter is allowed to vary in the fit, differentiating (2) and (3) yields;

$\sigma_{\chi_{aa}} = \sigma\sqrt{\sum w_i} \; / \sum w_i \, x_i$ when $\chi_{bb}-\chi_{cc}$ const.

$\sigma_{\chi_{bb}-\chi_{cc}} = \sigma/\sqrt{\sum w_i}$ when χ_{aa} const.

The Fortran IV program Chi, a listing of which is given at the end of this section, performs the computations here outlined.

Generalisation to include P- and R- Branches

The change in Y (I,J,F), for P- and R-branch transitions, prevents the procedure applicable to Q-branch data from being used. Other methods must therefore be employed.

By defining;

$$\chi_{J\tau} = \frac{2}{J(J+1)} \sum_{g=a,b,c} \chi_{gg} \langle P_g^2 \rangle = \frac{(2J+3)}{J} eQq_{J\tau}$$

The χ's used in the Q-branch fit become;

$$\chi = \chi_{J\tau'} - \chi_{J\tau}$$

and $\Delta\nu_q = \chi_{J\tau'}\ Y(I,J,F) - \chi_{J\tau} Y(I,J,F)$

with $\Delta F = 0$

For R- and P-branches

$$\pm\Delta\nu_q = \chi_{J'\tau'}\ Y(I,J',F') - \chi_{J\tau} Y(I,J,F)$$

with $\Delta F = \pm 1$

Special Case

$$\chi_{322} = 0$$

This follows from the Laplace condition and because, for the 3_{22} level

$$\langle P_a^2 \rangle = \langle P_b^2 \rangle = \langle P_c^2 \rangle = 4$$

The $\chi_{J\tau}$ for a level connected by a transition to the 3_{22} level can therefore be obtained directly from the observed line splitting. This $\chi_{J\tau}$ can then be fitted along with Q-branch data provided that $\langle P_g^2 \rangle$ values are given to the program instead of $\partial\nu/\partial G$ values.

General Case

It is possible, in principle, to solve a P- or R-branch quadrupole pattern for the relative contributions of $\chi_{J+1,\tau'}$ and $\chi_{J\tau}$. However, on account of the subtlety of the change in Y(I,J,F) with J, the parameters so determined will

usually have a large correlated error. This difficulty can be overcome by solving for

$$\chi = \chi_{J+1,\tau'} - \chi_{J\tau}$$

Fitting to $\chi_{J+1,\tau'} - \chi_{J\tau}$

$$\chi_{J+1,\tau'} - \chi_{J\tau} = \frac{2}{(J+1)(J+2)}\left[\sum_{g=a,b,c} \chi_{gg} \langle P_g'^2 \rangle\right] - \frac{2}{J(J+1)}\left[\sum \chi_{gg} \langle P_g^2 \rangle\right]$$

$$= \frac{2}{J(J+1)} \sum \chi_{gg}\left(\frac{\langle P_g'^2 \rangle}{(1+2/J)} - \langle P_g^2 \rangle\right)$$

Therefore, the linear combination $\chi_{J+1,\tau'} - \chi_{J\tau}$ can be fitted along with Q-branch data provided that $\frac{\langle P_g'^2 \rangle}{(1+2/J)} - \langle P_g^2 \rangle$ values are given to the program instead of $\partial\nu/\partial G$ values. As a check on the transformation, account may be taken of the condition;

$$\sum_g \left(\frac{\langle P_g'^2 \rangle}{(1+2/J)} - \langle P_g^2 \rangle\right) = 0$$

which is also the condition applicable to the sum of Q-branch $\partial\nu/\partial G$ (but not to P- or R-branch $\partial\nu/\partial G$) and follows from;

$$\langle p_a^2 \rangle + \langle P_b^2 \rangle + \langle P_c^2 \rangle = J(J+1)$$

Uncertainty in χ Values

From the difference between two line frequencies

$$\chi_{obs} = C(\nu_2 - \nu_1)$$

where C is a coefficient dependent on Casimir's function.

In the regime where measurement accuracy is governed by spectrometer limitations, all measured lines have the same uncertainty σ and;

$$\sigma_\chi = C\sqrt{2\sigma^2}$$

Each independent line splitting observed in a given quadrupole pattern provides a separate estimate for χ. Combination of two such estimates is best made by means of the uncertainty weighted average.

$$\chi = (w_1\chi_1 + w_2\chi_2)/(w_1 + w_2)$$

where $w_i = 1/\sigma_i^2$

When two non-independent splittings are available (e.g. from three components), uncertainty correlation difficulties can be overcome by combining two of the components;

e.g.

$$\chi_{obs} = C\,[\nu_1 - (\nu_2+\nu_3)/2]$$

$$\sigma_\chi = C\sqrt{\frac{3}{2}\sigma^2}$$

The simple average of ν_2 and ν_3 is only justified if the two lines are fully resolved since, in the limit that they become completely unresolved, the intensity weighted average becomes appropriate.

PROGRAM CHI INPUT FORMAT

Line 1 Title (10A8)

Line 2 ifix1, ifix2, χ_{aa}, χ_{bb}-χ_{cc} (2I2, 2F11.5)

Line 3 J, Text, , U , D_a, D_b, D_c (I2,2A8,5F11.5)

Notes:

If ifix1 > 0 the input value of χ_{aa} is used as a constant.

If ifix2 > 0 the input value of χ_{bb}-χ_{cc} is used as a constant.

'Text' allows user information about the observation to be input and printed out.

Only relative uncertainties need to be input. The program calculated weights and then normalises them so that the most accurate observation in the input data has weight = 1

$D_g = \partial\nu/\partial G$ for Q-branches

$= \langle P_g^2 \rangle$ for levels

$= \frac{\langle P_g'^2 \rangle}{(1+2/J)} - \langle P_g^2 \rangle$ for P- and R-branches

A quantity 'checksum' appears in the output to help ensure that the derivatives have been correctly input.

Checksum = $D_a + D_b + D_c$

= J(J+1) for levels

= 0 otherwise

```
c Program Chi.  By D.W.Knight  july 1984.
c For calculation of quadrupole coupling constants.
      implicit real*8 (a-h,o-z)
      dimension title(10),j(100),text(100,2)
      dimension chizz(100),u(100),y(100),x(100)
      dimension pasq(100),pbsq(100),pcsq(100)
      dimension g(100),w(100),check(100)
      equivalence (pasq(1),check(1)),(pbsq(1),g(1)),(pcsq(1),w(1))
c
      read(5,500)title
      write(6,600)
      write(6,605)title
      read(5,510)ifix1,ifix2,chiaa,chibc
      if (ifix1.gt.0) write(6,606)
      if (ifix2.gt.0) write(6,607)
c
      do 10 i=1,100
      read(5,520,end=15)j(i),text(i,1),text(i,2),chizz(i),u(i),
     *pasq(i),pbsq(i),pcsq(i)
      if (j(i).le.0)go to 15
      if (u(i).le.0.0) u(i)=1.0
      x(i)=(2.0*pasq(i)-pbsq(i)-pcsq(i))/(pbsq(i)-pcsq(i))
      check(i)=pasq(i)+pbsq(i)+pcsq(i)
      g(i)=(float(j(i)*(j(i)+1)))/(pbsq(i)-pcsq(i))
      y(i)=g(i)*chizz(i)
      w(i)=1.0/(u(i)*u(i)*g(i)*g(i))
      if (u(i).ge.1000.0) w(i)=0.0
   10 continue
      i=101
   15 n=i-1
      write(6,610)n
c
      sw=0.0
      swy=0.0
      swx=0.0
      swxy=0.0
      swxx=0.0
      do 20 i=1,n
      sw=sw+w(i)
      swy=swy+w(i)*y(i)
      swx=swx+w(i)*x(i)
      swxy=swxy+w(i)*x(i)*y(i)
      swxx=swxx+w(i)*x(i)*x(i)
   20 continue
      denom=sw*swxx-swx*swx
      id=1
      if (denom.eq.0.0) id=0
      if ((id+ifix1+ifix2).eq.0) stop "Inadequate data."
c
      if ((ifix1+ifix2).le.0) chiaa=(sw*swxy-swy*swx)/denom
      if (ifix2.gt.0) chiaa=(swxy-chibc*swx)/swxx
      if (ifix2.le.0) chibc=(swy-chiaa*swx)/sw
c
      sum1=0.0
      sum2=0.0
      if ((ifix1+ifix2).gt.0) go to 23
      do 22 i=1,n
      c1=sw*x(i)-swx
      c2=swxx-swx*x(i)
      sum1=sum1+c1*c1*w(i)
      sum2=sum2+c2*c2*w(i)
   22 continue
   23 continue
c
```

```
      write(6,615)
      neff=n
      do 25 i=1,n
      w(i)=1.0/(u(i)*u(i))
      if (u(i).ge.1000.0) neff=neff-1
      if (u(i).ge.1000.0) w(i)=0.0
   25 continue
      wmax=w(1)
      do 30 i=2,n
      if (w(i).gt.wmax) wmax=w(i)
   30 continue
c
      swrr=0.0
      wt=0.0
      do 40 i=1,n
      res=chizz(i)-(chiaa*x(i)+chibc)/g(i)
      swrr=swrr+res*res*w(i)
      if (wmax.gt.0.0) wt=w(i)/wmax
      write(6,620)j(i),text(i,1),text(i,2),chizz(i),res,wt,check(i)
   40 continue
c
      sigma=0.0
      eaa=0.0
      ebc=0.0
      np=2-ifix1-ifix2
      ndf=neff-np
      if (ndf.le.0) go to 60
      sigma=sqrt(swrr/float(ndf))
      esd=sigma/sqrt(wmax)
      write(6,625)esd
      if (id.eq.0) go to 50
      eaa=sigma*sqrt(sum1)/denom
      ebc=sigma*sqrt(sum2)/denom
   50 continue
      if (ifix2.gt.0) eaa=sigma*sqrt(sw)/swx
      if (ifix1.gt.0) ebc=sigma/sqrt(sw)
      if (ifix1.gt.0) eaa=0.0
      if (ifix2.gt.0) ebc=0.0
   60 write(6,630)chiaa,eaa
      write(6,635)chibc,ebc
      chibb=(-chiaa+chibc)/2.0
      chicc=(-chiaa-chibc)/2.0
      ebb=sqrt(eaa*eaa+ebc*ebc)/2.0
      write(6,640)chibb,ebb
      write(6,645)chicc,ebb
      stop
c
  500 format(10a8)
  510 format(2i2,2f11.5)
  520 format(i2,2a8,5f11.5)
c
  600 format(/x,13h Program Chi.)
  605 format(/x,10a8)
  606 format(x,26h       Chiaa held constant.)
  607 format(x,26hChibb-Chicc held constant.)
  610 format(/x,25h Number of observations = ,i3)
  615 format(/x,2h J,20x,40hObs/MHz     Res/MHz     Weight     Checksum/)
  620 format(x,i2,2a8,4f11.5)
  625 format(/4x,30hE.S.D. of an Observation/MHz =,f11.5,
     *13h/sqrt(Weight))
  630 format(/7x,7hChiaa =,f11.5,9h MHz  esd,f11.5)
  635 format(x,13hChibb-Chicc =,f11.5,9h MHz  esd,f11.5)
  640 format(7x,7hChibb =,f11.5,9h MHz  esd,f11.5)
  645 format(7x,7hChicc =,f11.5,9h MHz  esd,f11.5)
      end
```

APPENDIX 5

EVALUATION OF THE MOLECULAR INTERNAL ROTATION CONSTANT

When one part of a molecule (the top) rotates with respect to the rest of the molecule (the frame), calculation of the energy levels associated with the process requires knowledge of the reduced moment of inertia for internal rotation. This quantity is always less than the moment of inertia of the top about its rotation (z) axis (except when the frame is infinitely massive) because, when the top rotates there is a reaction in the frame. The reduced moment of inertia ($I_{effective}$) is, in effect, the angular momentum analogue of the reduced mass required for the calculation of vibrational energies.

Evaluation of I_{eff}

The rotational kinetic energy of a molecule is given by

$$T = \tfrac{1}{2}\omega^{\dagger} I \omega$$

and includes contributions from internal and overall angular momentum.

The molecule as a whole is viewed from its principal axis system (a,b,c) in order to dispense with products of inertia. The top is considered to have its own axis system (x,y,z) which rotates relative to the frame about the z axis. α is the internal rotation angle, defined as the angle between the projections onto the x,y plane, of a line from the z axis to a point on the top, and a line from the z axis to a point on the frame.

Special Case, The Symmetric Internal Rotor

When the top is symmetric about the z axis, the elements of the inertial tensor (I) are independent of α. I_{eff} is obtained by expanding the kinetic energy as follows;[5,15]

$$2T = \begin{bmatrix} \omega_a, \omega_b, \omega_c, d\alpha/dt \end{bmatrix} \begin{bmatrix} I_a & 0 & 0 & \lambda_{az} I_a \\ 0 & I_b & 0 & \lambda_{bz} I_b \\ 0 & 0 & I_c & \lambda_{cz} I_c \\ \lambda_{az} I_a & \lambda_{bz} I_b & \lambda_{cz} I_c & I_\alpha \end{bmatrix} \begin{bmatrix} \omega_a \\ \omega_b \\ \omega_c \\ d\alpha/dt \end{bmatrix}$$

Where the λ_{gz} are direction cosines relating the axes.

$d\alpha/dt$ is the angular velocity of the top with respect to the frame.

I_α is the moment of inertia of the top about the z axis.

Thus;

$$2T = \left[\sum_{g=a,b,c} I_g \omega_g^2\right] + I_\alpha \left(\frac{d\alpha}{dt}\right)^2 + 2I_\alpha \frac{d\alpha}{dt} \sum_{g=a,b,c} \lambda_{gz}\, \omega_g$$

To find the angular momentum about an axis use $P = dT/d\omega$

Thus;

$$P_g = \partial T/\partial \omega_g = I_g \omega_g + \lambda_{gz} I_\alpha \frac{d\alpha}{dt}$$

$$P_\alpha = \frac{\partial T}{\partial(\frac{d\alpha}{dt})} = I_\alpha \frac{d\alpha}{dt} + I_\alpha \sum_g \lambda_{gz} \omega_g$$

It is therefore not possible to separate internal and overall angular momentum (just as, it is not possible to completely separate vibrational momentum from overall angular momentum).

Substituting for ω_g gives;

$$P_\alpha = I_\alpha \frac{d\alpha}{dt} + I_\alpha \left[\sum_g \lambda_{gz} \frac{P_g}{I_g}\right] - I_\alpha^2 \frac{d\alpha}{dt} \sum_g \frac{\lambda_{gz}^2}{I_g}$$

Let $p = I_\alpha \sum_g \lambda_{gz} \frac{P_g}{I_g}$

Then the 'relative' angular momentum of the top, which has its conjugate operator associated with an observable, is;

$$(P_\alpha - p) = I_\alpha \frac{d\alpha}{dt} [1 - \sum_g \lambda_{gz}^2 \frac{I_\alpha}{I_g}]$$

The reduced moment of inertia is therefore

$$I_{eff} = rI_\alpha = I_\alpha [1 - \sum_g \lambda_{gz}^2 \frac{I_\alpha}{I_g}]$$

General Case

In the general case, the principal moments of inertia of the molecule and the orientations of the principal axes with respect to z all become functions of α. $I_{eff}(\alpha)$ is then best obtained by evaluating it at several values of α and constructing a Fourier series[112,122]. The general form for the instantaneous

values of I_{eff} required for this construction has been given by K.S. Pitzer;[123]

$$I_{eff} = I_{\alpha} - \frac{U^2}{M} - \sum_{g} \frac{\beta_g^2}{I_g}$$

where $U = \sum_{top} m_i \varkappa_i$, the Unbalance Factor.

M = molecular mass

$$\beta_g = \lambda_{gz} I_{\alpha} - \lambda_{gx} I_{xz} - \lambda_{gy} I_{yz} + U(\lambda_{(g-1),y} \cdot r_{(g+1)} - \lambda_{(g+1),y} \cdot r_{(g-1)})$$

z is the internal rotation axis

x is made to pass through the centre of mass of the top

y is chosen so that the x,y,z co-ordinate system has the same handedness as the a,b,c system (i.e. $\det\lambda = +1$)

I_{ff}, are products of inertia (f = x,y,z).

(g-1),(g+1) refer to cyclic permutations of a,b,c. ie, if g=a, g-1 = c etc.

r_g are the elements of the vector from the centre of mass of the molecule to the origin of co-ordinates of the top.

In calculating the top moments and products of inertia, atoms on the z axis are excluded.

GENERAL ALGORITHM FOR THE CALCULATION OF I_{eff}

I_{eff} for a given value of α can be computed from a knowledge of the instantaneous relative positions of the atoms in the molecule. The algorithm described here makes use of the masses and principal axis co-ordinates of the atoms and requires a knowledge of the two points on the internal rotation axis. It is given at the end of this section as a computer program designed to be called by a structure program. It requires the above mentioned information along with the molecular mass and the identify of the top atoms. The procedure for calculating I_{eff} is then as follows:

1) Find the Direction Cosines of the z Axis Viewed from the Principal Axis System (P.A.S)

$P_1(a_1,b_1,c_1)$ and $P_2(a_2,b_2,c_2)$ are two points on the z axis (see Figure 1).

$$\lambda_{gz} = (g_2 - g_1)/r' \qquad g=a,b,c$$

where $r' = \sqrt{(a_2 - a_1)^2 + (b_2 - b_1)^2 + (c_2 - c_1)^2}$

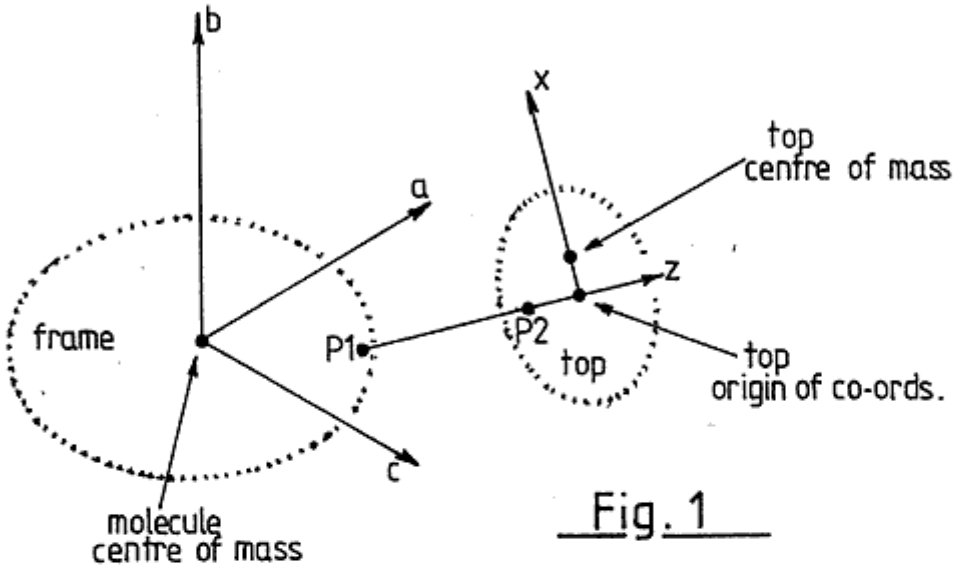

Fig. 1

2) Find the P.A.S. Co-ordinates of the Top Centre of Mass

$$\bar{g} = \sum_{top} m_i g_i / M_t$$

$$M_t = \sum_{top} m_i$$

3) Locate the Top Origin of Co-ordinates

Any point (a', b', c') in a plane satisfies; $la' + mb' + nc' = p$

l,m,n are direction cosines of a perpendicular from the plane to the origin of co-ordinates.

p = perpendicular distance from the plane to the origin of co-ordinates.

Both the top centre of mass $(\bar{a},\bar{b},\bar{c})$ and the top origin of co-ordinates $(\tilde{a},\tilde{b},\tilde{c})$ lie in the x,y plane. Translate the top centre of mass into a system parallel to the P.A.S. but centred on P_1. Then;

$r'' = (\bar{a}-a_1)\lambda_{az} + (\bar{b}+b_1)\lambda_{bz} + (\bar{c}-c_1)\lambda_{cz}$,

is the distance from P_1 to the top origin of co-ordinates.

$(\tilde{a},\tilde{b},\tilde{c})$ lies on the z axis, so the equation of the z axis can be given as;

$$\frac{\tilde{a} - a_1}{\lambda_{az}} = \frac{\tilde{b} - b_1}{\lambda_{bz}} = \frac{\tilde{c} - c_1}{\lambda_{cz}} = r''$$

hence $\tilde{g} = g_1 - \lambda_{gz} \cdot r''$. g=a,b,c.

4) Check for Symmetry of the Top

If the distance from the top centre of mass to the origin of co-ordinates is zero, then the top is balanced (and probably symmetric). In any case, I_{eff} reduces to the symmetric form and the direction of the x axis must be defined arbitrarily. This can be done by making one of the top atoms lie in the x,y plane, i.e. substitute the co-ordinates of the chosen atom in place of $(\bar{a},\bar{b},\bar{c})$ and return to step 3.

5) Find the Direction Cosines of the x Axis

Both the origin of co-ordinates and the top centre of mass (or the arbitrary point) lie on the x axis.

The equation of the x axis can therefore be given as;

$$\frac{\bar{a} - \tilde{a}}{\lambda_{ax}} = \frac{\bar{b} - \tilde{b}}{\lambda_{bx}} = \frac{\bar{c} - \tilde{c}}{\lambda_{cx}} = r'''$$

Where $r''' = \sqrt{(\bar{a}-\tilde{a})^2 + (\bar{b}-\tilde{b})^2 + (\bar{c}-\tilde{c})^2}$

therefore $\lambda_{gx} = (\bar{g} - \tilde{g})/r'''$

r''' is the distance from the origin to the centre of mass, and is the quantity required for the check made in step 4.

6) Define the y Axis so that the x,y,z, System has the same Handedness as the P.A.S.

$$\lambda = \begin{bmatrix} \lambda_{ax} & \lambda_{ay} & \lambda_{az} \\ \lambda_{bx} & \lambda_{by} & \lambda_{bz} \\ \lambda_{cx} & \lambda_{cy} & \lambda_{cz} \end{bmatrix}$$

Since both co-ordinate systems are Cartesian, the sum of squares along any row or column of λ is 1.

Also (see ref. 134, P.236);

$$\lambda_{ax}\lambda_{bx} + \lambda_{ay}\lambda_{by} + \lambda_{az}\lambda_{bz} = 0$$
$$\lambda_{bx}\lambda_{cx} + \lambda_{by}\lambda_{cy} + \lambda_{bz}\lambda_{cz} = 0$$
$$\lambda_{ax}\lambda_{cx} + \lambda_{ay}\lambda_{cy} + \lambda_{az}\lambda_{cz} = 0$$

therefore;

$$\left|\lambda_{gy}\right| = \sqrt{1-\lambda_{gx}^2 - \lambda_{gz}^2}$$

In order to avoid being fooled by a plane of symmetry (in which case λ will have zero entries) evaluate all three $\left|\lambda_{gy}\right|$ and see which is largest. Then, if $\left|\lambda_{gy}\right|$ now refers to the largest, temporarily define $\lambda_{gy} = \left|\lambda_{gy}\right|$ then, temporarily

$$\lambda_{(g\pm1),y} = -(\lambda_{gx} \cdot \lambda_{(g\pm1)x} + \lambda_{gz} \cdot \lambda_{(g\pm1)z}) / \lambda_{gy}$$

Now, check to see if $\det\lambda$ is +1, if not, reverse the sign of all λ_{gy}.

7) Translate the Co-ordinates of the Top Atoms into a System Centred on the Top Origin

$$g'_n = g_n - \tilde{g} \qquad g=a,b,c$$

8) Rotate the Top Atoms into the z,y,z System

$$f'_n = a'_n \lambda_{af} + b'_n \lambda_{bf} + c'_n \lambda_{cf} \qquad f=x,y,z$$

9) Evaluate I_α, I_{xz}, I_{yz}, U and Hence I_{eff}.

$$I_\alpha = \sum_{top} m_i (x_i^2 + y_i^2)$$
$$I_{xz} = \sum_{top} m_i x_i z_i$$
$$I_{yz} = \sum_{top} m_i y_i z_i$$
$$U = \sum m_i x_i$$

The above and also $r_g = \tilde{g}$ and the λ_{gf}, are the quantities required in the application of Pitzer's equation.

The internal rotation constant is then;

$$F = \frac{h}{8\pi^2 I_{eff}} .$$

Notes on the Application of the Method

The definitions of the top and frame are interchangeable and the same result is obtained either way unless (as is often the case) spectroscopic principal moments of inertia are substituted for the structural principal moments. If the operationally defined structure does not quite reproduce the observed rotational constants, evaluation of I_{eff} from the most convenient end of the molecule then produces a biased result. For this reason, the computer program given calculates I_{eff} from both ends if the molecule (one end is called the top, the other end the anti-top) and gives the option of using the average. This average does not necessarily converge with the purely structural result.

In the case where there are more than two atoms on the z axis (e.g. dimethyl acetylene), in considering all of the atoms in the molecule, the program may give an erroneous result. this problem may be avoided by; ignoring the result for the top containing on-axis atoms (unless the top is symmetric), excluding the data for extra on-axis atoms from the information passed by the calling program, or modifying the program itself.

The Fortran IV program which follows requires the following parameters.

NTOP - The number of atoms in the top (excluding atoms on the z axis).

IOBS - A flag to tell it to read rotational constants, convert them into moments and substitute them for the structural moments.

WTMOL - The molecular mass.

PMOM(3) - The principal moments calculated from structure.

P(50,3) - The principal axis co-ordinates of the atoms.

WT(20) - A library of atomic masses.

Mass(50)- The library location of the mass of the atom in question defined such that the mass of the ith atom = Wt (Mass(I))

NATM - The number of atoms in the molecule (the program will ignore atoms having indeces greater than NATM).

```
      SUBROUTINE PITZER(NTOP,IOBS,WTMOL,PMOM)
C By D.W.Knight  Jan. 1985
Calculates the internal rotation constant for a general internal top
C using the method given by K.S.Pitzer (1946) J.Chem.Phys.14,239.
C A line joining atoms 1 and 2 is taken to be the z (internal
C rotation) axis. If there are not two atoms on the z axis, then
C define dummy atoms of mass 0. NTOP is the number of atoms in the
C top.  The top atoms must be input as atoms 3 to NTOP+2  (atoms on
C the z axis are not part of the top).  The remaining atoms,
C NTOP+3 to NATM are called the anti-top.
      IMPLICIT REAL*8 (A-H,O-Z)
      COMMON P(50,3),         WT(20),NATM,        MASS(50)
      DIMENSION DIR(3,3),TOP(2),ABC(3),RBAR(3),RTILDE(3),RU(3),
     *ATMAS(20),TOPX(20),TOPY(20),TOPZ(20),BETA(3),PMOM(3)
      DATA TOP/8H      Top,8HAnti-top/
      WRITE(6,600)
      IF(IOBS.LE.0)GO TO 10
      READ(5,500,END=10)ABC
      DO 5 I=1,3
    5 PMOM(I)=505379.0/ABC(I)
      WRITE(6,610)PMOM
C Find direction cosines of the z axis.
   10 AAZ=P(2,1)-P(1,1)
      BBZ=P(2,2)-P(1,2)
      CCZ=P(2,3)-P(1,3)
      R21=SQRT(AAZ*AAZ+BBZ*BBZ+CCZ*CCZ)
      DIR(1,3)=AAZ/R21
      DIR(2,3)=BBZ/R21
      DIR(3,3)=CCZ/R21
      ISTART=3
      IEND=NTOP+2
      ICALC=1
      NT=NTOP
      RIOLD=0.0
   20 JJ=ISTART-1
      ISYM=0
      WRITE(6,615)TOP(ICALC),ISTART,IEND
C Find top (or anti-top) centre of mass
      SMA=0.0
      SMB=0.0
      SMC=0.0
      TOPMAS=0.0
      DO 30 I=ISTART,IEND
      WTI=WT(MASS(I))
      TOPMAS=TOPMAS+WTI
      SMA=SMA+WTI*P(I,1)
      SMB=SMB+WTI*P(I,2)
   30 SMC=SMC+WTI*P(I,3)
      RBAR(1)=SMA/TOPMAS
      RBAR(2)=SMB/TOPMAS
      RBAR(3)=SMC/TOPMAS
      WRITE(6,620)TOP(ICALC),RBAR
C Find top origin of co-ordinates.
   35 RXY1=(RBAR(1)-P(1,1))*DIR(1,3) + (RBAR(2)-P(1,2))*DIR(2,3)
     *    + (RBAR(3)-P(1,3))*DIR(3,3)
      DO 40 I=1,3
   40 RTILDE(I)=P(1,I) + DIR(I,3)*RXY1
Check for symmetry of the top.
      AAX=RBAR(1)-RTILDE(1)
      BBX=RBAR(2)-RTILDE(2)
      CCX=RBAR(3)-RTILDE(3)
      RCMO=SQRT(AAX*AAX+BBX*BBX+CCX*CCX)
      IF(RCMO.GT.1.0D-6) GO TO 60
```

```
C For symmetric top, make x axis pass through atom JJ.
      JJ=JJ+1
      IF(JJ.GT.IEND) GO TO 160
      DO 50 I=1,3
   50 RBAR(I)=P(JJ,I)
      ISYM=1
      GO TO 35
   60 IF(ISYM.EQ.0)WRITE(6,630)TOP(ICALC),RTILDE
C Find direction cosines of the x axis.
      DIR(1,1)=AAX/RCMO
      DIR(2,1)=BBX/RCMO
      DIR(3,1)=CCX/RCMO
C Make initial choice for direction cosines of the y axis.
      DAX=DIR(1,1)
      DBX=DIR(2,1)
      DCX=DIR(3,1)
      DAZ=DIR(1,3)
      DBZ=DIR(2,3)
      DCZ=DIR(3,3)
      DIR(1,2)=SQRT(ABS(1.0-DAX*DAX-DAZ*DAZ))
      DIR(2,2)=SQRT(ABS(1.0-DBX*DBX-DBZ*DBZ))
      DIR(3,2)=SQRT(ABS(1.0-DCX*DCX-DCZ*DCZ))
      BIGD=DIR(1,2)
      ID=1
      DO 62 I=2,3
      IF(DIR(I,2).GT.BIGD)ID=I
   62 IF(ID.EQ.I)BIGD=DIR(I,2)
      IF(ID.NE.3)GO TO 64
      DIR(1,2)=-(DAX*DCX+DAZ*DCZ)/BIGD
      DIR(2,2)=-(DBX*DCX+DBZ*DCZ)/BIGD
      GO TO 68
   64 IF(ID.NE.2)GO TO 66
      DIR(1,2)=-(DAX*DBX+DAZ*DBZ)/BIGD
      DIR(3,2)=-(DBX*DCX+DBZ*DCZ)/BIGD
      GO TO 68
   66 DIR(2,2)=-(DAX*DBX+DAZ*DBZ)/BIGD
      DIR(3,2)=-(DAX*DCX+DAZ*DCZ)/BIGD
Check to see if determinant of direction cosines is +1
   68 DETLAM=DIR(1,1)*(DIR(2,2)*DIR(3,3)-DIR(2,3)*DIR(3,2) )
     *       -DIR(1,2)*(DIR(2,1)*DIR(3,3)-DIR(2,3)*DIR(3,1) )
     *       +DIR(1,3)*(DIR(2,1)*DIR(3,2)-DIR(2,2)*DIR(3,1) )
      IF(DETLAM.GT.0.0)GO TO 80
      DO 70 I=1,3
   70 DIR(I,2)=-DIR(I,2)
   80 WRITE(6,640)
      IF(ISYM.GT.0)GO TO 90
      WRITE(6,641)(DIR(J,1),J=1,3)
      WRITE(6,642)(DIR(J,2),J=1,3)
   90 WRITE(6,643)(DIR(J,3),J=1,3)
C Translate top atoms into system centred on top origin of co-ords.
      K=ISTART-1
      DO 100 I=1,NT
      J=I+K
      TOPX(I)=P(J,1)-RTILDE(1)
      TOPY(I)=P(J,2)-RTILDE(2)
      TOPZ(I)=P(J,3)-RTILDE(3)
  100 ATMAS(I)=WT(MASS(J))
C Rotate top atoms into x,y,z co-ord. system.
      DO 110 I=1,NT
      TA=TOPX(I)
      TB=TOPY(I)
      TC=TOPZ(I)
      TOPX(I)=TA*DIR(1,1)+TB*DIR(2,1)+TC*DIR(3,1)
      TOPY(I)=TA*DIR(1,2)+TB*DIR(2,2)+TC*DIR(3,2)
  110 TOPZ(I)=TA*DIR(1,3)+TB*DIR(2,3)+TC*DIR(3,3)
```

```
Calculate top moments and products of inertia and Unbalance factor.
      TIZ=0.0
      DO 120 I=1,NT
      TX=TOPX(I)
      TY=TOPY(I)
  120 TIZ=TIZ+ATMAS(I)*(TX*TX+TY*TY)
      WRITE(6,650)TIZ
      TIXZ=0.0
      TIYZ=0.0
      U=0.0
      IF(ISYM.GT.0)GO TO 140
      DO 130 I=1,NT
      TIXZ=TIXZ+ATMAS(I)*TOPX(I)*TOPZ(I)
      TIYZ=TIYZ+ATMAS(I)*TOPY(I)*TOPZ(I)
  130 U=U+ATMAS(I)*TOPX(I)
      WRITE(6,660)TIXZ,TIYZ,U
Calculate Ieff.
  140 RU(1)=U*(DIR(3,2)*RTILDE(2)-DIR(2,2)*RTILDE(3))
      RU(2)=U*(DIR(1,2)*RTILDE(3)-DIR(3,2)*RTILDE(1))
      RU(3)=U*(DIR(2,2)*RTILDE(1)-DIR(1,2)*RTILDE(2))
      TERM=0.0
      DO 150 I=1,3
      BETA(I)=DIR(I,3)*TIZ-DIR(I,1)*TIXZ-DIR(I,2)*TIYZ+RU(I)
      BETA(I)=BETA(I)*BETA(I)/PMOM(I)
  150 TERM=TERM+BETA(I)
      RIEFF=TIZ-(U*U/WTMOL)-TERM
      F=505379.0/RIEFF
      WRITE(6,670)RIEFF,F
      F=F/29979.2458D0
      WRITE(6,680)F
      IF(ICALC.EQ.1)RIOLD=RIEFF
      IF(ICALC.EQ.1)GO TO 160
      IF(RIOLD.EQ.0.0)RETURN
      RIEFF=(RIEFF+RIOLD)/2.0
      F=505379.0/RIEFF
      WRITE(6,690)
      WRITE(6,670)RIEFF,F
      F=F/29979.2458D0
      WRITE(6,680)F
      RETURN
  160 ICALC=ICALC+1
      IF(ICALC.GT.2)RETURN
      ISTART=NTOP+3
      IEND=NATM
      NT=NATM-NTOP-2
      IF(NT.LE.0)RETURN
      GO TO 20
C
  500 FORMAT(3F12.4)
  600 FORMAT(/X,'Internal Rotation Calculation.')
  610 FORMAT(X,'Using Observed Principal Moments of Inertia.'/X,
     *'Ia =',F12.6,8X,'Ib =',F12.6,8X,'Ic =',F12.6)
  615 FORMAT(/X,A8,' Atoms',I3,' to',I3)
  620 FORMAT( X,A8,' Centre of Mass at ',3F12.7)
  630 FORMAT( X,A8,' Origin of co-ords.',3F12.7)
  640 FORMAT(X,'Direction Cosines'/6X,'a',11X,'b',11X,'c')
  641 FORMAT(X,'x',3F12.8)
  642 FORMAT(X,'y',3F12.8)
  643 FORMAT(X,'z',3F12.8)
  650 FORMAT(/X,' Iz =',F14.8)
  660 FORMAT( X,'Ixz =',F14.8/X,'Iyz =',F14.8/X,'  U =',F14.8)
  670 FORMAT( X,'Ieff=',F14.8/X,'  F =',F14.3,' MHz')
  680 FORMAT( X,'  F =',F14.8,' cm**-1')
  690 FORMAT(/X,'Average Over the Molecule')
      END
```

APPENDIX 6

DETERMINATION OF THE TORSIONAL HINDERING POTENTIAL FROM SPECTROSCOPIC DATA

As pointed out by Pickett[27], rotation-vibration interactions need not be considered in a theory of pure vibrational spectra, provided that the complete vibrational Hamiltonian is used. Therefore, insofar as a molecule is rigid except for its large-amplitude torsional degree of freedom, the problem of calculating its vibrational energy levels reduces to that of solving the one-dimensional Schroedinger equation arising from the Hamiltonian;

$$\tfrac{1}{2}PI_{eff}^{-1}P + V(\alpha) = E$$

The substitution;

$$P = i\hbar \frac{d}{d\alpha}$$

is here used to obtain the Hamiltonian operator

$$\hat{H} = -\frac{d}{d\alpha}\cdot F \cdot \frac{d}{d\alpha} + V(\alpha)$$

where F is the internal rotation constant discussed in Appendix 5.
For molecules with a rigid symmetric internal top, F is a constant, but for an asymmetric internal top, F is a function of α. $F(\alpha)$ may conveniently be constructed as a Fourier series and, since the molecules under investigation here can all be considered to have symmetry about $\alpha=0$, only the cosine terms need to be included.

Hence;

$$F(\alpha) = F_0 + \sum_n F_n \cos n\alpha$$

Similarly, only cosine terms need to be included in the torsional potential function when it is expressed as a Fourier series. Such a series is conventionally re-arranged so that $V(0) = 0$

i.e. $V(\alpha) = \frac{1}{2} \sum_n V_n(1-\cos n\alpha)$

The expanded Hamiltonian operator is therefore;

$$\hat{H} = -\frac{d}{d\alpha}(F_0 + \sum_n F_n \cos n\alpha)\frac{d}{d\alpha} + \tfrac{1}{2}\sum_n V_n(1-\cos n\alpha)$$

The above Hamiltonian, which is a re-arrangmeent of that derived by Lewis Malloy Chao and Laane[122], is the basis of the torsional potential program given at the end of this section. The program sets up the Hamiltonian in the free rotor representation and diagonalises the resulting energy matrix numerically. Parameterisation of the spectroscopic data is achieved by non-linear least-squares fitting.

The Hamiltonian for the free rotor is;

$$\hat{H} = -F\frac{d^2}{d\alpha^2}$$

with eigenfunctions

$$\psi_m = \frac{1}{\sqrt{2\pi}} e^{im\alpha} \qquad m=0,\pm1,\pm2, \ldots.$$

and eigenvalues

$$E_m = Fm^2$$

The torsion Hamiltonian may be expanded in terms of the ψ_m, but calculation of energy levels is facilitated by performing the Wang transformation, which results in a factorisation of the energy matrix into odd and even blocks. In practice, this is the same as using the following sine and cosine basis functions;

$$\psi_m^{even} = \frac{1}{\sqrt{2\pi}} \qquad m=0$$

$$= \frac{1}{\sqrt{\pi}} \cos m\alpha \qquad m=1,2,3 \ldots.$$

$$\psi_m^{odd} = \frac{1}{\sqrt{\pi}} \sin m\alpha \qquad m=1,2,3 \ldots.$$

Matrix elements are then given by;

$$H_{m'm} = \langle m' \,|H|\, m\rangle = \langle m \,|H|\, m'\rangle$$

$$= \int_0^{2\pi} \psi_{m'} H \psi_m \, d\alpha$$

and have been evaluated as follows;

$$\langle m'|H|m\rangle = (F_0 m^2 + \tfrac{1}{2}\sum V_n)\delta_{mm'} \mp \tfrac{1}{4}\sum_n V_n \delta_{(m'+m),n} - \tfrac{1}{4}\sum_n V_n \delta_{|m'-m|,n}$$
$$\mp \tfrac{1}{2} mm' \sum_i F_i \delta_{(m'+m),i} + \tfrac{1}{2} mm' \sum_i F_i \delta_{|m'-m|,i} \qquad m=1,2,3, \ldots\ldots$$

Upper sign refers to cos block

Lower sign refers to sin block.

for the m=0 elements, which only occur in the cosine block;

$$\langle 0|H|m\rangle = \tfrac{1}{2}\sum_n V_n \delta_{o,m} - \frac{1}{2\sqrt{2}}\sum_n V_n \delta_{m,n}$$

Derivatives of Energy Levels with Respect to Parameters

Numerical diagonalisation of the energy matrix H is equivalent to a contact transformation

$$T^{-1} H T = H'$$

where T is the matrix of eigenvectors obtained by performing identical operations on a unit matrix as were performed on H in order to diagonalise it. A single eigenvalue is then given by;

$$E_k = \tilde{T}_k H T_k$$

where T_k is a single eigenvector, i.e. the k'th column of T. It therefore follows that;

$$\frac{\partial E_k}{\partial P_i} = \tilde{T}_k \left[\frac{\partial H}{\partial P_i}\right] T_k$$

where P_i is the ith parameter and $[\partial H/\partial P_i]$ is a matrix which has elements;

$$(\partial H/\partial P_i)_{m',m} = \frac{\partial}{\partial P_i}\langle m'|H|m\rangle$$

These matrix elements are easily obtained from the matrix elements of H, given earlier, and are as follows;

$$\frac{\partial}{\partial F_0}\langle m'|H|m\rangle = m^2 \delta_{mm'} \qquad m=1,2,3 \ldots\ldots$$

$$\frac{\partial}{\partial F_n}\langle m'|H|m\rangle = \frac{m'm}{2}\left[\delta_{|m'-m|,n} \mp \delta_{(m'+m),n}\right] \qquad m=1,2,3 \ldots\ldots$$

$$\frac{\partial}{\partial V_n}\langle m'|H|m\rangle = \frac{\delta_{mm'}}{2} \mp \frac{\delta_{(m'+m),n}}{4} - \frac{\delta_{|m'm|,n}}{4} \qquad m=0,1,2 \ldots\ldots$$

and, for the cos block only;

$$\frac{\partial}{\partial V_n} \langle 0|H|m\rangle = \frac{-\delta_{m,n}}{2\sqrt{2}} \qquad m=1,2,3 \ldots.$$

Performing the necessary matrix multiplications then results in the following expressions for the derivatives;

$$\frac{\partial E_k}{\partial F_0} = \sum_{m=1}^{\infty} (t_{mk})^2 \, m^2$$

where the t_{mk} are the elements of the eigenvector T_k.

$$\frac{\partial E_k}{\partial F_n} = \sum_{m'=1}^{\infty} \sum_{m=1}^{\infty} t_{m'k} \cdot t_{mk} \cdot \frac{m'm}{2} \cdot \left[\delta_{|m'-m|,n} \mp \delta_{(m'+m),n}\right]$$

$$\frac{\partial E_k}{\partial V_n} = \frac{(t_{0k})^2}{2} + \frac{t_{0k} \cdot t_{nk}}{\sqrt{2}} + \sum_{m'=1}^{\infty} \sum_{m=1}^{\infty} t_{m'k} \, t_{mk} \left[\frac{\delta_{mm'}}{2} \mp \frac{\delta_{(m'+m),n}}{4} - \frac{\delta_{|m'-m|,n}}{4} \right]$$

Truncation of the Basis Set

All of the summations in the above run to infinity, but in practice the length of an eigenvector is the same as the order of H and H has to be limited to a manageable size.

An eigenfunction may be obtained from an eigenvector as a linear combination of basis functions;

$$\psi_k = \sum_m t_{mk} \quad \phi_m$$

where the ϕ_m, in this case, are the free-rotor functions given earlier. The order of H is therefore equivalent to the size of the set of basis functions used. Truncation of the basis set affects the accuracy of the calculated eigenvalues, but there is no point in calculating energies to an accuracy of more than a few orders of magnitude better than that of the spectroscopic data. a suitable truncation point may be decided by observing that the eigenvector elements t_{mk} become smaller as the difference between m and k increases. If T_k still has significantly large entries close to the truncation point, E_k will be inaccurate.

Weighted Non-Linear Least-Squares Fitting[134]

Data for the program consist principally of differences between torsional energy levels and can come from widely different experimental sources. This presents an unusual data adjustment problem since the program must be capable of fitting microwave ΔE values, with $\sigma \sim 0.1$ MHz, at the same time as it fits, for example, relative intensity data having $\sigma \sim 10$ or 20 cm^{-1}. Statistical weighting of the observations in the least-squares fit is therefore essential, as is double precision arithmetic (64 bit) to cope with weighting coefficients which can span sixteen orders of magnitude.

The initial calculated quantity $\nu_0(i)$, associated with the ith observation ν_i, can be expressed as a linear combination of the starting parameters;

$$\nu_0(i) = \frac{\partial \nu_i}{\partial P_1} p_1 + \frac{\partial \nu_i}{\partial P_2} p_2 + \ldots\ldots\ldots + \frac{\partial \nu_i}{\partial P_{np}} p_{np}$$

where $\nu_0(i) = E_{k'} - E_k$

$$\frac{\partial \nu_i}{\partial P_j} = \frac{\partial E_{k'}}{\partial P_j} - \frac{\partial E_k}{\partial P_j}$$

and n_p is the total number of parameters.

The object of least-squares fitting is to adjust the parameters in such a way as to simultaneously minimise all residuals (observed-calculated quantities). After parameter adjustment, the newly calculated quantity $\nu(i)$, on the assumption that the derivatives are constants, is given by;

$$\nu(i) = \frac{\partial \nu_i}{\partial P_1} (p_1 + \delta p_1) + \frac{\partial \nu_i}{\partial p_2} (p_2 + \delta p_2) + \ldots\ldots\ldots\ldots$$

i.e.;

$$\nu(i) = \nu_o(i) + \sum_{j}^{np} \frac{\partial \nu_i}{\partial p_j} \cdot \delta p_j$$

Observed and calculated quantities will, in general, be different;

$$\nu_i = \nu(i) + r_i$$

where r_i is the residual.

Simultaneous minimisation of all residuals can be accomplished by minimising the weighted square error sum S with respect of all parameter increments.

Now;

$$S = \sum_i W_i \, r_i^2$$

where $W_i = \frac{1}{\sigma_i^2}$ (making S dimensionless).

Therefore, substituting for r_i;

$$S = \sum_i W_i \left[\nu_i - \nu_o(i) - \sum_j^{n_p} \frac{\partial \nu_i}{\partial P_j} \delta P_j\right]^2$$

S is minimised by setting its derivative with respect to each parameter increment to zero.

$$\frac{\partial S}{\partial(\delta P_k)} = -2 \sum_i W_i \left[\nu_i - \nu_o(i) - \sum_j^{n_p} \frac{\partial \nu_i}{\partial P_j} \cdot \delta P_j\right] \frac{\partial \nu_i}{\partial P_k} = 0$$

i.e.;

$$\sum_i W_i [\nu_i - \nu_o(i)] \frac{\partial \nu_i}{\partial P_k} = \sum_i W_i \frac{\partial \nu_i}{\partial P_k} \sum_j^{n_p} \frac{\partial \nu_i}{\partial P_j} \delta P_j$$

Let;

$$a_k = \sum_i W_i \, [\nu_i - \nu_o(i)] \frac{\partial \nu_i}{\partial P_k}$$

and let;

$$a_{kj} = \sum_i W_i \frac{\partial \nu_i}{\partial P_k} \cdot \frac{\partial \nu_i}{\partial P_j}$$

therefore;

$$a_k = \sum_j^{n_p} a_{kj} \cdot \delta p_j$$

These are the n_p normal equations which can be arranged in matrix form;

$$\begin{bmatrix} a_1 \\ \cdot \\ \cdot \\ \cdot \\ a_{np} \end{bmatrix} = \begin{bmatrix} \\ a_{kj} \\ \\ \end{bmatrix} \begin{bmatrix} p_1 \\ \cdot \\ \cdot \\ \cdot \\ p_{np} \end{bmatrix}$$

or;

$$a = Ab$$

The elements of b are the required parameter shifts. Solution of the normal equations is then accomplished by pre-multiplying both sides of the above by A^{-1}, provided that such an inverse exists;

i.e.

$$A^{-1}a = b$$

The derivatives $\partial\nu_i/\partial p_j$ used in setting up the normal equations are in fact slowly varying functions of the parameters. As a consequence, the calculated parameter shifts will not usually produce the smallest possible S. It is therefore necessary to approach the optimum parameter set by a process of iteration. The calculated shifts are added on to the old parameters to produce a new parameter set. The new parameters are then used to calculate eigenvalues, residuals, eigenvectors and derivatives from scratch and a new least-squares fitting calculation is performed. Iteration is continued in this fashion until the calculated parameter shifts are several orders of magnitude smaller than the estimated uncertainties in the parameters themselves.

Estimation of Uncertainties[134]

The estimated standard deviation of an observation of unit weight, σ, is given by;

$$\sigma = \sqrt{\frac{S_{old}}{n_{eff} - n_{vp}}}$$

Where n_{eff} is the number of observations with finite weight, n_{vp} is the number of parameters allowed to vary in the fit, and $n_{eff}-n_{vp}$ is the number of degrees of freedom for the fit.

$$S_{old} = \sum_i W_i \, (\nu_i - \nu_o(i))^2$$

i.e. The best estimator of σ makes use of the residuals as they are, not as they are projected to be after parameter adjustment. The predicted value of σ after parameter adjustment is, however, a useful quantity since it is often a very good estimate of what σ will be at the convergence point. It is obtained by replacing S_{old} with S_{new}, where;

$$S_{new} = \sum_i W_i \, [\nu_i - \nu_o(i) - \sum_j^{n_p} \frac{\partial\nu_i}{\partial p_j} \cdot \delta p_j]^2$$

which, after some manipulation, can be put in the convenient form;

$$S_{new} = S_{old} - \sum_{k}^{n_p} a_k \delta p_k$$

Parameter Uncertainties and Correlation Coefficients[134]

Estimated parameter uncertainties are given by;

$$\sigma_j = \sqrt{\sigma^2 a^{jj}}$$

where the a^{jj} are the elements of the inverse of the normal matrix A^{-1}.

Parameter correlation coefficients are given by;

$$\rho_{jk} = \sqrt{\frac{\sigma^2 a^{jk}}{\sigma_j \sigma_k}}$$

i.e.;

$$\rho_{jk} = \frac{a^{jk}}{\sqrt{a^{jj} a^{kk}}}$$

REFINEMENTS TO THE PROGRAM

Preferred Conformational Angles

In addition to fitting torsional energy differences, any internal rotation model must reproduce preferred conformational angles (obtainable from structure and other sources) as minima in the potential energy surface.

A preferred value of α (α_{min}) is a root of the equation;

$$\frac{dV(\alpha_{min})}{d\alpha} = 0$$

when;

$$\frac{d^2V(\alpha_{min})}{d\alpha^2} > 0$$

For the purpose of least-squares fitting, it is necessary to obtain calculated α_{min} from the parameters and compare them with observed α_{min} input as data. Since $V(\alpha)$ is a smoothly varying function, this is most easily accomplished by taking an observed α_i and using it as the starting point for a Newton-Raphson iteration to find the calculated $\alpha_o(i)$.

i.e.;

$$\alpha_{next} = \alpha_{last} - \frac{f(\alpha_{last})}{f'(\alpha_{last})}$$

α in radians.

α_{last} is the initial approximation, α_{next} is the result of a round of iteration.

Where;

$$f(\alpha) = \frac{dV(\alpha)}{d\alpha} = \tfrac{1}{2} \sum_n n\, V_n \sin n\alpha$$

$$f'(\alpha) = \frac{d^2V(\alpha)}{d\alpha^2} = \tfrac{1}{2} \sum n^2\, V_n \cos n\alpha$$

The Newton-Raphson procedure converges very rapidly. Typically, for a calculation involving a three-fold dominated potential, adjustments of less than 10^{-10} radians will be achieved after four cycles of iteration, starting from a guess which was 10% in error.

By analogy with the other spectroscopic data discussed earlier, $\alpha(i)$ must now be expressed as a linear combination of parameters.

Before a round of least-squares adjustment;

$$\alpha_o(i) = \sum_n \frac{\partial \alpha}{\partial V_n} \cdot V_n$$

After adjustment;

$$\alpha(i) = \sum_n \frac{\partial \alpha}{\partial V_n} (V_n + \delta V_n)$$

$$= \alpha_o(i) + \sum_n \frac{\partial \alpha}{\partial V_n} \cdot \delta V_n$$

Now, α_o is defined when;

$$\frac{dV}{d\alpha} = f(\alpha_o, V_1, V_2, \ldots\ldots) = 0$$

The partial derivatives at the point $\alpha = \alpha_o$ are therefore;

$$\frac{\partial \alpha}{\partial V_n} = -\left(\frac{\partial f}{\partial V_n}\right) \Big/ \left(\frac{\partial f}{\partial \alpha}\right) = \frac{-\tfrac{1}{2} n \sin n\alpha_o}{\left(\frac{d^2V(\alpha_o)}{d\alpha^2}\right)}$$

Centrifugal Distortion

It is well known that centrifugal distortion produces terms in p^4, p^6, etc., in the overall rotation Hamiltonian. Internal rotation is entirely analogous in this respect. Terms in p^4 and p^6 have therefore been included in the final Hamiltonian in order to assess their importance to the internal-rotation process.

The total Hamiltonian operator becomes;

$$\hat{H}_{tot} = \hat{H} + \hat{H}_{c.d}$$

where;

$$\hat{H}_{c.d} = DF_1\left(\frac{p}{\hbar}\right)^4 + DF_2\left(\frac{p}{\hbar}\right)^6$$

$$= DF_1 \frac{\partial^4}{\partial\alpha^4} - DF_2 \frac{\partial^6}{\partial\alpha^6}$$

Hence;

$$\langle m' \left| H_{c.d} \right| m\rangle = (DF_1\, m^4 + DF_2\, m^6)\,\delta_{mm'}$$

and

$$\frac{\partial}{\partial DF_1} \langle m' \left| H_{tot} \right| m\rangle = m^4 \delta_{mm'}$$

$$\frac{\partial}{DF_2} \langle m' \left| H_{tot} \right| m\rangle = m^6 \delta_{mm'}.$$

Program Vfit Input Format

Line 1	Title (10A8)
Line 2	Nbasis (I3)
Line 3	Ifix, F_o (I2, 2X, F16.8)
Lines 4	Iend, Ifix, n, F_n (2I1, I2, F16.8)
Lines 5	Iend, Ifix, n, DF_n (2I1, I2, F16.8)
Lines 6	Iend, Ifix, n, V_n (2I1, I2, F16.8)
Line 7	Ncycle, Icov, Icc, New (4I3) If Ncycle = 0 go to line 10
Lines 8	Text, α_{min}, U (A8, 8x, 2F16.8) Blank line terminates list.
Lines 9	Text, M_u, M_L, Obs, U (A8, X, I3, X, I3, 2 F16.8) Blank line terminates list.
Line 10	Npred, Iplot, Imat, Ivec, Ider (5I3)

Notes

Nbasis = Number of basis functions
= Order of Hamiltonian matrix.

Ifix = 0 parameter held constant in fit.
Ifix = 1 parameter allowed to vary in fit.

Lines 3, 4 and 5 are lists of parameters. A '1' in the first column (Iend) is taken to terminate the list in each case. E.g. if no 'F_n' parameters are required, give a single line 4 with a '1' in column 1, then move on to lines 5.

Ncycle - maximum number of least-squares fitting cycles.

Icov = 0 does not print correlation matrix.
= 1 prints correlation matrix after convergence
>1 prints correlation matrix after each round of fitting.

Icc (convergence criterion) Default 10
If calc. shift < (parameter esd)/(ICC)^3 for all variable parameters, program exits from least-squares fitting routine.

New >0 prints an updated version of the input file containing the adjusted parameters.

Text - allows user information to be input and printed out with each observation.

α_{min} - preferred conformational angle in degrees.

Mu, Ml Upper and lower level limiting free-rotor quantum numbers.

Obs - Observation (preferably in cm^{-1})

U - Uncertainty in same units as the observation.
Weight of an observation is $1/U^2$

Npred - Number of energy levels to be predicted in each Wang block.

Iplot > 0 prints values of the potential function at intervals of (Iplot) degrees.

Imat > 0 prints a portion of the Hamiltonian matrix prior to diagonalisation.

Ivec > 0 prints out eigenvectors in blocks of 12, with Ivec specifying the start of the block.

Ider > 0 prints out ∂(Energy Level) / ∂(Parameter)

Acknowledgements

The code for subroutine Gaujdn was taken from Program Malon (Appendix 7).

Subroutine Hdiag is a modified NAG routine.

```
C Program Vfit-666. By D.W.Knight. Dec 1984.
C Solution of Schroedinger Eqn. for Periodic Potential and
C Alpha and Omega dependence of Internal Rot. Const.
C Reverts to Hamiltonian of Lewis et al., (J Mol Struct (1972),
C 12,449) in absence of Distortion Constants.
      IMPLICIT REAL*8 (A-H,O-Z)
      COMMON/MATRIX/H(100,100),VECT(100,100,2),ESIN(100)
      COMMON/PARMTR/F0,FN(8),DF(8),VN(12),NF,ND,NV,NP,NBASIS
      COMMON/FIX/IFIXF0,IFIXF(8),IFIXD(8),IFIXV(12)
      COMMON/DATA/TEXT(50),MMM(100),OMR(150),NOBS,NANG
      COMMON/INFO/LABEL(29)
      COMMON/MISC/TITLE(10)
C Reading Title (10A8).
      READ(5,500) TITLE
      WRITE(6,600) TITLE
C Reading Order of Matrix (No. of Basis Funcs.)
      READ(5,510) NBASIS
      IF (NBASIS.GT.100) NBASIS=100
      IF (NBASIS.LT.12) NBASIS=12
C Reading F0, the Internal Potation Const.
      READ(5,520) IFIXF0,F0
      NF=0
      ND=0
      NV=0
      DO 10 I=1,8
      FN(I)=0.0
      IFIXF(I)=0
      DF(I)=0.0
   10 IFIXD(I)=0
      DO 20 I=1,12
      VN(I)=0.0
   20 IFIXV(I)=0
C Reading Alpha Dependence Parameters Fn.
      DO 30 I=1,8
      READ(5,530) IEND,IFIX,N,P
      IF(IEND.NE.0)GO TO 40
      FN(N)=P
      IFIXF(N)=IFIX
   30 NF=N
C Reading Distortion Parameters DFn.
   40 DO 50 I=1,8
      READ(5,530) IEND,IFIX,N,P
      IF(IEND.NE.0)GO TO 60
      DF(N)=P
      IFIXD(N)=IFIX
   50 ND=N
   60 NVDOM=0
      VDOM=0.0
C Reading Potential Coeffs. Vn.
      DO 70 I=1,12
      READ(5,530) IEND,IFIX,N,P
      IF(IEND.NE.0)GO TO 80
      VN(N)=P
      IFIXV(N)=IFIX
      IF(ABS(P).GT.ABS(VDOM))NVDOM=N
      IF(NVDOM.EQ.N)VDOM=P
   70 NV=N
   80 IF(VDOM.EQ.0.0)NVDOM=0
      IF(NVDOM.EQ.0)WRITE(6,602)
      IF(NVDOM.GT.0)WRITE(6,604)NVDOM
      NP=17+NV
C Least squares Fitting Routine.
      READ(5,510)NCYCLE,ICOV,ICC,NEW
      IF(NCYCLE.EQ.0)GO TO 90
      WRITE(6,610)NBASIS
      CALL LEASQ(NCYCLE,ICOV,ICC)
```

```
C Energy Levels, Potential Func, Matrix, Eigenvectors, Derivatives.
   90 READ(5,510,END=200)NPRED,IPLOT,IMAT,IVEC,IDER
      IF(NEW.GT.0)CALL NUFILE(NCYCLE,ICOV,ICC,
     *NPRED,IPLOT,IMAT,IVEC,IDER)
      IF(IPLOT.GT.0) CALL VPLOT(IPLOT,NVDOM)
      IF(NPRED.EQ.0) STOP
      IF(NPRED.GE.NBASIS)NPRED=NBASIS-1
      IF(NCYCLE.GT.0)GO TO 100
      WRITE(6,610)NBASIS
      WRITE(6,620)F0
      IF(NF.GT.0)WRITE(6,630)(FN(I),I=1,NF)
      IF(ND.GT.0)WRITE(6,640)(DF(I),I=1,ND)
      IF (IPLOT.GT.0) GO TO 100
      IF(NV.GT.0)WRITE(6,650)(VN(I),I=1,NV)
  100 CALL SETUP(-1.0D0)
      IF(IMAT.GT.0)CALL MPRINT(0)
      IV=0
      IF(IVEC.GT.0)IV=1
      IF(IDER.GT.0)IV=1
      CALL HDIAG(NBASIS,IV)
      DO 110 I=1,NPRED
  110 ESIN(I)=H(I,I)
      CALL SETUP(1.0D0)
      IF(IMAT.GT.0)CALL MPRINT(1)
      IF(IVEC.GT.0)IV=2
      IF(IDER.GT.0)IV=2
      CALL HDIAG(NBASIS,IV)
      WRITE(6,660)
      WRITE(6,665)H(1,1)
      DO 130 I=1,NPRED
      J=I+1
  130 WRITE(6,670)I,ESIN(I),H(J,J)
      IF(IVEC.GT.0)CALL VPRINT(NBASIS,IVEC)
      IF(IDER.GT.0)CALL DERPR(NPRED,NVDOM)
  200 STOP
C
  500 FORMAT(10A8)
  510 FORMAT(5I3)
  520 FORMAT(I2,2X,F16.8)
  530 FORMAT(2I1,I2,F16.8)
C
  600 FORMAT(X,10A8/X,'Torsional Potential Program VFIT')
  602 FORMAT(X,'Free Rotor.')
  604 FORMAT(X,I3,' Fold Dominated Potential')
  610 FORMAT(/X,I3,' Basis Functions')
  620 FORMAT(/X,'F0='F12.8)
  630 FORMAT(/X,'Coeffs Fn of F(alpha)=F0+SigmaFn*Cos(n*alpha)'
     */(x,5F16.8))
  640 FORMAT(/X,'Distortion Coeffs DFn'
     */(x,5F16.8))
  650 FORMAT(/X,'Coeffs Vn of V(alpha)=SigmaVn(1-Cos(n*alpha))/2'
     */(x,5F16.8))
  660 FORMAT(/X,'Energy Levels'//2X,
     *'Iml   Odd (Sin) Wfn. Even (Cos) Wfn.'/)
  665 FORMAT(3X,'0',16X,F16.8)
  670 FORMAT(X,I3,2F16.8)
      END
C-----------------------------------------------------------------
      BLOCK DATA
      IMPLICIT REAL*8 (A-H,O-Z)
      COMMON/INFO/LABEL(29)
      DATA LABEL/4H   F0,4H  F1,4H  F2,4H  F3,4H  F4,4H  F5,4H  F6,
     *4H  F7,4H  F8,4H DF1,4H DF2,4H DF3,4H DF4,4H DF5,4H DF6,4H DF7,
     *4H DF8,4H  V1,4H  V2,4H  V3,4H  V4,4H  V5,4H  V6,4H  V7,4H  V8,
     *4H  V9,4H V10,4H V11,4H V12/
      END
C-----------------------------------------------------------------
```

```
      SUBROUTINE NUFILE(NCYCLE,ICOV,ICC,NPRED,IPLOT,IMAT,IVEC,IDER)
C Outputs an Updated Version of the Input File to Device 09.
      IMPLICIT REAL*8 (A-H,O-Z)
      COMMON/INFO/LO,LF(8),LD(8),LV(12)
      COMMON/MISC/TITLE(10)
      COMMON/PARMTR/FO,FN(8),DF(8),VN(12),NF,ND,NV,NP,NBASIS
      COMMON/FIX/IFO,IFF(8),IFD(8),IFV(12)
      COMMON/DATA/TEXT(50),MU(50),ML(50),OBS(50),W(50),RES(50),
     *NOBS,NANG
      IF(NCYCLE.EQ.0) RETURN
      WRITE(9,900)TITLE
      WRITE(9,910)NBASIS
      WRITE(9,920)IFO,FO,LO
      IF(NF.EQ.0)GO TO 20
      DO 10 I=1,NF
   10 WRITE(9,925)IFF(I),I,FN(I),LF(I)
   20 IF(NF.LT.8)WRITE(9,930)
      IF(ND.EQ.0)GO TO 40
      DO 30 I=1,ND
   30 WRITE(9,925)IFD(I),I,DF(I),LD(I)
   40 IF(ND.LT.8)WRITE(9,930)
      IF(NV.EQ.0)GO TO 60
      DO 50 I=1,NV
   50 WRITE(9,925)IFV(I),I,VN(I),LV(I)
   60 IF(NV.LT.12)WRITE(9,930)
      NEW=1
      WRITE(9,910)NCYC_F,ICOV,ICC,NEW
      IF(NANG.EQ.0)GO TO 68
      DO 62 I=1,NANG
      IF(W(I).EQ.0.0)W(I)=1.0D-6
      U=1.0/SQRT(W(I))
   62 WRITE(9,935)TEXT(I),OBS(I),U,RES(I)
   68 WRITE(9,950)
      IE1=NANG+1
      DO 70 I=IE1,NOBS
      U=1.0/SQRT( W(I) )
   70 WRITE(9,940)TEXT(I),MU(I),ML(I),OBS(I),U,RES(I)
      WRITE(9,950)
      WRITE(9,910)NPRED,IPLOT,IMAT,IVEC,IDER
      RETURN
C
  900 FORMAT(10A8)
  910 FORMAT(5I3)
  920 FORMAT(I2,2X,F16.8,2X,A4)
  925 FORMAT(2I2,F16.8,2X,A4)
  930 FORMAT('1')
  935 FORMAT(A8,8X,3F16.3)
  940 FORMAT(A8,X,I3,X,I3,3F16.8)
  950 FORMAT(X)
      END
C-----------------------------------------------------------------------
      SUBROUTINE VPLOT(ISTEP,NDOM)
Calculates Points for Plotting the Potential Func. V(alpha).
      IMPLICIT REAL*8 (A-H,O-Z)
      COMMON/PARMTR/F(17),V(12),NF,ND,NV,NP,NBASIS
      IF(NDOM.EQ.0)RETURN
      WRITE(6,600)
      WRITE(6,610)(I,I=1,NV)
      WRITE(6,620)(V(I),I=1,NV)
      WRITE(6,630)
      IF(ISTEP.GT.360) ISTEP=30
      IALFA=0
      DO 20 I=1,360
      RALFA=FLOAT(IALFA)*1.74532925199D-02
      VALFA=0.0
```

```
      DO 10 N=1,NV
   10 VALFA=VALFA + V(N)*(1.0-DCOS(FLOAT(N)*RALFA) )/2.0
      WRITE(6,640)IALFA,VALFA
      IALFA=IALFA+ISTEP
      IF(IALFA.GE.360) RETURN
   20 CONTINUE
C
  600 FORMAT(/X,'Potential Function ',
     *'V(alpha)=SigmaVn(1-Cos(n*alpha))/2')
  610 FORMAT(X,'n'5X,I2,11(8X,I2))
  620 FORMAT(X,'Vn',12F10.4)
  630 FORMAT(/X,'alpha',6X,'V(alpha)')
  640 FORMAT(X,I4,F15.5)
      END
C-----------------------------------------------------------------
      SUBROUTINE MPRINT(L)
C Prints Out Initial Matrix Elements.
      IMPLICIT REAL*8 (A-H,O-Z)
      COMMON/MATRIX/H(100,100),V(100,100,2),E(100)
      IF (L.EQ.0) WRITE(6,600)
      IF (L.EQ.1) WRITE(6,610)
      DO 20 I=1,12
   20 WRITE(6,620)(H(I,J),J=1,12)
      RETURN
  600 FORMAT(/X,'Hamiltonian Matrix in the Sin(m*alpha) Basis. ',
     *'Top Left is (1|H|1).'/)
  610 FORMAT(/X,'Hamiltonian Matrix in the Cos(m*alpha) Basis. ',
     *'Top Left is (0|H|0).'/)
  620 FORMAT(X,12F10.3)
      END
C-----------------------------------------------------------------
      SUBROUTINE VPRINT(NB,IV)
C Prints  Eigenvectors in Blocks of 12. IV Specifies Start of Block.
      IMPLICIT REAL*8 (A-H,O-Z)
      COMMON/MATRIX/H(100,100),V(100,100,2),E(100)
      DIMENSION IDENT(12)
      IF(IV.GE.NB) IV=NB-11
      IE=IV+11
      WRITE(6,600)
      WRITE(6,630)(I,I=IV,IE)
      DO 10 I=1,NB
   10 WRITE(6,620)(V(I,K,1),K=IV,IE)
      WRITE(6,610)
      DO 15 I=IV,IE
   15 IDENT(I)=I-1
      WRITE(6,630)(IDENT(I),I=IV,IE)
      DO 20 I=1,NB
   20 WRITE(6,620)(V(I,K,2),K=IV,IE)
      RETURN
  600 FORMAT(/X,'Eigenvectors Transforming From the Sin Basis'/)
  610 FORMAT(/X,'Eigenvectors Transforming From the Cos Basis'/)
  620 FORMAT(X,12F10.6)
  630 FORMAT(2X,I3,11(7X,I3))
      END
C-----------------------------------------------------------------
      SUBROUTINE DERPR(NPRED,NVDOM)
C Prints Out Energy Level Derivatives w.r.t Parameters.
      IMPLICIT REAL*8(A-H,O-Z)
      COMMON/PARMTR/P(20),NF,ND,NV,MAXV,NBASIS
      COMMON/FIX/IFIX(29)
      COMMON/DERIVS/DER(50,29)
      DIMENSION DL(29)
      DATA DL/8H dE/dF0 ,8H dE/dF1 ,8H dE/dF2 ,8H dE/dF3 ,8H dE/dF4 ,
     *8H dE/dF5 ,8H dE/dF6 ,8H dE/dF7 ,8H dE/dF8 ,8H dE/dDF1,
     *8H dE/dDF2,8H dE/dDF3,8H dE/dDF4,8H dE/dDF5,8H dE/dDF6,
     *8H dE/dDF7,8H dE/dDF8,8H dE/dV1 ,8H dE/dV2 ,8H dE/dV3 ,
     *8H dE/dV4 ,8H dE/dV5 ,8H dE/dV6 ,8H dE/dV7 ,8H dE/dV8 ,
     *8H dE/dV9 ,8H dE/dV10,8H dE/dV11,8H dE/dV12/
```

```
      IFIX(1)=1
      DO 10 I=2,29
   10 IF(P(I).NE.0.0)IFIX(I)=1
      IF(NV.EQ.0)GO TO 30
      DO 20 I=18,MAXV
      IF(IFIX(I).GT.0)MINV=I
      IF(IFIX(I).GT.0)GO TO 30
   20 CONTINUE
   30 IF(ND.EQ.0)GO TO 50
      MAXD=ND+9
      DO 40 I=10,MAXD
      IF(IFIX(I).GT.0)MIND=I
      IF(IFIX(I).GT.0)GO TO 50
   40 CONTINUE
   50 IF(NF.EQ.0)GO TO 65
      MAXF=NF+1
      DO 60 I=2,MAXF
      IF(IFIX(I).GT.0)MINF=I
      IF(IFIX(I).GT.0)GO TO 65
   60 CONTINUE
   65 IF(NV.GT.0)GO TO 68
      MAXV=18
      MINV=18
      NV=1
   68 IF(ND.GT.0)GO TO 70
      MAXD=10
      MIND=10
      ND=1
   70 IF(NF.GT.0)GO TO 71
      MAXF=NVDOM+1
      IF(NVDOM.EQ.0)MAXF=2
      IF(MAXF.GT.9)MAXF=2
      MINF=MAXF
      NF=NVDOM
      IF(NF.GT.9)NF=1
      IF(NVDOM.EQ.0)NF=1
   71 DO 72 I=MINF,MAXF
   72 IFIX(I)=1
      DO 73 I=MIND,MAXD
   73 IFIX(I)=1
      DO 74 I=MINV,MAXV
   74 IFIX(I)=1
      WRITE(6,600)
      ISIGN=-1
      ISHIFT=0
      DO 90 IW=1,2
      IF(IW.EQ.1)WRITE(6,610)
      IF(IW.EQ.2)WRITE(6,620)
      WRITE(6,630)DL(1),(DL(J),J=MINF,MAXF),(DL(K),K=MIND,MAXD)
     *,(DL(L),L=MINV,MAXV)
      DO 80 I=1,NPRED
      M=I*ISIGN-ISHIFT
      DO 75 II=1,MAXV
   75 DER(1,II)=0.0
      CALL DERCAL(1,M,1.0D0)
   80 WRITE(6,640)M,DER(1,1),(DER(1,J),J=MINF,MAXF),(DER(1,K),
     *K=MIND,MAXD),(DER(1,L),L=MINV,MAXV)
      ISIGN=1
   90 ISHIFT=1
      RETURN
  600 FORMAT(/X,'Energy Level Derivatives w.r.t Parameters.')
  610 FORMAT(/X,'Sin Block.')
  620 FORMAT(/X,'Cos Block.')
  630 FORMAT(/4X,'n',12(2X,A8)/5X,12(2X,A8)/5X,5(2X,A8))
  640 FORMAT(X,I4,12F10.3/5X,12F10.3/5X,5F10.3)
      END
C -----------------------------------------------------------------
```

```
      SUBROUTINE LEASQ(NCYCLE,ICOV,ICC)
      IMPLICIT REAL*8 (A-H,O-Z)
      COMMON/MATRIX/H(100,100),VECT(100,100,2),ESIN(100)
      COMMON/PARMTR/P(29),NF,ND,NV,NP,NBASIS
      COMMON/FIX/IFIX(29)
      COMMON/DERIVS/DER(50,29)
      COMMON/NORM/A(29,29)
      DIMENSION Y(29),DP(29),ALFA(2)
      COMMON/DATA/TEXT(50),MU(50),ML(50),OBS(50),WEIGHT(50),RES(50),
     *NOBS,NANG
      COMMON/INFO/LABEL(29)
      DATA ALFA/8Halphamin,8Halphamax/
      IF(ICC.EQ.0)ICC=10
      JCC=ICC
      CC=FLOAT(JCC*JCC*JCC)
C Writing out the Starting Parameters.
      WRITE(6,630)
      DO 5 I=1,NP
      IF(P(I).EQ.0.0)GO TO 5
      IF(IFIX(I).EQ.0)WRITE(6,640)LABEL(I),P(I)
      IF(IFIX(I).GT.0)WRITE(6,650)LABEL(I),P(I)
    5 CONTINUE
C Reading Input Data, Deciding Which Wang Blocks are Needed,
Calculating Weights and Degrees of Freedom.
      NEFF=0
      DO 6 I=1,10
      READ(5,510)TEXT(I),OBS(I),U
      IF(OBS(I).EQ.0.0)GO TO 7
      MU(I)=1
      WEIGHT(I)=1.0
      IF(U.GE.1.0D-6)WEIGHT(I)=1/(U*U)
    6 IF(WEIGHT(I).GT.1.0D-4)NEFF=NEFF+1
    7 NANG=I-1
      IE1=I
      ICOS=0
      ISIN=0
      MMAX=0
      DO 10 I=IE1,50
      READ(5,500,END=20)TEXT(I),MU(I),ML(I),OBS(I),U
      MMU=ABS(MU(I))
      MML=ABS(ML(I))
      IF((MMU+MML).EQ.0)GO TO 20
      IF(MU(I).GE.0)ICOS=1
      IF(ML(I).GE.0)ICOS=1
      IF(MU(I).LT.0)ISIN=1
      IF(ML(I).LT.0)ISIN=1
      IF(MMU.GT.MMAX)MMAX=MMU
      IF(MML.GT.MMAX)MMAX=MML
      WEIGHT(I)=1.0
      IF(U.GE.1.0D-8)WEIGHT(I)=1/(U*U)
   10 IF(WEIGHT(I).GT.1.0D-6)NEFF=NEFF+1
   20 NOBS=I-1
      IF(MMAX.EQ.0)RETURN
      IF(MMAX.GE.NBASIS)NBASIS=MMAX+1
      IF(NBASIS.GT.100)STOP'Illegal Quantum Number in input data.'
      NVP=0
      DO 25 I=1,NP
   25 IF(IFIX(I).GT.0)NVP=NVP+1
      NDF=NEFF-NVP
      IF(NDF.LE.0)STOP'More Parameters than Useful Observations.'
      WRITE(6,605)NDF
      FNDF=FLOAT(NDF)
C Least Squares Fitting Cycle.
      DO 900 IROUND=1,NCYCLE
      WRITE(6,600)IROUND
```

```
Calculating Energies, Residuals and Derivatives.
      WRITE(6,610)
      SWRR=0.0
      IF(NANG.EQ.0)GO TO 29
      DO 27 I=1,NANG
      DO 26 J=1,NP
   26 DER(I,J)=0.0
      CALL NEWTON(I,ITS)
      WRITE(6,615)TEXT(I),ALFA(MU(I)),OBS(I),RES(I),WEIGHT(I),ITS
   27 SWRR=SWRR+WEIGHT(I)*RES(I)*RES(I)
   29 IF(ISIN.EQ.0)GO TO 40
      CALL SETUP(-1.0D0)
      CALL HDIAG(NBASIS,1)
      DO 30 I=1,MMAX
   30 ESIN(I)=H(I,I)
   40 IF(ICOS.EQ.0)GO TO 50
      CALL SETUP(1.0D0)
      CALL HDIAG(NBASIS,2)
   50 DO 60 I=IE1,NOBS
      MMU=ABS(MU(I))
      MML=ABS(ML(I))
      IF(MU(I).LT.0)EUP=ESIN(MMU)
      IF(MU(I).GE.0)EUP=H(MMU+1,MMU+1)
      IF(ML(I).LT.0)ELO=ESIN(MML)
      IF(ML(I).GE.0)ELO=H(MML+1,MML+1)
      RES(I)=OBS(I)-EUP+ELO
      WRITE(6,620)TEXT(I),MU(I),ML(I),OBS(I),RES(I),WEIGHT(I)
      SWRR=SWRR+WEIGHT(I)*RES(I)*RES(I)
      DO 55 J=1,NP
   55 DER(I,J)=0.0
      CALL DERCAL(I,MU(I),1.0D0)
      CALL DERCAL(I,ML(I),-1.0D0)
   60 CONTINUE
      DO 75 K=1,NP
      DO 70 J=1,NP
   70 A(K,J)=0.0
      DP(K)=0.0
      Y(K)=0.0
   75 CONTINUE
      SIGMA=SQRT(SWRR/FNDF)
      WRITE(6,660)SIGMA
      IF(IROUND.EQ.1)GO TO 78
      IF(SIGMA.GT.SIGOLD)WRITE(6,685)
      IF(SIGMA.LE.SIGOLD)WRITE(6,684)
C Setting Up and Solving the Normal Equations.
   78 DO 90 I=1,NOBS
      DO 80 J=1,NP
      Y(J)=Y(J)+WEIGHT(I)*RES(I)*DER(I,J)
      DO 80 K=J,NP
      A(K,J)=A(K,J)+WEIGHT(I)*DER(I,K)*DER(I,J)
      A(J,K)=A(K,J)
   80 CONTINUE
   90 CONTINUE
      DO 100 J=1,NP
  100 IF(IFIX(J).EQ.0) A(J,J)=1.0
      CALL GAUJDN(NP)
      DO 110 J=1,NP
      DO 110 K=1,NP
  110 DP(J)=DP(J) + A(J,K)*Y(K)
C Parameter Adjustments.
      WRITE(6,665)
      IFLAG=0
      DS=0.0
```

```
      DO 120 J=1,NP
      DS=DS+DP(J)*Y(J)
      IF(IFIX(J).GT.0) GO TO 115
      IF(P(J).EQ.0.0) GO TO 120
      WRITE(6,680) LABEL(J),P(J)
      GO TO 120
  115 P(J)=P(J)+DP(J)
      ESD=SIGMA*SQRT(A(J,J))
      WRITE(6,670) LABEL(J),P(J),ESD,DP(J)
      CCP=ESD/CC
      IF(ABS(DP(J)).GT.CCP) IFLAG=1
  120 CONTINUE
      SIGNEW=SQRT( (SWRR-DS)/FNDF )
      WRITE(6,682) SIGNEW
      IF(ICOV.GT.1)CALL RHOCAL(NP,NVP)
      IF(IFLAG.EQ.0) GO TO 950
      SIGOLD=SIGMA
  900 CONTINUE
      IF(ICOV.EQ.1)CALL RHOCAL(NP,NVP)
      RETURN
  950 WRITE(6,690)
      IF(ICOV.EQ.1)CALL RHOCAL(NP,NVP)
      RETURN
C
  500 FORMAT(A8,X,I3,X,I3,2F16.8)
  510 FORMAT(A8,8X,2F16.8)
C
  600 FORMAT(/X,'Cycle Number',I3/)
  605 FORMAT(/X,I3,' Degrees of Freedom.')
  610 FORMAT(13X,'mu  ml',7X,'Obs',14X,'Obs-Calc',9X,'Weight')
  615 FORMAT(X,A8,2X,A8,2(X,F16.8),X,G16.5,4X,I3)
  620 FORMAT(X,A8,3X,I3,X,I3,2(X,F16.8),X,G16.5)
  630 FORMAT(/X,'Least Squares Fitting Routine'/X,'Initial Parameters')
  640 FORMAT(X,A4,F16.8,'  Const')
  650 FORMAT(X,A4,F16.8)
  660 FORMAT(/X,'E.S.D. of an Observation =',F16.8,'/Sqrt(Weight)')
  665 FORMAT(/2X,'Estimated Parameters',7X,'E.S.D.',7X,'Shift from Old')
  670 FORMAT(X,A4,3(X,F16.8))
  680 FORMAT(X,A4,X,F16.3,7X,'Const.')
  682 FORMAT(/X,'New Expected S.D. of Obs.=',F16.8,'/Sqrt(Weight)')
  684 FORMAT(X,'Converging.')
  686 FORMAT(X,'Diverging.')
  690 FORMAT(/X,'Refinement Terminated.')
      END
C-----------------------------------------------------------------
      SUBROUTINE RHOCAL(NP,NVP)
C Prints the Parameter Correlation Coeffs.
      IMPLICIT REAL*8 (A-H,O-Z)
      COMMON/NORM/A(29,29)
      COMMON/FIX/IFIX(29)
      COMMON/INFO/LABEL(29)
      DIMENSION IV(29),RTD(29),RHO(29)
      IF(NVP.EQ.0)RETURN
      WRITE(6,600)
      K=1
      DO 20 I=1,NVP
      DO 10 J=K,NP
      IF(IFIX(J).GT.0) GO TO 15
   10 CONTINUE
   15 IV(I)=J
   20 K=J+1
      WRITE(6,610)(LABEL(IV(I)),I=1,NVP)
      DO 30 I=1,NVP
      K=IV(I)
   30 RTD(I)=SQRT(A(K,K))
```

```
      DO 50 I=1,NVP
      DO 40 J=1,I
   40 RHO(J)=A(IV(I),IV(J))/(RTD(I)*RTD(J))
   50 WRITE(6,620)(RHO(J),J=1,I)
      RETURN
  600 FORMAT(/X,'Correlation Coefficients.')
  610 FORMAT(3X,A4,14(4X,A4)/3X,A4,13(4X,A4))
  620 FORMAT(X,15F8.4/X,14F8.4)
      END
C-----------------------------------------------------------------
      SUBROUTINE DERCAL(IOBS,M,SIGN)
Calculates Derivatives Using the Hellmann-Feynman Theorem and the
C fact that Eigenfunc(k)=Sum Over i of Eigenvect(i,k)*Basisfunc(i).
      IMPLICIT REAL*8 (A-H,O-Z)
      COMMON/MATRIX/H(100,100),VECT(100,100,2),ESIN(100)
      COMMON/PARMTR/P(29),NF,ND,NV,NP,NBASIS
      COMMON/FIX/IFIX(29)
      COMMON/DERIVS/DER(50,29)
      IVT=2
      IF(M.LT.0)IVT=1
      WANG=1.0
      IF(M.LT.0)WANG=-1.0
      ISHIFT=0
      IF(M.GE.0)ISHIFT=1
      ISTART=1+ISHIFT
      K=ABS(M)+ISHIFT
C dE/dF0
      IF(IFIX(1).EQ.0)GO TO 20
      DO 10 I=ISTART,NBASIS
      FM=FLOAT(I-ISHIFT)
      VV=VECT(I,K,IVT)
   10 DER(IOBS,1)=DER(IOBS,1)+SIGN*VV*VV*FM*FM
C dE/dFn
   20 IF(NF.EQ.0)GO TO 50
      NPE=NF+1
      DO 40 IP=2,NPE
      IF(IFIX(IP).EQ.0)GO TO 40
      N=IP-1
      DO 30 I=ISTART,NBASIS
      ML=I-ISHIFT
      FML=FLOAT(ML)
      DO 30 J=ISTART,NBASIS
      MR=J-ISHIFT
      FMR=FLOAT(MR)
      DELTA1=0.0
      IF(ABS(ML-MR).EQ.N)DELTA1=1.0
      DELTA2=0.0
      IF((ML+MR).EQ.N)DELTA2=1.0
   30 DER(IOBS,IP)=DER(IOBS,IP)+SIGN*VECT(I,K,IVT)*VECT(J,K,IVT)*
     *FML*FMR*(DELTA1-WANG*DELTA2)/2.0
   40 CONTINUE
C dE/dDFn
   50 IF(ND.EQ.0)GO TO 100
      IF(IFIX(10).EQ.0)GO TO 70
      DO 60 I=ISTART,NBASIS
      FM=FLOAT(I-ISHIFT)
      VV=VECT(I,K,IVT)
   60 DER(IOBS,10)=DER(IOBS,10)+SIGN*VV*VV*FM*FM*FM*FM
   70 IF(IFIX(11).EQ.0)GO TO 90
      DO 80 I=ISTART,NBASIS
      FM=FLOAT(I-ISHIFT)
      VV=VECT(I,K,IVT)
   80 DER(IOBS,11)=DER(IOBS,11)+SIGN*VV*VV*FM*FM*FM*FM*FM*FM
   90 NPE=ND+9
```

```
C dE/dVn
  100 IF(NV.EQ.0)RETURN
      DO 200 IP=18,NP
      IF(IFIX(IP).EQ.0)GO TO 200
      N=IP-17
      V0=VECT(1,K,2)
      IF(IVT.NE.2)GO TO 120
      DER(IOBS,IP)=DER(IOBS,IP)+SIGN*(0.5*V0*V0-V0*VECT(N+1,K,2)*
     * 0.707106781186548 D0 )
  120 DO 140 I=ISTART,NBASIS
      ML=I-ISHIFT
      DO 140 J=ISTART,NBASIS
      MR=J-ISHIFT
      DELTA1=0.0
      IF(ML.EQ.MR)DELTA1=1.0
      DELTA2=0.0
      IF((ML+MR).EQ.N))DELTA2=1.0
      DELTA3=0.0
      IF(ABS(ML-MR).EQ.N)DELTA3=1.0
  140 DER(IOBS,IP)=DER(IOBS,IP)+SIGN*VECT(I,K,IVT)*VECT(J,K,IVT)*
     *(0.5*DELTA1-0.25*(WANG*DELTA2+DELTA3 ) )
  200 CONTINUE
      RETURN
      END
C-----------------------------------------------------------------
      SUBROUTINE NEWTON(IOBS,ITS)
      IMPLICIT REAL*8 (A-H,O-Z)
      COMMON/PARMTR/P(17),V(12),NF,ND,NV,NP,NBASIS
      COMMON/FIX/IFIX(17),IFV(12)
      COMMON/DERIVS/DER(50,29)
      COMMON/DATA/TEXT(50),MU(50),ML(50),OBS(50),WT(50),RES(50),
     *NOBS,NANG
      DATA CONV/1.745329251990-02/
C Newton-Raphson iteration to find potential turning point.
      ALAST=OBS(IOBS)*CONV
      DO 20 I=1,100
      D1V=0.0
      D2V=0.0
      DO 10 J=1,NV
      FN=FLOAT(J)
      D1V=D1V+(FN*V(J)*DSIN(FN*ALAST))/2.0
      D2V=D2V+(FN*FN*V(J)*DCOS(FN*ALAST))/2.0
   10 CONTINUE
      DELTA=-D1V/D2V
      ANEXT=ALAST+DELTA
      IF(ABS(DELTA).LT.1.0D-10)GO TO 30
      ALAST=ANEXT
   20 CONTINUE
      WT(IOBS)=0.0
      RETURN
   30 ITS=I
      RES(IOBS)=OBS(IOBS)-ANEXT/CONV
      IF(D2V.GT.0.0)GO TO 40
      WT(IOBS)=0.0
      MU(IOBS)=2
      RETURN
Calculation of the dAlpha/dVn coeffs.
   40 DO 50 I=1,NV
      IF(IFV(I).EQ.0)GO TO 50
      FN=FLOAT(I)
      DER(IOBS,I)=-FN*DSIN(FN*ANEXT)/(2.0*D2V*CONV)
   50 CONTINUE
      RETURN
      END
C-----------------------------------------------------------------
```

```
      SUBROUTINE SETUP(WANG)
      IMPLICIT REAL*8 (A-H,O-Z)
      COMMON/MATRIX/H(100,100),VECT(100,100,2),ESIN(100)
      COMMON/PARMTR/FO,FN(8),DF(8),VN(12),NF,NO,NV,NP,NBASIS
C Wang=-1 for Sin (odd) Basis, Wang=+1 for Cos (even) Basis.
      DO 10 I=1,NBASIS
      DO 10 J=1,NBASIS
   10 H(I,J)=0.0
      SV=0.0
      IF(NV.LT.1)GO TO 25
      DO 20 I=1,NV
   20 SV=SV+VN(I)
      SV=SV/2.0
   25 ISHIFT=0
      IF(WANG.GT.0.0)ISHIFT=1
      ISTART=1+ISHIFT
C For cos basis H(1,1)=(0|H|0). For sin basis H(1,1)=(1|H|1).
      DO 30 I=1,NBASIS
      M=I-ISHIFT
      FM=FLOAT(M)
   30 H(I,I)=FO*FM*FM+SV
      IF(NV.LT.1)GO TO 80
      IF(WANG.LT.0.0)GO TO 50
      RT8=SQRT(8.0)
      MAX=NV+1
      DO 40 I=2,MAX
      M=I-1
   40 H(1,I)=-VN(M)/RT8
   50 DO 65 I=ISTART,NBASIS
      ML=I-ISHIFT
      K=I+1
      DO 60 J=K,NBASIS
      MR=J-ISHIFT
      IF((MR-ML).GT.NV)GO TO 62
      H(I,J)=H(I,J)-VN(MR-ML)/4.0
   60 CONTINUE
   62 CONTINUE
   65 CONTINUE
      DO 75 I=ISTART,NBASIS
      ML=I-ISHIFT
      DO 70 J=I,NBASIS
      MR=J-ISHIFT
      IF((ML+MR).GT.NV)GO TO 72
      H(I,J)=H(I,J)-WANG*VN(ML+MR)/4.0
   70 CONTINUE
   72 CONTINUE
   75 CONTINUE
   80 IF(NF.LT.1)GO TO 110
      DO 95 I=ISTART,NBASIS
      ML=I-ISHIFT
      FML=FLOAT(ML)
      K=I+1
      DO 90 J=K,NBASIS
      MR=J-ISHIFT
      IF((MR-ML).GT.NF)GO TO 92
      FMR=FLOAT(MR)
      H(I,J)=H(I,J)+FML*FMR*FN(MR-ML)/2.0
   90 CONTINUE
   92 CONTINUE
   95 CONTINUE
      DO 105 I=ISTART,NBASIS
      ML=I-ISHIFT
      FML=FLOAT(ML)
      DO 100 J=I,NBASIS
```

```
      MR=J-ISHIFT
      IF((ML+MR).GT.NF)GO TO 102
      FMR=FLOAT(MR)
      H(I,J)=H(I,J)-WANG*FML*FMR*FN(ML+MR)/2.0
  100 CONTINUE
  102 CONTINUE
  105 CONTINUE
  110 IF(ND.LT.1)RETURN
      DO 120 I=ISTART,NBASIS
      FM=FLOAT(I-ISHIFT)
      FM4=FM*FM*FM*FM
      FM6=FM4*FM*FM
  120 H(I,I)=H(I,I)+DF(1)*FM4 +DF(2)*FM6
      RETURN
      END
C-------------------------------------------------------------
      SUBROUTINE GAUJDN(N)
C GAUSS-JORDAN ALGORITHM FOR INVERSION OF A POSITIVE DEFINITE MATRIX.
      IMPLICIT REAL*8 (A-H,O-Z)
      DIMENSION H(29)
      COMMON/NORM/A(29,29)
      IF (N.LE.1) GO TO 8
      K=N
      DO 5 KK=1,N
      P=A(1,1)
      IF (P.LE.0.0)STOP'Normal matrix fails to invert'
      DO 3 I=2,N
      Q=A(I,1)
      QM=-Q
      IF (I.GT.K) QM=Q
      H(I)=QM/P
      DO 2 J=2,I
    2 A(I-1,J-1)=A(I,J)+Q*H(J)
    3 CONTINUE
      A(N,N)=1.0/P
      DO 4 I=2,N
    4 A(N,I-1)=H(I)
    5 K=K-1
      DO 6 J=1,N
      DO 6 K=1,J
    6 A(K,J)=A(J,K)
      RETURN
    8 A(1,1)=1.0/A(1,1)
      RETURN
      END
C-------------------------------------------------------------------
      SUBROUTINE HDIAG(N,IVECT)
C Jacobi Diagonalisation for Symmetric Matrices. Only the Upper
C Triangle is Used. N=Order of Matrix, NDM=Max Order of Matrix.
C Eigenvalues are not ordered so that Correlation between Basis
C Funcs. and Energies is Preserved.
C Dimension Statement in Calling Prog. is H(NDM,NDM),
C U(NDM,NDM,2). U=Storage For two sets of Eigenvectors Loaded
C according to IVECT=1,2. If IVECT=0 Eigenvectors are not calcd.
C NDM and NDG=NDM+1 are set by the Data Statement.
      IMPLICIT REAL*8 (A-H,O-Z)
      COMMON/MATRIX/H(10000),U(10000,2),ESIN(100)
      DATA NDM,NDG,ERA,ERB/100,101,0.0001,0.00000001/
      NR=0
      N1=N-1
      IF(IVECT.EQ.0) GO TO 97
C INITIALISE EIGENVECTORS IF WANTED
      KK=1
      KD=1
```

```
      DO 101 I=1,N
      K=KK
      DO 100 J=1,N
      U(K,IVECT)=0
  100 K=K+1
      U(KD,IVECT)=1.0
      KD=KD+NDG
  101 KK=KK+NDM
   97 IF(N1.LE.0)RETURN
C FIND ABSOLUTELY LARGRST ELEMENT OF H
      HTOP=0.
      KD=1
      DO 103 I=1,N
      K=KD
      DO 104 J=I,N
      Q=DABS(H(K))
      IF(HTOP-Q) 105,104,104
  105 HTOP=Q
  104 K=K+1
  103 KD=KD+NDG
      IF(HTOP.LE.0.0)RETURN
CALCULATE THE PIVOT THRESHOLD -- THRSH
      AVGF=FLOAT(N*N1)*.55
      D=0
      KS=NDG
      DO 107 JJ=1,N1
      K=KS
      DO 108 J=JJ,N1
      Q=SNGL(H(K))/HTOP
      D=D+Q*Q
  108 K=K+NDG
  107 KS=KS+NDM
      DSTOP=ERA*D
      THRSH=SQRT(D/AVGF)*HTOP
  110 IFLAG=0
C START A SWEEP
      KDD=NDM
      JJT=0
      DO 111 JJ=1,N1
      K=KDD+1
      MS=1
      DO 112 J=JJ,N1
      HIJ=H(K)
      AHIJ=DABS(HIJ)
CHECK TO SEE IF PIVOT IS ABOVE THRESHOLD
      IF(AHIJ-THRSH) 113,113,114
  114 KI=K-KDD
      HII=H(KI)
      KJ=JJ+K
      HJJ=H(KJ)
      S=HJJ-HII
      AS=DABS(S)
CHECK TO SEE IF ROTATION IS SIGNIFICANT
      IF(AHIJ-ERD*AS) 113,113,115
  115 IFLAG=1
CHECK FOR ROTATION CLOSE TO  45 DEGREES
      IF(1.E-10*AHIJ-AS) 116,117,117
  117 S=0.70710678118654 3D+00
      C=S
      IF(HIJ.LT.0) S=-S
      GO TO 118
CALCULATE ROTATION WHICH IS NOT CLOSE TO 45 DEGREES -- COS=C,SIN=S
  116 T=HIJ/S
      TT=0.25/DSQRT(0.25+T*T)
      C=DSQRT(0.5+TT)
      TT=T*TT/C
      IF(S) 140,141,141
```

```
  140 S=-C
      C=TT+TT
      GO TO 118
  141 S=TT+TT
CALCULATE NEW ELEMENTS OF H
  118 KK=MS+KDD
      DO 119 M=MS,<I
      T=H(M)
      TT=H(KK)
      H(M)=C*T-S*TT
      H(KK)=S*T+C*TT
  119 KK=KK+1
      MI=KI
      IF(JJT) 122,122,120
  120 MSS=KK+1
      DO 121 M=MSS,KJ
      MI=MI+NDM
      T=H(MI)
      TT=H(KK)
      H(MI)=C*T-S*TT
      H(KK)=S*T+C*TT
  121 KK=M
  122 H(KJ)=S*HIJ+C*HJJ
      H(KI)=C*H(KI)-S*(C*HIJ-S*HJJ)
      M=KJ
      DO 123 I=J,N1
      MI=MI+NDM
      T=H(MI)
      TT=H(M)
      H(MI)=C*T-S*TT
      H(M)=S*T+C*TT
  123 M=M+NDM
      NR=NR+1
      IF(IVECT.EQ.0) GO TO 98
CALCULATE NEW EIGENVECTORS IF NEEDED
      MSS=MS+N1
      DO 125 I=MS,MSS
      M=I+KDD
      T=U(I,IVECT)
      TT=U(M,IVECT)
      U(I,IVECT)=C*T-S*TT
  125 U(M,IVECT)=S*T+C*TT
   98 Q=AHIJ/HTOP
      D=D-Q*Q
CALCULATE THRESHOLD FROM SCRATCH IF ROUND-OFF GETTING LARGE
      IF(D-DSTOP) 126,129,129
  126 D=0.
      MSS=NDG
      DO 127 KK=1,N1
      M=MSS
      DO 128 I=KK,N1
      Q=SNGL(H(M))/HTOP
      D=D+Q*Q
  128 M=M+NDG
  127 MSS=MSS+NDM
      DSTOP=ERA*D
CALCULATE NEW THRESHOLD
  129 THRSH=SQRT(D/AVSF)*HTOP
  113 K=K+NDG
  112 MS=MS+NDM
      JJT=JJ
  111 KDD=KDD+NDM
C STOP IF THERE WERE NO SIGNIFICANT ROTATIONS AROUND PIVOTS ABOVE
C        THRESHOLD
      IF(IFLAG) 110,199,110
  199 RETURN
      END
```

APPENDIX 7

COMPUTER PROGRAM MALON

Program Malon is a least-squares fitting and prediction program designed to treat the vibration-rotation interaction in molecules having a single aperiodic tunnelling co-ordinate. The original version of the program was written by L. Halonen and P.H. Turner at Reading University. The version described here is a modification of the original, which in addition to fitting data and calculating line frequencies and intensities, also calculates energy levels, intermediate results for the quadrupole coupling problem and rotational constants transformed into the principal axis system. The program has also been modified to write out an updated version of its own input file, containing the least-squares adjusted parameters in place of their initial estimates.

The program sets up a version of Pickett's reduced-axis system (RAS) Hamiltonian[27] including all possible quartic terms in the interaction Hamiltonian H_{01}. In addition, the program includes quartic and sextic centrifugal distortion (c.d.) terms in Watson's A reduction[38].

$$H = \begin{bmatrix} H_0 & H_{01} \\ H_{01} & H_1 \end{bmatrix}$$

$$H_0 = X_0 P_x^2 + Y_0 P_y^2 + Z_0 P_z^2 + \text{c.d.}$$

$$H_1 = X_1 P_x^2 + Y_1 P_y^2 + Z_1 P_z^2 + \text{c.d.} + \Delta E_+^-$$

$$H_{01} = [T_{xy} + T_j P^2][P_x,P_z]_+ + T_{k1}[P_z^2,[P_x,P_z]_+]_+ + T_{k2}[(P_x^2-P_y^2),[P_x,P_z]_+]_+ + \Delta D$$

where $[A,B]_+ = AB + BA$

ΔE_+^- is the zero-point energy difference between the V=0 (+) and V=1 (-) states.

ΔD is the energy difference between the minima in the potential energy surface ($\Delta D=0$ for the symmetric double minimum problem).

A,B,C are related to X,Y,Z according to representation;

	I^r	II^r	III^r
x	B	C	A
y	C	A	B
z	A	B	C

Choice of representation is limited by the fact that coupling is only allowed along the y axis.

T_{xz} is the expectation value of the xz element of the inverse inertial tensor.

i.e. $T_{xz} = \langle I^{-1}_{xz} \rangle$

For further discussion of the RAS Hamiltonian, see Chapter 2, page 20 onwards.

PROGRAM MALON. INPUT FORMAT.

line 1 Title (10A8)

line 2 Rep (I3)

1,2 or 3 for I^r, II^r or III^r

lines 3-38 Fix, End, Parameter (F1.0, I1, X, F15.6)

Fix = 0 → fixed parameter
Fix = 1 → variable parameter

End = 1 terminates list of parameters at previous line → go to line 39

Parameters in order are;

$\Delta E_{\pm}$, T_{xz}, (MHz)

T_J, T_{K1}, T_{K2}, (KHz)

ΔD, (MHz)

X_0, Y_0, Z_0, X_1, Y_1, Z_1, (MHz)

ΔJ_0, ΔJK_0, ΔK_0, δJ_0, δK_0, (KHz)

ΔJ_1, ΔJK_1, ΔK_1, δJ_1, δK_1, (KHz)

HJ_0, HJK_0, HKJ_0, HK_0, hJ_0, hJK_0, hK_0, (Hz)

HJ_1, HJK_1, HKJ_1, HK_1, hJ_1, hJK_1, hK_1. (Hz)

line 39 Ncycle, Idrc, Iupd, Nopr (4I3)

Ncycle = max. No. of least-squares fitting cycles.
if Ncycle = 0 go to line 41

Idrc = 1 prints effective rotational constants and constants transformed into the principal axis system.

Iupd = 1 → Updated input file will be output on device 09 if Ncycle > 0

Nopr = 1 → Prints correlation matrix after each round of fitting.

line 40 v', v, J', K_a', K_c', J, K_a, K_c, Obs/MHz, Uncertainty/MHz

(8I4, 2F11.3) list of observations. Prime refers to upper state. max. list length 150 observations

If uncertainty = 0 or blank, weight = 1
uncertainty > 0, weight = 1/uncertainty^2.

Blank line terminates list if No. of observations is < 150.

line 41 JE_{min}, JE_{max}, J_{min}, J_{max}, χ_{aa}, χ_{bb}, χ_{cc}

(4I4, 3F9.4)

No further input is required if $J_{max} = 0$

JE → J range for energy level calculation
J → J range for predicted spectrum
The program calculates up to J = 30

χ_{aa} etc. (in MHz) are used in the energy level routine to calculate;

chi = $\chi_{aa}\langle P_a^2\rangle + \chi_{bb}\langle P_b^2\rangle + \chi_{cc}\langle P_c^2\rangle$

Thence, when $T_{xz} = 0$ (i.e. in the principal axis system);

$E_q(J,\tau)$ = Chi x Y(I,J,F)

chi = $\chi_{J\tau}$ as defined in Appendix 4.

line 42 μ_a, μ_b, μ_c, $D\mu_a$, $D\mu_b$, $D\mu_c$ (6F12.6)

Dipole moments and dipole derivatives (Debeye). Use dipole derivative if inversion occurs about the axis in question.

line 43 F_{min}, F_{max} (2F12.6) in MHz.

Upper and lower predicted frequency limits
Default 7900 - 42000 MHz.

line 44 Xlim (D12.4)

Intensity limit for predicted transitions.

Default 10^{-10}/cm. Min. 10^{-18}/cm.

line 45 T, HWHM (2F12.6)

Temperature/K. Default 195.
Half width at half max./MHz/Torr. Default 20.

line 46 Boltzmann Factor (F9.3)

Default 1.0.

line 47 Symmetry No. (F12.6)

Order of rotational subgroup. Default 1.0.

line 48 SP1, SP2 (2F12.6)

Spin weights. Default 1.0.

PROGRAM MALON LISTING (FORTRAN IV)

Input on device 05. The updated input file is output on device 09. All other output is on device 06.

```
C Original By L.Halonen and P.H.Turner, Reading Univ.
      IMPLICIT REAL*8 (A-H,O-Z)
      COMMON/BLANK/H(62,8),V(62,62),HS(62,56)
      COMMON/ROTPAR/P(36),PFIX(36),FJK(30),FJK1(30),PLABEL(36)
      COMMON/FREQS/OBS(150),WT(150)
      COMMON/VDATA/IVU(150),IVL(150)
      COMMON/DERIVS/DER(150,36),CAL(150),DUM(9826)
      COMMON/INTDAT/DIP(5),FLOW,FUP,SIGMA,T,HWHM,Q,EXX,S,XINT,XLIM,
     *SP1,SP2
      COMMON/TAU/IT(62),ITU(150),ITL(150)
      COMMON/LDATA/LU(150),LL(150)
      COMMON/JDATA/JU(150),JL(150)
      COMMON/PDATA/IPU(150),IPL(150)
      DIMENSION TITLE(10),IX(24),REP(3),CHY(3)
      DATA IX/4,1,2,3,2,4,1,3,1,2,4,3,2,3,4,1,3,1,4,2,1,2,4,3/
      DATA REP/5H  IR ,5H IIR ,5H IIIR/
C
      WRITE(6,900)
      READ(5,800)(TITLE(I),I=1,10)
      WRITE(6,901)(TITLE(I),I=1,10)
      READ(5,930)IREP
      WRITE(6,902)REP(IREP)
      DO 6 I=1,36
      READ(5,945)PFIX(I),IPEND,P(I)
      IF (IPEND)6,6,7
    6 CONTINUE
    7 NOOP=I-1
      IF (IPEND.EQ.0) NOOP=36
      DO 10 I=3,5
   10 P(I)=P(I)*1.0D-3
      DO 11 I=13,22
   11 P(I)=P(I)*1.0D-3
      DO 12 I=23,36
   12 P(I)=P(I)*1.0D-6
      READ(5,930)NCYCLE,IDRC,IUPD,NOPR
      IF (NCYCLE)13,13,1
C Least squares fitting routine follows
    1 CALL INPUT(JRMIN,JRMAX,NUM)
      WRITE(6,903)NUM
      DO 14 I=1,NUM
C Identification of upper and lower level symy blocks
C for each transition input.
      IODD=MOD(JU(I),2)
      LXY=MOD(JU(I)-ITJ(I),4)
      IF(LXY.EQ.0)LXY=4
      TEMP=IX(IODD*12+4*(IREP-1)+LXY)
      LU(I)=1
      IF(TEMP.EQ.1.OR.TEMP.EQ.4)LU(I)=2
      IODD=MOD(JL(I),2)
      LXY=MOD(JL(I)-ITL(I),4)
      IF(LXY.EQ.0)LXY=4
      TEMP=IX(IODD*12+4*(IREP-1)+LXY)
      LL(I)=1
      IF(TEMP.EQ.1.OR.TEMP.EQ.4)LL(I)=2
   14 CONTINUE
      TEST=1.0D+7
      DO 15 ICYCLE=1,NCYCLE
      WRITE(6,904)ICYCLE
```

```
      DO 16 I=1,NUM
      DO 17 J=1,NOOP
   17 DER(I,J)=0.0
   16 CAL(I)=0.0
      IODD=MOD(JRMIN,2)
      J=JRMIN
   27 IND1=0
      IND2=0
      DO 18 I=1,NUM
      IF(JU(I).NE.J.AND.JL(I).NE.J)GO TO 18
      IND2=I
      IF (IND1.EQ.0)IND1=I
   18 CONTINUE
      IF(IND1.EQ.0)GO TO 19
      RK=0.0
      RJ=FLOAT(J*(J+1))
      DO 20 I=1,J
      FJK(I)=SQRT((RJ-RK*(RK+1.0))*(RJ-(RK+1.0)*(RK+2.0)))
      FJK1(I)=SQRT(RJ-RK*(RK+1.0))
   20 RK=RK+1.0
      LMAX=2
      IF(J.EQ.0)LMAX=1
      DO 21 L=1,LMAX
      ITEMP=0
      DO 22 I=IND1,IND2
      IF(JU(I).EQ.J.AND.LU(I).EQ.L)ITEMP=1
      IF(JL(I).EQ.J.AND.LL(I).EQ.L)ITEMP=1
   22 CONTINUE
      IF(ITEMP.EQ.0)GO TO 21
      CALL SETUP(J,L,N)
      M=MIN0(7,N-1)
      CALL BANDIG(N,M)
      CALL ASSIGN(N,L,J,IREP,NO,NCYCLE)
      DO 23 I=IND1,IND2
      IF(JU(I).NE.J)GO TO 24
      N1=1+IVU(I)*NO
      N2=NO+IVU(I)*(N-NO)
      DO 25 K=N1,N2
      IF(IT(K).EQ.ITU(I))CALL DERCAL(K,I,1.0D0,N,NOOP)
   25 CONTINUE
   24 IF(JL(I).NE.J)GO TO 23
      N1=1+IVL(I)*NO
      N2=NO+IVL(I)*(N-NO)
      DO 26 K=N1,N2
      IF(IT(K).EQ.ITL(I))CALL DERCAL(K,I,-1.0D0,N,NOOP)
   26 CONTINUE
   23 CONTINUE
   21 CONTINUE
   19 IODD=1-IODD
      J=J+1
      IF(J.LE.JRMAX)GO TO 27
      WRITE(6,705)
      CALL LSQ(NUM,NOOP,TEST,IREP,NOPR,SDF)
      IF(TEST)28,15,15
   15 CONTINUE
   28 CONTINUE
      IF (IUPD) 55,55,39
C Writing to updated input file
   39 WRITE(9,600)(TITLE(I),I=1,10)
      WRITE(9,610)IREP
      DO 40 I=1,NOOP
      IPF=0
      IF (PFIX(I).EQ.1.0) IPF=1
      CONST=1.0
      IF (I.GE.3.AND.I.LE.5) CONST=1.0D3
      IF (I.GE.13) CONST=1.0D3
```

```
      IF (I.GE.23) CONST=1.0D6
      PAR=CONST*P(I)
      WRITE(9,620)IPF,PAR,PLABEL(I)
   40 CONTINUE
      IF (NOOP.LT.36) WRITE(9,625)
      WRITE(9,630)NCYCLE,IDRC,NOPR,SDF
      DO 50 I=1,NUM
      RES=OBS(I)-CAL(I)
      KAU=(ITU(I)+JU(I)+1)/2
      KCU=KAU-ITU(I)
      KAL=(ITL(I)+JL(I)+1)/2
      KCL=KAL-ITL(I)
      IF (WT(I).NE.1.0) GO TO 45
      WRITE(9,634)IVU(I),IVL(I),JU(I),KAU,KCU,JL(I),KAL,KCL,OBS(I),
     *RES
      GO TO 50
   45 U=SQRT(1.0/WT(I))
      WRITE(9,635)IVU(I),IVL(I),JU(I),KAU,KCU,JL(I),KAL,KCL,OBS(I),
     *U,RES
   50 CONTINUE
      IF (NUM.LT.150)WRITE(9,640)
C
   55 IF (IDRC) 13,13,56
C Calculation of determinable rot. consts. and conversion to P.A.S.
   56 X0=P(7)+2.0*P(13)+P(14)-2.0*P(15)-2.0*P(17)
      Y0=P(8)+2.0*P(13)+P(14)+2.0*P(16)+2.0*P(17)
      Z0=P(9)+2.0*P(13)
      X1=P(10)+2.0*P(18)+P(19)-2.0*P(21)-2.0*P(22)
      Y1=P(11)+2.0*P(18)+P(19)+2.0*P(21)+2.0*P(22)
      Z1=P(12)+2.0*P(18)
      WRITE(6,914)X0,Y0,Z0,X1,Y1,Z1
      IF (ABS(P(2)).LT.0.001) GO TO 13
      WRITE(6,915)
      CALL ROTATE(P(7),P(8),P(9),P(10),P(11),P(12),0)
      WRITE(6,916)
      CALL ROTATE(X0,Y0,Z0,X1,Y1,Z1,1)
C
   13 READ(5,940)JEMIN,JEMAX,JMIN,JMAX,CHY
      IF (JEMAX.GT.30) JEMAX=30
      IF (JMAX.GT.30) JMAX=30
      IF(IUPD.EQ.1.AND.NCYCLE.GT.0)WRITE(9,655)JEMIN,JEMAX,JMIN,JMAX,
     *CHY
      IF (JEMAX.LE.0) GO TO 70
C
C Energy level prediction follows
      WRITE (6,900)
      WRITE (6,909) CHY
      IF (NCYCLE.GT.0) GO TO 75
      WRITE (6,906)
      DO 80 I=1,NOOP
      IF (P(I).EQ.0.0) GO TO 80
      CONST=1.0
      IF (I.GE.3.AND.I.LE.5) CONST=1.0D3
      IF (I.GE.13) CONST=1.0D3
      IF (I.GE.23) CONST=1.0D6
      PAR=CONST*P(I)
      WRITE(6,907)PLABEL(I),PAR
   80 CONTINUE
   75 CONTINUE
      CALL ENCAL(JEMIN,JEMAX,IREP,NOOP,CHY)
C
   70 IF(JMAX.LE.0) STOP
C Calculation of spectrum follows
      WRITE(6,900)
      WRITE(6,905)
      IF (NCYCLE) 72,72,30
```

```
   72 IF (JEMAX) 73,73,30
   73 WRITE(6,906)
      DO 31 I=1,NOOP
      IF (P(I).EQ.0.0) GO TO 31
      CONST=1.0
      IF(I.GE.3.AND.I.LE.5)CONST=1.0D3
      IF(I.GE.13)CONST=1.0D3
      IF(I.GE.23)CONST=1.0D6
      PAR=CONST*P(I)
      WRITE(6,907)PLABEL(I),PAR
   31 CONTINUE
   30 N=1
      READ(5,950,END=90)DIP
      READ(5,950,END=90)FLOW,FUP
      READ(5,960,END=90)XLIM
      IF (XLIM.LT.1.0D-18) XLIM=1.0D-10
      READ(5,950,END=90)T,HWHM
      IF (T.LT.1.0D0) T=195.0
      IF(HWHM.LT.1.0D-5)HWHM=20.0
      READ(5,950,END=90)Q
      IF (Q.EQ.0.0) Q=1.0
      READ(5,950,END=90)SIGMA
      READ(5,950,END=90)SP1,SP2
      IF(SIGMA.LT.1.0D-5)SIGMA=1.0
      SUM=SP1+SP2
      CONST=0.0
      IF(SUM.LT.1.0D-5)CONST=1.0
      SP1=SP1+CONST
      SP2=SP2+CONST
C
      IF (IUPD) 90,90,61
   61 IF (NCYCLE) 90,90,62
C Writing to updated input file
   62 WRITE (9,645)(DIP(I),I=1,6)
      WRITE(9,645)FLOW,FUP
      WRITE(9,650)XLIM
      WRITE(9,645)T,HWHM
      WRITE(9,645)Q
      WRITE(9,645)SIGMA
      WRITE(9,645)SP1,SP2
C
   90 WRITE(6,908)T
      WRITE(6,910)(DIP(I),I=1,6)
      WRITE(6,911)HWHM,SIGMA
      WRITE(6,912)SP1,SP2
      WRITE(6,913)Q
      WRITE(6,918)JMIN,JMAX
      WRITE(6,919)FLOW,FUP
      WRITE(6,920)XLIM
      WRITE(6,705)
      CALL PREDICT(JMIN,JMAX,IREP)
      STOP
C
  600 FORMAT(10A8)
  610 FORMAT(I3)
  620 FORMAT(I1,2X,F15.6,2X,A8)
  625 FORMAT(X,1H1)
  630 FORMAT(2I3,2X,1H1,I3,43X,F12.4)
  634 FORMAT(8I4,F11.3,12X,F12.4)
  635 FORMAT(8I4,2F11.3,X,F12.4)
  640 FORMAT(X)
  645 FORMAT(6(F9.3,3X))
  650 FORMAT(D12.4)
  655 FORMAT(4I4,3F9.4)
  705 FORMAT(/25H UPPER LEVEL  LOWER LEVEL,37X,8HV=0 CHAR/10H  V  J Ka ,
     *60HKc   V  J Ka Kc     OBS/MHz   OBS-CALC     WEIGHT    %U    %L/)
```

```
706 FORMAT(/7X,24HUPPER LEVEL  LOWER LEVEL,12X,8HROT LINE,15X,8HV=0 CH
   *AR/74H  TYPE  V  J Ka Kc   V  J Ka Kc  FREQ/MHz  STRENGTH  INTENS*
   *cm     %U     %L/)
709 FORMAT(D10.4)
800 FORMAT(10A8)
900 FORMAT(/1X,30(4H----))
901 FORMAT(/X,10A8,3X,14H PROGRAM MALON)
902 FORMAT(/1X,11HA REDUCTION,10X,14HREPRESENTATION,A5)
903 FORMAT(/1X,I3,12H TRANSITIONS)
904 FORMAT(/1X,12HCYCLE NUMBER,I2)
905 FORMAT(/20H CALCULATED SPECTRUM/)
906 FORMAT(20H MOLECULAR CONSTANTS/)
907 FORMAT(1X,A8,F14.6)
908 FORMAT(//7H TEMP/K,10X,F7.3)
909 FORMAT(/7H CHIaa=,F9.4,9H   CHIbb=,F9.4,9H   CHIcc=,F9.4,4H MHz//
   *25H CALCULATED ENERGY LEVELS/)
910 FORMAT(12H DIPOLE(A)/D,5X,F7.3/12H DIPOLE(B)/D,5X,F7.3/
   *12H DIPOLE(C)/D,5X,F7.3/18H DIPOLE DERIV(A)/D,5X,F7.3/
   *18H DIPOLE DERIV(B)/D,5X,F7.3/18H DIPOLE DERIV(C)/D,5X,F7.3)
911 FORMAT(17H HWHM/(MHz/TORR) ,F7.3/11H SYM NUMBER,7X,F6.3)
912 FORMAT(14H NSPINWT (SP1) ,4X,F7.5/9X,5H(SP2),4X,F7.5)
913 FORMAT(/17H VIB BOLTZ FACTOR,4X,F10.5)
914 FORMAT(/30H     EFFECTIVE ROT. CONSTS./MHz
   */11H  V0 STATE ,3F14.6/11H  V1 STATE ,3F14.6)
915 FORMAT(/37H A REDUCED PRINCIPAL AXIS CONSTS./MHz)
916 FORMAT(/40H     EFFECTIVE PRINCIPAL AXIS CONSTS./MHz)
918 FORMAT(/1X,4HJMIN,I3,/1X,4HJMAX,I3)
919 FORMAT(/15H MIN FREQ/MHz  ,F12.4/15H MAX FREQ/MHz  ,F12.4)
920 FORMAT(/25H INTENSITY LIMIT/CM**-1  ,D10.4)
930 FORMAT(4I3)
940 FORMAT(4I4,3F9.4)
945 FORMAT(F1.0,I1,X,F15.6)
950 FORMAT(6F12.6)
960 FORMAT(D12.4)
    END
```

```
    BLOCK DATA
    IMPLICIT REAL*8 (A-H,O-Z)
    COMMON/ROTPAR/P(36),PFIX(36),FJK(60),PLABL(36)
    COMMON/ITAB/II(8,36)
    COMMON/INTDAT/BRIAN(18)
    DATA PFIX/36*0.0/,P/36*0.0/
    DATA PLABL/8H  DE/MHz,8H Txz/MHz,8H  Tj/KHz,8H Tk1/KHz,8H Tk2/KHz,
   *8H  DD/MHz,8H  XD/MHz,8H  YD/MHz,8H  ZD/MHz,8H  X1/MHz,8H  Y1/MHz,
   *8H  Z1/MHz,8H DJD/KHz,8HDJKD/KHz,8H DKD/KHz,8H dJD/KHz,8H dKD/KHz,
   *8H DJ1/KHz,8HDJK1/KHz,8H DK1/KHz,8H dJ1/KHz,8H dK1/KHz,8H  HJD/Hz,
   *8H HJKD/Hz,8H HKJD/Hz,8H  HKD/Hz,8H  hJD/Hz,8H hJKD/Hz,8H  hKD/Hz,
   *8H  HJ1/Hz,8H HJK1/Hz,8H HKJ1/Hz,8H  HK1/Hz,8H  hJ1/Hz,8H hJK1/Hz,
   *8H  hK1/Hz/
    DATA II/1,8*0,2,0,3,5*0,4,0,5,5*0,6,0,7,5*0,8,0,9,0,10,0,11,0,12,
   *6*0,13,3*0,14,3*0,15,3*0,16,3*0,17,7*0,18,3*0,19,3*0,20,3*0,21,
   *3*0,22,7*0,23,7*0,24,7*0,25,7*0,26,3*0,27,3*0,28,3*0,29,3*0,30,
   *7*0,31,7*0,32,7*0,33,3*0,34,3*0,35,3*0,36,3*0,37,7*0,38,7*0,39,
   *7*0,40,7*0,41,3*0,42,3*0,43,3*0,44,3*0,45,3*0,46,3*0,47,7*0,48,
   *7*0,49,7*0,50,7*0,51,3*0,52,3*0,53,3*0,54,3*0,55,3*0,56,3*0/
    DATA BRIAN/2.262,0.516,4*0.0,7900.0,42500.0,1.0,195.0,20.0,1.0,
   *3*0.0,1.0D-8,2*1.0/
    END
```

```
    SUBROUTINE ROTATE (X0,Y0,Z0,X1,Y1,Z1,IBAV)
    IMPLICIT REAL*8 (A-H,O-Z)
    COMMON/ROTPAR/P(36),PFIX(36),FJK(30),FJK1(30),PL(36)
    DX=X1-X0
    DYR=Y1-Y0
    DZ=Z1-Z0
    DXZ=(DX+DZ)/2.0
    XR=(X0+X1)/2.0
    Y=(Y0+Y1)/2.0
```

```
      ZR=(Z0+Z1)/2.0
      R2D=P(1)+DYR+DXZ
      ETAR=ZR-XR
      ETAP=SQRT(4.0*P(2)*P(2)+ETAR*ETAR)
      P2D=(R2D*ETAR)/ETAP
      DYP=P2D-P(1)-DXZ
      E11=(XR+ZR)/2.0
      XP=E11-ETAP/2.0
      ZP=E11+ETAP/2.0
      X1P=XP+DX/2.0
      X0P=XP-DX/2.0
      Y1P=Y+DYP/2.0
      Y0P=Y-DYP/2.0
      Z1P=ZP+DZ/2.0
      Z0P=ZP-DZ/2.0
      WRITE(6,10)X0P,Y0P,Z0P,X1P,Y1P,Z1P
      IF (IBAV.LT.1) RETURN
      QY=(R2D*P(2))/ETAP
      WRITE(6,20)QY
      WRITE(6,30)XP,Y,ZP
      RETURN
   10 FORMAT(11H (+) STATE ,3F14.6/11H (-) STATE ,3F14.6)
   20 FORMAT(/26H HIROTA'S PARAMETER Qy/MHz,F14.6)
   30 FORMAT(/28H  EFFECTIVE ROT. CONSTS./MHz/11x,3F14.6)
      END
```

```
      SUBROUTINE ENCAL(JEMIN,JEMAX,IREP,NOOP,CHY)
      IMPLICIT REAL*8 (A-H,O-Z)
      COMMON/BLANK/H(62,3),V(62,52),HS(62,56)
      COMMON/TAU/IT(62),ITT(300)
      COMMON/VDATA/NV(300)
      COMMON/PDATA/IP(300)
      COMMON/DERIVS/DER(150,36),CAL(150),DUM(9826)
      COMMON/ROTPAR/P(36),PFIX(36),FJK(30),FJK1(30),PL(36)
      DIMENSION CHY(3),NR(3,3)
      DATA NR/9,7,8,8,9,7,7,8,9/
      M1=NR(1,IREP)
      M2=NR(2,IREP)
      M3=NR(3,IREP)
      M4=M1+3
      M5=M2+3
      M6=M3+3
      CHI=0.0
C
      WRITE(6,20)
      J=JEMIN
      IODD=MOD(J,2)
   10 NA=2*J+2
      DO 13 I=1,NA
      H(I,1)=0.0
      IT(I)=0
      IP(I)=0
      DO 11 JA=1,NA
   11 V(JA,I)=0.0
   13 CONTINUE
      RK=0.0
      RJ=FLOAT(J*(J+1))
      DO 14 I=1,J
      FJK(I)=SQRT((RJ-RK*(RK+1.0))*(RJ-(RK+1.0)*(RK+2.0)))
      FJK1(I)=SQRT(RJ-RK*(RK+1.0))
      RK=RK+1.0
   14 CONTINUE
      LMAX=2
      IF (J.EQ.0) LMAX=1
      DO 16 L=1,LMAX
      CALL SETUP(J,L,N)
      M=MIN0(7,N-1)
```

```
      CALL BANDIG(N,M)
      CALL ASSIGN(N,L,J,IREP,NO,1)
      DO 18 I=1,NO
      IA=I+NO
      NV(I)=0
      NV(IA)=1
   18 CONTINUE
      DO 15 I=1,N
      IF (DABS(H(I,1)).LT.1.0D-5) GO TO 15
      DO 19 ID=1,12
      DER(I,ID)=0.0
   19 CONTINUE
      CALL DERCAL(I,I,1.0D0,N,12)
      KA=(J+IT(I)+1)/2
      KC=KA-IT(I)
      IF (J.EQ.0) GO TO 12
      RV=NV(I)
      CHI=(2.0/RJ)*(CHY(1)*(DER(I,M1)+DER(I,M4))+CHY(2)*(DER(I,M2)+
     *DER(I,M5))+CHY(3)*(DER(I,M3)+DER(I,M6)))
   12 WRITE(6,30)IP(I),NV(I),J,KA,KC,H(I,1),DER(I,1),DER(I,2),
     *DER(I,M1),DER(I,M2),DER(I,M3),DER(I,M4),DER(I,M5),DER(I,M6),CHI
   15 CONTINUE
   16 CONTINUE
      J=J+1
      IODD=1-IODD
      IF (JEMAX-J)17,10,10
   17 RETURN
   20 FORMAT(/50H %VO V  J Ka Kc   Energy/MHz   dE/dDE    dE/dT    ,
     *54HdE/dA0      dE/dB0      dE/dC0      dE/dA1      dE/dB1,
     *24H      dE/dC1     Chi/MHz/)
   30 FORMAT(X,I3,I2,3I3,F13.3,2F9.3,5F12.6,F10.4)
      END
```

```
      SUBROUTINE PREDICT(JMIN,JMAX,IREP)
      IMPLICIT REAL*8 (A-H,O-Z)
      COMMON/BLANK/H(62,3),V(62,62),HS(62,56)
      COMMON/FREQS/ES(300)
      COMMON/LDATA/IL(300)
      COMMON/TAU/IT(62),ITT(300)
      COMMON/VDATA/NV(300)
      COMMON/PDATA/IP(300)
      COMMON/DERIVS/VV(62,248)
      COMMON/ROTPAR/P(36),PFIX(36),FJK(30),FJK1(30),PLABEL(36)
      J=JMIN
      IODD=MOD(J,2)
      DO 10 I=1,62
      H(I,1)=0.0
      IT(I)=0
      DO 11 J1=1,62
   11 V(J1,I)=0.0
   10 CONTINUE
      DO 12 I=1,248
      ES(I)=0.0
      NV(I)=0
      ITT(I)=0
      IL(I)=0
      IP(I)=0
      DO 13 J1=1,62
   13 VV(J1,I)=0.0
   12 CONTINUE
   21 RK=0.0
      RJ=FLOAT(J*(J+1))
      DO 14 I=1,J
      FJK(I)=SQRT((RJ-RK*(RK+1.0))*(RJ-(RK+1.0)*(RK+2.0)))
      FJK1(I)=SQRT(RJ-RK*(RK+1.0))
      RK=RK+1.0
   14 CONTINUE
```

```
      LMAX=2
      IF(J.EQ.0)LMAX=1
      IF(J.EQ.JMIN)GO TO 15
C Move result of calc for previous J up to top half of each array
      DO 16 I=1,124
      II=I+124
      ES(II)=ES(I)
      IL(II)=IL(I)
      ES(I)=0.0
      IL(I)=0
      NV(II)=NV(I)
      NV(I)=0
      ITT(II)=ITT(I)
      ITT(I)=0
      IP(II)=IP(I)
      IP(I)=0
      DO 17 JJ=1,62
      VV(JJ,II)=VV(JJ,I)
      VV(JJ,I)=0.0
   17 CONTINUE
   16 CONTINUE
C
   15 DO 18 L=1,LMAX
      CALL SETUP(J,L,N)
      M=MINO(7,N-1)
      CALL BANDIG(N,M)
      CALL ASSIGN(N,L,J,IREP,NO,0)
      IND=62*(L-1)
      DO 19 I=1,N
      II=I+IND
      ES(II)=H(I,1)
      ITT(II)=IT(I)
      IL(II)=L
      DO 20 JJ=1,N
   20 VV(JJ,II)=V(JJ,I)
   19 CONTINUE
   18 CONTINUE
      CALL SELECT(J,IREP,JMIN)
      J=J+1
      IODD=1-IODD
      IF (J.LE.JMAX) GO TO 21
      RETURN
      END
```

```
      SUBROUTINE SELECT(J,IREP,JMIN)
      IMPLICIT REAL*8 (A-H,O-Z)
      LOGICAL ISEL
      COMMON/ROTPAR/P(6),X,Y,Z,SPARE(159)
      COMMON/FREQS/E(300)
      COMMON/LDATA/ILL(300)
      COMMON/TAU/IXY(62),IT(300)
      COMMON/VDATA/VV(300)
      COMMON/DERIVS/VV(62,248)
      COMMON/INTDAT/DIP(6),FLOW,FUP,SIGMA,T,HWHM,Q,EN,S,XINT,XLIM,SP1,
     *SP2
      COMMON/PDATA/IP(243),LEAVE(52)
      DIMENSION LB(9),TYPE(4)
      DATA TYPE/4H   A,4H   B,4H   C,4H   0/
      DATA LB/3,1,2,2,3,1,1,2,3/
      KD=0
      DO 13 KA=4,6
      IF(DIP(KA).LT.1.0D-6)GO TO 13
      KD=LB(KA-3+3*(IREP-1))
      KDA=KA
   13 CONTINUE
      DO 1 KA=1,3
```

```
      IF(DIP(KA).LT.1.0D-6)GO TO 1
      KX=LB(KA+3*(IREP-1))
      DO 2 IU=1,124
      IF(ILL(IU).EQ.0)GO TO 2
      KAU=(J+IT(IU)+1)/2
      KCU=KAU-IT(IJ)
      I1=IU+1
C Selection of Q branch transitions
      DO 3 IL=I1,124
      IF(ILL(IL).EQ.0.OR.IL.EQ.125)GO TO 3
      KX=LB(KA+3*(IREP-1))
      ISEL=.FALSE.
      IUL=ILL(IU)-ILL(IL)
      IF(KX.EQ.1.AND.IJL.NE.0)ISEL=.TRUE.
      IF(KX.EQ.2.AND.IUL.EQ.0)ISEL=.TRUE.
      IF(KX.EQ.3.AND.IJL.NE.0)ISEL=.TRUE.
      IF(.NOT.ISEL)GO TO 3
      EN=E(IU)-E(IL)
      IF(ABS(EN).LT.FLOW.OR.ABS(EN).GT.FUP)GO TO 3
      JL=J
      CALL INTENS(J,JL,KX,KD,KA,KDA,IU,IL)
      IF(XINT.LT.XLIM)GO TO 3
      KAL=(J+IT(IL)+1)/2
      KCL=KAL-IT(IL)
      IX=4
      MA=MOD(IABS(KAU-KAL),2)
      MC=MOD(IABS(KCU-KCL),2)
      IF((MA.EQ.0).AND.(MC.EQ.1)) IX=1
      IF((MA.EQ.1).AND.(MC.EQ.1)) IX=2
      IF((MA.EQ.1).AND.(MC.EQ.0)) IX=3
      IF(EN.GT.0)WRITE(6,20)TYPE(IX),NV(IU),J,KAU,KCU,NV(IL),J,KAL,KCL,
     *EN,S,XINT,IP(IU),IP(IL)
      EX=-EN
      IF(EN.LT.0)WRITE(6,20)TYPE(IX),NV(IL),J,KAL,KCL,NV(IU),J,KAU,KCU,
     *EX,S,XINT,IP(IL),IP(IU)
    3 CONTINUE
      IF (J.EQ.JMIN) GO TO 2
C Selection of P and R branch transitions
      DO 8 IL=125,248
      IF(ILL(IL).EQ.0) GO TO 8
      KX=LB(KA+3*(IREP-1))
      ISEL=.FALSE.
      IUL=ILL(IU)-ILL(IL)
      IF(KX.EQ.1.AND.IJL.EQ.0)ISEL=.TRUE.
      IF(KX.EQ.2.AND.IJL.NE.0)ISEL=.TRUE.
      IF(KX.EQ.3.AND.IJL.EQ.0)ISEL=.TRUE.
   12 IF(.NOT.ISEL) GO TO 8
      EN=E(IU)-E(IL)
      IF(ABS(EN).LT.FLOW.OR.ABS(EN).GT.FUP) GO TO 8
      JL=J-1
      CALL INTENS(J,JL,KX,KD,KA,KDA,IU,IL)
      IF(XINT.LT.XLIM) GO TO 8
      KAL=(J+IT(IL))/2
      KCL=KAL-IT(IL)
      IX=4
      MA=MOD(IABS(KAU-KAL),2)
      MC=MOD(IABS(KCU-KCL),2)
      IF ((MA.EQ.0).AND.(MC.EQ.1)) IX=1
      IF ((MA.EQ.1).AND.(MC.EQ.1)) IX=2
      IF ((MA.EQ.1).AND.(MC.EQ.0)) IX=3
      IF(EN.GT.0)WRITE(6,20)TYPE(IX),NV(IU),J,KAU,KCU,NV(IL),JL,KAL,KCL,
     *EN,S,XINT,IP(IU),IP(IL)
      EX=-EN
      IF(EN.LT.0)WRITE(6,20)TYPE(IX),NV(IL),JL,KAL,KCL,NV(IU),J,KAU,KCU,
     *EX,S,XINT,IP(IL),IP(IU)
    8 CONTINUE
    2 CONTINUE
```

```
    1 CONTINUE
   20 FORMAT(X,A4,I4,3I3,2H -,I2,3I3,F11.3,X,F7.3,3X,D9.3,I6,3H - ,I3)
      RETURN
      END
```

```
      SUBROUTINE INTENS(JU,JL,KX,KD,KA,KDA,IU,IL)
C Do not input non-zero Y-type dipole moment derivatives.
      IMPLICIT REAL*8 (A-H,O-Z)
      COMMON/ROTPAR/P(6),X,Y,Z,SPARE(159)
      COMMON/FREQS/E(300)
      COMMON/LDATA/ILL(300)
      COMMON/PDATA/IP(300)
      COMMON/DERIVS/V(62,248)
      COMMON/INTDAT/DIP(6),FLOW,FUP,SIGMA,T,HW,Q,EN,S,XINT,XLIM,SP1,
     *SP2
C
      S2=0.0
      S1=0.0
      I9=0
    4 S=0.0
      ID1=0
      IF (I9.EQ.1) ID1=1
      DO 7 I=1,2
      NV=I-1
      IX1=1+NV+ID1
      JL1=JL+1
      JU1=JU+1
      KL=0
      IF (ILL(IL).EQ.2)KL=1
      ML=KL+1
      KU=0
      IF (ILL(IU).EQ.2)KJ=1
      MU=KU+1
      DO 2 L1=ML,JL1
      KU=0
      IF (ILL(IU).EQ.2)KJ=1
      IX=1+NV
      DO 3 L2=MU,JU1
      IF(KX.EQ.3.AND.KL.EQ.KU)S=S+PHI(KX,JL,JU,KL,KU)*V(IX,IU)*V(IX1,IL)
      IF(KX.NE.3.AND.IABS(KL-KU).EQ.1)S=S+PHI(KX,JL,JU,KL,KU)*
     *V(IX,IU)*V(IX1,IL)
      IX=IX+2
      KU=KU+1
    3 CONTINUE
      IX1=IX1+2
      KL=KL+1
    2 CONTINUE
      IF (I9.EQ.1) ID1=-1
    7 CONTINUE
      IF (KX.EQ.2.AND.EN.LT.0) S=-S
      J=JL
      XJ=FLOAT(J)
      AX=1.0/(4.0*(XJ+1.0))
      IF (JU.EQ.JL) AX=AX*(2.0*XJ+1.0)/XJ
      IF (I9.EQ.0) S1=DIP(KA)*SQRT(AX)*S
      I9=I9+1
      IF (I9.EQ.2) GO TO 6
      KX=KD
      IF (KX.NE.0) GO TO 4
    6 IF (KX.NE.0) S2=DIP(KDA)*SQRT(AX)*S
      BETA=SP1
      IF (ILL(IL).EQ.2) BETA=SP2
      S=BETA*(S1+S2)*(S1+S2)
      ER=DMIN1(E(IU),E(IL))
      E7=EXP(-4.79927455D-5*ER/T)
      XINT=1.15210D-11*SQRT(X*Y*Z)*S*EN**2*SIGMA*Q*E7/(HW*T**3.5)
      RETURN
      END
```

```
      FUNCTION PHI(IALPHA,JL,JU,KL,KU)
      IMPLICIT REAL*8 (A-H,O-Z)
      J=JL
      IF (IALPHA.NE.3) GO TO 1
      PHI=2.0*FLOAT(KU)
      IF (JL.NE.JU) PHI=2.0*SQRT(FLOAT((J+1)*(J+1)-KU*KU))
      RETURN
    1 IF (JL.NE.JU) GO TO 2
      K=MINO(KU,KL)
      PHI=SQRT(FLOAT(J*(J+1)-K*(K+1)))
      IF (K.EQ.0) PHI=SQRT(2.0)*PHI
      IF (IALPHA.EQ.2.AND.KU.GT.KL) PHI=-PHI
      RETURN
    2 K=KL
      IF (KL.GT.KU) GO TO 3
      PHI=-SQRT(FLOAT((J+K+1)*(J+K+2)))
      IF (K.EQ.0) PHI=SQRT(2.0)*PHI
      RETURN
    3 PHI=SQRT(FLOAT((J-K+1)*(J-K+2)))
      IF((K-1).EQ.0) PHI=SQRT(2.0)*PHI
      IF (IALPHA.EQ.2) PHI=-PHI
      RETURN
      END
```

```
      SUBROUTINE INPUT (JRMIN,JRMAX,NUM)
      IMPLICIT REAL*8 (A-H,O-Z)
      COMMON/FREQS/OBS(150),WT(150)
      COMMON/VDATA/IVU(150),IVL(150)
      COMMON/JDATA/JU(150),JL(150)
      COMMON/TAU/IT(62),JTU(150),JTL(150)
      JRMAX=0
      JRMIN=101
      DO 2 I=1,150
      READ(5,20)IVU(I),IVL(I),JU(I),KAU,KCU,JL(I),KAL,KCL,OBS(I),U
      IF(JU(I)+JL(I))1,3,1
    1 JRMIN=MINO(JRMIN,JU(I),JL(I))
      JRMAX=MAXO(JRMAX,JU(I),JL(I))
      WT(I)=1.0
      IF (U.GT.1.0D-6)WT(I)=1.0/(U*U)
      JTU(I)=KAU-KCU
      JTL(I)=KAL-KCL
    2 CONTINUE
    3 NUM=I-1
      N1=NUM-1
      DO 5 I=1,N1
      J1=JU(I)
      K=I
      I1=I+1
      DO 4 J=I1,NUM
      IF (JU(J)-J1)6,6,4
    6 K=J
      J1=JU(J)
    4 CONTINUE
      IF (K-I)7,5,7
    7 JU(K)=JU(I)
      JU(I)=J1
      J1=JTU(K)
      JTU(K)=JTU(I)
      JTU(I)=J1
      J1=JL(K)
      JL(K)=JL(I)
      JL(I)=J1
      J1=JTL(K)
      JTL(K)=JTL(I)
      JTL(I)=J1
      J1=IVU(K)
```

```
      IVU(K)=IVU(I)
      IVU(I)=J1
      J1=IVL(K)
      IVL(K)=IVL(I)
      IVL(I)=J1
      U=OBS(K)
      OBS(K)=OBS(I)
      OBS(I)=U
      U=WT(K)
      WT(K)=WT(I)
      WT(I)=U
    5 CONTINUE
      RETURN
   20 FORMAT(8I4,2F11.3)
      END
```

```
      SUBROUTINE SETUP(J,L,N)
      IMPLICIT REAL*8 (A-H,O-Z)
      COMMON/BLANK/H(62,3),V(62,62),HS(62,56)
      COMMON/ROTPAR/EX,T1,T2,T3,T4,DD,X(6),D(10),HH(14),PFIX(36),
     *FJK(30),FJK1(30),PLABEL(36)
      DIMENSION HD(62,5),HE(62,1)
      DA=0.0
      DB=0.0
      DC=0.0
      DE1=0.0
      D1=0.5*(DB+DC)
      D2=DA-D1
      D3=0.5*(DB-DC)
      F1=FLOAT(J*(J+1))
      F2=F1*F1
      F3=F1*F2
      DO 10 I=1,62
      DO 11 K=1,8
   11 H(I,K)=0.0
      DO 12 K=1,56
   12 HS(I,K)=0.0
      DO 14 I1=1,5
      HD(I,I1)=0.0
   14 CONTINUE
   10 CONTINUE
      I=1
      ZI=1
      IF (L-1) 1,1,2
    1 K=0
      ZI=SQRT(2.0)
      YI=-1.0
      GO TO 7
    2 K=1
      YI=1.0
      GO TO 7
    5 I=I+1
      IODD=MOD(I,2)
      K=K+IODD
      IF (K.EQ.0) ZI=SQRT(2.0)
    7 IF (K.GT.J) GO TO 6
      C1=FLOAT(K*K)
      C2=C1*C1
      C3=C1*C2
      RK=FLOAT(K)
      IODD=MOD(I,2)
      ODD=FLOAT(IODD)
      EVEN=1.0-ODD
      HS(I,1)=1.0*EVEN
      HS(I,12)=1.0*ODD
      HD(I,1)=F1*ODD
      HD(I,2)=C1*ODD
```

```
      IF (K.EQ.1) HD(I,5)=ODD*YI*F1*0.5
      HS(I,13)=(F1-C1)*ODD/2
      HS(I,15)=HS(I,13)
      HS(I,18)=(F1-C1)*EVEN/2
      HS(I,20)=HS(I,18)
      HS(I,17)=C1*ODD
      HS(I,22)=C1*EVEN
      HS(I,23)=-F2*ODD
      HS(I,30)=-F2*EVEN
      HS(I,24)=-F1*C1*ODD
      HS(I,31)=-F1*C1*EVEN
      HS(I,25)=-C2*ODD
      HS(I,32)=-C2*EVEN
      HS(I,37)=F3*ODD
      HS(I,47)=F3*EVEN
      HS(I,38)=F2*C1*ODD
      HS(I,48)=F2*C1*EVEN
      HS(I,39)=F1*C2*ODD
      HS(I,49)=F1*C2*EVEN
      HS(I,40)=C3*ODD
      HS(I,50)=C3*EVEN
      IF (K.NE.1) GO TO 8
      HS(I,13)=HS(I,13)+0.25*YI*F1*ODD
      HS(I,18)=HS(I,18)+0.25*YI*F1*EVEN
      HS(I,15)=HS(I,15)-0.25*YI*F1*ODD
      HS(I,20)=HS(I,20)-0.25*YI*F1*EVEN
      HS(I,26)=-YI*F2*ODD
      HS(I,33)=-YI*F2*EVEN
      HS(I,28)=-YI*F1*ODD
      HS(I,35)=-YI*F1*EVEN
      HS(I,41)=YI*F3*ODD
      HS(I,51)=YI*F3*EVEN
      HS(I,43)=YI*F2*ODD
      HS(I,53)=YI*F2*EVEN
      HS(I,45)=YI*F1*ODD
      HS(I,55)=YI*F1*EVEN
    8 IF (K.GE.(J-2)) GO TO 9
      B1=FJK1(K+1)
      B2=FJK1(K+2)
      B3=FJK1(K+3)
      R3=2.0*RK+3
      HS(I,10)=0.5*R3*B1*B2*B3*ZI*EVEN
      HS(I,11)=0.5*R3*B1*B2*B3*ZI*ODD
    9 IF (K.GE.(J-1)) GO TO 25
      A=FJK(K+1)/4.0
      C4=(RK+2.0)*(RK+2.0)
      HS(I,14)=ZI*A*ODD
      HS(I,19)=ZI*A*EVEN
      HS(I,16)=-HS(I,14)
      HS(I,21)=-HS(I,19)
      HS(I,27)=-4.0*A*F1*ZI*ODD
      HS(I,34)=-4.0*A*F1*ZI*EVEN
      HS(I,29)=-2.0*A*(C4+C1)*ZI*ODD
      HS(I,36)=-2.0*A*(C4+C1)*ZI*EVEN
      HS(I,42)=4.0*A*F2*ZI*ODD
      HS(I,52)=4.0*A*F2*ZI*EVEN
      HS(I,44)=-HS(I,29)*F1
      HS(I,54)=-HS(I,35)*F1
      HS(I,46)=2.0*A*(C2+C4*C4)*ZI*ODD
      HS(I,56)=2.0*A*(C2+C4*C4)*ZI*EVEN
      HD(I,4)=0.5*ZI*ODD*4.0*A
      HD(I,3)=0.5*ZI*EVEN*4.0*A
   25 IF (K.GE.J) GO TO 15
      B1=FJK1(K+1)
      R1=RK*(RK+1.0)
      R2=2.0*RK+1.0
```

```
      HS(I,2)=0.5*R2*SQRT(F1-R1)*ZI*EVEN
      HS(I,3)=0.5*R2*SQRT(F1-R1)*ZI*ODD
      HE(I,1)=0.5*R2*SQRT(F1-R1)*ZI
      HS(I,4)=HS(I,2)*F1
      HS(I,5)=HS(I,3)*F1
      HS(I,6)=(2.0*C1*C1+R2)*HS(I,2)
      HS(I,7)=(2.0*C1*C1+R2)*HS(I,3)
      R4=2.0*RK-1.0
      R5=RK*(RK-1.0)
      R6=(RK+1.0)*(RK+1.0)
      R7=2.0*RK+3.0
      HS(I,8)=(0.25*R4*(F1-R5)+0.25*R7*(F1-R6))*B1*ZI*EVEN
      HS(I,9)=(0.25*R4*(F1-R5)+0.25*R7*(F1-R6))*B1*ZI*ODD
      IF (K.NE.1) GO TO 15
      HS(I,8)=HS(I,8)+YI*0.5*F1*EVEN
      HS(I,9)=HS(I,9)+YI*0.5*F1*ODD
   15 ZI=1.0
      GO TO 5
    6 N=I-1
      DO 13 I=1,N
      H(I,1)=HS(I,1)*EX+HS(I,13)*X(1)+HS(I,15)*X(2)+HS(I,17)*X(3)
     !+HS(I,18)*X(4)+HS(I,20)*X(5)+HS(I,22)*X(6)+HS(I,23)*D(1)
     !+HS(I,24)*D(2)+HS(I,25)*D(3)+HS(I,26)*D(4)+HS(I,28)*D(5)
     !+HS(I,30)*D(6)+HS(I,31)*D(7)+HS(I,32)*D(8)+HS(I,33)*D(9)
     !+HS(I,35)*D(10)+HS(I,37)*HH(1)+HS(I,38)*HH(2)+HS(I,39)*HH(3)
     !+HS(I,40)*HH(4)+HS(I,41)*HH(5)+HS(I,43)*HH(6)+HS(I,45)*HH(7)
     !+HS(I,47)*HH(8)+HS(I,48)*HH(9)+HS(I,49)*HH(10)+HS(I,50)*HH(11)
     !+HS(I,51)*HH(12)+HS(I,53)*HH(13)+HS(I,55)*HH(14)
      IF (I.EQ.N) RETURN
      H(I,2)=HS(I,2)*T1+HS(I,4)*T2+HS(I,6)*T3+HS(I,8)*T4+HS(I,12)*DD
     !+HD(I,1)*D1+HD(I,2)*D2+HD(I,5)*D3
      IF (I.EQ.(N-1)) GO TO 13
      H(I,3)=HE(I,1)*DE1
      IF (I.EQ.(N-2)) GO TO 13
      H(I,4)=HS(I,3)*T1+HS(I,5)*T2+HS(I,7)*T3+HS(I,9)*T4+HD(I,3)*D3
      IF (I.EQ.(N-3)) GO TO 13
      H(I,5)=HS(I,14)*X(1)+HS(I,16)*X(2)+HS(I,19)*X(4)+HS(I,21)*X(5)
     !+HS(I,27)*D(4)+HS(I,29)*D(5)+HS(I,34)*D(9)+HS(I,36)*D(10)
     !+HS(I,42)*HH(5)+HS(I,44)*HH(6)+HS(I,46)*HH(7)+HS(I,52)*HH(12)
     !+HS(I,54)*HH(13)+HS(I,56)*HH(14)
      IF (I.EQ.(N-4)) GO TO 13
      H(I,6)=HS(I,10)*T4+HD(I,4)*D3
      IF (I.EQ.(N-5)) GO TO 13
      H(I,8)=HS(I,11)*T4
   13 CONTINUE
      END
```

```
      SUBROUTINE ASSIGN(N,L,J,IREP,NO,NCYCLE)
      IMPLICIT REAL*8 (A-H,O-Z)
      COMMON/BLANK/H(62,3),V(62,62),HS(62,56)
      COMMON/TAU/IT(62),IDUM(300)
      COMMON/VDATA/NV(300)
      COMMON/PDATA/IP(300)
      DIMENSION LB1(12),LB2(12)
      DATA LB1/3*0,1,0,0,1,2,1,0,2,1/
      DATA LB2/3,1,2,2,1,2,2,5*3/
      NO=N/2
      DO 1 I=1,NO
      TEMP=0.0
      DO 2 IZ=1,N,2
      T=V(IZ,I)
    2 TEMP=TEMP+T*T
      IX=I
      I1=I+1
      DO 3 IY=I1,N
      TEMP1=0.0
```

```
      DO 4 IZ=1,N,2
      T=V(IZ,IY)
    4 TEMP1=TEMP1+T*T
      IF (TEMP.GT.TEMP1) GO TO 5
      TEMP=TEMP1
      IX=IY
    5 CONTINUE
    3 CONTINUE
      TEMP=H(IX,1)
      H(IX,1)=H(I,1)
      H(I,1)=TEMP
      DO 6 IZ=1,N
      TEMP=V(IZ,I)
      V(IZ,I)=V(IZ,IX)
    6 V(IZ,IX)=TEMP
    1 CONTINUE
      N2=0
      N3=1
      N4=NO-1
      N5=NO
      IF (NO.EQ.1) GO TO 7
   12 DO 8 I=N3,N4
      TEMP=H(I,1)
      IX=I
      I1=I+1
      DO 9 IY=I1,N5
      IF (TEMP.GT.H(IY,1)) GO TO 9
      TEMP=H(IY,1)
      IX=IY
    9 CONTINUE
      H(IX,1)=H(I,1)
      H(I,1)=TEMP
      DO 10 IZ=1,N
      TEMP=V(IZ,I)
      V(IZ,I)=V(IZ,IX)
   10 V(IZ,IX)=TEMP
    8 CONTINUE
      N2=N2+1
      N3=NO+1
      N4=N-1
      N5=N
      IF (N2.EQ.1) GO TO 12
    7 CONTINUE
      JODD=MOD(J,2)
      IX1=IREP+3*JODD+6*(L-1)
      ITAU1=J-LB1(IX1)
      ITAU2=J-LB2(IX1)
      IND=62*(L-1)
      IODD=1
      DO 13 I=1,NO
      I1=I+NO
      IF (NCYCLE.NE.0) GO TO 16
      S1=0.0
      S2=0.0
      DO 15 IZ=1,N,2
      S1=S1+V(IZ,I)*V(IZ,I)
      S2=S2+V(IZ,I1)*V(IZ,I1)
   15 CONTINUE
      IP(I+IND)=IDINT(100.0*S1+0.5)
      IP(I1+IND)=IDINT(100.0*S2+0.5)
      NV(I+IND)=0
      NV(I1+IND)=1
   16 IF (IODD.EQ.0) GO TO 14
      IT(I)=ITAU1
      IT(I1)=ITAU1
      ITAU1=ITAU1-4
      GO TO 13
```

```
   14 IT(I)=ITAU2
      IT(I1)=ITAU2
      ITAU2=ITAU2-4
   13 IODD=1-IODD
      RETURN
      END
```

```
      SUBROUTINE DERCAL(K,I,XI,N,NOOP)
C The look up table "II(8,36)" is initialised as block data.
      IMPLICIT REAL*8 (A-H,O-Z)
      COMMON/ITAB/II(8,35)
      COMMON/BLANK/H(62,3),V(62,62),HS(62,56)
      COMMON/DERIVS/DER(150,36),CAL(150),DUM(9826)
      COMMON/PDATA/IPU(150),IPL(150)
C
      DO 3 M=1,NOOP
      L1=0
      DO 4 L=1,8
      K1=II(L,M)
      IF (K1) 4,4,1
    1 FACT=2.0*XI
      IF (L.EQ.1) FACT=XI
      DO 5 J=1,N
      J1=J+L1
      IF (J1-N) 2,2,5
    2 DER(I,M)=DER(I,M)+FACT*V(J,K)*V(J1,K)*HS(J,K1)
    5 CONTINUE
    4 L1=L1+1
    3 CONTINUE
      CAL(I)=CAL(I)+XI*H(K,1)
      S1=0.0
      DO 6 IZ=1,N,2
      S1=S1+V(IZ,K)*V(IZ,K)
    6 CONTINUE
      IF (XI.LT.0) IPL(I)=IDINT(100.0*S1+0.5)
      IF (XI.GT.0) IPU(I)=IDINT(100.0*S1+0.5)
      RETURN
      END
```

```
      SUBROUTINE LSQ(N,M,TEST,IREP,NOPR,EE)
      IMPLICIT REAL*8 (A-H,O-Z)
      DIMENSION DD(35),Y(36),E(35)
      COMMON/WIN/DWD(36,36)
      COMMON/ROTPAR/P(36),PFIX(35),FJK(30),FJK1(30),PLABEL(36)
      COMMON/DERIVS/D(150,36),C(150),DUM(9826)
      COMMON/FREQS/OBS(150),WT(150)
      COMMON/VDATA/IVU(150),IVL(150)
      COMMON/JDATA/JU(150),JL(150)
      COMMON/TAU/IT(62),JTU(150),JTL(150)
      COMMON/PDATA/IPU(150),IPL(150)
      S0=0.0
      S1=0.0
      S2=0.0
      DO 2 I=1,M
      DO 2 J=1,M
      Y(J)=0.0
    2 DWD(I,J)=0.0
      NEFF=0
      DO 3 I=1,N
      IF (WT(I).GT.1.0D-6) NEFF=NEFF+1
      S0=S0+WT(I)
      RES=OBS(I)-C(I)
      KAL=(JTL(I)+JL(I)+1)/2
      KCL=KAL-JTL(I)
      KAU=(JTU(I)+JU(I)+1)/2
      KCU=KAU-JTU(I)
```

```
      IF(WT(I).EQ.1.0)WRITE(6,85)IVJ(I),JU(I),KAU,KCU,IVL(I),JL(I),KAL,
     *KCL,OBS(I),RES,IPU(I),IPL(I)
      IF(WT(I).NE.1.0)WRITE(6,86)IVJ(I),JU(I),KAU,KCU,IVL(I),JL(I),KAL,
     *KCL,OBS(I),RES,WT(I),IPU(I),IPL(I)
      S1=S1+WT(I)*RES*RES
      S2=S2+WT(I)*C(I)*C(I)
      DO 40 J=1,M
      IF (PFIX(J).LT.0.5) D(I,J)=0.0
   40 CONTINUE
      DO 4 J=1,M
      Y(J)=Y(J)+WT(I)*RES*D(I,J)
      DO 4 K=J,M
      DWD(K,J)=DWD(K,J)+WT(I)*D(I,K)*D(I,J)
    4 DWD(J,K)=DWD(K,J)
    3 CONTINUE
      DO 30 J=1,M
      IF (PFIX(J).LT.0.5) DWD(J,J)=1.0
   30 CONTINUE
      CALL GAUJDN(M)
      DO 33 J=1,M
      DO 33 K=1,J
      DWD(K,J)=DWD(J,K)
   33 CONTINUE
      SO=SO/FLOAT(NEFF)
      S4=0.0
      DO 35 J=1,M
   35 S4=S4+PFIX(J)
      S4=FLOAT(NEFF)-S4
      F=SQRT(S1/S4)
      DO 5 J=1,M
      DD(J)=0.0
      DO 5 K=1,M
    5 DD(J)=DD(J)+DWD(J,K)*Y(K)
      WRITE(6,60)
      S3=0.0
      LFLAG=0
      DO 7 J=1,M
      S3=S3+DD(J)*Y(J)
      E(J)=F*SQRT(DWD(J,J))
      CONST=1.0
      IF (J.GE.3.AND.J.LE.5) CONST=1000.0
      IF (J.GE.13) CONST=1000.0
      IF (J.GE.23) CONST=1.0D6
      IF (PFIX(J)-0.5) 31,31,32
   31 E(J)=0.0
      DD(J)=0.0
      IF (P(J).EQ.0.0) GO TO 7
      PP1=CONST*P(J)
      WRITE(6,70)PLABEL(J),PP1
      GO TO 7
   32 P1=P(J)+DD(J)
      PP1=CONST*DD(J)
      PP2=CONST*P1
      PP3=CONST*E(J)
      WRITE(6,80)PLABEL(J),PP1,PP2,PP3
      P(J)=P1
      DD(J)=E(J)
    7 CONTINUE
      WRITE(6,9)
      S3=S1-S3
      WRITE(6,10)S1,S3
      S1=SQRT(S1/S2)
      EE=F/SQRT(SO)
      WRITE(6,11)EE,F
      IF (LFLAG) 49,49,51
```

```
   49 IF (ABS(TEST-S1)-1.0D-5) 50,51,51
   50 TEST=-999.0
      WRITE(6,16)
      GO TO 52
   51 TEST=S1
   52 IF (NOPR.NE.1) RETURN
      WRITE(6,12)
      J1=1
      DO 13 J=1,M
      IF(PFIX(J).LT.0.5) GO TO 13
      I1=1
      DO 14 I=1,J
      IF (PFIX(I).LT.0.5) GO TO 14
      DWD(J1,I1)=DWD(J,I)*F*F/(DD(I)*DD(J))
      I1=I1+1
   14 CONTINUE
      J1=J1+1
   13 CONTINUE
      J1=J1-1
      K=15
      L=1
   19 WRITE(6,17)
      DO 18 I=L,J1
      K1=MIN0(I,K)
   18 WRITE(6,15)(DWD(I,J),J=L,K1)
      L=L+15
      K=K+15
      IF (L.LE.J1) GO TO 19
      RETURN
   60 FORMAT(/49H PARAMETER    CALC SHIFT      NEW VALUE        E.S.D./)
   70 FORMAT(X,A8,6X,5HCONST,3X,F14.6)
   80 FORMAT(X,A8,3F14.6)
   85 FORMAT(X,I2,3I3,2H -,I2,3I3,2F11.3,14X,I3,3H - ,I3)
   86 FORMAT(X,I2,3I3,2H -,I2,3I3,3F11.3,3X,I3,3H - ,I3)
    8 FORMAT(1X,A8,F14.6,3F15.6,4X,A8)
    9 FORMAT(/32X,12HBEFORE CYCLE,8X,11HAFTER CYCLE)
   10 FORMAT(23H WEIGHTED SQ ERROR SUM ,2D20.5)
   11 FORMAT(/38H WEIGHTED STANDARD DEVIATION OF FIT IS,17X,
     *F15.6,5H  MHz/
     *55H STANDARD DEVIATION OF AN OBSERVATION OF UNIT WEIGHT IS,
     *F15.6,5H  MHz)
   12 FORMAT(/19H CORRELATION MATRIX)
   15 FORMAT(1X,15F8.3)
   16 FORMAT(/21H REFINEMENT CONVERGED)
   17 FORMAT(1H )
      END
```

```
      SUBROUTINE GAUJDN(N)
C GAUSS-JORDAN ALGORITHM FOR INVERSION OF A POSITIVE DEFINITE MATRIX.
C UPPER TRIANGLE RETAINS INPUT, LOWER TRIANGLE IS INVERSE.
      IMPLICIT REAL*8 (A-H,O-Z)
      DIMENSION H(36)
      COMMON/WIN/A(36,36)
      IF (N.LE.1) GO TO 8
      K=N
      DO 5 KK=1,N
      P=A(1,1)
      IF (P.LE.0.0)STOP'Normal matrix fails to invert'
      DO 3 I=2,N
      Q=A(I,1)
      QM=-Q
      IF (I.GT.K) QM=Q
      H(I)=QM/P
      DO 2 J=2,I
    2 A(I-1,J-1)=A(I,J)+Q*H(J)
    3 CONTINUE
```

```
      A(N,N)=1.0/P
      DO 4 I=2,N
    4 A(N,I-1)=H(I)
    5 K=K-1
      RETURN
    8 A(1,1)=1.0/A(1,1)
      RETURN
      END
```

```
      SUBROUTINE BANDIG(N,M)
C ADAPTED FROM LINEAR ALGEBRA BANDRD AND TQL2.
C
C BANDRD WITH TRANSFORMATION MATRIX SAVED.
C USING HOUSEHOLDER'S TRANSFORMATION, CONVERTS MATRIX TO BAND-DIAGONAL
      IMPLICIT REAL*8 (A-H,O-Z)
      DIMENSION D(62),E(62)
      COMMON/BLANK/A(62,8),V(62,62),HS(62,56)
      EQUIVALENCE (D(1),A(1,1)),(E(1),A(1,2))
      IN=N-1
      DO 1 I=1,IN
      V(I,I)=1.0
      K=I+1
      DO 1 J=K,N
      V(I,J)=0.0
    1 V(J,I)=0.0
      V(N,N)=1.0
      M1=M-1
      IF (M1) 100,99,98
   98 CONTINUE
      G=0.0
      N2=N-2
      DO 16 K=1,N2
      NK=N-K
      MAXR=MINO(NK,M)
      NR=MAXR
      DO 15 IR=2,MAXR
      KR=K+NR
      DO 14 J=KR,N,M
      IF (J-KR) 4,2,4
    2 IF (A(K,NR+1)) 3,15,3
    3 B=-A(K,NR)/A(K,NR+1)
      IU=K
      GO TO 6
    4 IF (G) 5,15,5
    5 B=-A(J-M-1,M+1)/G
      IU=J-M
    6 S=1.0/SQRT(1.0+B*B)
      C=B*S
      C2=C*C
      S2=S*S
      CS=C*S
      U=C2*A(J-1,1)-2.0*CS*A(J-1,2)+S2*A(J,1)
      U1=S2*A(J-1,1)+2.0*CS*A(J-1,2)+C2*A(J,1)
      A(J-1,2)=CS*(A(J-1,1)-A(J,1))+(C2-S2)*A(J-1,2)
      A(J-1,1)=U
      A(J,1)=U1
      J2=J-2
      DO 7 L=IU,J2
      U=C*A(L,J-L)-S*A(L,J-L+1)
      A(L,J-L+1)=S*A(L,J-L)+C*A(L,J-L+1)
    7 A(L,J-L)=U
      IF (J-KR) 8,9,8
    8 A(J-M-1,M+1)=C*A(J-M-1,M+1)-S*G
    9 NJ=N-J
      IF (NJ) 80,80,90
   90 MAXL=MINO(NJ,M1)
```

```
      DO 10 L=1,MAXL
      U=C*A(J-1,L+2)-S*A(J,L+1)
      A(J,L+1)=S*A(J-1,L+2)+C*A(J,L+1)
   10 A(J-1,L+2)=U
   80 IF (N-J-M) 12,11,11
   11 G=-S*A(J,M+1)
      A(J,M+1)=C*A(J,M+1)
   12 CONTINUE
      DO 13 L=1,N
      U=C*V(L,J-1)-S*V(L,J)
      V(L,J)=S*V(L,J-1)+C*V(L,J)
   13 V(L,J-1)=U
   14 CONTINUE
   15 NR=NR-1
   16 CONTINUE
   99 CONTINUE
      A(N,2)=0.0
C TQL2. QL ALGORITHM. CONVERTS BAND-DIAGONAL TO DIAGONAL MATRIX.
      E(N)=0.0
      B=0.0
      F=0.0
      EPS=1.0D-18
      DO 32 L=1,N
      J=0
      H=EPS*(DABS(D(L))+DABS(E(L)))
      B=DMAX1(B,H)
      DO 17 IM=L,N
      IF (B-ABS(E(IM))) 17,18,18
   17 CONTINUE
   18 IF (IM-L) 19,31,19
   19 IF (J.GE.30)STOP'Energy matrix fails to diagonalise'
      J=J+1
      G=D(L)
      P=(D(L+1)-G)/(2.0*E(L))
      R=SQRT(P*P+1.0)
      IF (P) 23,24,24
   23 P=P-R
      GO TO 25
   24 P=P+R
   25 D(L)=E(L)/P
      H=G-D(L)
      L1=L+1
      DO 26 I=L1,N
   26 D(I)=D(I)-H
      F=F+H
      P=D(IM)
      C=1.0
      S=0.0
      M1=IM-1
      I=M1
      DO 33 IL=L,M1
      G=C*E(I)
      H=C*P
      IF (DABS(P)-DABS(E(I))) 28,27,27
   27 C=E(I)/P
      R=SQRT(C*C+1.0)
      E(I+1)=S*P*R
      S=C/R
      C=1.0/R
      GO TO 29
   28 C=P/E(I)
      R=SQRT(C*C+1.0)
      E(I+1)=S*E(I)*R
      S=1.0/R
```

```
    C=C/R
 29 P=C*D(I)-S*G
    D(I+1)=H+S*(C*G+S*D(I))
    DO 30 K=1,N
    H=V(K,I+1)
    V(K,I+1)=S*V(K,I)+C*H
 30 V(K,I)=C*V(K,I)-S*H
 33 I=I-1
    E(L)=S*P
    D(L)=C*P
    IF (DABS(E(L))-B) 31,31,19
 31 D(L)=D(L)+F
 32 CONTINUE
100 CONTINUE
    RETURN
    END
```

REFERENCES

1. E.B. Wilson (1959) Adv. Chem. Phys., Vol. II, 367 - 393.

2. J.P. Lowe (1968) Progress in Physical Organic Chemistry, Vol.6, 1 - 80.

3. E.B. Wilson (1972) Chem. Soc. Rev., 1, 293 - 318.

4. W.J. Orville-Thomas (ed) Internal Rotation in Molecules, Wiley (1974). Ab-Initio Calculations; A. Veillard, Chapter 11.

5. D.G. Lister, J.N. MacDonald and N.L. Owen Internal Rotation and Inversion, Academic Press (1978).

6. C.R. Quade (1980) J. Chem. Phys., 73, 2107 - 2114.

7. P.A. Kollman and L.C. Allen (1970) Chem. Phys. Letts., 5, 75 - 76.

8. A.R. Mochel, L.L. Griffin, R.W. Kramling and J.E. Boggs (1973) J. Chem. Phys., 58, 4040 - 4041.

9. M.A. Basharov, M.V. Vol'Kenshtein, I.B. Golovanov, G.L. Ermakov, V.V. Nauchitel and V.M. Sobolev (1984) J. Struct. Chem. 25(1), 26 - 29.

   M.A. Basharov, M.V. Vol'Kenshtein, I.B. Golovanov and V.M. Sobolev (1984) J. Struct. Chem. 25(1) 30 - 34.

   M.A. Basharov, M.V. Vol'Kenshtein, I.B. Golovanov, G.L. Ermakov and V.M. Sobolev (1984) J. Struct. Chem. 25(2), 177 - 181.

10. R.M. Lees (1973) J. Chem. Phys., 59, 2690 - 2697.

11. C.E. Souter and J.L. Wood (1970) J. Chem. Phys., 52, 674 - 682.

12. A. Bauder and H.H. GÜnthard (1976) J. Mol. Spec., 60, 290 - 311.

13. C.E. Dykstra (1981) Ann. Rev. Phys. Chem., 35, 25 - 52.

14. D. Coffey, C.O. Britt and J.E. Boggs (1968) J. Chem. Phys., 49, 591 - 600.

15. C.C. Lin and J.D. Swalen (1959) Rev. Mod. Phys., 31, 841 - 892.

16. P.H. Turner (1976) PhD Thesis. Bristol University.

17. P.H. Turner and A.P. Cox (1978) J.C.S. Faraday II, 74, 533 - 559

18. W. Lüttke (1957) Z. Electrochem., 61, 302 - 313

19. A.J. Barnes, H.E. Hallam, S. Waring and R.J. Armstrong (1976) J.C.S. Faraday II, 72, 1 - 10.

20. C.R. Quade and C.C. Lin (1963) J. Chem. Phys., 38, 540 - 550.

21. R.W. Kilb, C.C. Lin and E.B. Wilson (1957) J. Chem. Phys., 26, 1695 - 1703.

22. P.H. Turner and A.P. Cox (1976) Chem. Phys. Letts., 42, 84 - 88.

Cont/d

23. D.C. McKean (1978) Chem. Soc. Rev., 7, 399 - 422.

24. P. Pulay (1984) Tenth Austin Symposium on Molecular-Structure, Austin, Texas. Paper TM1.

25. J.A. Hardy (1980) PhD Thesis. Bristol University.

26. P.H. Turner, A.P. Cox and J.A. Hardy (1981) J.C.S. Faraday II, 77, 1217 - 1231.

27. H.M. Pickett (1972) J. Chem. Phys., 56, 1715 - 1723.

28. C.S. Coe and T.F. Doumani (1948) J.A.C.S., 70, 1516 - 1519.

29. B.G. Gowenlock and J. Trotman (1955) J. Chem. Soc., 4190 - 4196.

30. D.C. Frost, W.M. Lau, C.A. McDowell and N.P.C. Westwood (1982) J. Phys. Chem., 86, 3577 - 3581.

31. B.G. Gowenlock and J. Trotman (1956) J. Chem. Soc., 1670 - 1675.

32. J.G. Calvert, S.S. Thomas and P.L. Hanst (1960) J.A.C.S., 82, 1 - 5.

33. G.R. McMillan, J.G. Calvert and S.S. Thomas (1964) J. Phys. Chem., 68, 116 - 120.

34. L. Batt, J.K. Brown, B.G. Gowenlock and K.E. Thomas (1962) J. Chem. Soc., 37 - 40.

35. J.O. Halford, L.C. Anderson and J.R. Bates (1934) J.A.C.S., 56, 491 - 492.

36. I.N. Levine (1962) PhD Thesis. Harvard University.

37. Eizi Hirota, Tomohiko Hirooka and Yonezo Morino (1968) J. Mol. Spec., 26, 351 - 367.

38. J.K.G. Watson (1977) Vibrational Spectra and Structure, 6, 1 - 89.

39. C. Eckart (1935) Phys. Rev., 47, 552 - 558.

40. B.P. VanEijck (1980) J. Mol. Spec., 82, 81 - 91.

41. H.M. Pickett and H.L. Strauss (1970) J.A.C.S., 92, 7281 - 7290.

42. W. Gordy and R.L. Cook, Microwave Molecular Spectra, Interscience (1970)

43. J.A. Hardy (1977) BSc Thesis. Bristol University.

44. J. Lawson (1981) BSc Thesis. Bristol University.

45. J.K. Bragg and S. Golden (1949) Phys. Rev., 75, 735 - 738.

46. E.A. Valenzuela and R.C. Woods (1974) J. Chem. Phys., 61, 4119 - 4128.

47. W. Bossert, J. Ekkers, A. Bauder and H.H. Günthard (1978) Chem. Phys. 27, 433 - 463.

Cont/d

48. G.L. Walker and C.R. Quade (1970) J. Chem. Phys., 52, 6427 - 6428.

49. T. Pedersen, A.P. Cox and D.W. Knight. Unpublished work.

50. B.P. VanEijck (1982) J. Mol. Spec., 91, 348 - 362.

51. E. Hirota (1966) J. Chem. Phys., 45, 1984 - 1990.

52. G.C. Petty (1984) PhD Thesis, Manchester (Victoria) University.

53. D.R. Herschbach (1959) J. Chem. Phys., 31, 91 - 108.

54. H. Hollenstein and F. Winther (1978) J. Mol. Spec., 71, 118 - 144.

55. J.S. Crighton and S. Bell (1985) J. Mol. Spec., 112, 315 - 327.

56. Takao Iijima and Shuzo Tsuchiya (1972) J. Mol. Spec., 44, 88 - 107.

57. J.S. Crighton and S. Bell (1985) J. Mol. Spec., 112, 285 - 303.

58. P. Nösberger, A. Bauder and H.H. Günthard (1973) Chem. Phys., 1, 418 - 425.

59. J.V. Knopp and C.R. Quade (1968) J. Chem. Phys., 48, 3317 - 3321.

60. Keietsu Tamagake and Masamichi Tsuboi (1974) J. Mol. Spec., 53, 204 - 220.

61. A. Serrallach, R. Meyer and H.H. Günthard (1974) J. Mol. Spec., 52, 94 - 129.

62. A. Serrallach and R. Meyer (1976) J. Mol. Spec., 60, 246 - 258.

63. Keietsu Tamagake, Masamichi Tsuboi and Akiko Y. Hirakawa (1969) J. Chem. Phys., 51, 2952 - 2603.

64. D.C. McKean and I.A. Ellis (1975) J. Mol Struct., 29, 81 - 96.

65. R.A. McPhail, R.G. Snyder and H.L. Strauss (1982) J. Chem. Phys., 77, 1118 - 1137.

66. R.M. Corn and H.L. Strauss (1982) J. Chem. Phys., 76, 4834 - 4843.

67. R.M. Corn and H.L. Strauss (1983) J. Chem. Phys., 79, 2641 - 2649.

68. Josef Pfab. Private Communication to A.P. Cox.

69. T.D. Allston, M.L. Fedyk and G.A. Takacs (1978) Chem. Phys. Letts., 60, 97 - 101.

70. M.J. Molina and F.S. Rowland (1974) Nature, 249, 810 - 812.

71. J.C. Farman, B.G. Gardiner and J.D. Shanklyn (1985) Nature, 315, 207 - 210.

'The Guardian' 30.5.85. Page 13.

Cont/d

72. J. Mason (1963) J. Chem. Soc., 4531 - 4544.

73. J. Mason (1953) J. Chem. Soc., 3755 - 3761

74. N.P. Ernsting and J. Pfab (1980) Spectrochim. Acta., 36A, 75 - 84.

75. N.P. Ernsting, J. Pfab, J.C. Green and J. Romelt (1980) J.C.S. Faraday II, 76, 844 - 859

76. B.M. DeKoven, Kwok Hang Fung, D.H. Levy, L.D. Hoffland and K.G. Spears (1981) J. Chem. Phys., 74, 4755 - 4764.

77. P.H. Turner and A.P. Cox (1976) Chem. Phys. Letts., 39, 585 - 587.

78. S.H. Bauer and A.L. Andreassen (1972) J. Phys. Chem., 76, 3099 - 3108.

79. A.P. Cox, G. Duxbury, J.A. Hardy and Yoshiyuki Kawashima (1980) J.C.S. Faraday II, 76, 339 - 350.

80. J.H. Carpenter (1974) J. Mol. Spec., 50, 182 - 201.

81. Allied Chemical Corp. (1959) U.S. Pat. No. 2,870,213.

82. B. Yamada, R.W. Campbell and O. Vogl (1977) J. Polym. Sci. Polym. Chem. ed., 15, 1123 - 1135.

83. P. Kubista and O. Vogl (1980) Polymer, 21, 525 - 532.

84. O.R. Pierce and T.G. Cane (1954) J.A.C.S., 76, 300 - 301.

85. M. Braid, H. Iserson and F.E. Lawlor (1954) J.A.C.S., 76, 4027.

86. R.C. Woods (1965) PhD Thesis. Harvard University, U.S.A.

87. R.C. Woods (1967) J. Chem. Phys., 46, 4789 - 4799.

88. J.H. Carpenter, J.D. Muse, C.E. Small and J.G. Smith (1982) J. Mol. Spec., 93, 286 - 306.

89. P.C. Cross, R.M. Hainer and G.W. King (1944) J. Chem. Phys., 12, 210 - 243.

90. A.P. Cox and J. Randell. Private Communication.

91. J. Kraitchman (1953) Amer. J. Phys., 21, 17 - 24.

92. Harutoshi Takeo and Chi Matsumura (1977) Bull. Chem. Soc. Japan, 50, 636 - 640.

93. J.L. Duncan (1974) Mol. Phys., 28, 1177 - 1191.

94. H. Hollenstein and H.H. Günthard (1971) Spetrochim. Acta., 27A, 2027 - 2060.

95. V. Jaccarino and J.G. King (1951) Phys. Rev., 83, 471 - 472.

96. A.W. Ellenbroek and A. Dynamus (1978) Chem. Phys., 35, 227 - 237.

Cont/d

97. R.G. Ford (1976) J. Chem. Phys., 65, 354 - 362.

98. R.H. Schwendeman (1965) J. Mol. Spec., 15, 451 - 461.

99. A.C. Legon (1980) Chem. Rev., 80, 231 - 262.

100. E. Hirota (1965) J. Chem. Phys., 42, 2071 - 2089.

101. T.B. Malloy and L.A. Carriera (1977) J. Chem. Phys., 66, 4246 - 4247.

102. K. Bolton and J. Sheridan (1970) Spectrochim. Acta., 26A, 1001 - 1006.

103. E. Saegebarth and E.B. Wilson (1967) J. Chem. Phys., 46, 3088 - 3098.

104. J.A. Pople and M. Gordon (1967) J.A.C.S., 89, 4253 - 4261.

105. L.C. Allen (1968) Chem. Phys. Letts., 2, 597 - 601.

106. A. Liberles, B. O'Leary, J.E. Eilers and D.R. Whitman (1972) J.A.C.S., 94, 6894 - 6898.

107. Shuji Saito and Fumio Makino (1974) Bull. Chem. Soc. Japan, 47, 1863 - 1867.

108. S.S. Butcher and E.B. Wilson (1964) J. Chem. Phys., 40, 1671 - 1678

109. H.M. Pickett and D.G. Scroggin (1974) J. Chem. Phys., 61, 3954 - 3958.

110. C.M.P. Brown (1985) BSc Thesis. Bristol University.

111. Shigeo Kondo, Eizi Hirota and Yonezo Morino (1968) J. Mol. Spec., 28, 471 - 489.

112. P. Meakin, D.O. Harris and E. Hirota (1969) J. Chem. Phys., 51, 3775 - 3788.

113. E. Hirota (1970) J. Mol. Spec., 35, 9 - 17.

114. Yuzuru Niide, Mitsuru Takano, Takeshi Satoh and Yoshiaki Sasada (1976) J. Mol. Spec., 63, 108 - 119.

Yoshiaki Sasada, Yuzuru Niide, Mitsuru Takano and Takeshi Satoh (1979) J. Mol. Spec., 75, 87 - 96.

115. Yoshiaki Sasada, Yuzuru Niide, Mitsuru Takano and Takeshi Satoh (1977) J. Mol. Spec., 66, 421 - 427.

Mitsuru Takano (1979) J. Mol. Spec., 75, 41 - 52.

116. K.M. Marstokk and H. Møllendal (1973) J. Mol. Struct., 16, 259 - 270.

117. I. Botskor and E. Hirota (1976) J. Mol. Spec., 61, 79 - 91.

118. A.D. English, L.H. Scharpen, K.W. Ewool, H.L. Strauss and D.O. Harris (1976) J. Mol. Spec., 60, 210 - 224.

119. J.A. Hardy, A.P. Cox, E. Fliege and H. Dreizler (1982) Z. Naturforsch, 37A, 1035 - 1037.

Cont/d

120. C.V. Berney (1969) Spectrochim. Acta., 25A, 793 - 809.

121. H.F. Shurvell, S.C. Dass and R.D. Gordon (1974) Can. J. Chem., 52, 3149 - 3157.

122. J.D. Lewis, T.B. Malloy, T.H. Chao and J. Laane (1972) J. Mol. Struct., 12, 427 - 449.

123. K.S. Pitzer (1946) J. Chem. Phys., 14, 239 - 243.

124. R.H. Schwendeman (1955) PhD Thesis. Michigan State University, U.S.A.

125. R. Wellington-Davis, M.C.L. Gerry and C.J. Marsden (1983) J. Mol. Spec., 101, 167 - 179.

126. T. Pedersen (1976) Mol. Phys., 32, 407 - 418.

127. J.E. Wollrab. Rotational Spectra and Molecular Structure. Academic Press (1967)

128. C.H. Townes and A.L. Schawlow. Microwave Spectroscopy. Dover (1975).

129. T.H. Boyer (1985) Scientific American. 253(2), 56 - 62.

130. H.D. Rudolf (1968) Z. Naturforsch, 23A, 540 - 543.

131. A.P. Cox and D.J. Finnigan (1973) J.C.S. Faraday II, 69, 49 - 55.

132. Yardley Beers. Introduction to the Theory of Error. Addison-Wesley (1962).

133. R.H. Bacon (1953) Amer. J. Phys., 21, 428 - 446.

134. K. Rectorys. Survey of Applicable Mathematics. M.I.T. Press (1969).

135. G. Graner and G. Guelachvili (1984) J. Mol. Spec., 107, 215 - 228.